

Dissertation zur Erlangung des Doktorgrades  
der Fakultät für Chemie und Pharmazie  
der Ludwig-Maximilians-Universität München

**Mechanism of talin recruitment to integrin  
adhesion sites**

Thomas Bromberger  
aus  
Starnberg

2019





### Erklärung

Diese Dissertation wurde im Sinne von § 7 der Promotionsordnung vom 28. November 2011 von Herrn Prof. Dr. Reinhard Fässler betreut.

### Eidesstattliche Versicherung

Diese Dissertation wurde eigenständig und ohne unerlaubte Hilfe erarbeitet.

München, am 03.12.2019

---

Thomas Bromberger

Dissertation eingereicht am:	03.12.2019
1. Gutachter:	Prof. Dr. Reinhard Fässler
2. Gutachter:	Prof. Dr. Markus Sperandio
Mündliche Prüfung am:	16.01.2020



# Table of contents

TABLE OF CONTENTS.....	V
LIST OF ABBREVIATIONS .....	VII
SUMMARY .....	IX
LIST OF PUBLICATIONS .....	XI
<b>A. INTRODUCTION .....</b>	<b>1</b>
1 THE INTEGRIN RECEPTOR FAMILY .....	1
1.1 <i>Integrin structure</i> .....	2
1.2 <i>Integrin ligands</i> .....	4
1.3 <i>Integrin activation</i> .....	5
1.4 <i>Integrin clustering and outside-in signaling</i> .....	7
1.4.1 Nascent adhesions, focal adhesions and fibrillar adhesions .....	10
1.4.2 Podosomes.....	11
2 TALIN.....	14
2.1 <i>Talin domain structure, binding partners and functional implications</i> .....	14
2.1.1 The talin head: an atypical FERM domain.....	14
2.1.2 Structure and function of the talin rod .....	17
2.2 <i>Talin autoinhibition</i> .....	19
2.3 <i>Regulation of talin activity</i> .....	20
2.3.1 The Talin/RIAM/Rap1 pathway .....	20
2.3.1.1 The adapter molecule RIAM .....	21
2.3.1.2 The small GTPase Rap1.....	23
2.3.2 Membrane lipids and the lipid kinase PIPKly in talin activation.....	26
2.3.3 Other regulators of talin activity .....	28
2.4 <i>The role of talin in different organisms</i> .....	29
2.4.1 <i>Dictyostelium</i> talinA and talinB .....	29
2.4.2 <i>Drosophila</i> talin .....	29
2.4.3 Vertebrate talin 1 and talin 2 .....	30
3 THE KINDLIN PROTEIN FAMILY .....	33
3.1 <i>Structure of kindlins</i> .....	33
3.2 <i>Expression and subcellular localization of kindlins</i> .....	34
3.3 <i>Kindlin interaction partners</i> .....	34
3.4 <i>Physiological and patho-physiological role of kindlin family proteins</i> .....	35
3.4.1 Non-mammalian kindlin homologs .....	35
3.4.2 Mammalian kindlins.....	36
3.4.2.1 Kindlin 1.....	36
3.4.2.2 Kindlin 2.....	37

3.4.2.3	Kindlin 3 .....	38
4	THE HEMATOPOIETIC SYSTEM.....	41
5	INTEGRINS IN PLATELET AND NEUTROPHIL FUNCTION .....	43
5.1	<i>Platelets</i> .....	43
5.1.1	Platelet formation and their physiological role.....	43
5.1.2	Regulation of platelet function .....	44
5.1.3	Integrins in platelet function.....	47
5.2	<i>Neutrophils</i> .....	48
5.2.1	Neutrophils and their function.....	48
5.2.2	Leukocyte-specific integrins.....	50
5.2.3	The leukocyte adhesion cascade.....	50
<b>B.</b>	<b>AIMS OF THE THESIS .....</b>	<b>54</b>
<b>C.</b>	<b>PAPER SUMMARIES .....</b>	<b>56</b>
1	PAPER 1: STRUCTURE OF RAP1B BOUND TO TALIN REVEALS A PATHWAY FOR TRIGGERING INTEGRIN ACTIVATION... 56	
2	PAPER 2: DIRECT RAP1/TALIN1 INTERACTION REGULATES PLATELET AND NEUTROPHIL INTEGRIN ACTIVITY IN MICE 57	
3	PAPER 3: A KINDLIN-3-LEUPAXIN-PAXILLIN SIGNALING PATHWAY REGULATES Podosome stability .....	58
4	PAPER 4: RAP1 AND MEMBRANE LIPIDS COOPERATIVELY RECRUIT TALIN TO TRIGGER INTEGRIN ACTIVATION .....	59
<b>D.</b>	<b>REFERENCES .....</b>	<b>60</b>
	<b>ACKNOWLEDGEMENT .....</b>	<b>82</b>
	<b>CURRICULUM VITAE.....</b>	<b>83</b>
	<b>APPENDIX .....</b>	<b>84</b>

## List of abbreviations

Å	Ångström
ABS	actin binding site
ADMIDAS	adjacent to MIDAS
ADP	adenosine diphosphate
AGM	aorto-gonado-mesonephros
ATP	adenosine triphosphate
CD	cluster of differentiation
CXCL	chemokine (CXC motif) ligand
CXCR	chemokine (CXC motif) receptor
DAG	diacyl glycerol
$\Delta G$	free energy
EGF	epidermal growth factor
EMT	epithelial to mesenchymal transition
ERK	extracellular signal regulated kinase
ESL	E-selectin ligand
FAK	focal adhesion kinase
FERM	4.1, ezrin, radixin, moesin
FGF	fibroblast growth factor
fMLP	formyl-methionyl-leucyl-phenylalanine
FRET	Förster resonance energy transfer
GAP	GTPase activating protein
GDP	guanosine diphosphate
GEF	guanine nucleotide exchange factor
GP	glycoprotein
GTP	guanosine triphosphate
h	hour
IBS	integrin binding site
ICAM	intercellular adhesion molecule
IKK	I $\kappa$ B kinase
IL	interleukin
ILK	integrin linked kinase
IPP	ILK-PINCH-parvin
IP <sub>3</sub>	inositol triphosphate
JAM	junctional adhesion molecule
JNK	Jun N-terminal kinase
K <sub>d</sub>	dissociation constant
LAD	leukocyte adhesion deficiency
LFA-1	leukocyte function associated molecule-1



LIMBS	ligand associated metal ion binding site
MAC-1	macrophage-1 antigen
MAPK	mitogen activated protein kinase
MEF	mouse embryonic fibroblast
MHC	myosin heavy chain
µm	micrometer
MIDAS	metal ion dependet adhesion site
MMP	matrix metalloproteinase
MTJ	myotendinous junction
NADPH	reduced nicotinamide adenine dinucleotide phosphate
NET	neutrophil extracellular trap
NF-κB	nuclear factor-κB
NMR	nuclear magnetic resonance
PECAM	platelet endothelial cell adhesion molecule
PGI <sub>2</sub>	prostaglandin I <sub>2</sub>
PIP2	phosphoinosito bisphosphate
PIP3	phosphoinosito triphosphate
PI3K	phosphoinositide 3 kinase
PKA/B/C	protein kinase A/B/C
PLC	phospholipase C
PMN	polymorphonuclear neutrophil
pN	piconewton
PTB	phosphor tyrosine binding
PSGL-1	P-selectin glycoprotein ligand 1
PSI	plexin, semaphorin, integrin
Rap	Ras-related protein
RapL	regulator for cell adhesion and polarization enriched in lymphoid tissues
Ras	Rat sarcoma
RIAM	Rap1-GTP-interacting adapter molecule
SILAC	stable isotope labeling by amino acids in cell culture
SyMBS	synergistic metal ion binding site
THATCH	talin-HIP1/R/Slap2p actin- tethering C-terminal homology (domain)
TPO	thrombopoietin
VCAM	vascular cell adhesion molecule
VEGF	vascular endothelium growth factor
VLA	very late antigen
vWF	von Willebrand factor

## Summary

Integrins are heterodimeric transmembrane receptors that facilitate the adhesion of cells to their surrounding extracellular matrix and to other cells. Integrins can adopt an inactive, thermodynamically favored or an active conformation with much higher ligand binding affinity. The latter is induced and stabilized by direct association with the intracellular adapter molecules talin and kindlin. The cellular signaling processes that trigger the formation of the high affinity conformation are named integrin inside-out signaling. Active integrins recruit a large complex of scaffold and signaling molecules that mediate integrin clustering, provide a link to the actin cytoskeleton and form signaling hubs regulating processes such as cell spreading, migration, adhesion stability, differentiation, proliferation and gene expression (outside-in signaling).

A series of cell biological studies raised the hypothesis that integrin inside-out activation requires a so-called trimeric “integrin activation complex” consisting of talin, the adapter protein RIAM and the small membrane-bound GTPase Rap1. However, *in vivo* studies revealed that this complex is only involved in regulating leukocyte  $\beta 2$  integrins. Based on these observations, the main aim of my doctoral thesis was to decipher an alternative, RIAM independent pathway of talin membrane recruitment and integrin activation. Following up a previously detected, but due to its very weak nature, not further studied direct interaction between Rap1 and the N-terminal talin F0 domain, a detailed biochemical and cell biological characterization confirmed specific GTP-dependent binding of Rap1 to talin F0 and revealed that this direct interaction is important to recruit talin to adhesion sites and to regulate adhesion and spreading of fibroblasts *in vitro* (paper 1). To assess the *in vivo* relevance of the talin F0/Rap1 interaction a Rap1-binding deficient talin 1 knockin mouse model carrying specific mutations in the talin 1 F0 domain was generated. A detailed characterization of these mice revealed impaired hemostasis and leukocyte adhesion and extravasation defects due to reduced integrin activity in platelets and neutrophils, respectively (paper 2). Since blocking the talin F0/Rap1 interaction only partially impaired integrin activity *in vitro* and *in vivo*, the contribution of other known talin interacting factors, such as membrane lipids and RIAM as well as the role of a second novel Rap1-binding site in the talin F1 domain for integrin activity regulation were investigated. These studies showed that binding of talin F0 and F1 domains to Rap1 and talin F2 domain to membrane lipids act synergistically on talin recruitment to adhesion sites and promote integrin activation, cell adhesion and spreading (paper 4).

In addition, I contributed to a project that identified and characterized the interaction of kindlin-3 and the paxillin family protein leupaxin. This study showed that kindlin-3 dependent recruitment of leupaxin into podosomes increases their lifetime by regulating PTP-PEST-mediated paxillin dephosphorylation (paper 3).



## List of publications

### Paper 1:

L. Zhu\*, J. Yang\*, **T. Bromberger\***, A. Holly, F. Lu, H. Liu, K. Sun, S. Klapproth, J. Hirbawi, T.V. Byzova, E.F. Plow, M. Moser, and J. Qin. **Structure of Rap1b bound to talin reveals a pathway for triggering integrin activation.** Nat Commun. 2017.

### Paper 2:

**T. Bromberger**, S. Klapproth, I. Rohwedder, L. Zhu, L. Mittmann, C.A. Reichel, M. Sperandio, J. Qin, and M. Moser. **Direct Rap1/Talin1 interaction regulates platelet and neutrophil integrin activity in mice.** Blood. 2018.

### Paper 3:

S. Klapproth, **T. Bromberger**, C. Türk, M. Krüger, M. Moser. **A kindlin-3-leupaxin-paxillin signaling pathway regulates podosome stability.** J Cell Biol. 2019.

### Paper 4:

**T. Bromberger\***, L. Zhu\*, S. Klapproth, J. Qin, M. Moser. **Rap1 and membrane lipids cooperatively recruit talin to trigger integrin activation.** J Cell Sci. 2019

---

\* equal contribution

## A. INTRODUCTION

### 1 The integrin receptor family

Integrins are heterodimeric cell adhesion receptors consisting of an  $\alpha$  and a  $\beta$  subunit. Integrins cluster and become organized into higher ordered adhesion structures that anchor cells on or within extracellular matrices or connect cells tightly with other cells by providing a link between the intracellular actin cytoskeleton and their ligand. Integrins are expressed in all metazoans but are absent in non-metazoan organisms. Mammals express 18 different  $\alpha$  and 8  $\beta$  subunits, which combine to 24 receptors with different ligand binding preferences and expression pattern (Hynes, 2002, Moser et al., 2009a).

Mammalian integrins are subdivided into four groups (Figure 1). The group of RGD-receptors comprises seven heterodimers:  $\alpha 5\beta 1$ ,  $\alpha 8\beta 1$ ,  $\alpha 11\beta 3$  and all  $\alpha V$  integrins. Integrins  $\alpha 3\beta 1$ ,  $\alpha 6\beta 1$ ,  $\alpha 7\beta 1$ , and  $\alpha 6\beta 4$  are laminin receptors and  $\alpha 1\beta 1$ ,  $\alpha 2\beta 1$ ,  $\alpha 10\beta 1$  and  $\alpha 11\beta 1$  are collagen receptors. The fourth group is made up by leukocyte-specific integrins  $\alpha 4\beta 7$  and  $\alpha E\beta 7$  as well as the set of  $\beta 2$  integrins ( $\alpha M\beta 2$ ,  $\alpha L\beta 2$ ,  $\alpha D\beta 2$  and  $\alpha X\beta 2$ ). The main ligands of the fourth integrin class are counter receptors presented by other cells (Hynes, 2002). In addition to the classification by their ligand binding preferences, integrins can be grouped by the presence or absence of an I domain in the  $\alpha$  subunit (see chapter 1.1).

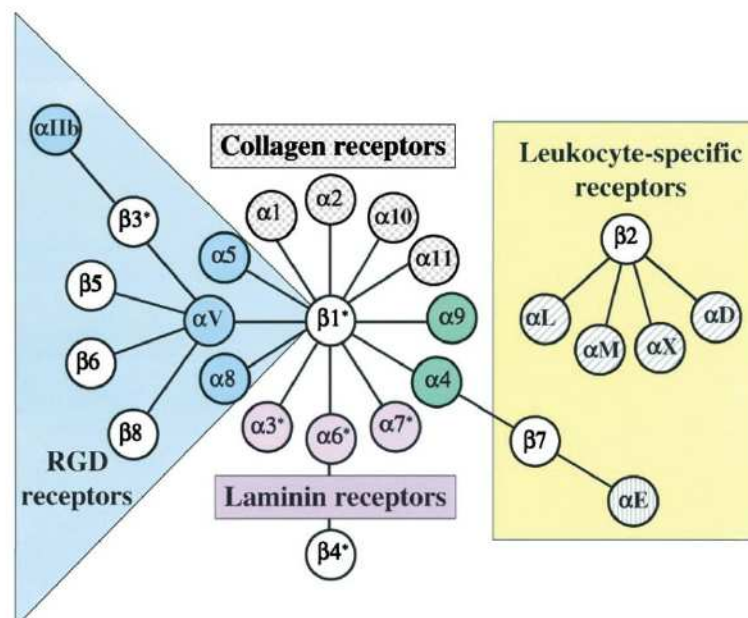


**Figure 1: Overview of integrin receptors.** Lines between subunits indicate their ability to form heterodimers. Subunits are assigned to collagen-, laminin- or RGD-binding integrins as well as integrins specifically expressed on leukocytes.  $\alpha$ -subunits are marked by grey patterned background (adapted with permission from Hynes, 2002).



In lower metazoans like fly or worm, the integrin repertoire is less diverse. *C. elegans* for instance expresses one  $\beta$  ( $\beta_{pat-3}$ ) and two  $\alpha$  subunits ( $\alpha_{pat-2}$  and  $\alpha_{ina-1}$ ), which assemble one RGD receptor ( $\alpha_{pat-2}/\beta_{pat-3}$ ) and one laminin receptor ( $\alpha_{ina-1}/\beta_{pat-3}$ ). In *Drosophila*, two  $\beta$  ( $\beta_{PS}$  and  $\beta_v$ ) and five  $\alpha$  subunits ( $\alpha_{PS1-5}$ ) are described (Hynes, 2002).

Due to their tissue and developmental stage specific expression patterns and functions, ablation of single integrin subunits in mice can cause diverse phenotypes with varying severity (Sheppard, 2000).  $\beta_1$  deficiency causes the most severe phenotype in mice showing early embryonic lethality after implantation at E6.5 highlighting its critical role in development (Fassler and Meyer, 1995). Other examples of phenotypes caused by integrin knockouts are leukocytosis, defective immune responses and cutaneous infections for integrin  $\beta_2$ , bleeding, bone and endothelial phenotypes for  $\beta_3$  and skin and epithelial defects for  $\beta_4$  (Hynes, 2002, Sheppard, 2000). The role of specific integrins in neutrophils and platelets will be discussed later in chapter 5.

### 1.1 Integrin structure

All integrin receptors are type I transmembrane proteins and share a similar domain structure (Figure 2). Both  $\alpha$ - and  $\beta$ -subunits comprise a big extracellular domain, a transmembrane helix of approximately 20 amino acids and a short cytoplasmic tail of 13 to 70 residues at the C-terminus (Moser et al., 2009a). The  $\alpha_6\beta_4$  integrin differs from all other integrins by the unusually large cytoplasmic domain of the  $\beta_4$  subunit (>1000 residues), which is untypically connected with the intermediate filament system (Hogervorst et al., 1990).

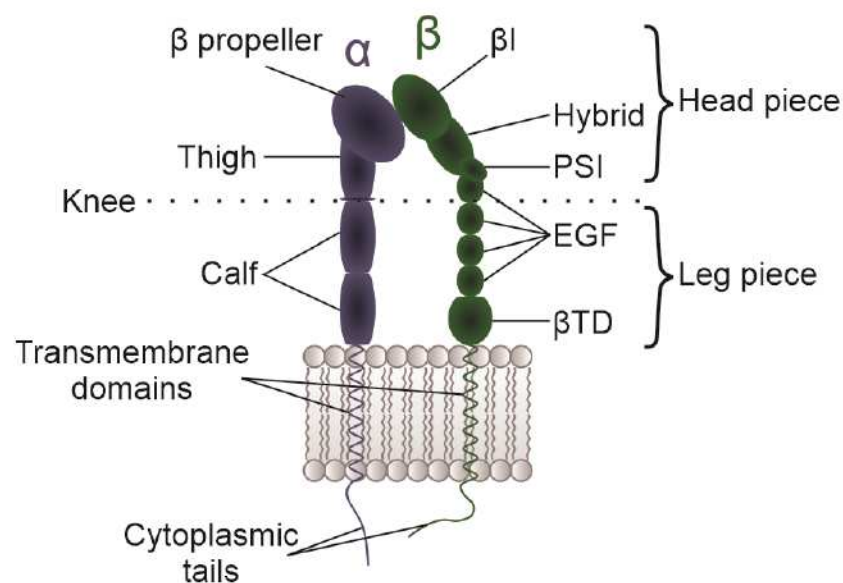


**Figure 2: Integrin domain structure (without  $\alpha$ I domain; in active conformation).**  $\alpha$ - and  $\beta$ -integrins are composed of extracellular domains with distinct structural modules, a transmembrane domain and a flexible cytoplasmic tail.

Extracellular domains of integrin  $\alpha$  subunits are composed of a seven-bladed  $\beta$  propeller at the N-terminus, followed by a thigh, a genu and two calf domains. Some  $\alpha$ -subunits (see Figure 1), have an additional domain referred to as  $\alpha$ I (also  $\alpha$ A) inserted into the  $\beta$ -propeller between blade 2 and 3.  $\beta$ -subunits comprise an I-like ( $\beta$ I or  $\beta$ A) domain, followed by a hybrid and a PSI (plexin, semaphorin, integrin) domain, four EGF (epidermal growth factor)-like modules and the  $\beta$ -terminal domain (Moser et al., 2009a).

Integrins bind their ligands via the interface between both subunits in the head area, whereas the  $\alpha$ I-domain alone serves as the ligand binding site in all  $\alpha$ I-containing integrins. Ligand binding depends on the association with divalent metal ions ( $Mn^{2+}$ ,  $Mg^{2+}$  and  $Ca^{2+}$ ). The ligand binding  $\alpha$ I and  $\beta$ I domains adopt a Rossmann fold comprising eight helices arranged around a  $\beta$  sheet in the center. Structural studies identified an ion binding site on top of the  $\alpha$ I domain termed metal ion-dependent adhesion site (MIDAS). The bound ion orients the ligand by directly interacting with acidic ligand side chains (Zhang and Chen, 2012). The  $\beta$ I domain contains a synergistic metal ion-binding site (SyMBS; or ligand associated metal binding site (LIMBS)) and an ADMIDAS (adjacent to MIDAS), which both bind  $Ca^{2+}$ , flanking a  $Mg^{2+}$ -bound MIDAS (Zhu et al., 2008). Both  $\alpha$  and  $\beta$ -subunit MIDAS, which are essential for ligand binding in the respective integrins, coordinate the metal ion by an Asp-X-Ser-X-Ser motif. Mutational studies suggested an inhibitory function of ADMIDAS and an activating role of SyMBS in regard of ligand binding (Zhang and Chen, 2012).

The transmembrane sequence of the different integrin  $\alpha$  and  $\beta$  subunits is highly conserved. A well-studied heterodimer regarding structural information on the transmembrane domain is integrin  $\alpha$ IIb $\beta$ 3 (Lau et al., 2009). NMR based assays on a C-terminal integrin  $\beta$ 3 peptide embedded in a bicelle showed that the  $\beta$ 3 transmembrane domain comprises a 29-amino acid  $\alpha$  helix from I693 to I721 spanning 43.5 Å. Given its linear arrangement, the mostly unpolar helix is tilted in a 20 to 30° angle to allow its full incorporation. Remarkably, K716 is located within the membrane segment despite its positive charge. However, the helix tilt allows an outward arrangement of its side chain in order to interact with negatively charged membrane lipid head groups (Lau et al., 2008b). In contrast, the  $\alpha$ IIb transmembrane domain spans only 24 amino acids and is not tilted.  $\alpha$  subunit transmembrane domains share high sequence similarity and carry a GFF motif (amino acids 991 to 993 in  $\alpha$ IIb) at the intracellular membrane border with the



phenylalanine side chains immersed into the hydrophobic membrane core leading to a reversal of the helix direction (Lau et al., 2008a).

A variety of studies using various techniques such as electron microscopy, mutational analysis, disulfide assays and FRET addressed the question, if and how  $\alpha$  and  $\beta$  transmembrane domains interact with each other. These studies indicated an association of both transmembrane helices of inactive integrins in an  $\alpha$  helical coiled-coil manner (Adair and Yeager, 2002, Ulmer, 2010, Luo et al., 2004, Campbell and Humphries, 2011). The interaction between the  $\alpha$  and  $\beta$  subunit is mainly facilitated by two motifs, the so called outer (OMC) and inner membrane clasps (IMC) in the outer and inner membrane leaflet, respectively: the OMC consists of glycine residues (for  $\alpha$ IIb $\beta$ 3: G972, G976 in  $\alpha$ IIb and G708 in  $\beta$ 3) and bigger hydrophobic amino acids on the opposing subdomain facing and gearing into each other. In the inner membrane clasp,  $\beta$ 3 residues L712, W715 and I719 form a groove that encloses  $\alpha$ IIb residues F992 and F993 (Lau et al., 2009, Ulmer, 2010). A salt bridge between the cytoplasmic tail residues  $\alpha$ IIb R995 and  $\beta$ 3 D723 close to the membrane also contributes to keep the integrin inactive (Hughes et al., 1996, Lau et al., 2009).

From a structural point of view, cytoplasmic domains have been shown to be highly flexible (Campbell and Humphries, 2011).

## **1.2 Integrin ligands**

The most prominent integrin recognition sequence consists of the three amino acid arginine, glycine and aspartic acid (RGD) motif. The RGD motif is present in a variety of extracellular matrix proteins and soluble ligands including fibronectin, vitronectin, fibrinogen, osteopontin, bone sialoprotein, complement factor C3bi, thrombospondin, von Willebrand factor, nidogen-1 and tenascin (Humphries, 1990). RGD-sequences are also present in laminin and collagen, however, they are inaccessible and thus don't serve as integrin binding sites (van der Flier and Sonnenberg, 2001). Structural data on integrin  $\alpha$ V $\beta$ 3 in complex with an RGD containing peptide provided insight into the binding mode to the RGD site. RGD binds to the interface between the  $\alpha$  and  $\beta$  subunit. Thereby, the arginine forms salt bridges to two aspartic acid residues in the  $\beta$  propeller and the RGD aspartic acid interacts with a  $Mg^{2+}$  ion bound in the MIDAS of the  $\beta$ I domain and some adjacent residues. Occupancy of the  $\beta$ I LIMBS stabilizes the binding interface (Xiong et al., 2002).

LDV motifs and related peptides are other common integrin binding sites. Fibronectin and VCAM-1 contain LDV motifs (Clements et al., 1994, Humphries et al., 2006). They

are recognized by integrins  $\alpha 4\beta 1$ ,  $\alpha E\beta 7$ ,  $\alpha 4\beta 7$  and  $\alpha 9\beta 1$  and  $\beta 2$  integrins. Receptors, which lack an  $\alpha$ I-domain, most likely bind to the LDV motif in a mode similar as the RGD site is bound by the respective integrins (Humphries et al., 2006).

Collagen binding integrins interact with a GFOGER peptide, which has been identified in the crystal structure of the  $\alpha$ -I domain of integrin  $\alpha 2$  with a collagen peptide (Emsley et al., 2000).

Further details on ligands for platelet and leukocyte integrins will follow in chapter 5.

### 1.3 Integrin activation

Integrins can reversibly shift between states with different ligand binding affinities. To achieve this, large conformational changes are necessary (Figure 3). Integrins can engage a low (bent-closed)-, intermediate (extended-closed)- or high-affinity conformation (extended-open) (Sun et al., 2019, Moser et al., 2009a). The low- and intermediate-affinity states are characterized by clasped transmembrane domains and leg pieces and closed ligand binding pockets in the I-domains. The transition from bent, low affinity to extended conformation involves unbending in the knee region. Opening of the ligand binding site, which is facilitated by a piston like movement of the I-domain  $\alpha 7$  helix away from the ligand binding site, in association with a swing-out of the hybrid domain and separation of the leg domains, facilitates the transition to the high-affinity conformation (Sun et al., 2019, Zhu et al., 2013). The opening results in a more than 5.000 fold higher ligand binding affinity from a  $K_d$  of 9  $\mu$ M for the ensemble of closed conformations to a  $K_d$  of 1.4 nM for extended open state in the case of integrin  $\alpha 5\beta 1$  (Li et al., 2017b). The affinity difference is smaller for  $\alpha 4\beta 1$  with only a 600-800 fold increase (Li and Springer, 2018).  $\alpha L\beta 2$  affinity to its ligand ICAM (intercellular adhesion molecule)-1 is around 10.000 fold higher in the open conformation (Shimaoka et al., 2001).

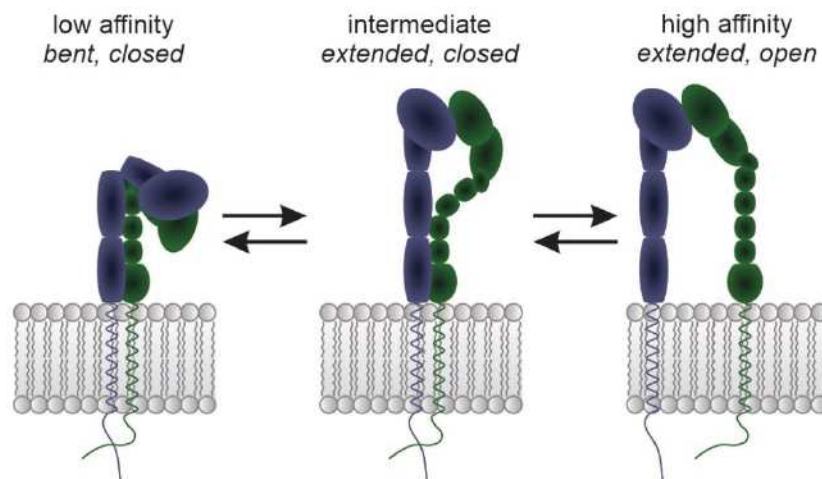




**Figure 3: Integrin ligand binding affinity depends on their conformation.** *Inactive integrins are in a bent, closed conformation, while intermediate affinity integrins are in an extended-closed and fully activated integrins in an extended-open state.*

The bent-closed conformation is thermodynamically favored. In K562 cells, 99.76% of  $\alpha 5 \beta 1$  integrins were shown to adopt the bent closed, 0.09% the extended closed and 0.15% the extended open conformation. Activation assays in the presence or absence of Fab fragments stabilizing either of the conformations showed that integrin extension requires a robust input of energy ( $\Delta G \approx 4.1$  kcal/mol), while the head piece opening is thermodynamically slightly favored ( $\Delta G \approx -0.4$  kcal/mol) (Li et al., 2017b). However, the exact ratios seem to be cell type and integrin specific. Similar measurements for integrin  $\alpha 4 \beta 1$  on different cell types revealed a smaller energy difference between conformations and a higher proportion of extended open integrins compared to  $\alpha 5 \beta 1$  (Li and Springer, 2018).

The stable shift towards the extended open conformation resulting in “integrin activation”, requires the stabilization of the active conformation. This is achieved by binding of the two cytoplasmic adapter protein families, talins and kindlins, to the  $\beta$  cytoplasmic tail. They bind integrins via a phospho-tyrosine binding motif within their F3 domains. Talin binds the membrane proximal NPXY motif and an additional site close to the  $\alpha/\beta$  tail interaction site in the membrane proximal region of the  $\beta$  tail. This leads to disruption of this interaction and tail separation triggering integrin activation (Moser et al., 2009a). Src mediated tyrosine phosphorylation of the NPXY-tyrosine inhibits talin binding and could therefore abolish integrin activation as shown for  $\beta 3$  integrins (Oxley et al., 2008). Kindlins bind the membrane distal NXXY motif via their F3 domain. Kindlin additionally requires a TT or ST motif located between both NXXY motives to bind  $\beta$  tails (Moser et al., 2009a).

Although it has been proven that talin or kindlin alone are not sufficient to achieve full integrin activation, it is not entirely clear yet, how they cooperate (Bledzka et al., 2012, Kahner et al., 2012, Ye et al., 2013b, Theodosiou et al., 2016). Functional studies on the leukocyte integrin LFA-1 and comparison of activation states with conformation specific antibodies suggested that talin binding induces the extension of the integrin ectodomain towards the intermediate affinity conformation. According to this model, subsequent kindlin recruitment facilitates the transition towards the high affinity conformation (Lefort et al., 2012). Another study, which addressed the specific roles of talin and kindlin in  $\alpha IIb \beta 3$  integrin activation claims that talin binding to the integrin tail alone is sufficient to increase integrin affinity and that kindlin binding is primarily involved in increasing adhesion strength in an avidity-based manner by promoting integrin clustering. The latter



model is mainly based on the observation that kindlin deficiency has a stronger effect on binding of multivalent than monovalent ligands, while the defect caused by talin deficiency was independent of the number of integrin binding sites of the ligand (Ye et al., 2013b).

Depending on the cell type and the integrin, different integrin activation models have been proposed. The “jack knife” or “switch blade” model suggests that integrins first need to adopt their active conformation by inside-out activation, which enables them to subsequently bind their ligands (Moser et al., 2009a). In contrast, according to the “dead bolt” model, ligand binding is the initial step to activate integrins and the intracellular complex of adapter molecules is assembled at the integrin tails in response to their activation (Moser et al., 2009a). This model of “outside-in” activation seems more applicable for integrins expressed on tissue resident cells, which are embedded within an extracellular matrix. Thus, respective integrin ligands are available at all time and integrins spontaneously bind (Klapholz and Brown, 2017). Integrins expressed on circulating hematopoietic cells such as immune cells and platelets are also permanently surrounded by their ligands exposed on endothelial cells or within the blood, respectively; however, uncontrolled integrin activation may induce severe pathologies such as heart attack and stroke or inflammations (Klapholz and Brown, 2017, Legate et al., 2009). Integrin activation in these cells has to be triggered by the activation of specific signaling pathways, for instance downstream of chemokine receptors or selectin ligands (Kuwano et al., 2010, Lefort et al., 2012). Thus, it is currently believed that circulating blood cells regulate their integrin activity by integrin inside-out activation.

Recent data suggest that integrin activation not only depends on these intra- and extracellular binding events but also on tensile forces. Force is physiologically applied intracellularly by the actin-myosin system or across the cell membrane by actin linkage in cooperation with external shear forces in hematopoietic cells. Li et al. showed that the level of active integrins correlates less with increasing concentrations of adapter proteins such as talin and kindlin if no force is applied to the bonds. At adapter concentrations equal to the  $K_d$  the proportion of active integrins increases with rising cytoskeletal force within a range of 0.1 to 4 pN (Li and Springer, 2018). Furthermore, tensile forces across active integrin  $\alpha L\beta 2$  generated by actin through talin and kindlin and bound ligand in migrating T cells were detected by FRET measurements (Nordenfelt et al., 2016). These findings suggest that talin and kindlin activate integrins not only by unclasping  $\alpha$  and  $\beta$  subunits but also by transducing the necessary forces (Sun et al., 2019).

#### **1.4 Integrin clustering and outside-in signaling**



Upon activation, which increases the affinity of individual integrin heterodimers, integrins cluster into adhesion structures. The increased avidity by the collective activity of clustered integrins enhances adhesion strength (Sun et al., 2019). Integrin clustering is facilitated by different mechanisms: One is mediated by the glycocalyx, a mucin/hyaluronan layer surrounding cells, which has a thickness of approximately twice the length of an extended integrin and limits diffusion of integrins along the membrane (Wehrle-Haller, 2012, Sun et al., 2019). Actin generated forces drive the formation of protrusions out of the glycocalyx to allow first contact of integrins to ligands, which enables ligand binding of surrounding integrins due to compression of the glycocalyx. In addition, talin and kindlin dimer formation and integrin binding to multivalent ligands (Li et al., 2017a, Ye et al., 2013a, Klapholz et al., 2015), together with pulling forces of the actin cytoskeleton and actin bundling by  $\alpha$ -actinin mediate integrin clustering (Sun et al., 2019).

As integrins reveal very short intracellular domains and do not exhibit any intrinsic enzymatic activity, integrins recruit a huge number of more than 200 adapter, scaffold and signaling molecules to adhesion sites (Schiller et al., 2011). This complex allows the modulation of numerous intracellular signaling pathways in a process termed integrin outside-in signaling (Legate et al., 2009, Sun et al., 2019).

The two key proteins of integrin activity regulation, talins and kindlins, serve also as seeds in initiating the formation of the adhesion complex by binding to a broad variety of proteins. Interactions of these proteins and their consequences are discussed in detail in chapters 2 and 3.

An important scaffold protein of focal adhesions is integrin linked kinase (ILK), a part of the IPP (ILK/PINCH/parvin) complex. The pseudokinase ILK, which comprises an ankyrin repeat domain, a PH domain and a C-terminal kinase domain lacking catalytic activity, can directly interact with integrin  $\beta$  tails. ILK contributes to the integrin/actin cytoskeleton linkage, as it indirectly binds to actin via parvin (Fukuda et al., 2009). ILK deficient mouse embryos die after implantation due to abnormal actin organization in epiblast cells leading to a failure in cell polarization. ILK deficient fibroblasts show uncommon aggregates of actin fibers and impaired cell spreading underlining its importance in the regulation of the actin cytoskeleton (Sakai et al., 2003). Direct interaction of ILK with kindlin was shown to recruit kindlin to adhesion sites. The kindlin/ILK complex is required for cell spreading (see also chapter 3.3) (Fukuda et al., 2014, Huet-Calderwood et al., 2014).



Moreover, paxillin provides a central adapter that is present in adhesion sites already early during their formation and regulates their assembly and turnover during cell migration (Lopez-Colome et al., 2017). It comprises five N terminal LD (leucine-aspartic acid-rich) and four C terminal LIM (Lin11, Isl-1, Mec-3) domains and provides various docking sites that can be modulated by tyrosine and serine phosphorylation in response to integrin binding to the extracellular matrix, most importantly of tyrosines 31 and 118 (Laukaitis et al., 2001, Legate et al., 2009, Webb et al., 2004). FAK and Src family kinases are major paxillin kinases, whose effect is antagonized by phosphatases such as PTP-Pest. Tyrosine 31 and 118 phosphorylation is associated with high adhesion turnover. Together with paxillin mediated regulation of Rho GTPases (see below), this effect has a major impact on cell migration (Lopez-Colome et al., 2017).

Besides proteins, membrane lipids provide a scaffold for the assembly of signaling molecules. Phospho-inositides are a class of membrane lipids, which are phosphorylated by different lipid kinases. Several of these kinases such as PIPK $\gamma$  (Phosphatidylinositol 4-phosphate 5-kinase type-1  $\gamma$ , see 2.3.2) and PI3K are recruited to adhesion sites by talin and FAK, respectively, and synthesize phospho-inositol bisphosphate (PIP<sub>2</sub>) or triphosphate (PIP<sub>3</sub>) (Legate et al., 2009, Bye et al., 2016), which are bound by talin and kindlins, respectively (Qu et al., 2011, Ye et al., 2016).

An important function of integrin downstream signaling is the regulation and rearrangement of the actin cytoskeleton resulting in cell polarization, migration and spreading (Legate et al., 2009). Actin polymerization is initiated by the Arp2/3 complex, which is recruited to focal adhesions by FAK, vinculin and kindlin 2 (Chorev et al., 2014, Serrels et al., 2007, Bottcher et al., 2017). Rho-GTPases function in the spatiotemporal regulation of actin dynamics. The active form of the Rho GTPase Rac1 is enriched at the leading edge of migrating cells, where it promotes lamellipodia formation by driving actin polymerization. It can be activated by FAK and/or paxillin dependent pathways (Legate et al., 2009). Paxillin associates with GIT-1 (G protein coupled receptor kinase interacting protein 1) in a phosphorylation dependent manner. GIT-1 in turn forms a complex with the kinase PAK (p21 associated kinase) and the Rac1 activator PIX (PAK interactive exchange factor) (Nayal et al., 2006). The Rho family member CDC42 is activated by ILK via  $\alpha$ PIX. This leads to spatial activity of the Arp2/3 complex and filopodia formation. While Rac1 and CDC42 activation result in formation of cell protrusions, RhoA enhances cell contractility by augmenting myosin II light chain phosphorylation (Legate et al., 2009).



Moreover, integrins contribute to the regulation of signal transduction and gene expression. An integrin associated complex of Src family kinases, which directly bind  $\beta$  integrin tails (Arias-Salgado et al., 2003), and FAK initiates different signaling cascades. A major target is the Ras-MEK-MAPK pathway. Activation of the MAP-kinase ERK (extracellular signal regulated kinase) promotes proliferation, cell cycle progression and survival (Walker et al., 2005, Webb et al., 2004). Signaling cascades involving the Ser/Thr kinase Akt also mediate cell survival. Akt is recruited by PIP3, which is generated by PI3K after recruitment by FAK (Legate et al., 2009).

#### **1.4.1 Nascent adhesions, focal adhesions and fibrillar adhesions**

Clustered integrins are organized in defined adhesion structures containing distinct cytoplasmic adapter and signaling proteins. Focal adhesion-like structures (nascent, focal and fibrillar adhesions) and the more dynamic invadosome type complexes (invadopodia and podosomes [chapter 1.4.2]) are the major types of cell adhesions, which appear in a cell type and/or time and localization dependent manner (Block et al., 2008).

Focal adhesion precursors termed nascent adhesions or focal complexes form in migrating or spreading cells at the tip of protrusions like lamellipodia and filopodia in order to provide a first link to the extracellular matrix. Despite their small size of only 0.5 to 1  $\mu\text{m}$  in diameter and the missing connection to actin stress fibers, they already contain the central signaling molecules also present in mature focal adhesions. These structures are instable and disappear after approximately 1 minute (Block et al., 2008, Sun et al., 2014). Eventually, some nascent adhesions mature into focal adhesions, which are associated with stress fibers. Further adhesome proteins are recruited by membrane lipids and scaffold proteins. These recruitment events are modulated by phosphorylation or applied tension (Wehrle-Haller, 2012). RhoA driven stress fiber formation and myosin II activity build up tension and thus promote focal adhesion growth. This effect also depends on the substrate rigidity (Schiller et al., 2013). In contrast to the dot shape of nascent adhesions, mature focal adhesions appear elongated and have a size of 3 to 10  $\mu\text{m}$  (Block et al., 2008).

Detailed analysis of focal adhesion structure by super resolution microscopy revealed their molecular organization in several layers (Figure 4). Signaling and regulatory proteins like FAK, paxillin, kindlin and the talin head localize in the integrin signaling layer close to the plasma membrane and integrins, while mediators of mechanical force such as talin rod and vinculin can be detected in the adjacent force transduction layer. Actin



regulators like VASP localize to a third layer and provide links to actin filaments. Talin is the central molecule, which connects all layers (Kanchanawong et al., 2010).

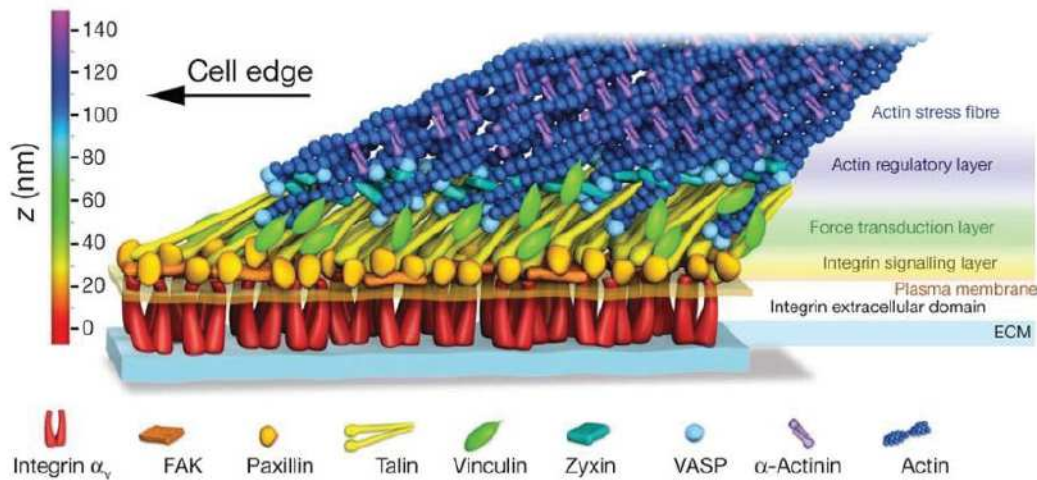


**Figure 4: Molecular composition and structure of focal adhesions.** Focal adhesions are formed by layers with distinct proteins facilitating integrin signaling, force transduction and regulation of the actin cytoskeleton (adapted with permission from Kanchanawong et al., 2010).

Fibrillar adhesions are the most mature type of focal adhesion-like structures. They promote fibronectin fibrillogenesis and their hallmark is the presence of tensin 1. Tensin can be recruited by ILK (Stanchi et al., 2009). Interestingly, it also binds like talin to the membrane proximal NPXY motif within the integrin tail. Tyrosine phosphorylation within this motif, which occurs during adhesion maturation, reduces talin affinity but has a negligible effect on tensin binding. Thus, tyrosine phosphorylation regulates the transition of focal adhesions to fibrillar adhesions (McCleverty et al., 2007).

#### 1.4.2 Podosomes

Podosomes form together with invadopodia the second group of cell-matrix adhesions, the invadosomes, and are usually made by macrophages, dendritic cells, osteoclasts and endothelial cells but have also been observed in tumor cells and src-transformed fibroblasts. They are critically involved in cell migration and remodeling of the extracellular matrix by secreting proteases (Linder and Aeppelbacher, 2003).

Although they comprise a similar set of proteins as focal adhesion like structures, their organization and morphological appearance are different (Figure 5). They contain a central actin core structure comprising actin filaments and actin regulatory proteins such as Arp2/3, WASP and cortactin (Kaverina et al., 2003, Mizutani et al., 2002, Tehrani et al., 2006). The core is surrounded by a ring of integrins and associated proteins such as talin, kindlin 3, paxillin and vinculin (Pfaff and Jurdic, 2001, Schmidt et al., 2011,

Zambonin-Zallone et al., 1989, Linder and Wiesner, 2016). The predominant integrin class in podosomes depends on the cell type. The principal integrin of osteoclasts is integrin  $\alpha V\beta 3$ , while macrophage podosomes primarily contain  $\beta 2$  integrins (Calle et al., 2006, Veillat et al., 2015). Integrins anchor the ring of adapter and signaling proteins on the extracellular matrix and the adhesion receptor CD44 provides a direct link between the actin core and the cell environment (Chabadel et al., 2007).

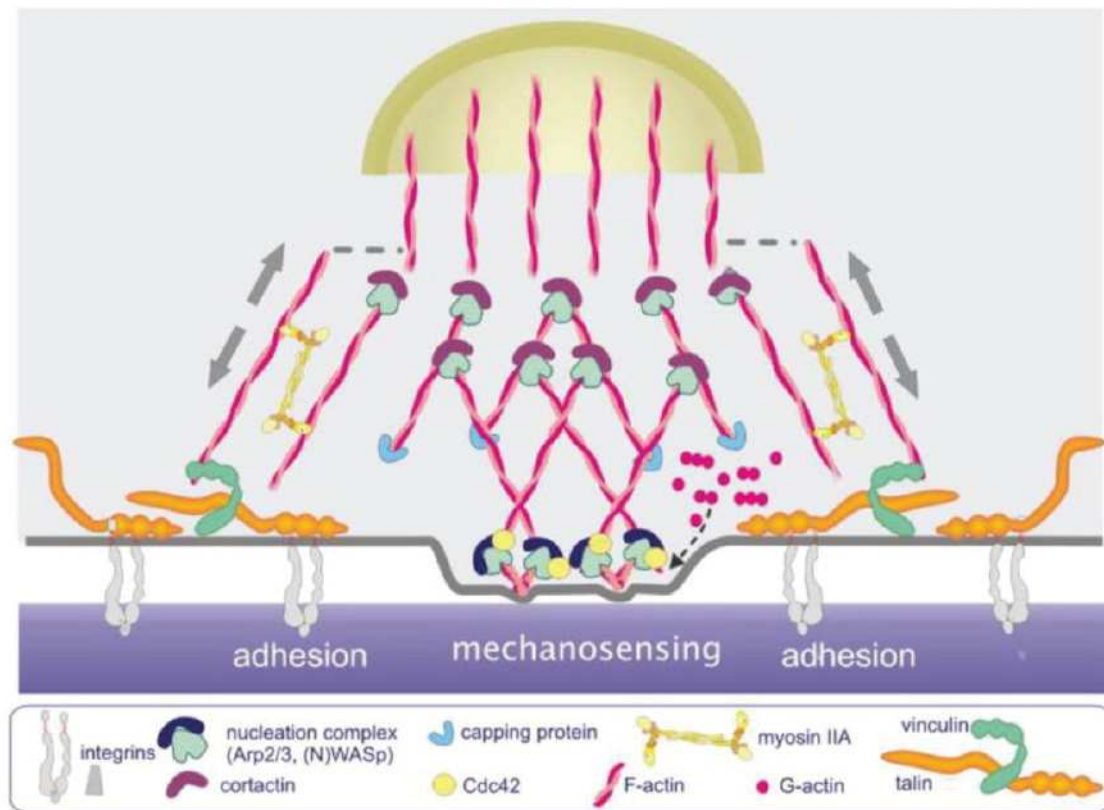


**Figure 5: Scheme of vertical middle section through podosomes.** The actin core is surrounded by a ring of plaque proteins including talin and vinculin, which is anchored to the extracellular matrix by integrins. Actin regulatory proteins like the Arp2/3 complex localize to the actin core (adapted with permission from Veillat et al., 2015).

Branched actin filaments in the core are nucleated by the Arp2/3 complex. Additional unbranched, long actin fibers provide a link between podosome core and ring structures and between different podosomes (Akisaka et al., 2008, Linder and Wiesner, 2016). These fibers nucleate at the top of the actin core, where a cap structure covers the whole complex. The podosome cap contains actin associated proteins such as supervillin, which regulates contractility by binding myosin (Bhuwania et al., 2012), the actin bundling protein fascin (Van Audenhove et al., 2015) and the formin family members INF2 and FMNL1, which initiate actin polymerization (Mersich et al., 2010, Panzer et al., 2016). The association with the actin/myosin network in combination with mechanosensitive



proteins like talin enables podosomes to sense substrate rigidity (Linder and Wiesner, 2016).

Furthermore, podosomes are critically involved in matrix degradation by secretion of proteases, specifically matrix metallo-proteases (MMPs), to enable invasive growth and protrusion formation. MMPs are transported to the adhesion sites via the microtubule network and are either secreted (e.g. MMP-2) or retained at the membrane (e.g. MT1-MMP) (Gawden-Bone et al., 2010, Guegan et al., 2008, Samanna et al., 2007, Wiesner et al., 2010).

Thus, podosomes function not only as mediators of cell adhesion and migration but also as centers of protein secretion and rigidity sensing.

## 2 Talin

As mentioned above, talin is crucial for all integrin-mediated processes by regulating both integrin inside-out and outside-in signaling. Furthermore, it connects the extracellular matrix with the intracellular actin cytoskeleton through direct integrin and actin filament binding. A great variety of studies addressed the physiological relevance of talin in different model systems, described the consequence of talin loss in whole organisms or particular organs and gave insight into the structure and regulation of talin, highlighting its importance in a broad variety of cell types and processes.

### 2.1 Talin domain structure, binding partners and functional implications

Talin is a large multi-domain protein composed of 2541 amino acids in the case of murine talin 1 and 2540 for murine talin 2. It comprises an N-terminal head domain consisting of a 400 amino acid FERM domain and a big rod domain of 2060 amino acids comprising 13  $\alpha$  helix bundles and a dimerization domain. Head and rod domain are connected by an unstructured linker region spanning 81 amino acids (Figure 6). The two mouse talin isoforms are structurally highly similar (Gough and Goult, 2018). The three-dimensional orientation of its single domains has been shown to be very flexible (Winkler et al., 1997). The protein contains two cleavage sites for the protease calpain 2, both playing a role in regulating the turnover of adhesion sites: one in the linker region between talin head and rod domain (Franco et al., 2004, Hayashi et al., 1999) and the second one between the C-terminal rod helix bundle 13 and the dimerization domain (Bate et al., 2012).

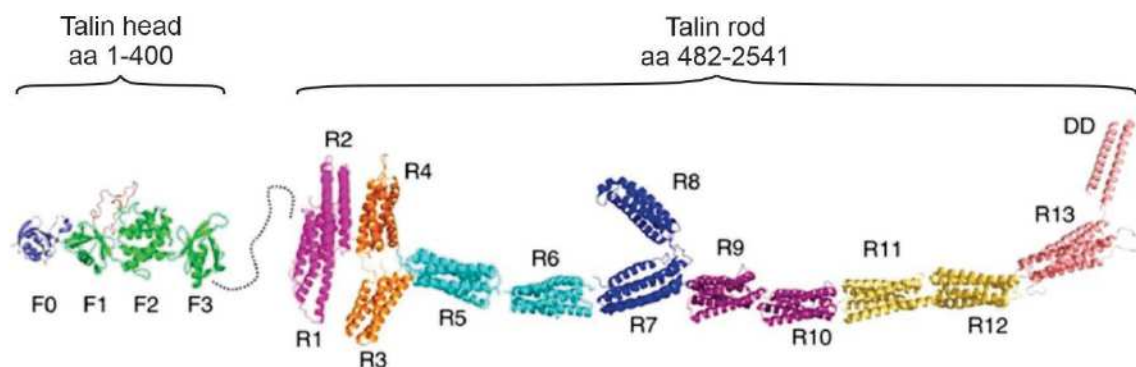


**Figure 6: Talin domain structure.** The head domain spans 400 amino acids and comprises a FERM domain containing the F0 domain (purple), the F1-F3 domains (green) and a loop (red) inserted within the F1 domain. The rod is composed of 13 bundles of 4 to 5  $\alpha$ -helices and the C-terminal dimerization domain spanning amino acids 482 to 2541. (figure adapted from Zhu et al., 2017; amino acid numbering corresponds to murine talin 1 according to Gough and Goult, 2018)

#### 2.1.1 The talin head: an atypical FERM domain



The talin head consists of a FERM (4.1, ezrin, radixin, moesin) domain with unique characteristics (Figure 7). FERM domains are typically found in proteins that provide a link from the membrane to the cytoskeleton (Klapholz and Brown, 2017). They are composed of three subdomains F1, F2 and F3. The FERM domain of talin contains an additional subdomain at its N-terminus, named F0, and an unstructured loop inserted into the F1 domain. These features are unique to talin and its closest homolog, the kindlin protein family (Goult et al., 2010a). Another anomaly of the talin FERM domain concerns its three-dimensional structure: the four subdomains in its activated membrane-attached state reveal a linear alignment, whereas other FERM domains usually adopt a cloverleaf-like conformation (Elliott et al., 2010).

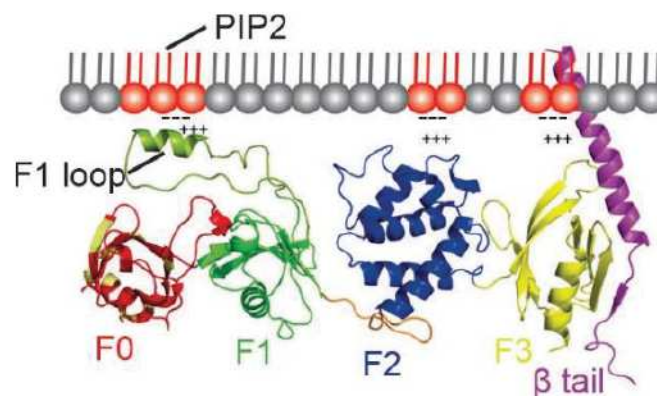


**Figure 7: Structure of the talin head domain.** The talin head consists of a linearly arranged FERM (F1, F2, F3) domain with an additional N-terminal F0 domain and an inserted loop in the F1 domain. This loop adopts a helical structure and interacts with negatively charged membrane lipids upon talin activation (adapted from Elliott et al., 2010).

The structure of the F0 domain, which spans amino acids 1 to 86, reveals an ubiquitin-like fold. It is composed of five  $\beta$  strands, forming a twisted  $\beta$  sheet, with an  $\alpha$  helix between strands 2 and 3 and a short helical turn between strands 4 and 5. A further feature of the F0 domain is a patch of basic amino acids at its surface (K15, R30, R35; Figure 8), which shares a high structural similarity with the Ras-binding site on the Ras-effector RalGDS. Ras-like GTPases contain negatively charged amino acids, which form salt bridges to such positively charged clusters of their binding partners. K7 and R33 further enhance the positive charge at this site (Goult et al., 2010a).



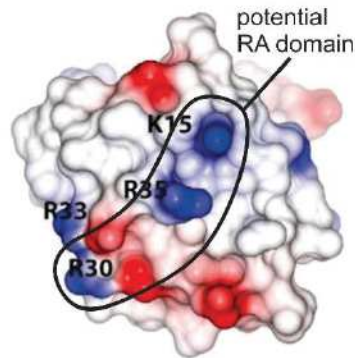


**Figure 8: Talin F0 domain structure.** Basic amino acids potentially resembling a Ras association (RA) domain are shown in blue (adapted from Goult et al., 2010a).

Talin's F1 domain is highly similar to the F0 domain, comprising the same secondary structural elements assembled in an ubiquitin-like fold and a similar amino acid sequence. The F1 domain contains an additional unstructured loop between  $\beta$  sheets 3 and 4 spanning amino acids 133 to 170 in mouse talin 1 and consisting of 60% charged residues. Upon talin activation and contact with negatively charged membrane lipids, the loop shifts towards a helical structure with positively charged amino acids facing the membrane (Figure 7) and thereby anchoring talin at the membrane (Goult et al., 2010a).

The F2 domain comprises two  $3_{10}$  helices and four  $\alpha$  helices. The F3 domain resembles a phospho-tyrosine binding (PTB) domain and is formed by a C-terminal  $\alpha$  helix, which is embedded between two  $\beta$  sheets containing four and three antiparallel strands, respectively. The PTB motif in F3 binds the membrane proximal NPXY motif of the  $\beta$  integrin cytoplasmic tail and thereby stabilizes the active integrin conformation (Garcia-Alvarez et al., 2003, Calderwood et al., 2002) as already mentioned in chapter 1.3. Structural analysis of talin F3/integrin  $\beta 3$  binding identified a mostly hydrophobic surface on F3 to be responsible for integrin binding. The  $\beta 3$  NPLY sequence forms a turn by intramolecular interactions and specifically the NPLY asparagine (N744) interacts with talin residues T354 and I356, while its tyrosine side chain is buried within a pocket containing acidic and hydrophobic residues. Additionally, talin F3 residues R358, W359 and I396 are critical for integrin binding. They interact with aromatic amino acids N-terminal of the NPXY motif (Garcia-Alvarez et al., 2003).

The F2 and F3 domains contain further patches of positively charged amino acids, which bind to negatively charged membrane lipids such as phosphatidyl-inositol diphosphate (PIP2; see chapter 2.3.2) (Martel et al., 2001, Saltel et al., 2009, Song et al., 2012) and interaction sites for a variety of binding partners (Figure 9). One of the three actin binding sites (ABS1) of talin is located within the F2/F3 segment (Lee et al., 2004). ABS1 binding



to actin blocks actin polymerization at barbed ends and caps actin filaments. This could potentially lead to increased tension exerted by the acto-myosin system on talin (Ciobanasu et al., 2018). F3 binds among others RIAM (Rap1-GTP interacting adapter molecule; see chapter 2.3.1.1) (Yang et al., 2014), FAK (focal adhesion kinase, see chapter 2.3.3) (Lawson et al., 2012), PIPK1 $\gamma$  (phosphatidylinositol 4-phosphate 5-kinase type-1 gamma; chapter 2.3.2) (de Pereda et al., 2005), G $\alpha$ 13 (see chapter 2.3.3) (Srinivasan et al., 2015, Schiemer et al., 2016) and TIAM1, a Rac1-GEF (Wang et al., 2012).

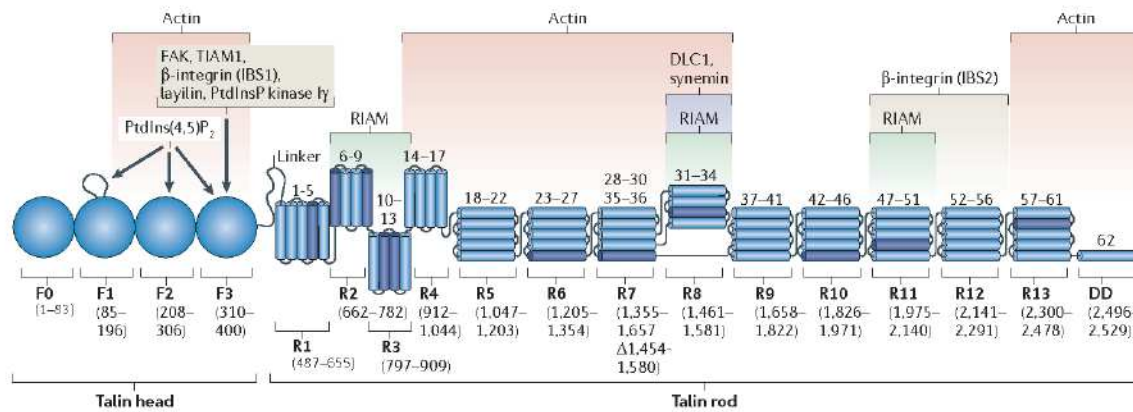


**Figure 9: Talin binding partners.** Talin head interaction partners include FAK, TIAM1, layilin, PIPK1 $\gamma$  and  $\beta$  integrin tails to the F3 domain, an actin binding site (ABS1) spanning F2 and F3 as well as membrane lipid binding sites. Major interactors of the rod are RIAM and actin, which has two binding sites: one spanning R4 to R8 and one in the R13/dimerization domain (ABS2 and ABS3). 11 cryptic vinculin binding sites are distributed over the whole rod domain (dark blue helices). R11 contains a second integrin binding site (adapted with permission from Calderwood et al., 2013).

### 2.1.2 Structure and function of the talin rod

The talin rod comprises more than 2000 amino acids and is organized into thirteen bundles, the R domains 1-13. They are composed of four (R2-4 and R8) or five (R1, R5-7 and R9-13)  $\alpha$ -helices and followed by a small dimerization domain at the very C-terminus consisting of only one helix. While the N-terminal domains R1-5 are assembled in a compact structure, the C-terminal helix bundles (R6-13) are linearly aligned (Calderwood et al., 2013).

A hallmark of talin is its function in the mechanical force transmission from the extracellular matrix to the actin cytoskeleton. A talin molecule in cultured fibroblasts bears forces between 7 and 10 pN (Austen et al., 2015, Ringer et al., 2017, Kumar et al., 2016). Integrin dependent attachments of developing flight muscles to tendon cells in *Drosophila* were used as a model to assess mechanical tension load across talin *in vivo*.



This study confirmed that some talin molecules experienced 7 to 10 pN of force. However, the proportion of talin molecules experiencing tension was much lower than *in vitro* and decreased further with development due to enhanced localization of talin to adhesion sites (Lemke et al., 2019). Those observations are particularly interesting due to the fact, that all rod segments except R8 unfold in a force-dependent manner at a range from 5 to 25 pN. This process is fully reversible, if the applied force drops beneath 3 pN (Yao et al., 2016). Importantly, the force dependent conformational changes induce displacement of binding partners such as RIAM but also recruitment of other interactors like vinculin or actin, a process that is crucial for signaling and adhesion maturation (Goult et al., 2018).

These pulling forces are exerted on talin by the actin cytoskeleton. The talin rod contains two actin binding sites (ABS2 and ABS3; see figure 9). Helix bundles R4 to R8 form ABS2 (Hemmings et al., 1996, Klapholz and Brown, 2017). ABS2 is more important in mature adhesion complexes than in initial adhesions and is engaged in a tension dependent manner (Atherton et al., 2015). Force measurements across talin revealed, that ABS2 bears most of the tension in mature focal adhesions and thus is critical for mechano-sensing (Kumar et al., 2016). R13 forms the C-terminal actin binding site (ABS3) together with the dimerization domain resembling a THATCH core domain. A common feature of THATCH domains is a helix at the C-terminus, which enhances actin binding by formation of homodimers. Indeed, dimerization of talin promotes R13 actin binding, although dimers bind only one actin filament via the C-terminal binding site (Gingras et al., 2008). Engagement of actin with ABS3 is thought to mediate initial formation of adhesion complexes and force-mediated unmasking of cryptic binding sites in the talin rod such as multiple vinculin binding sites and the ABS2 simultaneously with displacement of other interactors like RIAM (Atherton et al., 2015).

The adapter molecule RIAM binds to the talin rod at the domains R2, R3, R8 and R11 (Goult et al., 2013b). More details on the function of RIAM are provided in chapter 2.3.1 on the regulation of talin activity.

The talin rod contains eleven vinculin binding sites (Figure 9). Their consensus sequence spans nineteen amino acids and contains several hydrophobic residues at distinct positions within one  $\alpha$ -helix (Gingras et al., 2005). Structural analysis of the individual R domains confirmed the presence of vinculin binding sites in the R1/R2 segment (Goult et al., 2010b, Papagrigoriou et al., 2004), in R3, R6 (Goult et al., 2013b), R7, R8 (Gingras et al., 2010), R10 (Gingras et al., 2006, Goult et al., 2010b) and R11 (Goult et al., 2013b). However, most vinculin binding sites are cryptic and only exposed upon application of



mechanical forces and the resulting domain unfolding (Goult et al., 2010b, del Rio et al., 2009, Papagrigoriou et al., 2004, Goult et al., 2018). Vinculin is a 117 kDa protein that interacts with talin via its head domain and with actin via its tail. This leads to reinforcement of talin linkage to the actin cytoskeleton (Atherton et al., 2016).

Goult et al. reported a mutually exclusive binding of RIAM and vinculin to the talin rod R2R3 domains. While RIAM interacts with folded talin rod domains, which are not exposed to force and therefore present in nascent adhesions at the leading edge of migrating cells, vinculin is recruited to mature focal adhesions upon exposure of its binding sites by force dependent domain unfolding of talin rod helical bundles (Goult et al., 2013b).

R7 and 8 resemble a unique structure compared to all other rod domains, as the four-helix bundle of R8 is inserted into the loop connecting helices 3 and 4 of the R7 domain (Gingras et al., 2010). R7 bears the interaction site for Kank family proteins (Kidney ankyrin repeat protein), which regulate talin activity and force transduction by inhibiting actin binding to ABS2 (Sun et al., 2016). The R8 domain of talin competes with the vinculin rod for binding of the muscle intermediate filament protein  $\alpha$ -synemin (Sun et al., 2008), and binds the tumor suppressor DLC1 (deleted in liver cancer 1), which interacts with talin and FAK via a LD domain to reach its full activity (Li et al., 2011).

In addition to interaction sites for RIAM and vinculin, the R11 contains a second integrin binding site (IBS2) (Gingras et al., 2009). Structural and mutational analyses revealed the formation of a salt bridge between talin rod helix 50 residues K2085 and K2089 and the acidic amino acids E726 and E733 within the membrane proximal helix of the  $\beta$ 3 cytoplasmic tail (Rodius et al., 2008). While some information is available about the role of IBS2 in *Drosophila* (see chapter 2.4.2), its role in mammalian talin is largely unknown. One study addressing nascent adhesion formation in mouse embryonic fibroblasts (MEFs) suggested an involvement of IBS2 in nascent adhesion formation, as expression of the talin rod alone in talin deficient cells was sufficient to rescue nascent adhesion formation (Changade et al., 2015).

## **2.2 Talin autoinhibition**

The first insights into talin structure are based on electron microscopy studies, which described two different conformations: under low ionic strength of 5-20 mM NaCl talin adopted a globular shape, while the structure appeared more flexible and extended at high salt concentrations (Molony and Burridge, 1985). Subsequent studies showed an intramolecular interaction within talin between a positively charged loop in the F3 domain



and negatively charged residues in the talin rod domain R9, which results in masking of the PTB domain and talin autoinhibition. As talin in its autoinhibited conformation can neither bind integrins nor actin filaments, talin head alone has a higher potential to activate integrins compared to full-length talin in a CHO cell based overexpression model (Goksoy et al., 2008, Goult et al., 2009a, Zhang et al., 2016a, Banno et al., 2012). Additionally, intramolecular interaction of the N-terminal region of the talin rod with the F2/F3 domain masks membrane lipid binding sites and promotes the cytosolic localization of inactive talin (Banno et al., 2012). Song et al. supported this model of autoinhibition by showing that the closed conformation not only sterically inhibits binding to integrins but also electrostatically prevents association of the talin head with negatively charged membrane lipids, as a negatively charged surface in the R9 rod segment exerts repulsive effects (Song et al., 2012). Taking into account all of these findings, Goult et al. suggested inactive talin homodimers to adopt a donut-like shape with both rod domains forming a ring around the head domains, which are located in the center (Goult et al., 2013a). A recently published study that resolved the structure of full length talin 1 by cryo-electron microscopy confirmed the autoinhibitory intramolecular interactions between talin head F2 and F3 with rod R12 and R9 domains, respectively. However, multiple additional interactions between rod segments were found to maintain talin in its compact autoinhibited conformation (Dedden et al., 2019). The latter contradicts the model of Goult et al. suggesting a donut-shaped arrangement of the rod around the head domain.

### **2.3 Regulation of talin activity**

Talin activity depends on its conformation (auto-inhibited vs open) and its subcellular localization (cytosolic vs membrane bound). Both are regulated by different interactors and proteolysis by calpain-2 (Calderwood et al., 2013). The molecular steps that are involved in the release of autoinhibition and targeting of talin to the membrane, have been addressed by several studies but the mechanisms are not fully elucidated yet. The known regulation pathways are of different importance depending on the integrin and/or cell type. The following chapters summarize different mechanisms of talin activity regulation.

#### **2.3.1 The Talin/RIAM/Rap1 pathway**

One model of talin recruitment and talin mediated integrin activation involves a trimeric complex consisting of talin, the small GTPase Rap1 and the Rap1-GTP interacting adapter molecule (RIAM). In this model, RIAM acts as a linker connecting talin to the membrane-bound GTP-loaded Rap1 protein and thereby brings it in proximity to the

integrin (Figure 10). However, subsequent studies in RIAM deficient cells and mice indicated that this talin recruitment pathway is only relevant for a subclass of integrins, the  $\beta 2$  integrins, expressed on hematopoietic cells (Klapproth et al., 2015b, Stritt et al., 2015, Su et al., 2015).

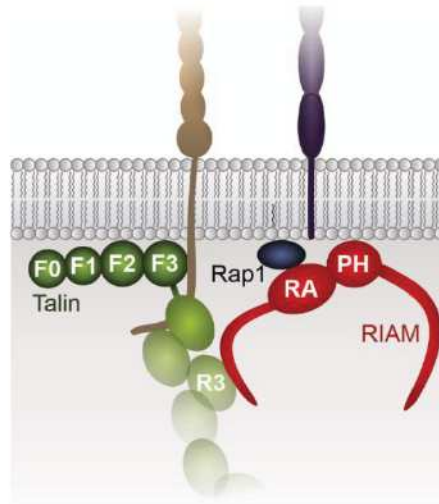


**Figure 10: Model of talin recruitment to the plasma membrane in a trimeric complex together with RIAM and Rap1.** RIAM (red) binds active membrane-bound Rap1 (blue) by its Ras-association (RA) domain and talin by its N-terminus leading to talin membrane targeting.

#### 2.3.1.1 The adapter molecule RIAM

RIAM, which is also named amyloid beta (A4) precursor protein-binding family B member 1-interacting protein (APBB1IP), is a member of the MRL (Mig-10/RIAM/Lamellipodin) protein family (Colo et al., 2012). Murine RIAM is a 670 amino acid protein. Its N-terminus comprises two coiled-coiled domains and a small proline rich region, which is followed by an RA (Ras association) domain, a PH (pleckstrin homology) domain and a big proline rich region at the C-terminus (Figure 11). It binds GTP-bound Rap1 and with lower affinity active Ras via its RA domain (Lafuente et al., 2004, Colo et al., 2012). Rap1 binding and interaction with phosphoinositol 4,5-bisphosphate facilitated by the PH domain cooperatively regulate plasma membrane association as shown in activated T cells (Wynne et al., 2012). Additionally, RIAM plays a role in driving actin polymerization, lamellipodia formation and cell spreading, as it contains binding motifs for profilin and EVH1 domains of Ena/VASP in both proline-rich regions (Lafuente et al., 2004, Jenzora et al., 2005).



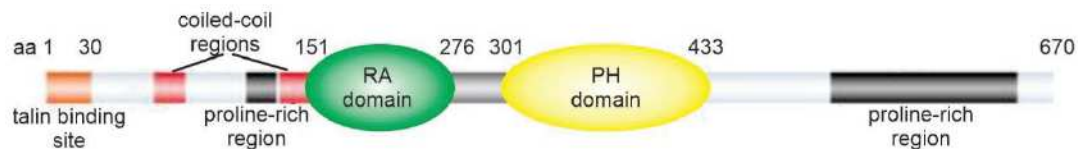


**Figure 11: Domain structure of Rap1-GTP interacting adapter molecule (RIAM).** RIAM contains N-terminal coiled-coil regions, a Ras-association (RA) domain, which binds Rap1, a Pleckstrin-homology (PH) domain facilitating membrane interactions and a proline rich region at the C terminus that binds profilin and Ena/VASP. Talin binds the N terminus (adapted with permission from Wynne et al., 2012; residue numbering of murine RIAM according to Jenzora et al., 2005).

The proposed model of a trimeric integrin activation complex consisting of GTP-bound Rap1, RIAM and talin is primarily based on experiments using a CHO cell based system (Han et al., 2006, Lee et al., 2009, Watanabe et al., 2008). This CHO cell model is frequently applied to study integrin  $\alpha\text{IIb}\beta 3$  inside-out signaling *in vitro*. Ectopic stable expression of human integrin  $\alpha\text{IIb}\beta 3$  in combination with overexpression of different proteins allows the assessment of their role in integrin  $\alpha\text{IIb}\beta 3$  activation by antibody binding assays using active conformation specific antibodies such as PAC-1 (Han et al., 2006, Lagarrigue et al., 2018). These studies revealed a reduction of talin mediated integrin activation in the absence of RIAM, suggesting that talin recruitment and integrin activation critically depend on RIAM (Han et al., 2006, Lee et al., 2009).

The importance of RIAM for the formation of protrusions during cell migration was confirmed by cell biological studies using different cell lines. They showed that a Rap1 dependent complex of talin, active integrin and RIAM can be found at the tips of protrusions like lamellipodia and filopodia (Lagarrigue et al., 2015). Biochemical analysis of the RIAM/talin interaction revealed a very similar binding mode between RIAM and the talin R3 and R8 domains, although R8 exhibited a higher affinity for RIAM. The talin binding site in RIAM consists of a helix, which is 55° kinked at the position of serine 13. Of note, this structural element is absent in lamellipodin despite the high similarity apart from that. As a consequence, talin interacts stronger with RIAM than with lamellipodin and RIAM shows a stronger ability to promote integrin activation (Chang et al., 2014). Yang et al. described a further RIAM interaction site within the talin F3 domain that sterically excludes the intramolecular F3/R9 interaction and concluded that RIAM is additionally involved in the conformational activation of talin (Yang et al., 2014).

Studies on RIAM knockout mice, however, question its importance for integrin activation. RIAM deficient mice are viable and fertile without any overt phenotype (Klapproth et al., 2015b, Stritt et al., 2015, Su et al., 2015). As various cells of the hematopoietic system strongly depend on rapid integrin inside-out activation, several studies on RIAM knockout mice focused on blood cells. RIAM knockout mice suffer from a severe leukocyte



adhesion defect, due to impaired  $\beta 2$  integrin activation, which results in strongly reduced leukocyte trafficking. While RIAM is primarily important for  $\beta 2$  integrin-mediated adhesion of neutrophils, T cells and macrophages, it is less involved in  $\alpha 4 \beta 1$  regulation (Klapproth et al., 2015b). This provides an explanation for the stronger adhesion defects of talin-deficient leukocytes, since here all integrin classes are affected. The development of B and T cells occurs normally in the absence of RIAM, however, the number of marginal zone B cells in spleens is reduced, trafficking of B and T cell populations to lymph nodes is diminished due to adhesion and migration defects and the humoral immune response is attenuated (Su et al., 2015). In strong contrast, platelets isolated from RIAM knockout mice exhibited normal activation of  $\alpha \text{IIb} \beta 3$  and  $\beta 1$  integrins, aggregation, adhesion under flow on collagen, clot retraction and spreading on fibrinogen. Furthermore, the mice did not show any bleeding tendency or delay in thrombus formation (Stritt et al., 2015). Together, these results show that leukocyte but not platelet integrin activation and function are RIAM dependent.

Non-mammalian MRL protein family members are mig-10 in *Caenorhabditis elegans* and the lamellipodin paralogue *pico* in *Drosophila*, which is expressed in two splice variants termed *pico* and *pico-L* (Colo et al., 2012). The N-terminal 128 of 1159 amino acids of *pico-L* are missing in *pico*. *pico* drives cell proliferation and tissue growth by binding effectors of EGF receptor signaling like Ras and modifies the actin cytoskeleton via *ena*. A constitutive knockout of the *pico* gene is lethal at larval stage (Lyulcheva et al., 2008).

The *C. elegans* member of the MRL family, mig-10, regulates axon outgrowth in neuronal development and filopodia formation in cooperation with the Ena/VASP related protein unc-34 and promotes adhesion of anchor cells during migration through the vulval and gonadal basement membrane at larval development (Chang et al., 2006, Wang et al., 2014).

Interestingly, no RIAM paralogue exists in *Dictyostelium*, although both Rap1 and talin proteins are expressed (Plak et al., 2016). DydA is the only MRL protein of *Dictyostelium*, however, it does not bind Rap1. Interestingly, the Rap1 effector Phg2, which is a Ser/Thr kinase and known to be important for cell motility regulation, might be involved in the regulation of talinA (Kolsch et al., 2013, Plak et al., 2016).

#### **2.3.1.2 The small GTPase Rap1**

Rap1a and Rap1b are two almost identical isoforms (95% protein identity) of the membrane-anchored small GTPase Rap1 (Ras-related protein 1) in vertebrates, which are expressed at different levels depending on the cell type. This family of small GTPases



plays a role in the regulation of a broad variety of cellular processes like adhesion, growth, migration and apoptosis (Jaskiewicz et al., 2018). Rap1, initially called Krev-1, has first been identified and described in 1989 as a Ras-related protein with tumor suppressing function (Kitayama et al., 1989) and was characterized as a Ras antagonist (Cook et al., 1993).

Similar to other small GTPases, Rap1 activity is directly modulated by two groups of enzymes: guanine nucleotide exchange factors (GEFs) and GTPase activating proteins (GAPs) (Figure 12). They control a cycle between inactive GDP-bound and active GTP-bound Rap1. GEFs induce an exchange of GDP by GTP, which shifts the protein into an active state. The intrinsic GTPase activity of Rap1 is enhanced by GAPs, which promote inactivation of the protein (Jaskiewicz et al., 2018).

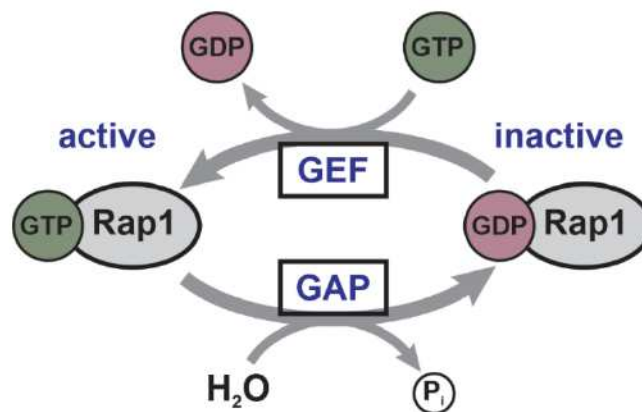


**Figure 12: Activation cycle of Rap1 GTPases.** Inactive Rap1 is activated by a GDP to GTP exchange catalyzed by guanine nucleotide exchange factors (GEFs), which is reversed by GTPase activating proteins (GAPs) that enhance its GTPase activity to get back to the GDP bound state.

Depending on the cell type, Rap1 activation involves various GEFs, whose activity in turn is triggered by different stimuli. For example, Epac is a Rap1-GEF activated by binding of the second messenger cAMP (cyclic adenosine monophosphate) (de Rooij et al., 1998). Epac1 is expressed ubiquitously while its homolog Epac2 is mainly expressed in endocrine and neuronal tissues (Ulucan et al., 2007). C3G is particularly important in mouse embryonic fibroblasts and during embryonic development (Ohba et al., 2001). In neutrophils, Rap1 activation depends on protein kinase C and elevation of intracellular  $\text{Ca}^{2+}$  levels upon stimulation with fMLP (formyl-Methionyl-Leucyl-Phenylalanine), GM-CSF (M'Rabet et al., 1998) or other agonists.  $\text{Ca}^{2+}$  is also involved in Rap1 activation in platelets (Franke et al., 1997, Stefanini and Bergmeier, 2010). In both cell types, it acts through the  $\text{Ca}^{2+}$  dependent CalDAG-GEFI, a GEF with highest expression levels in neuronal tissue and the hematopoietic system (Kawasaki et al., 1998, Stadtmann et al.,



2011, Stefanini and Bergmeier, 2010). Indeed, CalDAG-GEFI deficient mice suffer from severe platelet dysfunction due to defective integrin activation caused by inability to activate Rap1 (Crittenden et al., 2004).

While Rap1a/b double-knockout mice die during embryonic development before E10.5, mice deficient in only one isoform show a less severe phenotype (Chrzanowska-Wodnicka et al., 2015). Rap1a deficient mice on C57BL/6J background derived from heterozygous matings are born at a sub-mendelian ratio indicating partial embryonic lethality (Li et al., 2007). 85% of Rap1b knockout mice die before or shortly after birth due to hemorrhages. The surviving pups develop to adulthood despite a reduction in body size. Furthermore, they show impaired platelet function caused by a reduction in integrin activity and signaling to approximately 70% (Chrzanowska-Wodnicka et al., 2005, Zhang et al., 2011). The expression level of Rap1b in platelets is more than 20-times higher compared to Rap1a (Zeiler et al., 2014). However, both isoforms are involved in platelet integrin regulation. A platelet specific knockout of either isoform causes a defect in platelet function, which is more pronounced in the case of Rap1b deficiency. Knockout of both isoforms results in a stronger platelet defect (Stefanini et al., 2018). Loss of Rap1a in leukocytes impairs integrin-regulated processes, such as LFA-1 mediated lymphocyte and macrophage adhesion, oxidative burst as well as Mac-1/complement factor C3bi-mediated phagocytosis (Li et al., 2007, Caron et al., 2000, Katagiri et al., 2000, Duchniewicz et al., 2006). Surprisingly, Rap1b deficiency promotes neutrophil extravasation, however, this effect is rather due to enhanced PI3K-Akt signaling than screwed integrin activity (Kumar et al., 2014).

Specifically in migrating T cells, LFA-1 clustering at the leading edge is regulated by binding of the Rap1 effector RapL (regulator of adhesion and cell polarity enriched in lymphoid tissues) to the  $\alpha$ -subunit of the integrin dimer. RapL in turn is translocated to the leading edge by interacting with Rap1a (Katagiri et al., 2003). Cell polarization is cooperatively promoted by RapL and the protein Mst1 (Katagiri et al., 2006).

Additionally, both Rap1a and Rap1b have important integrin-dependent and independent regulatory functions during angiogenesis and in maintaining blood vessel integrity through VE-cadherin mediated cell-cell junction formation, which was shown in extensive studies on endothelial cells (Chrzanowska-Wodnicka et al., 2015). For instance, Rap1a recruits the cell-cell junction stabilizing protein KRIT-1, which negatively regulates  $\beta$ -catenin translocation to the nucleus by retaining it at cell junctions (Glading et al., 2007, Glading and Ginsberg, 2010). It promotes FGF2 (fibroblast growth factor-2)/FGFR1 (FGF receptor-1)-induced Rac activation as well as MAPKp38 (mitogen activated protein



kinase p38) and ERK (extracellular signal regulated kinase) phosphorylation (Yan et al., 2008) and Rap1b synergizes with integrin  $\alpha v \beta 3$  to enable VEGFR2 (vascular endothelial growth factor receptor-2) activation (Lakshmikanthan et al., 2011). Rap1a-mediated Rac1 activation is triggered by recruitment of Rac-GEFs like Tiam1 to protrusions (Arthur et al., 2004). An overview of Rap1 targets is shown in figure 13.

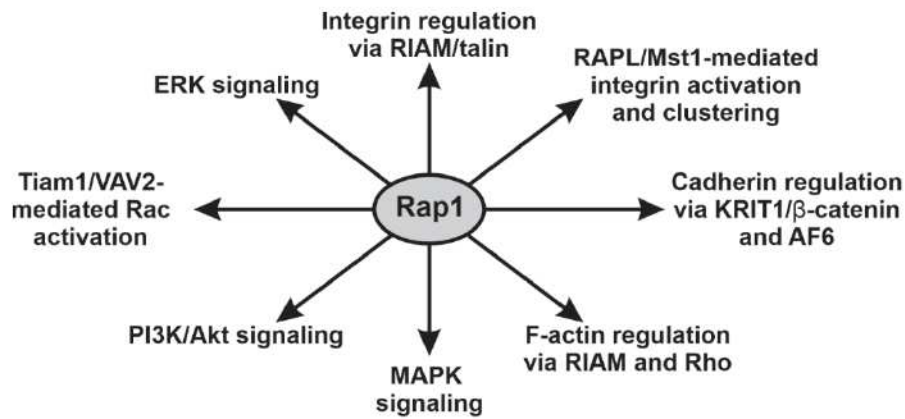


**Figure 13: Overview of Rap1 downstream effector functions.** This includes pathways that regulate integrin adhesion and signaling, formation and maintenance of cadherin mediated cell junctions, actin remodeling, proliferation and gene expression (according to Jaskiewicz et al., 2018).

Taken together, Rap1 GTPases are important signaling units that regulate cell adhesion, migration, proliferation and gene regulation not only by its integrin activating and F-actin regulatory activity through RIAM/talin but also by modulating a variety of other signaling pathways.

### 2.3.2 Membrane lipids and the lipid kinase PIPKly in talin activation

Interaction of talin with negatively charged membrane lipids mainly involving PIP2 participates in talin activation (Martel et al., 2001, Goksoy et al., 2008, Ye et al., 2016). This mechanism was also described for other FERM-domain containing proteins like ezrin (Barret et al., 2000, Fievet et al., 2004) and radixin (Hamada et al., 2000). A positively charged talin surface formed by basic residues K268/272/274/277/278 in the F2 domain and residues K322/324 in the F3 domain is attracted by negatively charged PIP2 patches within the plasma membrane (Saltel et al., 2009, Song et al., 2012). Consequently, in the autoinhibited form a patch of acidic amino acids (residues E1714/1794/1797/1798/1808) within the F3 interacting R9 domain is exposed to the negative charges of the membrane leading to a repulsive effect and thus release of the closed talin conformation (Song et al., 2012). This “pull/push” mechanism facilitates the

simultaneous recruitment of talin to the plasma membrane and its conformational activation (Figure 14).

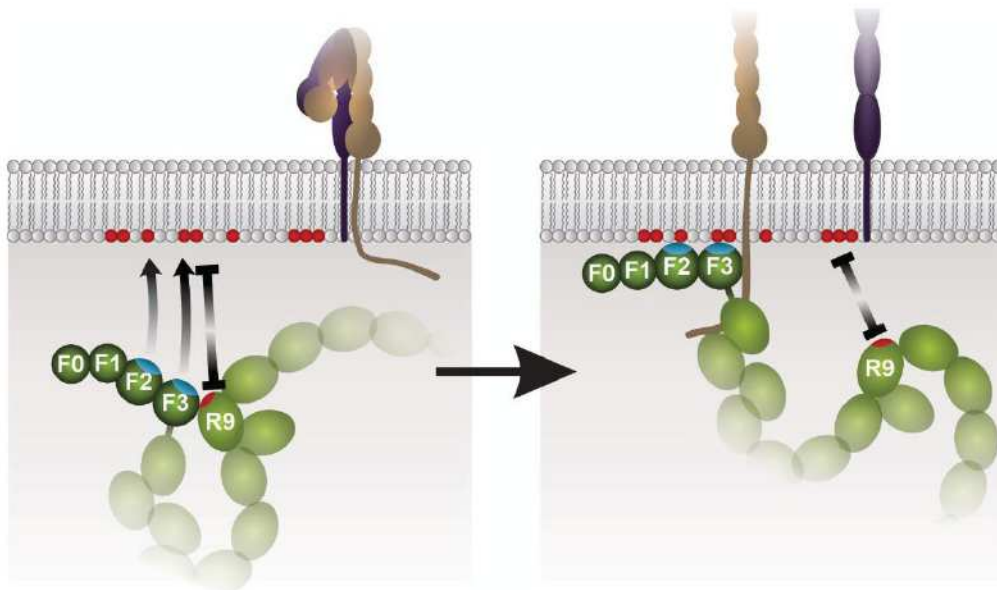


**Figure 14: Simultaneous talin recruitment and release of autoinhibition mediated by electrostatic interaction with PIP2.** Negatively charged PIP2 in the membrane (indicated by red dots) attracts positively charged amino acids on talin F2/F3 (blue) and repels negative charges in R9 (red), which leads to release of the autoinhibitory conformation.

Indeed, expression of talin variants carrying multiple point mutations within the positively charged patches of the F2/F3 domains in talin-null fibroblasts confirmed an important role of talin/membrane interactions for integrin activation and focal adhesion formation (Chinthalapudi et al., 2018).

Phosphatidylinositol 4-phosphate 5-kinase type-1  $\gamma$  (PIP5K1 $\gamma$ ; PIP5K1C) belongs to the PIP5-kinase family, which is expressed in three isoforms in mouse and catalyzes the reaction of phosphatidylinositol-4-phosphate to phosphatidylinositol-4,5-bisphosphate (PIP2) (van den Bout and Divecha, 2009). PIP5K1 $\gamma$ -deficiency in mice results in embryonic lethality due to abnormal development of the nervous system and cardiovascular system (Wang et al., 2007). The kinase is regulated by a variety of proteins, for example Rho and Rac GTPases and the ADP-ribosylation factor ARF6. ARF6 has been suggested to directly activate PIP5Ks and to promote the production of phosphatidic acid, which regulates the affinity of the kinase to its substrate, by phospholipase D (van den Bout and Divecha, 2009).

The larger splice variant PIP5K1 $\gamma$ 661 (661 amino acids; also PIP5K1 $\gamma$ 90 for 90 kDa) but not PIP5K1 $\gamma$ 635 (or PIP5K1 $\gamma$ 87), which lacks the interaction site, is recruited to focal adhesions



by interacting with the talin FERM domain. This effect is enhanced upon Src-mediated phosphorylation of the kinase. A high local concentration of PIPKly increases PIP2 content in the membrane at focal adhesion sites and results in recruitment of further proteins such as FAK, vinculin and talin itself (Di Paolo et al., 2002, Ling et al., 2002, Ye et al., 2016).

Since the SPLH (residues 645-648) motif of PIPKly661 binds to a region in the talin F3 domain, which is also involved in integrin binding, this competition may displace talin from focal adhesions (de Pereda et al., 2005, Ling et al., 2002). This might also explain the finding that PIPKly661 is a negative regulator of LFA-1 mediated adhesion and immune synapse formation in T cells (Wernimont et al., 2010). In contrast, abolishing focal adhesion targeting of PIPKly in murine fibroblasts by deleting the respective sequence in exon 17 of the encoding gene decreases local PIP2 levels and impairs recruitment of talin and vinculin to newly formed adhesions leading to a transient defect in integrin mediated adhesion (Legate et al., 2011).

### **2.3.3 Other regulators of talin activity**

Kank2 was identified as a further talin activator by interacting with the R7 domain via its KN motif (Sun et al., 2016). Kank (Kidney ankyrin repeat domain) family proteins, which are encoded by four genes (Kank1-4) in vertebrates, comprise a KN (Kank N-terminal) domain, coiled-coil domains and ankyrin repeats at the C-terminus (Kakinuma et al., 2009). In addition to mediating talin activation, Kank regulates cell migration and reduces force across focal adhesions by interfering with actin binding to talin ABS2. Furthermore, it provides a link between microtubules and the actin cytoskeleton (Chen et al., 2018, Sun et al., 2016).

The G protein subunit  $G\alpha_{13}$  also represents a regulator of talin activity in platelets. G proteins are heterotrimers composed of an  $\alpha$ ,  $\beta$  and  $\gamma$  subunit in association with a G protein coupled receptor. Upon receptor activation by respective agonists, a GDP to GTP exchange in the G protein leads to dissociation of the  $\alpha$  from the  $\beta\gamma$  subunit, which both trigger downstream signaling. Switch region 2 of the  $\alpha$  subunit  $G\alpha_{13}$  has been shown to interact with the F3 domain of talin and thereby displace the autoinhibitory rod interaction. Inhibition of the interaction in platelets slightly impairs adhesion to collagen, hemostasis and thrombus formation, but does not completely abolish these processes (Srinivasan et al., 2015, Schiemer et al., 2016).

Furthermore, FAK has been suggested to be involved in talin recruitment to nascent adhesions. According to this model, FAK is targeted to nascent adhesions of mouse



embryonic fibroblasts by clustered integrins and subsequently recruits talin. Moreover, abolishing FAK binding to talin increases the lifetime of adhesion sites due to reduced talin cleavage by calpain-2, which is in turn recruited by FAK (Lawson et al., 2012).

## **2.4 The role of talin in different organisms**

### **2.4.1 *Dictyostelium* talinA and talinB**

Two variants of talin, talinA and talinB, with distinct functions exist in the slime mold *Dictyostelium discoideum*. This is particularly interesting as *Dictyostelium* does not express integrins (Klapholz and Brown, 2017). *Dictyostelium* talins show a similar domain structure as vertebrate talins comprising membrane binding and actin interacting domains in the head and rod, respectively. Of note, talinB contains a villin headpiece-like domain at the C-terminus, which is a unique feature compared to other talins and most likely provides an additional actin binding site (Tsujioka et al., 1999). While talinA deficient amoebae develop normally despite reduced adhesion and slightly impaired cytokinesis (Niewohner et al., 1997, Tsujioka et al., 2008), impaired migration of talinB mutants causes a defect in multicellular aggregation, which stops at the so-called mound stage, and abolishes the formation of fruiting bodies (Tsujioka et al., 2004). TalinA/talinB double deficient cells exhibit a more pronounced phenotype with a developmental arrest at early mound stage pointing to a partial redundancy of both talin isoforms (Tsujioka et al., 2008).

### **2.4.2 *Drosophila* talin**

The talin homolog of *Drosophila* is encoded by the gene *rhea* and structurally resembles vertebrate talin. A knockout of *rhea* in *Drosophila* is lethal at larval stage, in most cases due to defective germband retraction, a remodeling process during embryonic development, which involves cell migration (Brown et al., 2002, Camp et al., 2018). Talin becomes enriched at membranes of muscle attachment sites and in the mid gut during embryonic development. Attachment of muscle to tendon cells is severely impaired in the absence of talin. Although integrins initially bind the extracellular matrix, a link to the cytoskeleton is missing, which abolishes force transduction and integrin clustering (Brown et al., 2002, Ellis et al., 2014). In adult flies, a lack of talin causes a wing blistering phenotype due to instable attachment of the two epithelial layers forming the wing (Brown et al., 2002). Talin is also essential for formation and growth of the *Drosophila* heart, which is formed by a tube-like arrangement of cardiomyocytes. Talin knockdown leads to cardiomyopathies due to a reduction in number and length of myofibrils and instable cell contacts (Bogatan et al., 2015, Vanderploeg and Jacobs, 2015).



To further explain and specify the observed phenotypes, different studies addressed the role of talin IBS1 and IBS2 as well as the C-terminal actin binding site *in vivo* by rescue experiments using the respective binding mutants of talin in *Drosophila* as a model organism (Ellis et al., 2011, Franco-Cea et al., 2010, Klapholz et al., 2015, Tanentzapf and Brown, 2006, Ellis et al., 2014). These studies showed that talin can be recruited to adhesions by directly interacting with integrin tails at the NPXY and membrane proximal regions (Tanentzapf et al., 2006). However, also a full length IBS1 mutant talin (R367A) localizes to adhesions, most likely due to IBS2. Despite proper localization this mutant cannot compensate talin deficiency completely. It can partially compensate the developmental and wing phenotypes, but is incapable of rescuing the muscle detachment phenotype in the embryo, although a link to the cytoskeleton is provided and adhesion complexes are assembled. Nevertheless, the muscle cells detach from the extracellular matrix indicating that integrins cannot resist the tension of muscle contractions in the absence of talin head binding (Tanentzapf and Brown, 2006). However, integrin affinity is not, like in some vertebrate cells, modulated by talin mediated inside-out activation in *Drosophila*, as shown by activation specific antibody binding assays to integrin  $\alpha$ PS2 $\beta$ PS (Helsten et al., 2008). In line, studies comparing the specific involvement of IBS1 and IBS2 in muscle attachments confirmed that IBS1 engagement stabilizes integrin/extracellular matrix connections, while IBS2 bound talin primarily serves as a scaffold for assembling other intracellular adhesome proteins at the integrin. However, talin head binding is not important for integrin activation, but is required for integrin clustering, which reinforces integrin mediated muscle attachment to tendons (Ellis et al., 2014, Ellis et al., 2011).

Analysis of talin orientation towards the membrane by FRET and superresolution microscopy using different deletion mutants revealed a tissue specific engagement of IBS2 in wing and also during germ band retraction but not in muscles, where actin pulling forces perpendicular to the membrane act on talin. Based on these results a role of talin in crosslinking integrins by engagement of both integrin binding sites and dimerization was suggested in wings. Due to the dimerization behavior and engagement of vinculin, this is partially possible even in the absence of IBS1 (Klapholz et al., 2015).

### **2.4.3 Vertebrate talin 1 and talin 2**

Vertebrates express two talin isoforms: the ubiquitously expressed talin 1 and its homolog talin 2, which reveals a more distinct expression pattern with particularly high expression in brain, kidney and heart muscle (Gough and Goult, 2018). Interestingly, talin 1 arose by duplication of the talin 2 locus (Senetar and McCann, 2005).



The physiological role of talin 1 was extensively studied by constitutive and conditional knockout approaches in mice. Constitutive talin 1 deletion results in early lethality at embryonic day 8.5 (E8.5) to E9.5 of development, although first abnormalities are already visible at gastrulation stage (E6.5 to E7.5). The milder phenotype compared to integrin  $\beta$ 1 deficient mice, which die already at E6.5, might be explained by partial compensation by talin 2 or residual parental talin in the embryos (Monkley et al., 2000).

Cells of the hematopoietic system serve as excellent tools to study integrin-mediated processes. Therefore, conditional deletion of talin 1 in platelets and leukocytes revealed its essential role in regulating integrin function. Talin-null platelets are dysfunctional. They fail to activate integrins, aggregate, adhere, spread and retract fibrin clots. The integrin activation defect causes defective hemostasis and spontaneous bleedings and protects the mice from pathological thrombus formation (Haling et al., 2011, Nieswandt et al., 2007, Petrich et al., 2007). Moreover, talin 1 is essential for the regulation of leukocyte integrins (Lefort et al., 2012). Loss of talin in the hematopoietic system causes a severe leukocyte adhesion deficiency and leukocytosis due to abolished activation of all expressed integrin classes (Klapproth et al., 2015b). In T cells, talin is not only crucial for integrin  $\beta$ 2-mediated cell trafficking but is also required for integrin  $\alpha$ L $\beta$ 2 dependent formation of immune synapses and efficient T cell activation upon contact with antigen presenting cells (Simonson et al., 2006, Wernimont et al., 2011). The latter in turn has an impact on the maintenance of the central and effector Treg (regulatory T cell) pool (Klann et al., 2017).

A number of studies addressed the role of talin in non-hematopoietic cells. While hematopoietic cells express only talin 1, many non-hematopoietic cell types express both talin isoforms. In contrast to talin 1, talin 2 is less well investigated. Talin 2 deficiency in mice causes no overt phenotype (Debrand et al., 2012). The talin isoforms differ in their subcellular localization. Talin 1 mainly localizes to focal adhesions at the cell periphery of cultured mouse embryonic fibroblasts, smooth and striated muscle cells, whereas talin 2 can be detected in fibrillar adhesions (Praekelt et al., 2012, Senetar et al., 2007).

Mature skeletal muscle cells express high levels of talin 2, which is upregulated during differentiation (~8-fold) and localizes to costameres (Senetar et al., 2007, Conti et al., 2008, Senetar and McCann, 2005). Costameres are protein complexes, which anchor actin filaments of myofibrils to the membrane at z-lines, the interface between two sarcomeres (Samarel, 2005). Talin 1 does not localize to costameres, but both isoforms are present in myotendinous junctions (MTJ), another type of force transducing adhesion structures of muscle cells (Conti et al., 2008) that anchor muscle fibers to tendons, which

comprise extracellular matrix (mainly collagen) and tenocytes and connect muscle to bone (Valdivia et al., 2017). Although talin 1 or 2 deficiency in skeletal muscles allows formation of MTJs most likely due to partial mutual compensation, they are unstable and less force resistant resulting in muscular dystrophy with increasing age of mice. This phenotype is more pronounced in talin 2 deficient animals (starting at an age of 3 months) than in skeletal muscle specific talin 1 deficient mice, in which abnormalities emerge at 6 months of age (Conti et al., 2008, Conti et al., 2009). Mice expressing no talin in skeletal muscle die postnatally. Muscle talin 1/2 double-deficient E17.5 embryos showed highly abnormal muscle organization caused by defects in integrin adhesion structure formation, disruptions of myofilaments and impaired myoblast fusion during muscle maturation (Conti et al., 2009). Muscle specific integrin  $\beta 1$  deficiency causes a similar phenotype (Conti et al., 2009, Schwander et al., 2003). As initial integrin activation was shown to be normal in talin 1/2 double deficient muscle cells, the phenotype seems to be primarily caused by defective linkage between integrins and the actin cytoskeleton here (Conti et al., 2009).

Like in skeletal muscles, talin 2 is the dominant isoform in adult cardiomyocytes, where it also localizes to costameres. Cardiac talin 1 expression is upregulated upon mechanical stress induced by transverse aortic constriction in mice eventually resulting in hypertrophy (Manoso et al., 2013). Despite downregulation of integrin  $\beta 1D$ , a muscle specific integrin  $\beta 1$  isoform, deletion of talin 2 allows normal heart development. As integrin  $\beta 1D$  shows a stronger affinity for talin 2 than talin 1, talin 2/ $\beta 1D$  interaction provides the most stable actin to integrin linkage. On the contrary, loss of both talin isoforms in cardiac muscle of mice causes cardiomyopathy and destabilization of costameres leading to impairment of cardiac functions and lethality within six months. This indicates a compensatory effect between the two proteins (Manoso et al., 2017).



### 3 The kindlin protein family

The murine and human genomes encode three kindlin orthologues (also called Fermitin family homologues). The name kindlin is derived from “Kindler syndrome”, a hereditary skin disease, which has been first described by Theresa Kindler in 1954 (Kindler, 1954). After identifying the causative locus harboring loss of function mutations in Kindler syndrome patients, the encoded gene was named KIND1 (protein name: kindlin 1). Two homologous genes were identified in the human genome encoding for proteins with a similar domain structure and size: MIG-2 encodes a protein that shares 62% amino acid sequence identity with kindlin 1, and was renamed KIND2 (kindlin 2). Another gene encoded on chromosome 11q13.1 was identified as the third family member and named KIND3 (kindlin 3) (Siegel et al., 2003). Alternative names for kindlin 1 and kindlin 3 are URP1 and URP2 (unc-112 related protein), respectively, due to their similarity to the *C. elegans* protein unc-112 (Weinstein et al., 2003). The human kindlin 3 amino acid sequence is 49% identical to kindlin 1 and 53% to kindlin 2 (Siegel et al., 2003).

#### 3.1 Structure of kindlins

All kindlins share a FERM domain as major structural element, which is similar to the talin head comprising F0, F1, F2 and F3 domains (Figure 15). Kindlin’s F0 domain also adopts an ubiquitin-like fold. The unstructured F1 loop that has been described for talin is also present in kindlins, however, this loop is bigger than in talin and the sequence is not conserved (Goult et al., 2009b). The F2 domain of kindlin proteins is split by the insertion of a PH (pleckstrin homology) domain. The PH domain binds membrane phosphoinositides, preferentially phosphoinositol-triphosphate (PIP3) via its  $\beta 1$ - $\beta 2$  loop, which promotes kindlin recruitment to adhesion sites and integrin activation (Qu et al., 2011, Ni et al., 2017, Yates et al., 2012b). Interestingly, the F2 domain was also shown to serve as an interface for kindlin 2 homodimerization (Li et al., 2017a). As in talin, the F3 domain contains an integrin binding PTB domain (Moser et al., 2009b).

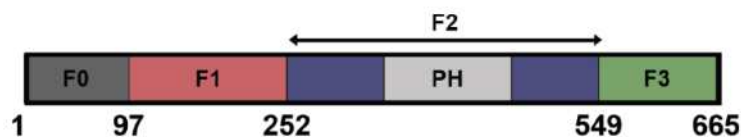


**Figure 15: Domain structure of kindlins.** The general domain structure is conserved within the protein family. Here, amino acid numbering corresponds to mouse kindlin 3. Kindlins comprises an atypical FERM domain containing an N-terminal F0 domain and F1, F2 and F3 modules. A PH domain is inserted into F2.

In contrast to the linear alignment of the subdomains in the talin FERM domain, kindlin FERM domains adopt a cloverleaf-like conformation (Kammerer et al., 2017, Li et al., 2017a).

### **3.2 Expression and subcellular localization of kindlins**

Mammalian kindlins are expressed in a tissue specific pattern. While kindlin 1 is expressed in epithelial cells (primarily keratinocytes and epithelial cells of the gut), kindlin 2 is almost ubiquitously expressed except for hematopoietic cells and particularly high levels are found in striated and smooth muscle cells. Kindlin 3 expression is restricted to all lineages of the hematopoietic system (Ussar et al., 2006).

Kindlin 1 and 2 localize to focal adhesions, while the third family member kindlin 3 is found in podosomes in hematopoietic cells (Ussar et al., 2006). Moreover, kindlin 2 was found at adherence junctions in different cell types such as keratinocytes, gut epithelial cells and cardiomyocytes (He et al., 2014, Dowling et al., 2008a, Ussar et al., 2008). Furthermore, kindlin 1 and 2 localization to the nucleus has been described (Lai-Cheong et al., 2008, Yu et al., 2012).

### **3.3 Kindlin interaction partners**

Kindlin 2 is the most extensively studied family member and most interactions have been shown for kindlin 2. Due to the high structural homology and sequence similarity between the kindlin family members, many interactors are shared by them (Goult et al., 2009b).

The most important kindlin interaction partners are integrins. Kindlins bind the membrane distal NXXY motif of the  $\beta$  integrin tail via their F3 domains, which is an essential step during integrin activation (Moser et al., 2009a, Yates et al., 2012a).

Migfilin was the first identified kindlin interactor that binds to all kindlins (Brahme et al., 2013, Malinin et al., 2010, Tu et al., 2003). It comprises an N-terminal domain spanning 85 amino acids, followed by a proline rich region and three C-terminal LIM domains. Kindlin 1 and 2 interact with the migfilin LIM domains via their N-terminus (Brahme et al., 2013, Tu et al., 2003). Interaction of the migfilin N-terminus with the actin binding protein filamin provides a link to the cytoskeleton. Migfilin deficient cells show a spreading defect and reduced amount of filamentous actin (Tu et al., 2003). It is recruited to focal adhesions by kindlin (Brahme et al., 2013). As filamin reveals an integrin inactivating function, migfilin indirectly promotes integrin activation by competing with integrin  $\beta$  tails for filamin binding (Das et al., 2011, Ithychanda et al., 2009, Lad et al., 2008).



An  $\alpha$ -helix between the F2 and the PH domain of kindlins binds ILK, which forms together with PINCH and parvin the IPP (ILK, PINCH, parvin) complex. This interaction was proposed to be crucial for kindlin recruitment to adhesion sites, cell spreading (Fukuda et al., 2014) and integrin activation (Huet-Calderwood et al., 2014). ILK interaction was shown to be much stronger for kindlin 2 than for kindlin 3, which was explained by sequence differences in the PH domain. Consequently, the effect of ILK on focal adhesion targeting of overexpressed GFP-tagged kindlins in CHO cells is much weaker for kindlin 3 compared to kindlin 2. These results give a possible explanation for functional differences among kindlin proteins (Huet-Calderwood et al., 2014). The IPP complex provides another connection of kindlin to the actin cytoskeleton through the actin binding capability of parvin (Fukuda et al., 2009).

Paxillin was shown to interact with the kindlin 2 F0 and PH domains (Bottcher et al., 2017, Theodosiou et al., 2016). NMR based characterization of the complex confirmed that the kindlin 2 F0 domain interacts specifically with the C-terminal LIM4 domain of paxillin (Zhu et al., 2019). Kindlin 2 mediated paxillin recruitment to focal adhesions induces cell spreading in a FAK/Rac1 dependent manner. FAK assembles a complex of p130Cas, Dock180 and Crk, which in turn activates Rac1 (Theodosiou et al., 2016). In addition to paxillin, kindlin 2 recruits the actin nucleating Arp2/3 complex, which is necessary for Rac1-mediated cell spreading (Bottcher et al., 2017). Besides its role in cell spreading, the kindlin F0/paxillin interaction was shown to promote integrin  $\alpha$ IIb $\beta$ 3 activation in platelets by linking kindlin to talin and thereby stabilizing talin binding to the integrin. Therefore, abolishing the interaction of kindlin 3 with paxillin and its relative Hic-5 by mutating the so-called M3 loop within the F0 domain in platelets attenuates fibrinogen binding in response to different agonists, platelet spreading and thrombus formation (Gao et al., 2017).

Additionally to the already mentioned links between kindlins and the actin cytoskeleton via kindlin interacting proteins, a direct actin binding site had been proposed in the kindlin 2 F0 domain. Mutation of this site resulted in reduced cell spreading and actin organization (Bledzka et al., 2016).

As kindlins recruit their interactors to adhesions sites, they are not only critical for integrin activation but also for integrin-mediated signaling.

### **3.4 Physiological and patho-physiological role of kindlin family proteins**

#### **3.4.1 Non-mammalian kindlin homologs**



The *C. elegans* kindlin homolog unc-112 was the first described kindlin protein. It colocalizes with pat-3 and pat-4 corresponding to  $\beta$  integrin and ILK in embryonic body wall muscles. There, unc-112 is crucial for pat-3 localization and organization in the membrane. Some adhesion complexes have been observed in muscles of unc-112 mutant embryos, however, unlike the usually distinct organization in structures termed M-lines and dense bodies, adhesion sites of mutant embryos are highly disorganized revealing its critical role in assembly of muscle attachment sites and muscular function (Rogalski et al., 2000, Mackinnon et al., 2002).

Furthermore, two kindlin homologs, Fermitin1 and Fermitin2, exist in *Drosophila*. However, they have not been extensively studied so far. Both proteins were identified in an RNAi screen for genes that are important for muscle integrity. Further *in vivo* knockdown experiments confirmed this finding, as muscles rounded up completely in the absence of both fermitins. This phenotype was also observed but weaker, when only one homolog was missing, indicating a functional redundancy (Bai et al., 2008). Similarly, cardiac silencing of one or both fermitins showed a redundant role of both fermitins. A cardiac fermitin double knockdown resulted in impaired heart development and cardiomyopathies (Catterson et al., 2013).

### **3.4.2 Mammalian kindlins**

#### **3.4.2.1 Kindlin 1**

Kindlin 1 is involved in a variety of signaling pathways both in an integrin dependent and independent manner, which is reflected in the symptoms exhibited by Kindler syndrome patients (Rognoni et al., 2016). Kindler syndrome patients suffer from skin blistering, wrinkling, atrophy, pigmentation defects, increased photosensitivity and increased cancer risk already early in childhood (Siegel et al., 2003). In addition to the mentioned skin defects, patients have a tendency to develop gut inflammation (ulcerative colitis) (Sadler et al., 2006).

A knockout of kindlin 1 in mice is lethal within three to five days after birth. In line with the Kindler syndrome symptoms, the animals suffer from a severe intestinal inflammation, as the gut epithelial cells detach due to strongly reduced integrin activity, and from skin atrophy (Ussar et al., 2008). Although kindlin 2 is also expressed in keratinocytes and gut epithelial cells, it cannot compensate for a loss of kindlin 1, most likely due to their different subcellular localization. Kindlin 1 is found in adhesions to the epithelial basal membrane and kindlin 2 in cell-cell junctions, which remains unchanged in the absence of kindlin 1 (Ussar et al., 2008).



Furthermore, a skin specific deletion of kindlin 1 in mice promotes tumor development in the skin. Kindlin 1 but not kindlin 2 can induce integrin  $\alpha V\beta 6$  mediated release of TGF $\beta$ , which is immobilized in the extracellular matrix of hair follicles and keeps stem cells quiescent in skin upon release. In addition, kindlin 1 suppresses Wnt signaling. Therefore, kindlin 1 is an essential regulator in epithelial stem cells homeostasis. Together with inflammations caused by impaired integrin mediated adhesion of keratinocytes, loss of these functions increases tumor risk (Rognoni et al., 2014).

An oncogenic function of kindlin 1 by modulating different signaling pathways was shown in a variety of other tumors. Its expression level negatively correlates with patients' survival. For instance, kindlin 1 promotes migratory and invasive processes in pancreatic cancer (Mahawithitwong et al., 2013) and colorectal cancer (Kong et al., 2016), and its expression is increased and correlated to poor outcome in hepatocellular carcinoma (Ma et al., 2015). It facilitates lung metastasis in breast cancer patients by increasing cell motility and enabling  $\alpha 4\beta 1$ /VCAM-1 interaction of intravasated tumor cells with pulmonary endothelial cells (Sarvi et al., 2018, Sin et al., 2011). A common reason for these tumor-promoting effects of kindlin 1 is its capability of modulating TGF $\beta$  and Smad3 signaling (Kong et al., 2016, Sarvi et al., 2018, Sin et al., 2011).

#### **3.4.2.2 Kindlin 2**

The kindlin 2 gene was initially named mitogen inducible gene-2 (Mig-2), as it was identified in a screen for genes with differential expression during the cell cycle (Ussar et al., 2006, Wick et al., 1994). Loss of kindlin 2, which is the only kindlin expressed in embryonic stem cells, causes embryonic lethality at implantation stage in mice (Dowling et al., 2008a, Montanez et al., 2008). The lack of integrin activity results in cell detachment from the basal membrane and impedes proper formation of primitive ectoderm and endoderm (Montanez et al., 2008).

As kindlin 2 is highly expressed in heart, where it localizes to cell-cell contacts (intercalated discs) and costamers, its role in heart development and function was extensively studied (Dowling et al., 2008a). Kindlin 2 promotes muscle tube formation by allowing myoblasts to adhere, elongate and spread and also ensures muscle function by anchoring myofibrils at the membrane as shown by *in vitro* and zebra fish studies (Dowling et al., 2008a, Dowling et al., 2008b). A  $\beta$ -MHC (myosin heavy chain)-Cre mouse line was used to deplete kindlin 2 in cardiac muscle cells of the developing mouse heart around birth and an inducible cardiac specific Cre allowed kindlin 2 ablation in adult mice. These mice survive for several months without cardiac kindlin 2 until they die from cardiomyopathy (Zhang et al., 2016b).



A reduction or abolishment of kindlin 2 expression in endothelial cells results in impaired angiogenesis and leads to formation of fewer, immature and leaky blood vessels, as shown in different mouse models. These endothelial cells reveal defects in adhesion, migration and spreading, which are mainly mediated by integrin  $\alpha V\beta 3$  (Pluskota et al., 2011).

Kindlin 2 is a driver of epithelial to mesenchymal transition (EMT) by promoting TGF $\beta$ , ERK and Akt signaling (Wei et al., 2014, Guo et al., 2015). Kindlin 2 mediated ERK and Akt signaling were shown to promote EMT of human kidney tubular epithelial cells and the activation of both signaling pathways in mice with unilateral ureteral obstruction is impaired in absence of kindlin 2. As a major part of the matrix secreting myofibroblasts causing kidney fibrosis are derived from tubular epithelial cells, which underwent EMT, these results indicate that kindlin 2 promotes kidney fibrosis (Wei et al., 2014).

Like kindlin 1, kindlin 2 has an impact on Wnt signaling and can potentially promote tumor progression. It was shown to bind and stabilize both cytoplasmic and nuclear active  $\beta$  catenin and thus increase the transcription of the Wnt target gene axin2, which in turn enhances invasiveness by upregulating the EMT-driver Snail-1 (Yu et al., 2012). However, kindlin 2 exhibits either oncogenic or tumor suppressing behavior depending on the tumor type (Rognoni et al., 2016).

#### **3.4.2.3 Kindlin 3**

Kindlin 3 was the first family member that was proven to promote integrin mediated cell adhesion (Moser et al., 2009a, Moser et al., 2008). Kindlin 3 deficiency in mice is lethal within one week after birth due to severe hemorrhages and a strong bleeding phenotype. Kindlin 3 knockout platelets reveal a pronounced integrin activation defect resulting in impaired adhesion and aggregation (Moser et al., 2008). Furthermore, as kindlin 3 deficient neutrophils lack  $\beta 2$  integrin activity, adhesion and extravasation are abolished as shown in *ex vivo* and *in vivo* mouse experiments (Moser et al., 2009a).

These platelet and neutrophil phenotypes resemble the most critical symptoms observed in leukocyte adhesion deficiency type 3 (LAD-III) patients (Manevich-Mendelson et al., 2009, Mory et al., 2008, Svensson et al., 2009, Moser et al., 2009a, Kuijpers et al., 2009). LAD-III (or LAD-I variant) is a recessive hereditary disease combining symptoms of both the bleeding disorder Glanzmann's thrombasthenia (see chapter 5.1.3) and LAD-I. While a lack of or severely reduced  $\beta 2$  integrin surface levels cause LAD-I, integrin levels are normal in LAD-III patients. Bleedings and failure of clearing infections in LAD-III patients can be explained by a lack of platelet, neutrophil and lymphocyte  $\beta 1$ , 2 and 3 integrin



function. Analyses of three LAD-III patients from Turkish and Maltese families revealed that mutations in the kindlin 3 gene abolished kindlin 3 protein expression (in these cases by an early stop codon or impaired splicing) and are causative for the disease (Kasbekar et al., 2017, Mory et al., 2008, Svensson et al., 2009).

Furthermore, kindlin 3 promotes podosome and sealing zone formation in osteoclasts. Thus, kindlin 3 deficiency in mice results in defective bone resorption causing severe osteopetrosis, which is detectable already before birth (Schmidt et al., 2011). Of note, osteopetrosis is also observed in LAD-III patients (Mory et al., 2008).

In erythrocytes, kindlin 3 contributes to the assembly of the membrane skeleton, which determines their characteristic shape and size. The membrane skeleton comprises a distinct set of proteins including dematin, adducin-2, ankyrin-1 and band 4.1. Kindlin 3 deficient erythrocytes are irregularly shaped. SILAC based analysis of erythrocyte ghosts (isolated membranes) revealed, that these membrane skeleton proteins were not assembled at the membrane of kindlin 3 deficient erythrocytes (Kruger et al., 2008).

In T cells, kindlin 3 is required for integrin activation and stabilization of LFA-1 bonds to ICAM-1 (Feigelson et al., 2011, Moretti et al., 2013). Analysis of the role of kindlin 3 during lymph node trafficking revealed that adhesion of T cells to the vessel wall and extravascular migration but not transendothelial migration depend on kindlin 3 (Cohen et al., 2013). While the adult, fully vascularized thymus cannot be entered in the absence of kindlin 3, homing of T cell progenitors to the fetal thymus is kindlin 3 independent due to the very low shear forces in the non-vascularized thymus of the developing embryo (Moretti et al., 2018). Beyond T cell trafficking, kindlin 3 contributes to efficient T cell activation (Morrison et al., 2015) and LFA-1/ICAM dependent immune synapse formation (Kondo et al., 2017). The same is true for B cells. Kindlin 3 is required for both B cell trafficking and the induction of an efficient antigen response (Morrison et al., 2015, Hart et al., 2013).

Interestingly, the analysis of hypomorphic mice revealed that only 5% of wild-type kindlin 3 levels allow normal development and postnatal survival in contrast to complete loss of the protein. Nevertheless, reduced integrin activation in platelets and neutrophils results in a bleeding tendency as well as impaired neutrophil trafficking and bacterial clearance, respectively. This shows that low amounts of active integrins are sufficient for survival under basal conditions, however, high levels of integrin activation are required in stress situation like injury and infection (Klapproth et al., 2015a).

The formation of neutrophil extracellular traps (NETosis) is negatively regulated by kindlin 3, most likely in an integrin independent manner, as an integrin-binding deficient kindlin 3 mutant still suppresses NET formation (Xu et al., 2018). This suggests that kindlin 3 is involved in the regulation of several neutrophil functions. The underlying mechanism has not been described so far.

Like the other kindlin family members, enhanced kindlin 3 expression is associated with tumor development (Rognoni et al., 2016). Elevated kindlin 3 levels were detected in human breast cancer samples and kindlin 3 overexpression was shown to promote tumor growth and metastasis by enhancing angiogenesis upon implantation of breast cancer cells into mice (Sossey-Alaoui et al., 2014).



## 4 The hematopoietic system

The hematopoietic system comprises all organs and tissues that are involved in the formation of cellular blood components (hematopoiesis) and includes bone marrow, spleen, thymus and lymph nodes in mammals (Linden et al., 2011).

Hematopoiesis starts early during embryonic development and undergoes several phases. The first transient wave of blood cell generation referred to as primitive hematopoiesis starts at E7.25 in mice. At this stage, primitive hematopoietic stem cells cluster in so called blood islands within the yolk sac and give rise to primitive erythrocytes and progenitor cells of macrophages and megakaryocytes, which provide oxygen for the developing embryo and are involved in tissue remodeling, respectively (Lacaud and Kouskoff, 2017).

The first definitive hematopoietic stem cells emerge in the AGM (aorto-gonado-mesonephros) region of E9 embryos independently of primitive hematopoietic cells (Medvinsky and Dzierzak, 1996). The AGM region consists of the urogenital ridges and the dorsal aorta, where hematopoietic cells arise from the hemogenic endothelium in a process called endothelial-to-hematopoietic transition. Hematopoietic stem cells leave the AGM region starting at E10.5 and colonize the fetal liver. Upon formation of the bone marrow at E16.5, they reside in their niches within the bone marrow throughout life (Lacaud and Kouskoff, 2017).

Hematopoietic stem cells give rise to all hematopoietic cell types (Figure 16), guided by exposure to distinct sets of cytokines. All blood cells can be assigned to one of the two major hematopoietic lineages of myeloid and lymphoid cells except for dendritic cells, as they can be differentiated from both myeloid and lymphoid precursors (Wu and Liu, 2007). The lymphoid lineage comprises T cells, B cells and NK (natural killer) cells. Neutrophil, basophil and eosinophil granulocytes, monocytes, which further differentiate to macrophages upon tissue entry, as well as mast cells are part of the myeloid lineage. Erythrocytes and megakaryocytes, which give rise to platelets, also derive from a myeloid precursor (Drissen and Nerlov, 2016).

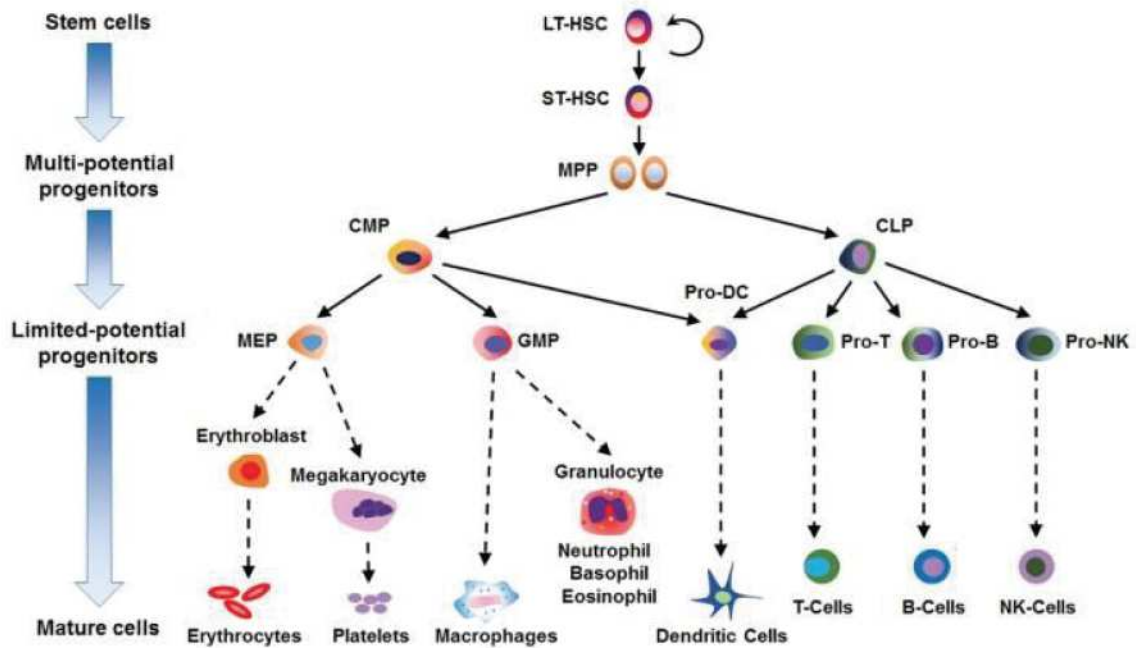


**Figure 16: Overview of hematopoietic cells.** Differentiation of mature hematopoietic cells from HSC (hematopoietic stem cells) is a multistep process going through several intermediate progenitor states, which all express a specific set of surface markers. [LT-HSC/ST-HSC: long term/short term repopulating HSC, MPP: multipotent progenitor, CLP: common lymphoid progenitor, CMP: common myeloid progenitor, MEP: megakaryocyte and erythroid progenitor, GMP: granulocyte and macrophage progenitor] (adapted with permission from Choi et al., 2015).



## 5 Integrins in platelet and neutrophil function

This chapter summarizes basic characteristics and the physiological role of platelets and neutrophils as well as the specific involvement of integrins in the according processes. These cell types serve as excellent tools to study integrin activation for several reasons: (I) Circulating blood cells activate their integrins in an agonist induced manner (Legate et al., 2009). (II) Specifically platelets and neutrophils depend on rapid integrin inside-out activation at vessel injuries or sites of infection, respectively. (III) Integrins are critically involved in all steps of platelet activity and during neutrophil trafficking (see chapters 5.1.3 and 5.2.3). Methods to study these functions both *ex vivo* and *in vivo* are well established. (IV) While talin mediated neutrophil  $\beta 2$  integrin activation takes place in a RIAM dependent manner (Klapproth et al., 2015a), this is not the case in platelets (Stritt et al., 2015) suggesting different mechanisms in both cell types. Unlike leukocytes, no dominant role of any talin activation pathway in platelets is known.

### 5.1 Platelets

#### 5.1.1 Platelet formation and their physiological role

Platelets are cell fragments that are released into the circulation from megakaryocytes, which reside in vascular niches close to sinusoidal blood vessels within the bone marrow (Grozovsky et al., 2015). Thus, platelets lack a nucleus and have a short lifetime of approximately ten days. Platelet concentrations in human blood range between 0.15 and 0.4 million per microliter (Grozovsky et al., 2015, Varga-Szabo et al., 2008) and average values of 1.1 million per microliter are reported for mice (Peters et al., 2005). The major regulator of megakaryocyte differentiation and growth is thrombopoietin (TPO). Genetic ablation of TPO or its receptor c-Mpl in mice causes severe thrombocytopenia, a condition of reduced platelet counts (Bunting et al., 1997, de Sauvage et al., 1996, Gurney et al., 1994). The chemokine CXCL12 (also called stromal-cell derived factor [SDF]-1), which binds its receptor CXCR4 on megakaryocyte precursors, potentiates megakaryopoiesis (Hodohara et al., 2000). Megakaryocytes interact with the endothelium by binding of integrin  $\alpha 4 \beta 1$  to endothelial VCAM-1. This interaction additionally promotes megakaryocyte maturation and growth (Fox and Kaushansky, 2005). During platelet formation, mature megakaryocytes extend large pseudopodia into blood vessels through the endothelium. These so called proplatelets then fragment into multiple platelets within the blood stream (Grozovsky et al., 2015).

The capability of platelets to adhere and aggregate at sites of blood vessel injuries makes them the critical component in primary hemostasis (Varga-Szabo et al., 2008).



Hemostasis is the process that assures maintenance of blood vessel integrity and prevention of blood loss upon vascular injuries. It occurs in two steps: primary or cellular hemostasis, which is facilitated by platelet aggregation at the site of injury, and secondary or plasmatic hemostasis, which is regulated by the coagulation cascade and leads to the formation of a fibrin clot (Versteeg et al., 2013).

Excessive, uncontrolled platelet activity or increased platelet counts can increase the risk of thrombotic events such as stroke, peripheral ischemia, and myocardial infarction, whereas thrombocytopenia can lead to impaired clot formation and increased bleeding risk. Arterial thrombosis usually occurs under high shear conditions upon rupture of atherosclerotic plaques, which can cause heart attacks or stroke (Koupenova et al., 2017). In venular blood vessels, where the exposure to shear forces is low compared to arteries, thrombus formation is initiated by activation of the endothelium, which causes upregulation of surface receptors and secretion of thrombogenic factors. The resulting thrombi are enriched in fibrin and red blood cells. Venular vessel occlusion can result in pulmonary embolism (Koupenova et al., 2017).

Due to the risk for pathological conditions, platelet function needs to be tightly regulated to assure immediate activation at sites of vessel injuries, but prevent excessive or uncontrolled platelet response.

### **5.1.2 Regulation of platelet function**

Platelet function is actively inhibited by the healthy endothelium primarily by production and secretion of nitric oxide and prostacyclin (also called prostaglandin  $I_2$ ;  $PGI_2$ ). Activation of the platelet prostaglandin receptor by  $PGI_2$  leads to adenylate cyclase mediated elevation of cAMP (cyclic adenosine-monophosphate). Cellular response to nitric oxide results in increased cGMP (cyclic guanosine-monophosphate) levels. cAMP and cGMP activate protein kinase A (PKA) and protein kinase G (PKG) (Smolenski, 2012), which phosphorylate an  $IP_3$  (inositol-triphosphate)-regulated  $Ca^{2+}$  channel.  $IP_3$  receptor phosphorylation finally blocks  $Ca^{2+}$  influx into the cytoplasm (Bye et al., 2016). These mechanisms prevent platelet activation, as cytoplasmic  $Ca^{2+}$  is an important activating component and the Rap1b activator CalDAG-GEFI depends on  $Ca^{2+}$  (see chapter 2.3.1.2). Furthermore, PKA and PKG phosphorylate Rap1b at serine 179, which induces a translocation of the protein from the plasma membrane into the cytosolic fraction (Altschuler and Lapetina, 1993, Bye et al., 2016, Lapetina et al., 1989).

At sites of vascular injury, activating stimuli via different agonist receptors, which in turn activate various central signaling cascades, prevail over inhibitory signals (Figure 17).



Platelet integrins are activated upon agonist stimulation and facilitate firm adhesion and aggregation (see chapter 5.3).

Thrombus formation is usually initiated by binding of von Willebrand factor (vWF) to the platelet receptor GP (glycoprotein)Ib-IX-V and association of collagen with the receptor GPVI. vWF is only accessible for platelets in injured vessels, where it is presented on the exposed collagen matrix (Bye et al., 2016, Varga-Szabo et al., 2008).

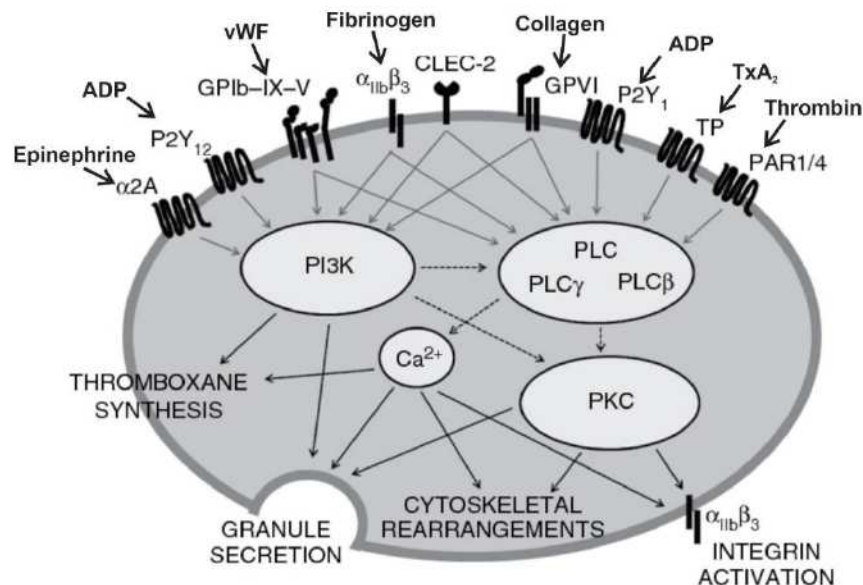


**Figure 17: Overview of the most important platelet activating receptors and pathways.** Platelets are activated by different agonists such as epinephrine, ADP, vWF, collagen, ADP, thromboxane and thrombin. PI3K, PLC and PKC are central signal mediators of platelet activation that trigger integrin activation, thromboxane synthesis, degranulation and cytoskeletal rearrangements. (adapted from Bye et al., 2016)

Upon initial activation, platelets release secondary activators such as thromboxane (TxA<sub>2</sub>), which is synthesized de novo, and ADP, which is stored in platelet granules, to boost the activation and trigger activation of further platelets by binding their receptors TP (TxA<sub>2</sub>) and P2Y<sub>1</sub> and P2Y<sub>12</sub> (ADP) (Bye et al., 2016). Platelets store different types of granules: α-granules comprise a broad variety of proteins that are important components in hemostasis, such as fibrinogen, vWF and coagulation factors. Additionally, they include proteins like growth factors, proteases and cytokines. Dense granules rather contain small molecules like the secondary platelet activator ADP (Whiteheart, 2011).

Thrombin reveals a key function in hemostasis and is locally generated by cleavage of its inactive precursor prothrombin by the prothrombinase complex. This complex assembles at phosphatidylserine-enriched regions on the membrane of activated platelets and is composed of coagulation factors Va and Xa (Koklic et al., 2009,



Majumder et al., 2008). Thrombin fulfills different thrombogenic functions: It is a strong platelet agonist, which acts through PARs (protease activated receptors) and thus activates and recruits further platelets to facilitate thrombus growth. Moreover, thrombin cleaves fibrinogen to fibrin, which forms a stable clot (secondary hemostasis) (Bye et al., 2016, Versteeg et al., 2013).

Activation of the respective receptors by their agonists induces intracellular signaling pathways. Phospholipase C isoforms PLC $\beta$  and PLC $\gamma$ 2 as well as the lipid kinase PI3K are key signal transducers of platelet activation (Bye et al., 2016). Four PI3K isoforms are expressed in platelets, which activate different signaling cascades including ERK, Akt and PLC $\gamma$  by phosphorylating PIP2. Depending on the upstream agonist receptor, distinct isoforms are preferentially activated. GPVI mainly activates PI3K $\beta$ , which in turn triggers Ca<sup>2+</sup> influx and PLC $\gamma$  activation, while PI3K $\gamma$  primarily transmits signals from the ADP receptor P2Y<sub>12</sub> (Bye et al., 2016). P2Y<sub>12</sub> induced PI3K signaling promotes thromboxane synthesis (Garcia et al., 2010). This pathway also promotes Rap1-mediated integrin activation in a Ca<sup>2+</sup> independent manner by inhibiting the Rap1 GAP RASA3 (Stefanini et al., 2015).

Platelet receptor GPVI, which is stimulated by exposed collagen at vessel wounds and by integrin outside-in signaling, signals via PLC $\gamma$ 2. PLC $\beta$  activity is triggered by G protein coupled receptors of secreted agonists such as the ADP receptor P2Y<sub>1</sub>, the thromboxane receptor and PAR receptors, which are bound by thrombin (Bye et al., 2016). The second messengers diacylglycerol (DAG) and IP<sub>3</sub> (inositol-triphosphate) are produced by PLC-mediated cleavage of PIP2. DAG activates protein kinase C (PKC) and IP<sub>3</sub> promotes Ca<sup>2+</sup> influx from the dense tubular system, an intracellular Ca<sup>2+</sup> store, into the cytoplasm (Harper and Poole, 2010). High cytoplasmic Ca<sup>2+</sup> concentrations trigger integrin activation via the Ca<sup>2+</sup> dependent Rap1 GEF CalDAG-GEFI (Stefanini and Bergmeier, 2010). PKC is a central regulator of platelet functions and promotes integrin activation in a CalDAG-GEFI independent manner by strong activation of Rap1 (Cifuni et al., 2008). Furthermore, PKC regulates cytoskeletal remodeling, thromboxane synthesis (Bye et al., 2016) and secretory activities, most likely by phosphorylating proteins such as the SNARE protein syntaxin 4 and the associated protein Munc18c. They regulate granule secretion by mediating fusion of granule membranes with the plasma membrane (Chung et al., 2000, Schraw et al., 2003). Cytoskeletal remodeling induces a shape change resulting in the formation of protrusions to increase platelet surface and adherent platelets spread by forming lamellipodia and filopodia (Bye et al., 2016).



Taken together platelet activation involves integrin activation, the synthesis of thromboxane, secretion of stored granules and platelet shape change (Bye et al., 2016, Varga-Szabo et al., 2008).

### **5.1.3 Integrins in platelet function**

Platelets express six different integrin heterodimers at different levels on their surface: the  $\beta 1$  integrins  $\alpha 2\beta 1$ ,  $\alpha 5\beta 1$  and  $\alpha 6\beta 1$ , the  $\beta 2$  integrin  $\alpha L\beta 2$  and the  $\beta 3$  integrins  $\alpha V\beta 3$  and  $\alpha IIb\beta 3$  (Zeiler et al., 2014).

The principal platelet integrin is the RGD-binding integrin  $\alpha IIb\beta 3$  (or glycoprotein GPIIb/IIIa) with approximately 120,000 copies per platelet (Zeiler et al., 2014). Its ligands include fibronectin, vWF, vitronectin, thrombospondin, fibrin and fibrinogen, which all contain RGD motifs. Integrin  $\alpha IIb\beta 3$  facilitates platelet adhesion and spreading on subendothelial extracellular matrix ligands such as immobilized vWF and fibronectin as well as aggregation by binding fibrinogen, which can crosslink platelets due to its multiple integrin binding sites (Huang et al., 2019, Varga-Szabo et al., 2008, Versteeg et al., 2013). Mice lacking either integrin  $\alpha IIb$  or  $\beta 3$  expression show spontaneous bleedings and prolonged tail bleeding times, resembling the symptoms of the bleeding disorder Glanzmann's thrombasthenia. Platelets isolated from these mice are unable to aggregate, bind fibrinogen and retract fibrin clots (Hodivala-Dilke et al., 1999, Tronik-Le Roux et al., 2000). Thus, integrin  $\alpha IIb\beta 3$  is the most essential integrin for platelet function.

Although with only 16,000 copies per platelet expressed at much lower levels than integrin  $\alpha IIb\beta 3$ , integrin  $\alpha 2\beta 1$  is considered as the second major platelet integrin, as it binds to collagen exposed at endothelial lesion sites. Despite conflicting results due to the use of different mouse models, disease models, pharmacological inhibitors or experimental approaches it is currently believed that integrin  $\alpha 2\beta 1$  together with the second platelet collagen receptor GPVI functions as an important platelet adhesion receptor (Chen et al., 2002, He et al., 2003, Holtkotter et al., 2002, Miller et al., 2009, Nissinen et al., 2010, Savage et al., 1998). More recent studies on platelets from mice expressing very little or an activation-deficient  $\beta 1$  integrin revealed that  $\beta 1$  integrins assemble important signaling platforms in platelets that initiate full-fledged platelet activation and granule secretion in response to collagen binding and that very low  $\beta 1$  integrin levels are sufficient to initiate this response (Petzold et al., 2013).

The  $\beta 1$  integrins  $\alpha 5\beta 1$  and  $\alpha 6\beta 1$  bind to fibronectin and laminin, respectively (Zeiler et al., 2014). A comparative analysis on the impact of different platelet integrins showed that integrin  $\alpha 5\beta 1$  and  $\alpha 6\beta 1$  contribute to adhesion to their respective ligands, however,

a loss of either of them is compensated by integrin  $\alpha\text{IIb}\beta 3$  (Gruner et al., 2003). Integrin  $\alpha 6\beta 1$  plays a specific role in laminin induced platelet spreading, as integrin mediated adhesion allows laminin mediated activation of GPVI, which in turn initiates protrusion formation (Inoue et al., 2006).

As integrins are involved in all steps of platelet activity, including firm adhesion and spreading, aggregation, clot retraction and regulation of signaling cascades by outside-in signaling, platelets serve as excellent tools to study integrin function.

## 5.2 Neutrophils

### 5.2.1 Neutrophils and their function

Neutrophils or polymorphonuclear leukocytes (PMNs) are characterized by segmentation of the nucleus and enrichment of cytoplasmic granules and vesicles (Figure 18). They are part of the innate immune system and typically among the first cells recruited to sites of inflammation (Kolaczowska and Kubes, 2013).

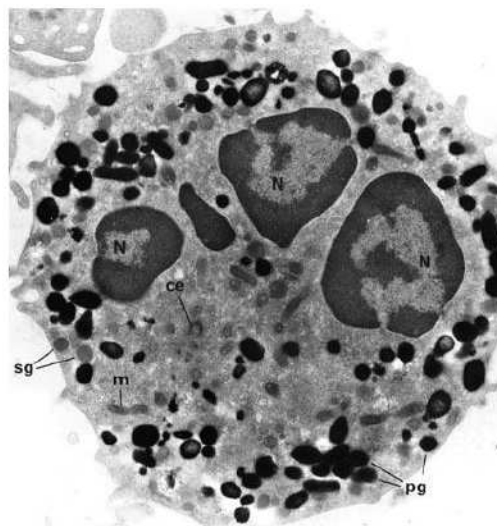


**Figure 18: Transmission electron micrograph of a neutrophil.** It shows the typical segmented nucleus and a great abundance of granules and vesicles throughout the cytoplasm. N: nucleus; pg/sg: primary/secondary granule (adapted with permission from Witko-Sarsat et al., 2000).

PMNs are derived from myeloid precursor cells located in the bone marrow. Differentiation is stimulated by exposure to G-CSF (granulocyte colony stimulating factor), which in turn is produced upon IL (interleukin)-17A secretion by a specific subset of regulatory T cells (Kolaczowska and Kubes, 2013). After differentiation within the bone marrow, where they are retained by VLA-4 binding to endothelial VCAM-1 and



CXCR4/CXCL12 interaction, PMN release to the circulation is triggered by CXCR2-mediated signals (Hong, 2017).

Circulating neutrophils have a very limited lifespan. However, usage of different techniques to analyze their half-life gave variable results. *Ex vivo* labeled neutrophils showed a blood half-life of 1.5 h in mice and 8 h in humans. In contrast, the half-life of  $^2\text{H}_2\text{O}$  *in vivo* labeled PMNs in mice and men was calculated to 12.5 h and 5.4 days, respectively (Pillay et al., 2010), although the latter is most likely an overestimation (Tofts et al., 2011). They are with 50-70% the major subset of circulating leukocytes in humans and with 10-25% less abundant in mice (Kolaczkowska and Kubes, 2013).

PMNs are part of the innate immune system and critically involved in the resolution of acute inflammation due to their antimicrobial functions (Kolaczkowska and Kubes, 2013). Neutrophils evolved three mechanisms to eliminate pathogens: The first one is phagocytosis, meaning the uptake of the pathogen, and the subsequent intracellular bacterial decomposition by reactive oxygen species and degradative enzymes in phagosomes (Kolaczkowska and Kubes, 2013). The key enzymes for the production of reactive oxygen species like superoxide anions and hydrogen peroxide are the membrane protein NADPH oxidase, which transfers electrons from cytoplasmic NADPH to phagosomes, and myeloperoxidase, which promotes superoxide production (Hager et al., 2010).

The second defense strategy is mediated by the release of antibacterial compounds such as lysozyme, cathepsins, neutrophil elastase, and lactoferrin from granules (Kolaczkowska and Kubes, 2013). They kill pathogens by different mechanisms like degradation of the bacterial cell wall, proteolytic activity or sequestration of nutrients to block bacterial growth (Teng et al., 2017). Neutrophil granules are subdivided into three types, which form successively during neutrophil maturation starting at promyelocyte stage and differ in their protein content: azurophil (or primary), specific (or secondary) and gelatinase (or tertiary) granules are characterized by an enrichment of myeloperoxidase, lactoferrin and gelatinase, respectively (Borregaard, 2010).

The third mechanism is the formation of neutrophil extracellular traps (NETs) (Kolaczkowska and Kubes, 2013). NETs are DNA structures decorated with histone and granule proteins. They bind and kill bacteria efficiently due to the antibacterial activity of histone and other proteins like cathepsin G and neutrophil elastase (Brinkmann et al., 2004).



In addition to resolving bacterial infections, PMNs show immune modulatory functions. For instance, specific neutrophil subsets were shown to reduce T cell activation by secretion of arginase 1 and promote splenic B cell activation in marginal zones by secreting BAFF (B cell activating factor) and other mediators. Additionally, PMNs were shown to modulate MHC expression by IFN (interferon)- $\gamma$  production or to transport antigens to sites of antigen presentation and T cell activation (Ellis and Beaman, 2002, Galli et al., 2011, Kolaczowska and Kubes, 2013, Puga et al., 2012).

### **5.2.2 Leukocyte-specific integrins**

Leukocytes critically depend on integrins for a variety of their functions. They primarily express  $\beta 2$  integrins. Depending on the leukocyte subset, different levels of  $\alpha L\beta 2$  (LFA [leukocyte function associated antigen]-1),  $\alpha M\beta 2$  (MAC [macrophage 1 antigen]-1),  $\alpha D\beta 2$  and  $\alpha X\beta 2$  are expressed. Additionally, integrins  $\alpha 4\beta 1$  (VLA [very late antigen]-4),  $\alpha 4\beta 7$  and  $\alpha E\beta 7$  can be found on blood cells (Mitroulis et al., 2015) as well as some extracellular matrix binding integrins such as  $\alpha 6\beta 1$ ,  $\alpha 5\beta 1$  and  $\alpha V\beta 3$ . The latter are critical for matrix adhesion and migration upon extravasation (see chapter 5.2.3) (Sixt et al., 2001).

$\alpha L\beta 2$  is the major integrin on many leukocytes. It is critically involved in leukocyte adhesion to the endothelium during leukocyte recruitment to sites of inflammation or T cell homing to lymphoid tissues. Furthermore, it is crucial for other processes such as immune synapse formation, where T cell  $\alpha L\beta 2$  binds ICAM-1 on antigen presenting cells to stabilize the T cell receptor/MHC (major histo-compatibility) complex (Bertoni et al., 2018, Nourshargh and Alon, 2014).

$\alpha M\beta 2$  expression levels are specifically high on PMNs and monocytes, which facilitates leukocyte migration and phagocytosis of complement opsonized pathogens. This is enabled by its binding capacity for complement factor C3b (Dustin, 2016). Integrins  $\alpha 4\beta 1$  and  $\alpha 4\beta 7$  are major T cell and monocyte integrins (Nourshargh and Alon, 2014). While  $\alpha 4\beta 1$  facilitates trafficking of lymphocytes to different tissues,  $\beta 7$  integrins are associated with gut homing (Bertoni et al., 2018).  $\alpha D\beta 2$  is expressed on monocytes and macrophages and was suggested to keep macrophages at sites of inflammation. Highest expression was found in specific macrophages within atherosclerotic lesions, the foam cells (Aziz et al., 2017, Yakubenko et al., 2008). Integrin  $\alpha X\beta 2$  expression can mainly be observed on dendritic cells and on a much lower level on macrophages (Mitroulis et al., 2015).

### **5.2.3 The leukocyte adhesion cascade**



Leukocyte trafficking between blood and tissues is essential for a number of immunological processes. Neutrophils that are recruited to a site of inflammation (Figure 19) or lymphocytes that leave the circulation and enter a lymph node undergo a sequence of events, which are described in the concept of the leukocyte adhesion cascade.

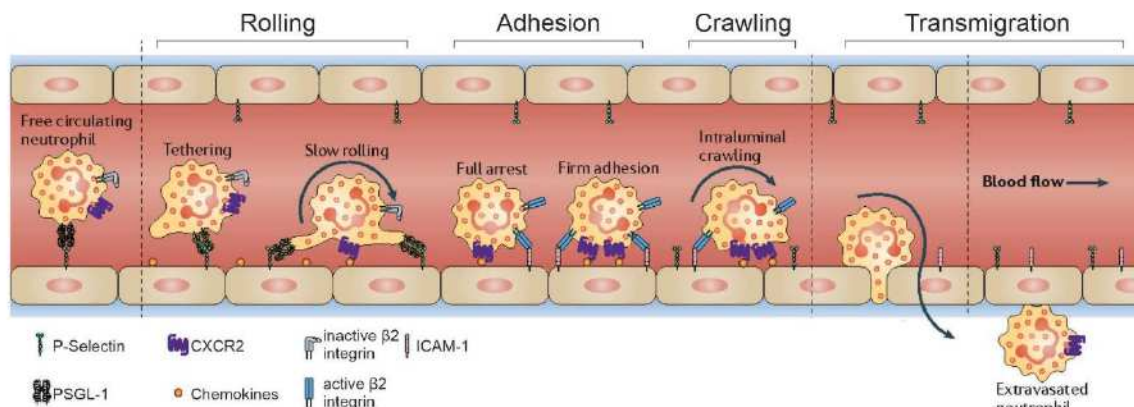


**Figure 19: The leukocyte adhesion cascade illustrated on neutrophils.** After initial contact of neutrophils to the endothelium through selectins, integrins facilitate slow rolling and upon chemokine binding to receptors like CXCR2 firm adhesion on ICAM-1, intraluminal crawling and diapedesis. While rolling and adhesion is mainly mediated by integrin  $\alpha\text{L}\beta 2$ ,  $\alpha\text{M}\beta 2$  facilitates intraluminal crawling (adapted with permission from Kolaczowska and Kubes, 2013).

In case of neutrophils, glycosylated ligands like PSGL-1 (P-selectin glycoprotein ligand), ESL-1 (E-selectin ligand-1) and CD44 bind to P- and E-selectins, which are upregulated on the luminal endothelial surface in inflamed tissues in response to chemokines or pattern recognition receptor activation. These interactions capture the neutrophils and they start rolling on the endothelium with the blood flow (Hidalgo et al., 2007, Kolaczowska and Kubes, 2013, Ley et al., 2007). The expression of L-selectin on neutrophils allows interaction of neutrophils among each other via PSGL-1 (Walcheck et al., 1996). Although the expression level of integrin  $\alpha 4\beta 1$  is rather low on neutrophils, its interaction with endothelial VCAM-1 also facilitates rolling (Alon et al., 1995, Henderson et al., 2001).

PSGL-1 engagement with selectins induces signaling through the tyrosine kinase Syk (spleen tyrosine kinase), which results in  $\alpha\text{L}\beta 2$  extension but not its full activation. Syk mediated phosphorylation of the Tec kinase Btk triggers activation of PI3K and PLC $\gamma 2$ , whose products DAG and IP $_3$  lead to activation of PKC and IP $_3$  receptor mediated  $\text{Ca}^{2+}$  influx, respectively (Mueller et al., 2010). The extended integrins bind to ICAM-1 with an intermediate affinity, resulting in deceleration of the rolling neutrophil (Kuwano et al.,



2010, Zarbock et al., 2007). Subsequently, slow rolling allows G-protein coupled receptor activation by chemokines presented on the endothelial surface, which promotes full  $\alpha\text{L}\beta 2$  activation and firm adhesion (Lefort et al., 2012). Chemokines initiating neutrophil activation and arrest include the CXCR2 ligands CXCL8 (or IL-8) in humans and CXCL1, CXCL2 and CXCL5 in mice (Sanz and Kubes, 2012). A study, which addressed the specific requirement of talin and kindlin 3 in this process, showed that the intermediate affinity  $\alpha\text{L}\beta 2$  conformation is stabilized by talin alone, while additional binding of kindlin 3 induces the shift to full activation (Lefort et al., 2012). After full arrest on the endothelium, integrin outside-in signaling facilitates adhesion strengthening and cell spreading (Ley et al., 2007).

While  $\alpha\text{L}\beta 2$  is the crucial integrin for neutrophil arrest,  $\alpha\text{M}\beta 2$  facilitates intraluminal crawling, the next step in the leukocyte adhesion cascade. By migration on the endothelial surface the cell scans the surrounding area for the optimal spot to transmigrate into the tissue (Phillipson et al., 2006).

Transendothelial migration is the final step of the leukocyte adhesion cascade, which includes the passage of the endothelial cell layer, the basement membrane and the pericyte layer. Neutrophil diapedesis relies on multiple interactions of neutrophil integrins with their endothelial counter receptors as well as homotypic interaction of other proteins expressed in endothelial cell junctions such as JAMs (junctional adhesion molecules), CD31 (platelet/endothelial cell adhesion molecule (PECAM)-1) and CD99 (Muller, 2003). Neutrophils preferentially take a paracellular route to emigrate, especially at contact points between three cells (Wang et al., 2006). Thereby, untightening of VE (vascular endothelial)-cadherin mediated endothelial cell junctions is necessary to allow leukocyte passage. This is accomplished by phosphorylation of VE-cadherin tyrosine 685 in response to inflammation and leukocyte-induced dephosphorylation of tyrosine 631 by SHP-2 (Src homology domain containing protein tyrosine phosphatase-2), which triggers VE-cadherin endocytosis (Gotsch et al., 1997, Wessel et al., 2014). The second way of extravasation is transcellular migration. This process is actively driven by endothelial cells. They encapsulate the extravasating neutrophil in dome-like structures by forming protrusions, which are rich in ICAM-1 and VCAM-1 (Kolaczowska and Kubes, 2013). However, neutrophils rarely use the transcellular route, although it has been observed more frequently, when crawling was inhibited like it is the case in  $\alpha\text{M}\beta 2$  deficient mice (Phillipson et al., 2006).

Major components of the basal membrane are laminins and collagens. Secretion of matrix metalloproteinases and other proteases such as neutrophil elastase facilitates



degradation of these extracellular matrix molecules to allow passage of the extravasating cells (Kolaczowska et al., 2009). Observations by intravital microscopy revealed that regions of less dense extracellular matrix regions are preferred routes for emigration of neutrophils. Of note, these areas were associated with gaps in the pericyte layer (Wang et al., 2006).

## B. Aims of the thesis

The main goal of this thesis was to assess the mechanism of talin mediated integrin activation (inside-out signaling) in different cell types. Previously, cell biological *in vitro* studies of integrin  $\alpha\text{IIb}\beta 3$  activation in a CHO cell based model system suggested that talin is activated and recruited to the plasma membrane as a trimeric complex in association with the small GTPase Rap1 and the adapter molecule RIAM (Han et al., 2006). However, in contrast to talin 1 deficient mice, RIAM-null mice are viable and do not show any overt phenotype, indicating that RIAM is not in general an essential component in integrin activation. Analysis of RIAM deficient mice revealed that RIAM is critically involved in leukocyte integrin  $\beta 2$  activation but dispensable in the context of other integrin classes or cell types including platelets (Klapproth et al., 2015b, Stritt et al., 2015, Su et al., 2015). Therefore, additional, RIAM independent pathways must exist to recruit talin to the plasma membrane and trigger integrin activation, which have not been described yet.

My PhD project followed the hypothesis of a direct Rap1/talin interaction to promote talin membrane recruitment and integrin activation, which was primarily based on three findings: (I) The N-terminal talin F0 domain structurally resembles a Ras-association domain (Goult et al., 2010a) and was shown to very weakly bind to Rap1. (II) Mutation of a critical amino acid (K16) in the potential Rap1 interaction site in *Dictyostelium* talin B resulted in impaired adhesion and multicellular aggregate formation (Plak et al., 2016). (III) Talin 1 and Rap1b but not RIAM are among the most abundant proteins in platelets and are expressed at very high and similar levels (Zeiler et al., 2014).

We first aimed to address our hypothesis by biochemical analyses of the interaction and *in vitro* cell biological studies. Previously established talin 1/2 double-knockout fibroblasts (Theodosiou et al., 2016) served as an excellent tool for rescue experiments with wild-type talin or variants carrying mutations in the putative Rap1 binding site to investigate integrin mediated functions like adhesion and spreading.

In the next step, we addressed the physiological relevance of the Rap1/talin pathway *in vivo* and specifically in the hematopoietic system. We targeted the talin 1 gene locus in embryonic stem cells with the help of the CRISPR/Cas9-technology, and generated a talin knockin mouse line carrying mutations in the Rap1 binding site. These mice were then analysed according to their integrin mediated functions in platelets and neutrophils *ex vivo* and *in vivo*.



Since Rap1-binding mutant talin knockin mice exhibited rather mild integrin defects in platelets and neutrophils, we next investigated and functionally compared the relative importance of different talin recruitment pathways. These included the Rap1 binding site within the F0 domain and a recently identified binding site in the F1 domain, binding of membrane lipids to the F2/F3 domain as well as RIAM binding to the talin rod. Expression of talin mutants, which abolish these interactions individually or in various combinations, in talin 1/2 double deficient fibroblasts allowed us to compare them to each other and to observe compensatory or synergistic effects.

## **C. Paper summaries**

### **1 Paper 1: Structure of Rap1b bound to talin reveals a pathway for triggering integrin activation**

This publication describes a novel RIAM-independent pathway of talin-mediated integrin activation in mice facilitated by a direct interaction of talin F0 domain with the small GTPase Rap1. My contribution to this work was the substantiation of the structural and biochemical data, which were generated in the lab of Jun Qin (Lerner Research Institute, Cleveland Clinic, USA), by cell biological experiments.

Pulldown and NMR experiments revealed a specific, GTP-dependent interaction of Rap1 with the F0 domain, albeit with a very low affinity ( $K_d=162\ \mu\text{M}$ ). NMR based structural analysis of the Rap1b/talin-F0 complex revealed an interaction mode similar to that of other Ras family proteins with their effectors. The small differences between the talin-F0 Rap1 binding site and other Ras-association domains explain for instance, why talin-F0 binds specifically to Rap1 but not to the highly homologous H-Ras. Furthermore, the structure indicated a critical involvement of talin residues K15 and R35 in Rap1 binding, which is abolished by mutating these amino acids to alanines. We addressed the cell biological relevance of the interaction by expressing wild-type or Rap1-binding deficient talin 1 in talin 1/2 double-knockout fibroblasts. Despite the low affinity of the interaction, cells expressing a K15A/R35A talin mutant showed reduced adhesion and spreading compared to wild-type talin expressing cells. A detailed cell biological analysis of the adhesion sites revealed that cells expressing the Rap1-binding deficient talin mutant show fewer focal adhesions, which in sum cover a smaller area per cell, due to impaired talin recruitment to focal adhesion sites. Moreover, the impaired talin targeting to focal adhesions leads to reduced integrin activation. As talin recruitment is enhanced by interactions of the head domain with negatively charged membrane lipids, further biochemical experiments revealed stronger talin binding to Rap1 embedded in membrane vesicles than in solution.

Taken together, we confirmed a weak but specific interaction between the talin F0 domain and Rap1, which is strongly enhanced in the context of a membrane-anchored Rap1. Moreover, we characterized the binding interface and showed that this interaction promotes integrin mediated adhesion and spreading by contributing to talin focal adhesion recruitment in fibroblasts.



## **2 Paper 2: Direct Rap1/Talin1 interaction regulates platelet and neutrophil integrin activity in mice**

The central aim of the second study was to assess, whether the direct interaction between Rap1 and talin, described in paper 1, is of physiological relevance *in vivo*.

To address this point, we generated a talin 1 knockin mouse strain expressing K15A/R30A/R35A triple-mutant talin 1, which was shown to be functionally and biochemically similar to the Rap1-binding deficient K15A/R35A mutant analysed in fibroblasts. The mutant allele was inherited at Mendelian ratio and homozygous mice were viable and fertile without showing an obvious phenotype, which might be due to compensatory expression of talin 2 in many cell types. Importantly, hematopoietic cells do not express significant amounts of talin 2. We extensively studied platelet function, and showed that platelet integrin activation is reduced in Rap1-binding deficient talin knockin mice, resulting in impaired aggregation, adhesion under flow and delayed spreading due to reduced actin polymerization *in vitro*. *In vivo* experiments revealed that this leads to defective hemostasis and delayed microvascular thrombosis in the mutant mice. We then investigated, whether the role of the direct Rap1/talin interaction is also involved in leukocyte integrin regulation. Neutrophils isolated from talin 1 knockin mice showed reduced adhesion to different ligands and  $\beta 2$  integrin-mediated phagocytosis. The *in vivo* relevance of the talin/Rap1 interaction for leukocyte adhesion and extravasation was further confirmed in cremaster experiments under inflammatory conditions.

In sum, we showed that the direct Rap1/talin-F0 interaction contributes to talin mediated integrin regulation in platelets and neutrophils *in vitro* and *in vivo*.

### **3 Paper 3: A kindlin-3-leupaxin-paxillin signaling pathway regulates podosome stability**

This study dealt with the role of kindlin 3 in the regulation of podosomes, which are specialized adhesion structures mainly found in myeloid cells and are comprised of an actin core surrounded by a ring of adhesion and signaling proteins.

Based on a yeast-two-hybrid screen, we found a direct interaction of kindlin 3 with the paxillin family member leupaxin. The interaction sites were mapped to the M3 loop in the kindlin 3 F0 domain and the C-terminal LIM domains of leupaxin. The functional consequences were addressed using pre-osteoclasts differentiated from bone marrow of kindlin 3 hypomorphic mice, which express only 5% of wild-type kindlin 3 levels, and the murine macrophage-like RAW 265.7 cell line, in which we deleted kindlin 3, leupaxin or paxillin by CRISPR/Cas9 technology. We could show that kindlin 3 mediates leupaxin podosomal targeting. If leupaxin is not present in podosomes either due to genetic deletion or impaired recruitment because of strongly reduced or no kindlin 3 expression or because the leupaxin binding site was mutated in kindlin 3, paxillin phosphorylation on tyrosines 31 and 118 was increased. Our study strongly suggests that the phosphatase PTP-Pest dephosphorylates paxillin and that its phosphatase activity depends on the presence of leupaxin within podosomes. Since high paxillin phosphorylation levels promote adhesion disassembly, we measured reduced podosome lifetimes in kindlin 3 hypomorphic and leupaxin deficient cells. Surprisingly, cells lacking paxillin or both paxillin and leupaxin could still assemble podosomes, although podosome actin core size and podosome lifetime were reduced. Of note, the expression of the third paxillin family member Hic-5 was not induced in paxillin/leupaxin double knockout cells and could not compensate for the deficiencies. Loss of leupaxin, paxillin or both affected cell functions assessed in migration and matrix degradation assays. Both paxillin and leupaxin knockout cells showed reduced gelatin degradation, which was even more pronounced in double-deficient cells. Cell migration was impaired in paxillin and double deficient cells, but enhanced in leupaxin-null cells.

In summary, we showed that leupaxin is recruited to podosomes by kindlin 3, where it promotes PTP-Pest mediated paxillin dephosphorylation and thereby stabilizes podosomes. Paxillin family members are dispensable for podosome assembly but of critical importance for podosome function.



## **4 Paper 4: Rap1 and membrane lipids cooperatively recruit talin to trigger integrin activation**

Direct Rap1/talin-F0 binding contributes to talin-mediated integrin regulation, but its disruption does not abolish integrin activation and function. Therefore, we aimed to address the relative importance of different talin recruitment and activation pathways and their cooperative potential.

Expression of talin mutants, which abolish Rap1/F0, PIP2/F2 or RIAM/R3R8 interaction, in talin 1/2 double-deficient fibroblasts revealed a contribution of both Rap1 and PIP2 in talin-mediated integrin activation and function, while RIAM was dispensable in this model. Furthermore, we deciphered the role of a second recently proposed Rap1-binding site in the talin-F1 domain, which structurally resembles the talin-F0 domain and in which positively charged residues that are crucial for Rap1/F0 interaction, are conserved. Although the Rap1 interaction with the F1 domain is threefold weaker compared to F0, abolishing the Rap1/F1 interaction caused a similar phenotype as disruption of the F0 interaction, when the respective mutants were expressed in talin 1/2 double-deficient fibroblasts. The defects in cell adhesion, spreading, talin recruitment and integrin activation were further enhanced in cells transduced with a talin variant, in which both Rap1 binding domains were mutated.

Based on these findings and previously published work, we suggest a three-step mechanism of talin activation: (I) The process is initiated by talin binding to Rap1 by its F0 domain in response to Rap1 activation, followed by (II) reinforcement of the interaction by the lower-affinity talin-F1/Rap1 binding. Finally, (III) the talin head is stabilized and properly oriented by electrostatic attraction of positive charges on talin-F2 and F3 domains to negatively charged lipid patches in the membrane, which leads to a simultaneous displacement of the talin rod upon repulsion of negative charges in the F3 interacting R9 segment from the membrane. The proposed model explains simultaneous talin recruitment and release of autoinhibition.



## D. References

- ADAIR, B. D. & YEAGER, M. 2002. Three-dimensional model of the human platelet integrin alpha IIb beta 3 based on electron cryomicroscopy and x-ray crystallography. *Proc Natl Acad Sci U S A*, 99, 14059-64.
- AKISAKA, T., YOSHIDA, H., SUZUKI, R. & TAKAMA, K. 2008. Adhesion structures and their cytoskeleton-membrane interactions at podosomes of osteoclasts in culture. *Cell Tissue Res*, 331, 625-41.
- ALON, R., KASSNER, P. D., CARR, M. W., FINGER, E. B., HEMLER, M. E. & SPRINGER, T. A. 1995. The integrin VLA-4 supports tethering and rolling in flow on VCAM-1. *J Cell Biol*, 128, 1243-53.
- ALTSCHULER, D. & LAPETINA, E. G. 1993. Mutational analysis of the cAMP-dependent protein kinase-mediated phosphorylation site of Rap1b. *J Biol Chem*, 268, 7527-31.
- ARIAS-SALGADO, E. G., LIZANO, S., SARKAR, S., BRUGGE, J. S., GINSBERG, M. H. & SHATTIL, S. J. 2003. Src kinase activation by direct interaction with the integrin beta cytoplasmic domain. *Proc Natl Acad Sci U S A*, 100, 13298-302.
- ARTHUR, W. T., QUILLIAM, L. A. & COOPER, J. A. 2004. Rap1 promotes cell spreading by localizing Rac guanine nucleotide exchange factors. *J Cell Biol*, 167, 111-22.
- ATHERTON, P., STUTCHBURY, B., JETHWA, D. & BALLESTREM, C. 2016. Mechanosensitive components of integrin adhesions: Role of vinculin. *Exp Cell Res*, 343, 21-27.
- ATHERTON, P., STUTCHBURY, B., WANG, D. Y., JETHWA, D., TSANG, R., MEILER-RODRIGUEZ, E., WANG, P., BATE, N., ZENT, R., BARSUKOV, I. L., GOULT, B. T., CRITCHLEY, D. R. & BALLESTREM, C. 2015. Vinculin controls talin engagement with the actomyosin machinery. *Nat Commun*, 6, 10038.
- AUSTEN, K., RINGER, P., MEHLICH, A., CHROSTEK-GRASHOFF, A., KLUGER, C., KLINGNER, C., SABASS, B., ZENT, R., RIEF, M. & GRASHOFF, C. 2015. Extracellular rigidity sensing by talin isoform-specific mechanical linkages. *Nat Cell Biol*, 17, 1597-606.
- AZIZ, M. H., CUI, K., DAS, M., BROWN, K. E., ARDELL, C. L., FEBBRAIO, M., PLUSKOTA, E., HAN, J., WU, H., BALLANTYNE, C. M., SMITH, J. D., CATHCART, M. K. & YAKUBENKO, V. P. 2017. The Upregulation of Integrin alphaDbeta2 (CD11d/CD18) on Inflammatory Macrophages Promotes Macrophage Retention in Vascular Lesions and Development of Atherosclerosis. *J Immunol*, 198, 4855-4867.
- BAI, J., BINARI, R., NI, J. Q., VIJAYAKANTHAN, M., LI, H. S. & PERRIMON, N. 2008. RNA interference screening in Drosophila primary cells for genes involved in muscle assembly and maintenance. *Development*, 135, 1439-49.
- BANNO, A., GOULT, B. T., LEE, H., BATE, N., CRITCHLEY, D. R. & GINSBERG, M. H. 2012. Subcellular localization of talin is regulated by inter-domain interactions. *J Biol Chem*, 287, 13799-812.
- BARRET, C., ROY, C., MONTCOURRIER, P., MANGEAT, P. & NIGGLI, V. 2000. Mutagenesis of the phosphatidylinositol 4,5-bisphosphate (PIP(2)) binding site in the NH(2)-terminal domain of ezrin correlates with its altered cellular distribution. *J Cell Biol*, 151, 1067-80.
- BATE, N., GINGRAS, A. R., BACHIR, A., HORWITZ, R., YE, F., PATEL, B., GOULT, B. T. & CRITCHLEY, D. R. 2012. Talin contains a C-terminal calpain2 cleavage site important in focal adhesion dynamics. *PLoS One*, 7, e34461.
- BERTONI, A., ALABISO, O., GALETTO, A. S. & BALDANZI, G. 2018. Integrins in T Cell Physiology. *Int J Mol Sci*, 19.
- BHUWANIA, R., CORNFINE, S., FANG, Z., KRUGER, M., LUNA, E. J. & LINDER, S. 2012. Supervillin couples myosin-dependent contractility to podosomes and enables their turnover. *J Cell Sci*, 125, 2300-14.



- BLEDZKA, K., BIALKOWSKA, K., SOSSEY-ALAOUI, K., VAYNBERG, J., PLUSKOTA, E., QIN, J. & PLOW, E. F. 2016. Kindlin-2 directly binds actin and regulates integrin outside-in signaling. *J Cell Biol*, 213, 97-108.
- BLEDZKA, K., LIU, J., XU, Z., PERERA, H. D., YADAV, S. P., BIALKOWSKA, K., QIN, J., MA, Y. Q. & PLOW, E. F. 2012. Spatial coordination of kindlin-2 with talin head domain in interaction with integrin beta cytoplasmic tails. *J Biol Chem*, 287, 24585-94.
- BLOCK, M. R., BADOWSKI, C., MILLON-FREMILLON, A., BOUVARD, D., BOUIN, A. P., FAUROBERT, E., GERBER-SCOKAERT, D., PLANUS, E. & ALBIGES-RIZO, C. 2008. Podosome-type adhesions and focal adhesions, so alike yet so different. *Eur J Cell Biol*, 87, 491-506.
- BOGATAN, S., CEVIK, D., DEMIDOV, V., VANDERPLOEG, J., PANCHBHAYA, A., VITKIN, A. & JACOBS, J. R. 2015. Talin Is Required Continuously for Cardiomyocyte Remodeling during Heart Growth in *Drosophila*. *PLoS One*, 10, e0131238.
- BORREGAARD, N. 2010. Neutrophils, from Marrow to Microbes. *Immunity*, 33, 657-670.
- BOTTCHER, R. T., VEELDERS, M., ROMBAUT, P., FAIX, J., THEODOSIOU, M., STRADAL, T. E., ROTTNER, K., ZENT, R., HERZOG, F. & FASSLER, R. 2017. Kindlin-2 recruits paxillin and Arp2/3 to promote membrane protrusions during initial cell spreading. *Journal of Cell Biology*, 216, 3785-3798.
- BRAHME, N. N., HARBURGER, D. S., KEMP-O'BRIEN, K., STEWART, R., RAGHAVAN, S., PARSONS, M. & CALDERWOOD, D. A. 2013. Kindlin binds migfilin tandem LIM domains and regulates migfilin focal adhesion localization and recruitment dynamics. *J Biol Chem*, 288, 35604-16.
- BRINKMANN, V., REICHARD, U., GOOSMANN, C., FAULER, B., UHLEMANN, Y., WEISS, D. S., WEINRAUCH, Y. & ZYCHLINSKY, A. 2004. Neutrophil extracellular traps kill bacteria. *Science*, 303, 1532-1535.
- BROWN, N. H., GREGORY, S. L., RICKOLL, W. L., FESSLER, L. I., PROUT, M., WHITE, R. A. & FRISTROM, J. W. 2002. Talin is essential for integrin function in *Drosophila*. *Dev Cell*, 3, 569-79.
- BUNTING, S., WIDMER, R., LIPARI, T., RANGELL, L., STEINMETZ, H., CARVER-MOORE, K., MOORE, M. W., KELLER, G. A. & DE SAUVAGE, F. J. 1997. Normal platelets and megakaryocytes are produced in vivo in the absence of thrombopoietin. *Blood*, 90, 3423-9.
- BYE, A. P., UNSWORTH, A. J. & GIBBINS, J. M. 2016. Platelet signaling: a complex interplay between inhibitory and activatory networks. *J Thromb Haemost*, 14, 918-30.
- CALDERWOOD, D. A., CAMPBELL, I. D. & CRITCHLEY, D. R. 2013. Talins and kindlins: partners in integrin-mediated adhesion. *Nat Rev Mol Cell Biol*, 14, 503-17.
- CALDERWOOD, D. A., YAN, B., DE PEREDA, J. M., ALVAREZ, B. G., FUJIOKA, Y., LIDDINGTON, R. C. & GINSBERG, M. H. 2002. The phosphotyrosine binding-like domain of talin activates integrins. *J Biol Chem*, 277, 21749-58.
- CALLE, Y., BURNS, S., THRASHER, A. J. & JONES, G. E. 2006. The leukocyte podosome. *Eur J Cell Biol*, 85, 151-7.
- CAMP, D., HAAGE, A., SOLIANOVA, V., CASTLE, W. M., XU, Q. A., LOSTCHUCK, E., GOULT, B. T. & TANENTZAPF, G. 2018. Direct binding of Talin to Rap1 is required for cell-ECM adhesion in *Drosophila*. *J Cell Sci*, 131.
- CAMPBELL, I. D. & HUMPHRIES, M. J. 2011. Integrin structure, activation, and interactions. *Cold Spring Harb Perspect Biol*, 3.
- CARON, E., SELF, A. J. & HALL, A. 2000. The GTPase Rap1 controls functional activation of macrophage integrin alphaMbeta2 by LPS and other inflammatory mediators. *Curr Biol*, 10, 974-8.
- CATTERSON, J. H., HECK, M. M. & HARTLEY, P. S. 2013. Fermitins, the orthologs of mammalian Kindlins, regulate the development of a functional cardiac syncytium in *Drosophila melanogaster*. *PLoS One*, 8, e62958.



- CHABADEL, A., BANON-RODRIGUEZ, I., CLUET, D., RUDKIN, B. B., WEHRLE-HALLER, B., GENOT, E., JURDIC, P., ANTON, I. M. & SALTEL, F. 2007. CD44 and beta3 integrin organize two functionally distinct actin-based domains in osteoclasts. *Mol Biol Cell*, 18, 4899-910.
- CHANG, C., ADLER, C. E., KRAUSE, M., CLARK, S. G., GERTLER, F. B., TESSIER-LAVIGNE, M. & BARGMANN, C. I. 2006. MIG-10/lamellipodin and AGE-1/PI3K promote axon guidance and outgrowth in response to slit and netrin. *Curr Biol*, 16, 854-62.
- CHANG, Y. C., ZHANG, H., FRANCO-BARRAZA, J., BRENNAN, M. L., PATEL, T., CUKIERMAN, E. & WU, J. 2014. Structural and mechanistic insights into the recruitment of talin by RIAM in integrin signaling. *Structure*, 22, 1810-1820.
- CHANGÉDE, R., XU, X., MARGADANT, F. & SHEETZ, M. P. 2015. Nascent Integrin Adhesions Form on All Matrix Rigidities after Integrin Activation. *Dev Cell*, 35, 614-621.
- CHEN, J., DIACOVO, T. G., GRENAME, D. G., SANTORO, S. A. & ZUTTER, M. M. 2002. The alpha(2) integrin subunit-deficient mouse: a multifaceted phenotype including defects of branching morphogenesis and hemostasis. *Am J Pathol*, 161, 337-44.
- CHEN, N. P., SUN, Z. & FASSLER, R. 2018. The Kank family proteins in adhesion dynamics. *Curr Opin Cell Biol*, 54, 130-136.
- CHINTHALAPUDI, K., RANGARAJAN, E. S. & IZARD, T. 2018. The interaction of talin with the cell membrane is essential for integrin activation and focal adhesion formation. *Proc Natl Acad Sci U S A*, 115, 10339-10344.
- CHOI, J. S., MAHADIK, B. P. & HARLEY, B. A. 2015. Engineering the hematopoietic stem cell niche: Frontiers in biomaterial science. *Biotechnol J*, 10, 1529-45.
- CHOREV, D. S., MOSCOVITZ, O., GEIGER, B. & SHARON, M. 2014. Regulation of focal adhesion formation by a vinculin-Arp2/3 hybrid complex. *Nat Commun*, 5, 3758.
- CHYZANOWSKA-WODNICKA, M., SMYTH, S. S., SCHOENWAEELDER, S. M., FISCHER, T. H. & WHITE, G. C., 2ND 2005. Rap1b is required for normal platelet function and hemostasis in mice. *J Clin Invest*, 115, 680-7.
- CHYZANOWSKA-WODNICKA, M., WHITE, G. C., 2ND, QUILLIAM, L. A. & WHITEHEAD, K. J. 2015. Small GTPase Rap1 Is Essential for Mouse Development and Formation of Functional Vasculature. *PLoS One*, 10, e0145689.
- CHUNG, S. H., POLGAR, J. & REED, G. L. 2000. Protein kinase C phosphorylation of syntaxin 4 in thrombin-activated human platelets. *J Biol Chem*, 275, 25286-91.
- CIFUNI, S. M., WAGNER, D. D. & BERGMEIER, W. 2008. CalDAG-GEFI and protein kinase C represent alternative pathways leading to activation of integrin alpha IIb beta 3 in platelets. *Blood*, 112, 1696-1703.
- CIOBANASU, C., WANG, H., HENRIOT, V., MATHIEU, C., FENTE, A., CSILLAG, S., VIGOUROUX, C., FAIVRE, B. & LE CLAINCHE, C. 2018. Integrin-bound talin head inhibits actin filament barbed-end elongation. *J Biol Chem*, 293, 2586-2596.
- CLEMENTS, J. M., NEWHAM, P., SHEPHERD, M., GILBERT, R., DUDGEON, T. J., NEEDHAM, L. A., EDWARDS, R. M., BERRY, L., BRASS, A. & HUMPHRIES, M. J. 1994. Identification of a key integrin-binding sequence in VCAM-1 homologous to the LDV active site in fibronectin. *J Cell Sci*, 107 ( Pt 8), 2127-35.
- COHEN, S. J., GUREVICH, I., FEIGELSON, S. W., PETROVICH, E., MOSER, M., SHAKHAR, G., FASSLER, R. & ALON, R. 2013. The integrin coactivator Kindlin-3 is not required for lymphocyte diapedesis. *Blood*, 122, 2609-17.
- COLO, G. P., LAFUENTE, E. M. & TEIXIDO, J. 2012. The MRL proteins: adapting cell adhesion, migration and growth. *Eur J Cell Biol*, 91, 861-8.
- CONTI, F. J., FELDER, A., MONKLEY, S., SCHWANDER, M., WOOD, M. R., LIEBER, R., CRITCHLEY, D. & MULLER, U. 2008. Progressive myopathy and defects in the maintenance of myotendinous junctions in mice that lack talin 1 in skeletal muscle. *Development*, 135, 2043-53.



- CONTI, F. J., MONKLEY, S. J., WOOD, M. R., CRITCHLEY, D. R. & MULLER, U. 2009. Talin 1 and 2 are required for myoblast fusion, sarcomere assembly and the maintenance of myotendinous junctions. *Development*, 136, 3597-606.
- COOK, S. J., RUBINFELD, B., ALBERT, I. & MCCORMICK, F. 1993. RapV12 antagonizes Ras-dependent activation of ERK1 and ERK2 by LPA and EGF in Rat-1 fibroblasts. *EMBO J*, 12, 3475-85.
- CRITTENDEN, J. R., BERGMEIER, W., ZHANG, Y., PIFFATH, C. L., LIANG, Y., WAGNER, D. D., HOUSMAN, D. E. & GRAYBIEL, A. M. 2004. CalDAG-GEFI integrates signaling for platelet aggregation and thrombus formation. *Nat Med*, 10, 982-6.
- DAS, M., ITHYCHANDA, S. S., QIN, J. & PLOW, E. F. 2011. Migfilin and filamin as regulators of integrin activation in endothelial cells and neutrophils. *PLoS One*, 6, e26355.
- DE PEREDA, J. M., WEGENER, K. L., SANTELLI, E., BATE, N., GINSBERG, M. H., CRITCHLEY, D. R., CAMPBELL, I. D. & LIDDINGTON, R. C. 2005. Structural basis for phosphatidylinositol phosphate kinase type Igamma binding to talin at focal adhesions. *J Biol Chem*, 280, 8381-6.
- DE ROOIJ, J., ZWARTKRUIS, F. J., VERHEIJEN, M. H., COOL, R. H., NIJMAN, S. M., WITTINGHOFER, A. & BOS, J. L. 1998. Epac is a Rap1 guanine-nucleotide-exchange factor directly activated by cyclic AMP. *Nature*, 396, 474-7.
- DE SAUVAGE, F. J., CARVER-MOORE, K., LUOH, S. M., RYAN, A., DOWD, M., EATON, D. L. & MOORE, M. W. 1996. Physiological regulation of early and late stages of megakaryocytopoiesis by thrombopoietin. *J Exp Med*, 183, 651-6.
- DEBRAND, E., CONTI, F. J., BATE, N., SPENCE, L., MAZZEO, D., PRITCHARD, C. A., MONKLEY, S. J. & CRITCHLEY, D. R. 2012. Mice carrying a complete deletion of the talin2 coding sequence are viable and fertile. *Biochem Biophys Res Commun*, 426, 190-5.
- DEDDEN, D., SCHUMACHER, S., KELLEY, C. F., ZACHARIAS, M., BIERTUMPFEL, C., FASSLER, R. & MIZUNO, N. 2019. The Architecture of Talin1 Reveals an Autoinhibition Mechanism. *Cell*, 179, 120-131 e13.
- DEL RIO, A., PEREZ-JIMENEZ, R., LIU, R., ROCA-CUSACHS, P., FERNANDEZ, J. M. & SHEETZ, M. P. 2009. Stretching single talin rod molecules activates vinculin binding. *Science*, 323, 638-41.
- DI PAOLO, G., PELLEGRINI, L., LETINIC, K., CESTRA, G., ZONCU, R., VORONOV, S., CHANG, S., GUO, J., WENK, M. R. & DE CAMILLI, P. 2002. Recruitment and regulation of phosphatidylinositol phosphate kinase type 1 gamma by the FERM domain of talin. *Nature*, 420, 85-9.
- DOWLING, J. J., GIBBS, E., RUSSELL, M., GOLDMAN, D., MINARCIK, J., GOLDEN, J. A. & FELDMAN, E. L. 2008a. Kindlin-2 is an essential component of intercalated discs and is required for vertebrate cardiac structure and function. *Circ Res*, 102, 423-31.
- DOWLING, J. J., VREEDE, A. P., KIM, S., GOLDEN, J. & FELDMAN, E. L. 2008b. Kindlin-2 is required for myocyte elongation and is essential for myogenesis. *BMC Cell Biol*, 9, 36.
- DRISSEN, R. & NERLOV, C. 2016. Hematopoietic Lineage Diversification, Simplified. *Cell Stem Cell*, 19, 148-150.
- DUCHNIEWICZ, M., ZEMOJTEL, T., KOLANCZYK, M., GROSSMANN, S., SCHEELE, J. S. & ZWARTKRUIS, F. J. 2006. Rap1A-deficient T and B cells show impaired integrin-mediated cell adhesion. *Mol Cell Biol*, 26, 643-53.
- DUSTIN, M. L. 2016. Complement Receptors in Myeloid Cell Adhesion and Phagocytosis. *Microbiol Spectr*, 4.
- ELLIOTT, P. R., GOULT, B. T., KOPP, P. M., BATE, N., GROSSMANN, J. G., ROBERTS, G. C., CRITCHLEY, D. R. & BARSUKOV, I. L. 2010. The Structure of the talin head reveals a novel extended conformation of the FERM domain. *Structure*, 18, 1289-99.
- ELLIS, S. J., LOSTCHUCK, E., GOULT, B. T., BOUAQUINA, M., FAIRCHILD, M. J., LOPEZ-CEBALLOS, P., CALDERWOOD, D. A. & TANENTZAPF, G. 2014. The talin head domain reinforces



- integrin-mediated adhesion by promoting adhesion complex stability and clustering. *PLoS Genet*, 10, e1004756.
- ELLIS, S. J., PINES, M., FAIRCHILD, M. J. & TANENTZAPF, G. 2011. In vivo functional analysis reveals specific roles for the integrin-binding sites of talin. *J Cell Sci*, 124, 1844-56.
- ELLIS, T. N. & BEAMAN, B. L. 2002. Murine polymorphonuclear neutrophils produce interferon-gamma in response to pulmonary infection with *Nocardia asteroides*. *Journal of Leukocyte Biology*, 72, 373-381.
- EMSLEY, J., KNIGHT, C. G., FARNDAL, R. W., BARNES, M. J. & LIDDINGTON, R. C. 2000. Structural basis of collagen recognition by integrin  $\alpha 2\beta 1$ . *Cell*, 101, 47-56.
- FASSLER, R. & MEYER, M. 1995. Consequences of lack of beta 1 integrin gene expression in mice. *Genes Dev*, 9, 1896-908.
- FEIGELSON, S. W., GRABOVSKY, V., MANEVICH-MENDELSON, E., PASVOLSKY, R., SHULMAN, Z., SHINDER, V., KLEIN, E., ETZIONI, A., AKER, M. & ALON, R. 2011. Kindlin-3 is required for the stabilization of TCR-stimulated LFA-1:ICAM-1 bonds critical for lymphocyte arrest and spreading on dendritic cells. *Blood*, 117, 7042-52.
- FIEVET, B. T., GAUTREAU, A., ROY, C., DEL MAESTRO, L., MANGEAT, P., LOUVARD, D. & ARPIN, M. 2004. Phosphoinositide binding and phosphorylation act sequentially in the activation mechanism of ezrin. *J Cell Biol*, 164, 653-9.
- FOX, N. E. & KAUSHANSKY, K. 2005. Engagement of integrin  $\alpha 4\beta 1$  enhances thrombopoietin-induced megakaryopoiesis. *Exp Hematol*, 33, 94-9.
- FRANCO-CEA, A., ELLIS, S. J., FAIRCHILD, M. J., YUAN, L., CHEUNG, T. Y. & TANENTZAPF, G. 2010. Distinct developmental roles for direct and indirect talin-mediated linkage to actin. *Dev Biol*, 345, 64-77.
- FRANCO, S. J., RODGERS, M. A., PERRIN, B. J., HAN, J., BENNIN, D. A., CRITCHLEY, D. R. & HUTTENLOCHER, A. 2004. Calpain-mediated proteolysis of talin regulates adhesion dynamics. *Nat Cell Biol*, 6, 977-83.
- FRANKE, B., AKKERMAN, J. W. & BOS, J. L. 1997. Rapid  $\text{Ca}^{2+}$ -mediated activation of Rap1 in human platelets. *EMBO J*, 16, 252-9.
- FUKUDA, K., BLEDZKA, K., YANG, J., PERERA, H. D., PLOW, E. F. & QIN, J. 2014. Molecular basis of kindlin-2 binding to integrin-linked kinase pseudokinase for regulating cell adhesion. *J Biol Chem*, 289, 28363-75.
- FUKUDA, K., GUPTA, S., CHEN, K., WU, C. & QIN, J. 2009. The pseudoactive site of ILK is essential for its binding to alpha-Parvin and localization to focal adhesions. *Mol Cell*, 36, 819-30.
- GALLI, S. J., BORREGAARD, N. & WYNN, T. A. 2011. Phenotypic and functional plasticity of cells of innate immunity: macrophages, mast cells and neutrophils. *Nature Immunology*, 12, 1035-1044.
- GAO, J., HUANG, M., LAI, J., MAO, K., SUN, P., CAO, Z., HU, Y., ZHANG, Y., SCHULTE, M. L., JIN, C., WANG, J., WHITE, G. C., XU, Z. & MA, Y. Q. 2017. Kindlin supports platelet integrin  $\alpha \text{IIb}\beta 3$  activation by interacting with paxillin. *J Cell Sci*, 130, 3764-3775.
- GARCIA-ALVAREZ, B., DE PEREDA, J. M., CALDERWOOD, D. A., ULMER, T. S., CRITCHLEY, D., CAMPBELL, I. D., GINSBERG, M. H. & LIDDINGTON, R. C. 2003. Structural determinants of integrin recognition by talin. *Mol Cell*, 11, 49-58.
- GARCIA, A., KIM, S., BHAVARAJU, K., SCHOENWAEELDER, S. M. & KUNAPULI, S. P. 2010. Role of phosphoinositide 3-kinase beta in platelet aggregation and thromboxane A2 generation mediated by Gi signalling pathways. *Biochem J*, 429, 369-77.
- GAWDEN-BONE, C., ZHOU, Z., KING, E., PRESCOTT, A., WATTS, C. & LUCOCQ, J. 2010. Dendritic cell podosomes are protrusive and invade the extracellular matrix using metalloproteinase MMP-14. *J Cell Sci*, 123, 1427-37.
- GINGRAS, A. R., BATE, N., GOULT, B. T., HAZELWOOD, L., CANESTRELLI, I., GROSSMANN, J. G., LIU, H., PUTZ, N. S., ROBERTS, G. C., VOLKMANN, N., HANEIN, D., BARSUKOV, I. L. &



- CRITCHLEY, D. R. 2008. The structure of the C-terminal actin-binding domain of talin. *EMBO J*, 27, 458-69.
- GINGRAS, A. R., BATE, N., GOULT, B. T., PATEL, B., KOPP, P. M., EMSLEY, J., BARSUKOV, I. L., ROBERTS, G. C. & CRITCHLEY, D. R. 2010. Central region of talin has a unique fold that binds vinculin and actin. *J Biol Chem*, 285, 29577-87.
- GINGRAS, A. R., VOGEL, K. P., STEINHOFF, H. J., ZIEGLER, W. H., PATEL, B., EMSLEY, J., CRITCHLEY, D. R., ROBERTS, G. C. & BARSUKOV, I. L. 2006. Structural and dynamic characterization of a vinculin binding site in the talin rod. *Biochemistry*, 45, 1805-17.
- GINGRAS, A. R., ZIEGLER, W. H., BOBKOV, A. A., JOYCE, M. G., FASCI, D., HIMMEL, M., ROTHMUND, S., RITTER, A., GROSSMANN, J. G., PATEL, B., BATE, N., GOULT, B. T., EMSLEY, J., BARSUKOV, I. L., ROBERTS, G. C., LIDDINGTON, R. C., GINSBERG, M. H. & CRITCHLEY, D. R. 2009. Structural determinants of integrin binding to the talin rod. *J Biol Chem*, 284, 8866-76.
- GINGRAS, A. R., ZIEGLER, W. H., FRANK, R., BARSUKOV, I. L., ROBERTS, G. C., CRITCHLEY, D. R. & EMSLEY, J. 2005. Mapping and consensus sequence identification for multiple vinculin binding sites within the talin rod. *J Biol Chem*, 280, 37217-24.
- GLADING, A., HAN, J., STOCKTON, R. A. & GINSBERG, M. H. 2007. KRIT-1/CCM1 is a Rap1 effector that regulates endothelial cell cell junctions. *J Cell Biol*, 179, 247-54.
- GLADING, A. J. & GINSBERG, M. H. 2010. Rap1 and its effector KRIT1/CCM1 regulate beta-catenin signaling. *Dis Model Mech*, 3, 73-83.
- GOKSOY, E., MA, Y. Q., WANG, X., KONG, X., PERERA, D., PLOW, E. F. & QIN, J. 2008. Structural basis for the autoinhibition of talin in regulating integrin activation. *Mol Cell*, 31, 124-33.
- GOTSCH, U., BORGES, E., BOSSE, R., BOGGEMEYER, E., SIMON, M., MOSSMANN, H. & VESTWEBER, D. 1997. VE-cadherin antibody accelerates neutrophil recruitment in vivo. *J Cell Sci*, 110 ( Pt 5), 583-8.
- GOUGH, R. E. & GOULT, B. T. 2018. The tale of two talins - two isoforms to fine-tune integrin signalling. *FEBS Lett*, 592, 2108-2125.
- GOULT, B. T., BATE, N., ANTHIS, N. J., WEGENER, K. L., GINGRAS, A. R., PATEL, B., BARSUKOV, I. L., CAMPBELL, I. D., ROBERTS, G. C. & CRITCHLEY, D. R. 2009a. The structure of an interdomain complex that regulates talin activity. *J Biol Chem*, 284, 15097-106.
- GOULT, B. T., BOUAOUINA, M., ELLIOTT, P. R., BATE, N., PATEL, B., GINGRAS, A. R., GROSSMANN, J. G., ROBERTS, G. C., CALDERWOOD, D. A., CRITCHLEY, D. R. & BARSUKOV, I. L. 2010a. Structure of a double ubiquitin-like domain in the talin head: a role in integrin activation. *EMBO J*, 29, 1069-80.
- GOULT, B. T., BOUAOUINA, M., HARBURGER, D. S., BATE, N., PATEL, B., ANTHIS, N. J., CAMPBELL, I. D., CALDERWOOD, D. A., BARSUKOV, I. L., ROBERTS, G. C. & CRITCHLEY, D. R. 2009b. The structure of the N-terminus of kindlin-1: a domain important for alphaIIb beta3 integrin activation. *J Mol Biol*, 394, 944-56.
- GOULT, B. T., GINGRAS, A. R., BATE, N., BARSUKOV, I. L., CRITCHLEY, D. R. & ROBERTS, G. C. 2010b. The domain structure of talin: residues 1815-1973 form a five-helix bundle containing a cryptic vinculin-binding site. *FEBS Lett*, 584, 2237-41.
- GOULT, B. T., XU, X. P., GINGRAS, A. R., SWIFT, M., PATEL, B., BATE, N., KOPP, P. M., BARSUKOV, I. L., CRITCHLEY, D. R., VOLKMANN, N. & HANEIN, D. 2013a. Structural studies on full-length talin1 reveal a compact auto-inhibited dimer: implications for talin activation. *J Struct Biol*, 184, 21-32.
- GOULT, B. T., YAN, J. & SCHWARTZ, M. A. 2018. Talin as a mechanosensitive signaling hub. *J Cell Biol*, 217, 3776-3784.
- GOULT, B. T., ZACHARCHENKO, T., BATE, N., TSANG, R., HEY, F., GINGRAS, A. R., ELLIOTT, P. R., ROBERTS, G. C., BALLESTREM, C., CRITCHLEY, D. R. & BARSUKOV, I. L. 2013b. RIAM and



- vinculin binding to talin are mutually exclusive and regulate adhesion assembly and turnover. *J Biol Chem*, 288, 8238-49.
- GROZOVSKY, R., GIANNINI, S., FALET, H. & HOFFMEISTER, K. M. 2015. Novel mechanisms of platelet clearance and thrombopoietin regulation. *Curr Opin Hematol*, 22, 445-51.
- GRUNER, S., PROSTREDNA, M., SCHULTE, V., KRIEG, T., ECKES, B., BRAKEBUSCH, C. & NIESWANDT, B. 2003. Multiple integrin-ligand interactions synergize in shear-resistant platelet adhesion at sites of arterial injury in vivo. *Blood*, 102, 4021-7.
- GUEGAN, F., TATIN, F., LESTE-LASSERRE, T., DRUTEL, G., GENOT, E. & MOREAU, V. 2008. p190B RhoGAP regulates endothelial-cell-associated proteolysis through MT1-MMP and MMP2. *J Cell Sci*, 121, 2054-61.
- GUO, B., GAO, J., ZHAN, J. & ZHANG, H. 2015. Kindlin-2 interacts with and stabilizes EGFR and is required for EGF-induced breast cancer cell migration. *Cancer Lett*, 361, 271-81.
- GURNEY, A. L., CARVER-MOORE, K., DE SAUVAGE, F. J. & MOORE, M. W. 1994. Thrombocytopenia in c-mpl-deficient mice. *Science*, 265, 1445-7.
- HAGER, M., COWLAND, J. B. & BORREGAARD, N. 2010. Neutrophil granules in health and disease. *Journal of Internal Medicine*, 268, 25-34.
- HALING, J. R., MONKLEY, S. J., CRITCHLEY, D. R. & PETRICH, B. G. 2011. Talin-dependent integrin activation is required for fibrin clot retraction by platelets. *Blood*, 117, 1719-22.
- HAMADA, K., SHIMIZU, T., MATSUI, T., TSUKITA, S. & HAKOSHIMA, T. 2000. Structural basis of the membrane-targeting and unmasking mechanisms of the radixin FERM domain. *EMBO J*, 19, 4449-62.
- HAN, J., LIM, C. J., WATANABE, N., SORIANI, A., RATNIKOV, B., CALDERWOOD, D. A., PUZON-MCLAUGHLIN, W., LAFUENTE, E. M., BOUSSIOTIS, V. A., SHATTIL, S. J. & GINSBERG, M. H. 2006. Reconstructing and deconstructing agonist-induced activation of integrin  $\alpha$ IIb $\beta$ 3. *Curr Biol*, 16, 1796-806.
- HARPER, M. T. & POOLE, A. W. 2010. Diverse functions of protein kinase C isoforms in platelet activation and thrombus formation. *J Thromb Haemost*, 8, 454-62.
- HART, R., STANLEY, P., CHAKRAVARTY, P. & HOGG, N. 2013. The kindlin 3 pleckstrin homology domain has an essential role in lymphocyte function-associated antigen 1 (LFA-1) integrin-mediated B cell adhesion and migration. *J Biol Chem*, 288, 14852-62.
- HAYASHI, M., SUZUKI, H., KAWASHIMA, S., SAIDO, T. C. & INOMATA, M. 1999. The behavior of calpain-generated N- and C-terminal fragments of talin in integrin-mediated signaling pathways. *Arch Biochem Biophys*, 371, 133-41.
- HE, L., PAPPAN, L. K., GRENACHE, D. G., LI, Z., TOLLEFSEN, D. M., SANTORO, S. A. & ZUTTER, M. M. 2003. The contributions of the  $\alpha$ 2 $\beta$ 1 integrin to vascular thrombosis in vivo. *Blood*, 102, 3652-7.
- HE, Y., SONNENWALD, T., SPRENGER, A., HANSEN, U., DENGJEL, J., BRUCKNER-TUDERMAN, L., SCHMIDT, G. & HAS, C. 2014. RhoA activation by CNFy restores cell-cell adhesion in kindlin-2-deficient keratinocytes. *J Pathol*, 233, 269-80.
- HELSTEN, T. L., BUNCH, T. A., KATO, H., YAMANOUCHI, J., CHOI, S. H., JANNUZI, A. L., FERAL, C. C., GINSBERG, M. H., BROWER, D. L. & SHATTIL, S. J. 2008. Differences in regulation of Drosophila and vertebrate integrin affinity by talin. *Mol Biol Cell*, 19, 3589-98.
- HEMMINGS, L., REES, D. J., OHANIAN, V., BOLTON, S. J., GILMORE, A. P., PATEL, B., PRIDDLE, H., TREVITHICK, J. E., HYNES, R. O. & CRITCHLEY, D. R. 1996. Talin contains three actin-binding sites each of which is adjacent to a vinculin-binding site. *J Cell Sci*, 109 ( Pt 11), 2715-26.
- HENDERSON, R. B., LIM, L. H., TESSIER, P. A., GAVINS, F. N., MATHIES, M., PERRETTI, M. & HOGG, N. 2001. The use of lymphocyte function-associated antigen (LFA)-1-deficient mice to determine the role of LFA-1, Mac-1, and  $\alpha$ 4 integrin in the inflammatory response of neutrophils. *J Exp Med*, 194, 219-26.



- HIDALGO, A., PEIRED, A. J., WILD, M., VESTWEBER, D. & FRENETTE, P. S. 2007. Complete identification of E-selectin ligands on neutrophils reveals distinct functions of PSGL-1, ESL-1, and CD44. *Immunity*, 26, 477-489.
- HODIVALA-DILKE, K. M., MCHUGH, K. P., TSAKIRIS, D. A., RAYBURN, H., CROWLEY, D., ULLMAN-CULLERE, M., ROSS, F. P., COLLIER, B. S., TEITELBAUM, S. & HYNES, R. O. 1999. Beta3-integrin-deficient mice are a model for Glanzmann thrombasthenia showing placental defects and reduced survival. *J Clin Invest*, 103, 229-38.
- HODOHARA, K., FUJII, N., YAMAMOTO, N. & KAUSHANSKY, K. 2000. Stromal cell-derived factor-1 (SDF-1) acts together with thrombopoietin to enhance the development of megakaryocytic progenitor cells (CFU-MK). *Blood*, 95, 769-75.
- HOGERVORST, F., KUIKMAN, I., VON DEM BORNE, A. E. & SONNENBERG, A. 1990. Cloning and sequence analysis of beta-4 cDNA: an integrin subunit that contains a unique 118 kd cytoplasmic domain. *EMBO J*, 9, 765-70.
- HOLTKOTTER, O., NIESWANDT, B., SMYTH, N., MULLER, W., HAFNER, M., SCHULTE, V., KRIEG, T. & ECKES, B. 2002. Integrin alpha(2)-deficient mice develop normally, are fertile, but display partially defective platelet interaction with collagen. *Journal of Biological Chemistry*, 277, 10789-10794.
- HONG, C. W. 2017. Current Understanding in Neutrophil Differentiation and Heterogeneity. *Immune Netw*, 17, 298-306.
- HUANG, J. S., LI, X., SHI, X. F., ZHU, M., WANG, J. H., HUANG, S. J., HUANG, X., WANG, H. F., LI, L., DENG, H., ZHOU, Y. L., MAO, J. H., LONG, Z. B., MA, Z. X., YE, W. L., PAN, J. J., XI, X. D. & JIN, J. 2019. Platelet integrin alpha IIb beta 3: signal transduction, regulation, and its therapeutic targeting. *Journal of Hematology & Oncology*, 12.
- HUET-CALDERWOOD, C., BRAHME, N. N., KUMAR, N., STIEGLER, A. L., RAGHAVAN, S., BOGGON, T. J. & CALDERWOOD, D. A. 2014. Differences in binding to the ILK complex determines kindlin isoform adhesion localization and integrin activation. *J Cell Sci*, 127, 4308-21.
- HUGHES, P. E., DIAZ-GONZALEZ, F., LEONG, L., WU, C., MCDONALD, J. A., SHATTIL, S. J. & GINSBERG, M. H. 1996. Breaking the integrin hinge. A defined structural constraint regulates integrin signaling. *J Biol Chem*, 271, 6571-4.
- HUMPHRIES, J. D., BYRON, A. & HUMPHRIES, M. J. 2006. Integrin ligands at a glance. *Journal of Cell Science*, 119, 3901-3903.
- HUMPHRIES, M. J. 1990. The molecular basis and specificity of integrin-ligand interactions. *J Cell Sci*, 97 ( Pt 4), 585-92.
- HYNES, R. O. 2002. Integrins: bidirectional, allosteric signaling machines. *Cell*, 110, 673-87.
- INOUE, O., SUZUKI-INOUE, K., MCCARTY, O. J., MOROI, M., RUGGERI, Z. M., KUNICKI, T. J., OZAKI, Y. & WATSON, S. P. 2006. Laminin stimulates spreading of platelets through integrin alpha6beta1-dependent activation of GPIIb/IIIa. *Blood*, 107, 1405-12.
- ITHYCHANDA, S. S., DAS, M., MA, Y. Q., DING, K., WANG, X., GUPTA, S., WU, C., PLOW, E. F. & QIN, J. 2009. Migfilin, a molecular switch in regulation of integrin activation. *J Biol Chem*, 284, 4713-22.
- JASKIEWICZ, A., PAJAK, B. & ORZECOWSKI, A. 2018. The Many Faces of Rap1 GTPase. *International Journal of Molecular Sciences*, 19.
- JENZORA, A., BEHRENDT, B., SMALL, J. V., WEHLAND, E. & STRADAL, T. E. B. 2005. PREL1 provides a link from Ras signalling to the actin cytoskeleton via Ena/VASP proteins. *FEBS Letters*, 579, 455-463.
- KAHNER, B. N., KATO, H., BANNO, A., GINSBERG, M. H., SHATTIL, S. J. & YE, F. 2012. Kindlins, integrin activation and the regulation of talin recruitment to alphaIIb beta3. *PLoS One*, 7, e34056.
- KAKINUMA, N., ZHU, Y., WANG, Y., ROY, B. C. & KIYAMA, R. 2009. Kank proteins: structure, functions and diseases. *Cell Mol Life Sci*, 66, 2651-9.



- KAMMERER, P., ARETZ, J. & FASSLER, R. 2017. Lucky kindlin: A cloverleaf at the integrin tail. *Proc Natl Acad Sci U S A*, 114, 9234-9236.
- KANCHANAWONG, P., SHTENGEL, G., PASAPERA, A. M., RAMKO, E. B., DAVIDSON, M. W., HESS, H. F. & WATERMAN, C. M. 2010. Nanoscale architecture of integrin-based cell adhesions. *Nature*, 468, 580-4.
- KASBEKAR, S., BUEREN, J., THRASHER, A. J., KOHN, D. B., SEVILLA, J., SCHWARTZ, J. D. & ALMARZA, E. 2017. Leukocyte Adhesion Deficiency-I (LAD-I): A Comprehensive Review of Published Cases. *Blood*, 130.
- KATAGIRI, K., HATTORI, M., MINATO, N., IRIE, S., TAKATSU, K. & KINASHI, T. 2000. Rap1 is a potent activation signal for leukocyte function-associated antigen 1 distinct from protein kinase C and phosphatidylinositol-3-OH kinase. *Mol Cell Biol*, 20, 1956-69.
- KATAGIRI, K., IMAMURA, M. & KINASHI, T. 2006. Spatiotemporal regulation of the kinase Mst1 by binding protein RAPL is critical for lymphocyte polarity and adhesion. *Nat Immunol*, 7, 919-28.
- KATAGIRI, K., MAEDA, A., SHIMONAKA, M. & KINASHI, T. 2003. RAPL, a Rap1-binding molecule that mediates Rap1-induced adhesion through spatial regulation of LFA-1. *Nat Immunol*, 4, 741-8.
- KAVERINA, I., STRADAL, T. E. & GIMONA, M. 2003. Podosome formation in cultured A7r5 vascular smooth muscle cells requires Arp2/3-dependent de-novo actin polymerization at discrete microdomains. *J Cell Sci*, 116, 4915-24.
- KAWASAKI, H., SPRINGETT, G. M., TOKI, S., CANALES, J. J., HARLAN, P., BLUMENSTIEL, J. P., CHEN, E. J., BANY, I. A., MOCHIZUKI, N., ASHBACHER, A., MATSUDA, M., HOUSMAN, D. E. & GRAYBIEL, A. M. 1998. A Rap guanine nucleotide exchange factor enriched highly in the basal ganglia. *Proc Natl Acad Sci U S A*, 95, 13278-83.
- KINDLER, T. 1954. Congenital poikiloderma with traumatic bulla formation and progressive cutaneous atrophy. *Br J Dermatol*, 66, 104-11.
- KITAYAMA, H., SUGIMOTO, Y., MATSUZAKI, T., IKAWA, Y. & NODA, M. 1989. A ras-related gene with transformation suppressor activity. *Cell*, 56, 77-84.
- KLANN, J. E., REMEDIOS, K. A., KIM, S. H., METZ, P. J., LOPEZ, J., MACK, L. A., ZHENG, Y., GINSBERG, M. H., PETRICH, B. G. & CHANG, J. T. 2017. Talin Plays a Critical Role in the Maintenance of the Regulatory T Cell Pool. *J Immunol*, 198, 4639-4651.
- KLAPHOLZ, B. & BROWN, N. H. 2017. Talin - the master of integrin adhesions. *J Cell Sci*, 130, 2435-2446.
- KLAPHOLZ, B., HERBERT, S. L., WELLMANN, J., JOHNSON, R., PARSONS, M. & BROWN, N. H. 2015. Alternative mechanisms for talin to mediate integrin function. *Curr Biol*, 25, 847-57.
- KLAPPROTH, S., MORETTI, F. A., ZEILER, M., RUPPERT, R., BREITHAUPT, U., MUELLER, S., HAAS, R., MANN, M., SPERANDIO, M., FASSLER, R. & MOSER, M. 2015a. Minimal amounts of kindlin-3 suffice for basal platelet and leukocyte functions in mice. *Blood*, 126, 2592-600.
- KLAPPROTH, S., SPERANDIO, M., PINHEIRO, E. M., PRUNSTER, M., SOEHNLEIN, O., GERTLER, F. B., FASSLER, R. & MOSER, M. 2015b. Loss of the Rap1 effector RIAM results in leukocyte adhesion deficiency due to impaired beta2 integrin function in mice. *Blood*, 126, 2704-12.
- KOKLIC, T., MAJUMDER, R., WEINREB, G. E. & LENTZ, B. R. 2009. Factor XA binding to phosphatidylserine-containing membranes produces an inactive membrane-bound dimer. *Biophys J*, 97, 2232-41.
- KOLACZKOWSKA, E., GRZYBEK, W., VAN ROOIJEN, N., PICCARD, H., PLYTYCZ, B., ARNOLD, B. & OPDENAKKER, G. 2009. Neutrophil elastase activity compensates for a genetic lack of matrix metalloproteinase-9 (MMP-9) in leukocyte infiltration in a model of experimental peritonitis. *J Leukoc Biol*, 85, 374-81.



- KOLACZKOWSKA, E. & KUBES, P. 2013. Neutrophil recruitment and function in health and inflammation. *Nature Reviews Immunology*, 13, 159-175.
- KOLSCH, V., SHEN, Z. X., LEE, S., PLAK, K., LOTFI, P., CHANG, J., CHAREST, P. G., ROMERO, J. L., JEON, T. J., KORTHOLT, A., BRIGGS, S. P. & FIRTEL, R. A. 2013. Daydreamer, a Ras effector and GSK-3 substrate, is important for directional sensing and cell motility. *Molecular Biology of the Cell*, 24, 100-114.
- KONDO, N., UEDA, Y., KITA, T., OZAWA, M., TOMIYAMA, T., YASUDA, K., LIM, D. S. & KINASHI, T. 2017. NDR1-Dependent Regulation of Kindlin-3 Controls High-Affinity LFA-1 Binding and Immune Synapse Organization. *Mol Cell Biol*, 37.
- KONG, J., DU, J., WANG, Y., YANG, M., GAO, J., WEI, X., FANG, W., ZHAN, J. & ZHANG, H. 2016. Focal adhesion molecule Kindlin-1 mediates activation of TGF-beta signaling by interacting with TGF-betaRI, SARA and Smad3 in colorectal cancer cells. *Oncotarget*, 7, 76224-76237.
- KOUPENOVA, M., KEHREL, B. E., CORKREY, H. A. & FREEDMAN, J. E. 2017. Thrombosis and platelets: an update. *Eur Heart J*, 38, 785-791.
- KRUGER, M., MOSER, M., USSAR, S., THIEVESSEN, I., LUBER, C. A., FORNER, F., SCHMIDT, S., ZANIVAN, S., FASSLER, R. & MANN, M. 2008. SILAC mouse for quantitative proteomics uncovers kindlin-3 as an essential factor for red blood cell function. *Cell*, 134, 353-64.
- KUIJPERS, T. W., VAN DE VIJVER, E., WETERMAN, M. A., DE BOER, M., TOOL, A. T., VAN DEN BERG, T. K., MOSER, M., JAKOBS, M. E., SEEGER, K., SANAL, O., UNAL, S., CETIN, M., ROOS, D., VERHOEVEN, A. J. & BAAS, F. 2009. LAD-1/variant syndrome is caused by mutations in FERMT3. *Blood*, 113, 4740-6.
- KUMAR, A., OUYANG, M., VAN DEN DRIES, K., MCGHEE, E. J., TANAKA, K., ANDERSON, M. D., GROISMAN, A., GOULT, B. T., ANDERSON, K. I. & SCHWARTZ, M. A. 2016. Talin tension sensor reveals novel features of focal adhesion force transmission and mechanosensitivity. *J Cell Biol*, 213, 371-83.
- KUMAR, S., XU, J., KUMAR, R. S., LAKSHMIKANTHAN, S., KAPUR, R., KOFRON, M., CHRZANOWSKA-WODNICKA, M. & FILIPPI, M. D. 2014. The small GTPase Rap1b negatively regulates neutrophil chemotaxis and transcellular diapedesis by inhibiting Akt activation. *J Exp Med*, 211, 1741-58.
- KUWANO, Y., SPELTEN, O., ZHANG, H., LEY, K. & ZARBOCK, A. 2010. Rolling on E- or P-selectin induces the extended but not high-affinity conformation of LFA-1 in neutrophils. *Blood*, 116, 617-624.
- LACAUD, G. & KOUSKOFF, V. 2017. Hemangioblast, hemogenic endothelium, and primitive versus definitive hematopoiesis. *Exp Hematol*, 49, 19-24.
- LAD, Y., JIANG, P., RUSKAMO, S., HARBURGER, D. S., YLANNE, J., CAMPBELL, I. D. & CALDERWOOD, D. A. 2008. Structural basis of the migfilin-filamin interaction and competition with integrin beta tails. *J Biol Chem*, 283, 35154-63.
- LAFUENTE, E. M., VAN PUIJENBROEK, A. A., KRAUSE, M., CARMAN, C. V., FREEMAN, G. J., BEREZOVSKAYA, A., CONSTANTINE, E., SPRINGER, T. A., GERTLER, F. B. & BOUSSIOTIS, V. A. 2004. RIAM, an Ena/VASP and Profilin ligand, interacts with Rap1-GTP and mediates Rap1-induced adhesion. *Dev Cell*, 7, 585-95.
- LAGARRIGUE, F., GINGRAS, A. R., PAUL, D. S., VALADEZ, A. J., CUEVAS, M. N., SUN, H., LOPEZ-RAMIREZ, M. A., GOULT, B. T., SHATTIL, S. J., BERGMEIER, W. & GINSBERG, M. H. 2018. Rap1 binding to the talin 1 F0 domain makes a minimal contribution to murine platelet GPIIb-IIIa activation. *Blood Adv*, 2, 2358-2368.
- LAGARRIGUE, F., VIKAS ANEKAL, P., LEE, H. S., BACHIR, A. I., ABLACK, J. N., HORWITZ, A. F. & GINSBERG, M. H. 2015. A RIAM/lamellipodin-talin-integrin complex forms the tip of sticky fingers that guide cell migration. *Nat Commun*, 6, 8492.



- LAI-CHEONG, J. E., USSAR, S., ARITA, K., HART, I. R. & MCGRATH, J. A. 2008. Colocalization of kindlin-1, kindlin-2, and migfilin at keratinocyte focal adhesion and relevance to the pathophysiology of Kindler syndrome. *J Invest Dermatol*, 128, 2156-65.
- LAKSHMIKANTHAN, S., SOBCZAK, M., CHUN, C., HENSCH, A., DARGATZ, J., RAMCHANDRAN, R. & CHRZANOWSKA-WODNICKA, M. 2011. Rap1 promotes VEGFR2 activation and angiogenesis by a mechanism involving integrin  $\alpha v \beta 3$ . *Blood*, 118, 2015-26.
- LAPETINA, E. G., LACAL, J. C., REEP, B. R. & MOLINA Y VEDIA, L. 1989. A ras-related protein is phosphorylated and translocated by agonists that increase cAMP levels in human platelets. *Proc Natl Acad Sci U S A*, 86, 3131-4.
- LAU, T. L., DUA, V. & ULMER, T. S. 2008a. Structure of the integrin  $\alpha \text{IIb} \beta 3$  transmembrane segment. *J Biol Chem*, 283, 16162-8.
- LAU, T. L., KIM, C., GINSBERG, M. H. & ULMER, T. S. 2009. The structure of the integrin  $\alpha \text{IIb} \beta 3$  transmembrane complex explains integrin transmembrane signalling. *EMBO J*, 28, 1351-61.
- LAU, T. L., PARTRIDGE, A. W., GINSBERG, M. H. & ULMER, T. S. 2008b. Structure of the integrin  $\beta 3$  transmembrane segment in phospholipid bicelles and detergent micelles. *Biochemistry*, 47, 4008-16.
- LAUKAITIS, C. M., WEBB, D. J., DONAIS, K. & HORWITZ, A. F. 2001. Differential dynamics of  $\alpha 5$  integrin, paxillin, and  $\alpha$ -actinin during formation and disassembly of adhesions in migrating cells. *J Cell Biol*, 153, 1427-40.
- LAWSON, C., LIM, S. T., URYU, S., CHEN, X. L., CALDERWOOD, D. A. & SCHLAEPFER, D. D. 2012. FAK promotes recruitment of talin to nascent adhesions to control cell motility. *J Cell Biol*, 196, 223-32.
- LEE, H. S., BELLIN, R. M., WALKER, D. L., PATEL, B., POWERS, P., LIU, H., GARCIA-ALVAREZ, B., DE PEREDA, J. M., LIDDINGTON, R. C., VOLKMANN, N., HANEIN, D., CRITCHLEY, D. R. & ROBSON, R. M. 2004. Characterization of an actin-binding site within the talin FERM domain. *J Mol Biol*, 343, 771-84.
- LEE, H. S., LIM, C. J., PUZON-MCLAUGHLIN, W., SHATTIL, S. J. & GINSBERG, M. H. 2009. RIAM activates integrins by linking talin to ras GTPase membrane-targeting sequences. *J Biol Chem*, 284, 5119-27.
- LEFORT, C. T., ROSSAINT, J., MOSER, M., PETRICH, B. G., ZARBOCK, A., MONKLEY, S. J., CRITCHLEY, D. R., GINSBERG, M. H., FASSLER, R. & LEY, K. 2012. Distinct roles for talin-1 and kindlin-3 in LFA-1 extension and affinity regulation. *Blood*, 119, 4275-82.
- LEGATE, K. R., TAKAHASHI, S., BONAKDAR, N., FABRY, B., BOETTIGER, D., ZENT, R. & FASSLER, R. 2011. Integrin adhesion and force coupling are independently regulated by localized PtdIns(4,5)2 synthesis. *EMBO J*, 30, 4539-53.
- LEGATE, K. R., WICKSTROM, S. A. & FASSLER, R. 2009. Genetic and cell biological analysis of integrin outside-in signaling. *Genes Dev*, 23, 397-418.
- LEMKE, S. B., WEIDEMANN, T., COST, A. L., GRASHOFF, C. & SCHNORRER, F. 2019. A small proportion of Talin molecules transmit forces at developing muscle attachments in vivo. *PLoS Biol*, 17, e3000057.
- LEY, K., LAUDANNA, C., CYBULSKY, M. I. & NOURSHARGH, S. 2007. Getting to the site of inflammation: the leukocyte adhesion cascade updated. *Nat Rev Immunol*, 7, 678-89.
- LI, G., DU, X., VASS, W. C., PAPAGEORGE, A. G., LOWY, D. R. & QIAN, X. 2011. Full activity of the deleted in liver cancer 1 (DLC1) tumor suppressor depends on an LD-like motif that binds talin and focal adhesion kinase (FAK). *Proc Natl Acad Sci U S A*, 108, 17129-34.
- LI, H., DENG, Y., SUN, K., YANG, H., LIU, J., WANG, M., ZHANG, Z., LIN, J., WU, C., WEI, Z. & YU, C. 2017a. Structural basis of kindlin-mediated integrin recognition and activation. *Proc Natl Acad Sci U S A*, 114, 9349-9354.
- LI, J. & SPRINGER, T. A. 2018. Energy landscape differences among integrins establish the framework for understanding activation. *J Cell Biol*, 217, 397-412.



- LI, J., SU, Y., XIA, W., QIN, Y., HUMPHRIES, M. J., VESTWEBER, D., CABANAS, C., LU, C. & SPRINGER, T. A. 2017b. Conformational equilibria and intrinsic affinities define integrin activation. *EMBO J*, 36, 629-645.
- LI, Y., YAN, J., DE, P., CHANG, H. C., YAMAUCHI, A., CHRISTOPHERSON, K. W., 2ND, PARANAVITANA, N. C., PENG, X., KIM, C., MUNUGALAVADLA, V., KAPUR, R., CHEN, H., SHOU, W., STONE, J. C., KAPLAN, M. H., DINAUER, M. C., DURDEN, D. L. & QUILLIAM, L. A. 2007. Rap1a null mice have altered myeloid cell functions suggesting distinct roles for the closely related Rap1a and 1b proteins. *J Immunol*, 179, 8322-31.
- LINDEN, M., WARD, J. M. & CHERIAN, S. 2011. Hematopoietic and Lymphoid Tissues. *Comparative Anatomy and Histology: A Mouse and Human Atlas*, 309-338.
- LINDER, S. & AEPFELBACHER, M. 2003. Podosomes: adhesion hot-spots of invasive cells. *Trends Cell Biol*, 13, 376-85.
- LINDER, S. & WIESNER, C. 2016. Feel the force: Podosomes in mechanosensing. *Exp Cell Res*, 343, 67-72.
- LING, K., DOUGHMAN, R. L., FIRESTONE, A. J., BUNCE, M. W. & ANDERSON, R. A. 2002. Type I gamma phosphatidylinositol phosphate kinase targets and regulates focal adhesions. *Nature*, 420, 89-93.
- LOPEZ-COLOME, A. M., LEE-RIVERA, I., BENAVIDES-HIDALGO, R. & LOPEZ, E. 2017. Paxillin: a crossroad in pathological cell migration. *J Hematol Oncol*, 10, 50.
- LUO, B. H., SPRINGER, T. A. & TAKAGI, J. 2004. A specific interface between integrin transmembrane helices and affinity for ligand. *PLoS Biol*, 2, e153.
- LYULCHEVA, E., TAYLOR, E., MICHAEL, M., VEHLLOW, A., TAN, S., FLETCHER, A., KRAUSE, M. & BENNETT, D. 2008. Drosophila p115 and its mammalian ortholog lamellipodin activate serum response factor and promote cell proliferation. *Dev Cell*, 15, 680-90.
- M'RABET, L., COFFER, P., ZWARTKRUIS, F., FRANKE, B., SEGAL, A. W., KOENDERMAN, L. & BOS, J. L. 1998. Activation of the small GTPase rap1 in human neutrophils. *Blood*, 92, 2133-40.
- MA, H. X., SHU, Q. H., PAN, J. J., LIU, D., XU, G. L., LI, J. S., MA, J. L., JIA, W. D., YV, J. H. & GE, Y. S. 2015. Expression of Kindlin-1 in human hepatocellular carcinoma and its prognostic significance. *Tumour Biol*, 36, 4235-41.
- MACKINNON, A. C., QADOTA, H., NORMAN, K. R., MOERMAN, D. G. & WILLIAMS, B. D. 2002. C. elegans PAT-4/ILK functions as an adaptor protein within integrin adhesion complexes. *Curr Biol*, 12, 787-97.
- MAHAWITHITWONG, P., OHUCHIDA, K., IKENAGA, N., FUJITA, H., ZHAO, M., KOZONO, S., SHINDO, K., OHTSUKA, T., AISHIMA, S., MIZUMOTO, K. & TANAKA, M. 2013. Kindlin-1 expression is involved in migration and invasion of pancreatic cancer. *Int J Oncol*, 42, 1360-6.
- MAJUMDER, R., QUINN-ALLEN, M. A., KANE, W. H. & LENTZ, B. R. 2008. A phosphatidylserine binding site in factor Va C1 domain regulates both assembly and activity of the prothrombinase complex. *Blood*, 112, 2795-802.
- MALININ, N. L., PLOW, E. F. & BYZOVA, T. V. 2010. Kindlins in FERM adhesion. *Blood*, 115, 4011-7.
- MANEVICH-MENDELSON, E., FEIGELSON, S. W., PASVOLSKY, R., AKER, M., GRABOVSKY, V., SHULMAN, Z., KILIC, S. S., ROSENTHAL-ALLIERI, M. A., BEN-DOR, S., MORY, A., BERNARD, A., MOSER, M., ETZIONI, A. & ALON, R. 2009. Loss of Kindlin-3 in LAD-III eliminates LFA-1 but not VLA-4 adhesiveness developed under shear flow conditions. *Blood*, 114, 2344-53.
- MANSO, A. M., LI, R., MONKLEY, S. J., CRUZ, N. M., ONG, S., LAO, D. H., KOSHMAN, Y. E., GU, Y., PETERSON, K. L., CHEN, J., ABEL, E. D., SAMAREL, A. M., CRITCHLEY, D. R. & ROSS, R. S. 2013. Talin1 has unique expression versus talin 2 in the heart and modifies the hypertrophic response to pressure overload. *J Biol Chem*, 288, 4252-64.



- MANSO, A. M., OKADA, H., SAKAMOTO, F. M., MORENO, E., MONKLEY, S. J., LI, R., CRITCHLEY, D. R. & ROSS, R. S. 2017. Loss of mouse cardiomyocyte talin-1 and talin-2 leads to beta-1 integrin reduction, costameric instability, and dilated cardiomyopathy. *Proc Natl Acad Sci U S A*, 114, E6250-E6259.
- MARTEL, V., RACAUD-SULTAN, C., DUPE, S., MARIE, C., PAULHE, F., GALMICHE, A., BLOCK, M. R. & ALBIGES-RIZO, C. 2001. Conformation, localization, and integrin binding of talin depend on its interaction with phosphoinositides. *J Biol Chem*, 276, 21217-27.
- MCCLEVERTY, C. J., LIN, D. C. & LIDDINGTON, R. C. 2007. Structure of the PTB domain of tensin1 and a model for its recruitment to fibrillar adhesions. *Protein Sci*, 16, 1223-9.
- MEDVINSKY, A. & DZIERZAK, E. 1996. Definitive hematopoiesis is autonomously initiated by the AGM region. *Cell*, 86, 897-906.
- MERSICH, A. T., MILLER, M. R., CHKOURKO, H. & BLYSTONE, S. D. 2010. The formin FRL1 (FMNL1) is an essential component of macrophage podosomes. *Cytoskeleton (Hoboken)*, 67, 573-85.
- MILLER, M. W., BASRA, S., KULP, D. W., BILLINGS, P. C., CHOI, S., BEAVERS, M. P., MCCARTY, O. J., ZOU, Z., KAHN, M. L., BENNETT, J. S. & DEGRADO, W. F. 2009. Small-molecule inhibitors of integrin alpha2beta1 that prevent pathological thrombus formation via an allosteric mechanism. *Proc Natl Acad Sci U S A*, 106, 719-24.
- MITROULIS, I., ALEXAKI, V. I., KOURTZELIS, I., ZIOGAS, A., HAJISHENGALLIS, G. & CHAVAKIS, T. 2015. Leukocyte integrins: role in leukocyte recruitment and as therapeutic targets in inflammatory disease. *Pharmacol Ther*, 147, 123-135.
- MIZUTANI, K., MIKI, H., HE, H., MARUTA, H. & TAKENAWA, T. 2002. Essential role of neural Wiskott-Aldrich syndrome protein in podosome formation and degradation of extracellular matrix in src-transformed fibroblasts. *Cancer Res*, 62, 669-74.
- MOLONY, L. & BURRIDGE, K. 1985. Molecular shape and self-association of vinculin and metavinculin. *J Cell Biochem*, 29, 31-6.
- MONKLEY, S. J., ZHOU, X. H., KINSTON, S. J., GIBLETT, S. M., HEMMINGS, L., PRIDDLE, H., BROWN, J. E., PRITCHARD, C. A., CRITCHLEY, D. R. & FASSLER, R. 2000. Disruption of the talin gene arrests mouse development at the gastrulation stage. *Dev Dyn*, 219, 560-74.
- MONTANEZ, E., USSAR, S., SCHIFFERER, M., BOSL, M., ZENT, R., MOSER, M. & FASSLER, R. 2008. Kindlin-2 controls bidirectional signaling of integrins. *Genes Dev*, 22, 1325-30.
- MORETTI, F. A., KLAPPROTH, S., RUPPERT, R., MARGRAF, A., WEBER, J., PICK, R., SCHEIERMANN, C., SPERANDIO, M., FASSLER, R. & MOSER, M. 2018. Differential requirement of kindlin-3 for T cell progenitor homing to the non-vascularized and vascularized thymus. *Elife*, 7.
- MORETTI, F. A., MOSER, M., LYCK, R., ABADIER, M., RUPPERT, R., ENGELHARDT, B. & FASSLER, R. 2013. Kindlin-3 regulates integrin activation and adhesion reinforcement of effector T cells. *Proc Natl Acad Sci U S A*, 110, 17005-10.
- MORRISON, V. L., UOTILA, L. M., LLORT ASENS, M., SAVINKO, T. & FAGERHOLM, S. C. 2015. Optimal T Cell Activation and B Cell Antibody Responses In Vivo Require the Interaction between Leukocyte Function-Associated Antigen-1 and Kindlin-3. *J Immunol*, 195, 105-15.
- MORY, A., FEIGELSON, S. W., YARALI, N., KILIC, S. S., BAYHAN, G. I., GERSHONI-BARUCH, R., ETZIONI, A. & ALON, R. 2008. Kindlin-3: a new gene involved in the pathogenesis of LAD-III. *Blood*, 112, 2591.
- MOSER, M., BAUER, M., SCHMID, S., RUPPERT, R., SCHMIDT, S., SIXT, M., WANG, H. V., SPERANDIO, M. & FASSLER, R. 2009a. Kindlin-3 is required for beta2 integrin-mediated leukocyte adhesion to endothelial cells. *Nat Med*, 15, 300-5.
- MOSER, M., LEGATE, K. R., ZENT, R. & FASSLER, R. 2009b. The tail of integrins, talin, and kindlins. *Science*, 324, 895-9.
- MOSER, M., NIESWANDT, B., USSAR, S., POZGAJOVA, M. & FASSLER, R. 2008. Kindlin-3 is essential for integrin activation and platelet aggregation. *Nat Med*, 14, 325-30.



- MUELLER, H., STADTMANN, A., VAN AKEN, H., HIRSCH, E., WANG, D., LEY, K. & ZARBOCK, A. 2010. Tyrosine kinase Btk regulates E-selectin-mediated integrin activation and neutrophil recruitment by controlling phospholipase C (PLC) gamma2 and PI3Kgamma pathways. *Blood*, 115, 3118-27.
- MULLER, W. A. 2003. Leukocyte-endothelial-cell interactions in leukocyte transmigration and the inflammatory response. *Trends Immunol*, 24, 327-34.
- NAYAL, A., WEBB, D. J., BROWN, C. M., SCHAEFER, E. M., VICENTE-MANZANARES, M. & HORWITZ, A. R. 2006. Paxillin phosphorylation at Ser273 localizes a GIT1-PIX-PAK complex and regulates adhesion and protrusion dynamics. *J Cell Biol*, 173, 587-9.
- NI, T., KALLI, A. C., NAUGHTON, F. B., YATES, L. A., NANEH, O., KOZOROG, M., ANDERLUH, G., SANSOM, M. S. & GILBERT, R. J. 2017. Structure and lipid-binding properties of the kindlin-3 pleckstrin homology domain. *Biochem J*, 474, 539-556.
- NIESWANDT, B., MOSER, M., PLEINES, I., VARGA-SZABO, D., MONKLEY, S., CRITCHLEY, D. & FASSLER, R. 2007. Loss of talin1 in platelets abrogates integrin activation, platelet aggregation, and thrombus formation in vitro and in vivo. *J Exp Med*, 204, 3113-8.
- NIEWOHNER, J., WEBER, I., MANIAK, M., MULLER-TAUBENBERGER, A. & GERISCH, G. 1997. Talin-null cells of Dictyostelium are strongly defective in adhesion to particle and substrate surfaces and slightly impaired in cytokinesis. *J Cell Biol*, 138, 349-61.
- NISSINEN, L., PENTIKAINEN, O. T., JOUPPILA, A., KAPYLA, J., OJALA, M., NIEMINEN, J., LIPSANEN, A., LAPPALAINEN, H., ECKES, B., JOHNSON, M. S., LASSILA, R., MARJAMAKI, A. & HEINO, J. 2010. A small-molecule inhibitor of integrin alpha2 beta1 introduces a new strategy for antithrombotic therapy. *Thromb Haemost*, 103, 387-97.
- NORDENFELT, P., ELLIOTT, H. L. & SPRINGER, T. A. 2016. Coordinated integrin activation by actin-dependent force during T-cell migration. *Nat Commun*, 7, 13119.
- NOURSHARGH, S. & ALON, R. 2014. Leukocyte Migration into Inflamed Tissues. *Immunity*, 41, 694-707.
- OHBA, Y., IKUTA, K., OGURA, A., MATSUDA, J., MOCHIZUKI, N., NAGASHIMA, K., KUOKAWA, K., MAYER, B. J., MAKI, K., MIYAZAKI, J. & MATSUDA, M. 2001. Requirement for C3G-dependent Rap1 activation for cell adhesion and embryogenesis. *EMBO J*, 20, 3333-41.
- OXLEY, C. L., ANTHIS, N. J., LOWE, E. D., VAKONAKIS, I., CAMPBELL, I. D. & WEGENER, K. L. 2008. An integrin phosphorylation switch: the effect of beta3 integrin tail phosphorylation on Dok1 and talin binding. *J Biol Chem*, 283, 5420-6.
- PANZER, L., TRUBE, L., KLOSE, M., JOOSTEN, B., SLOTMAN, J., CAMBI, A. & LINDER, S. 2016. The formins FHOD1 and INF2 regulate inter- and intra-structural contractility of podosomes. *J Cell Sci*, 129, 298-313.
- PAPAGRIGORIOU, E., GINGRAS, A. R., BARSUKOV, I. L., BATE, N., FILLINGHAM, I. J., PATEL, B., FRANK, R., ZIEGLER, W. H., ROBERTS, G. C., CRITCHLEY, D. R. & EMSLEY, J. 2004. Activation of a vinculin-binding site in the talin rod involves rearrangement of a five-helix bundle. *EMBO J*, 23, 2942-51.
- PETERS, L. L., ZHANG, W., LAMBERT, A. J., BRUGNARA, C., CHURCHILL, G. A. & PLATT, O. S. 2005. Quantitative trait loci for baseline white blood cell count, platelet count, and mean platelet volume. *Mamm Genome*, 16, 749-63.
- PETRICH, B. G., MARCHESE, P., RUGGERI, Z. M., SPIESS, S., WEICHERT, R. A., YE, F., TIEDT, R., SKODA, R. C., MONKLEY, S. J., CRITCHLEY, D. R. & GINSBERG, M. H. 2007. Talin is required for integrin-mediated platelet function in hemostasis and thrombosis. *J Exp Med*, 204, 3103-11.
- PFAFF, M. & JURDIC, P. 2001. Podosomes in osteoclast-like cells: structural analysis and cooperative roles of paxillin, proline-rich tyrosine kinase 2 (Pyk2) and integrin alphaVbeta3. *J Cell Sci*, 114, 2775-86.
- PHILLIPSON, M., HEIT, B., COLARUSSO, P., LIU, L. X., BALLANTYNE, C. M. & KUBES, P. 2006. Intraluminal crawling of neutrophils to emigration sites: a molecularly distinct process



- from adhesion in the recruitment cascade. *Journal of Experimental Medicine*, 203, 2569-2575.
- PILLAY, J., DEN BRABER, I., VRISEKOOP, N., KWAST, L. M., DE BOER, R. J., BORGHANS, J. A., TESSELAAR, K. & KOENDERMAN, L. 2010. In vivo labeling with 2H<sub>2</sub>O reveals a human neutrophil lifespan of 5.4 days. *Blood*, 116, 625-7.
- PLAK, K., POTS, H., VAN HAASTERT, P. J. & KORTHOLT, A. 2016. Direct Interaction between TalinB and Rap1 is necessary for adhesion of Dictyostelium cells. *BMC Cell Biol*, 17, 1.
- PLUSKOTA, E., DOWLING, J. J., GORDON, N., GOLDEN, J. A., SZPAK, D., WEST, X. Z., NESTOR, C., MA, Y. Q., BIALKOWSKA, K., BYZOVA, T. & PLOW, E. F. 2011. The integrin coactivator kindlin-2 plays a critical role in angiogenesis in mice and zebrafish. *Blood*, 117, 4978-87.
- PRAEKELT, U., KOPP, P. M., REHM, K., LINDER, S., BATE, N., PATEL, B., DEBRAND, E., MANSO, A. M., ROSS, R. S., CONTI, F., ZHANG, M. Z., HARRIS, R. C., ZENT, R., CRITCHLEY, D. R. & MONKLEY, S. J. 2012. New isoform-specific monoclonal antibodies reveal different sub-cellular localisations for talin1 and talin2. *Eur J Cell Biol*, 91, 180-91.
- PUGA, I., COLS, M., BARRA, C. M., HE, B., CASSIS, L., GENTILE, M., COMERMA, L., CHORNY, A., SHAN, M. M., XU, W. F., MAGRI, G., KNOWLES, D. M., TAM, W., CHIU, A., BUSSEL, J. B., SERRANO, S., LORENTE, J. A., BELLOSILLO, B., LLORETA, J., JUANPERE, N., ALAMEDA, F., BARO, T., DE HEREDIA, R. D., TORAN, N., CATALA, A., TORREBADELL, M., FORTUNY, C., CUSI, V., CARRERAS, C., DIAZ, G. A., BLANDER, J. M., FARBER, C. M., SILVESTRI, G., CUNNINGHAM-RUNDLES, C., CALVILLO, M., DUFOUR, C., NOTARANGELO, L. D., LOUGARIS, V., PLEBANI, A., CASANOVA, J. L., GANAL, S. C., DIEFENBACH, A., AROSTEGUI, J. I., JUAN, M., YAGUE, J., MAHLAOU, N., DONADIEU, J., CHEN, K. & CERUTTI, A. 2012. B cell-helper neutrophils stimulate the diversification and production of immunoglobulin in the marginal zone of the spleen. *Nature Immunology*, 13, 170-180.
- QU, H., TU, Y., SHI, X., LARJAVA, H., SALEEM, M. A., SHATTIL, S. J., FUKUDA, K., QIN, J., KRETZLER, M. & WU, C. 2011. Kindlin-2 regulates podocyte adhesion and fibronectin matrix deposition through interactions with phosphoinositides and integrins. *J Cell Sci*, 124, 879-91.
- RINGER, P., WEISSEL, A., COST, A. L., FREIKAMP, A., SABASS, B., MEHLICH, A., TRAMIER, M., RIEF, M. & GRASHOFF, C. 2017. Multiplexing molecular tension sensors reveals piconewton force gradient across talin-1. *Nature Methods*, 14, 1090-+.
- RODIUS, S., CHALOIN, O., MOES, M., SCHAFFNER-RECKINGER, E., LANDRIEU, I., LIPPENS, G., LIN, M., ZHANG, J. & KIEFFER, N. 2008. The talin rod IBS2 alpha-helix interacts with the beta3 integrin cytoplasmic tail membrane-proximal helix by establishing charge complementary salt bridges. *J Biol Chem*, 283, 24212-23.
- ROGALSKI, T. M., MULLEN, G. P., GILBERT, M. M., WILLIAMS, B. D. & MOERMAN, D. G. 2000. The UNC-112 gene in *Caenorhabditis elegans* encodes a novel component of cell-matrix adhesion structures required for integrin localization in the muscle cell membrane. *J Cell Biol*, 150, 253-64.
- ROGNONI, E., RUPPERT, R. & FASSLER, R. 2016. The kindlin family: functions, signaling properties and implications for human disease. *J Cell Sci*, 129, 17-27.
- ROGNONI, E., WIDMAIER, M., JAKOBSON, M., RUPPERT, R., USSAR, S., KATSOUKRI, D., BOTTCHE, R. T., LAI-CHEONG, J. E., RIFKIN, D. B., MCGRATH, J. A. & FASSLER, R. 2014. Kindlin-1 controls Wnt and TGF-beta availability to regulate cutaneous stem cell proliferation. *Nat Med*, 20, 350-9.
- SADLER, E., KLAUSEGGER, A., MUSS, W., DEINSBERGER, U., POHLA-GUBO, G., LAIMER, M., LANSCHUETZER, C., BAUER, J. W. & HINTNER, H. 2006. Novel KIND1 gene mutation in Kindler syndrome with severe gastrointestinal tract involvement. *Arch Dermatol*, 142, 1619-24.
- SAKAI, T., LI, S. H., DOCHEVA, D., GRASHOFF, C., SAKAI, K., KOSTKA, G., BRAUN, A., PFEIFER, A., YURCHENCO, P. D. & FASSLER, R. 2003. Integrin-linked kinase (ILK) is required for



- polarizing the epiblast, cell adhesion, and controlling actin accumulation. *Genes & Development*, 17, 926-940.
- SALTEL, F., MORTIER, E., HYTONEN, V. P., JACQUIER, M. C., ZIMMERMANN, P., VOGEL, V., LIU, W. & WEHRLE-HALLER, B. 2009. New PI(4,5)P<sub>2</sub>- and membrane proximal integrin-binding motifs in the talin head control beta3-integrin clustering. *J Cell Biol*, 187, 715-31.
- SAMANNA, V., MA, T., MAK, T. W., ROGERS, M. & CHELLAIAH, M. A. 2007. Actin polymerization modulates CD44 surface expression, MMP-9 activation, and osteoclast function. *J Cell Physiol*, 213, 710-20.
- SAMAREL, A. M. 2005. Costameres, focal adhesions, and cardiomyocyte mechanotransduction. *Am J Physiol Heart Circ Physiol*, 289, H2291-301.
- SANZ, M. J. & KUBES, P. 2012. Neutrophil-active chemokines in in vivo imaging of neutrophil trafficking. *Eur J Immunol*, 42, 278-83.
- SARVI, S., PATEL, H., LI, J., DODD, G. L., CREEDON, H., MUIR, M., WARD, J., DAWSON, J. C., LEE, M., CULLEY, J., SALTER, D. M., SIMS, A. H., BYRON, A. & BRUNTON, V. G. 2018. Kindlin-1 Promotes Pulmonary Breast Cancer Metastasis. *Cancer Res*, 78, 1484-1496.
- SAVAGE, B., ALMUS-JACOBS, F. & RUGGERI, Z. M. 1998. Specific synergy of multiple substrate-receptor interactions in platelet thrombus formation under flow. *Cell*, 94, 657-66.
- SCHIEMER, J., BOHM, A., LIN, L., MERRILL-SKOLOFF, G., FLAUMENHAFT, R., HUANG, J. S., LE BRETON, G. C. & CHISHTI, A. H. 2016. Galpha13 Switch Region 2 Relieves Talin Autoinhibition to Activate alphaIIb beta3 Integrin. *J Biol Chem*, 291, 26598-26612.
- SCHILLER, H. B., FRIEDEL, C. C., BOULEGUE, C. & FASSLER, R. 2011. Quantitative proteomics of the integrin adhesome show a myosin II-dependent recruitment of LIM domain proteins. *EMBO Rep*, 12, 259-66.
- SCHILLER, H. B., HERMANN, M. R., POLLEUX, J., VIGNAUD, T., ZANIVAN, S., FRIEDEL, C. C., SUN, Z., RADUCANU, A., GOTTSCHALK, K. E., THERY, M., MANN, M. & FASSLER, R. 2013. beta1- and alpha-v-class integrins cooperate to regulate myosin II during rigidity sensing of fibronectin-based microenvironments. *Nat Cell Biol*, 15, 625-36.
- SCHMIDT, S., NAKCHBANDI, I., RUPPERT, R., KAWELKE, N., HESS, M. W., PFALLER, K., JURDIC, P., FASSLER, R. & MOSER, M. 2011. Kindlin-3-mediated signaling from multiple integrin classes is required for osteoclast-mediated bone resorption. *J Cell Biol*, 192, 883-97.
- SCHRAW, T. D., LEMONS, P. P., DEAN, W. L. & WHITEHEART, S. W. 2003. A role for Sec1/Munc18 proteins in platelet exocytosis. *Biochem J*, 374, 207-17.
- SCHWANDER, M., LEU, M., STUMM, M., DORCHIES, O. M., RUEGG, U. T., SCHITTNY, J. & MULLER, U. 2003. Beta1 integrins regulate myoblast fusion and sarcomere assembly. *Dev Cell*, 4, 673-85.
- SENETAR, M. A. & MCCANN, R. O. 2005. Gene duplication and functional divergence during evolution of the cytoskeletal linker protein talin. *Gene*, 362, 141-52.
- SENETAR, M. A., MONCMAN, C. L. & MCCANN, R. O. 2007. Talin2 is induced during striated muscle differentiation and is targeted to stable adhesion complexes in mature muscle. *Cell Motil Cytoskeleton*, 64, 157-73.
- SERRELS, B., SERRELS, A., BRUNTON, V. G., HOLT, M., MCLEAN, G. W., GRAY, C. H., JONES, G. E. & FRAME, M. C. 2007. Focal adhesion kinase controls actin assembly via a FERM-mediated interaction with the Arp2/3 complex. *Nature Cell Biology*, 9, 1046-U15.
- SHEPPARD, D. 2000. In vivo functions of integrins: lessons from null mutations in mice. *Matrix Biol*, 19, 203-9.
- SHIMAOKA, M., LU, C., PALFRAMAN, R. T., VON ANDRIAN, U. H., MCCORMACK, A., TAKAGI, J. & SPRINGER, T. A. 2001. Reversibly locking a protein fold in an active conformation with a disulfide bond: integrin alphaL I domains with high affinity and antagonist activity in vivo. *Proc Natl Acad Sci U S A*, 98, 6009-14.



- SIEGEL, D. H., ASHTON, G. H. S., PENAGOS, H. G., LEE, J. V., FEILER, H. S., WILHELMSSEN, K. C., SOUTH, A. P., SMITH, F. J. D., PRESCOTT, A. R., WESSAGOWIT, V., OYAMA, N., AKIYAMA, M., AL ABOUD, D., AL ABOUD, K., AL GITHAMI, A., AL HAWSAWI, K., AL ISMAILY, A., AL-SUWAID, R., ATHERTON, D. J., CAPUTO, R., FINE, J. D., FRIEDEN, I. J., FUCHS, E., HABER, R. M., HARADA, T., KITAJIMA, Y., MALLORY, S. B., OGAWA, H., SAHIN, S., SHIMIZU, H., SUGA, Y., TADINI, G., TSUCHIYA, K., WIEBE, C. B., WOJNAROWSKA, F., ZAGHLOUL, A. B., HAMADA, T., MALLIPEDDI, R., EADY, R. A. J., MCLEAN, W. H. I., MCGRATH, J. A. & EPSTEIN, E. H. 2003. Loss of kindlin-1, a human homolog of the *Caenorhabditis elegans* actin-extracellular-matrix linker protein UNC-112, causes Kindler syndrome. *American Journal of Human Genetics*, 73, 174-187.
- SIMONSON, W. T., FRANCO, S. J. & HUTTENLOCHER, A. 2006. Talin1 regulates TCR-mediated LFA-1 function. *J Immunol*, 177, 7707-14.
- SIN, S., BONIN, F., PETIT, V., MESEURE, D., LALLEMAND, F., BIECHE, I., BELLAHCENE, A., CASTRONOVO, V., DE WEVER, O., GESPACH, C., LIDEREAU, R. & DRIOUCH, K. 2011. Role of the Focal Adhesion Protein Kindlin-1 in Breast Cancer Growth and Lung Metastasis. *Journal of the National Cancer Institute*, 103, 1323-1337.
- SIXT, M., HALLMANN, R., WENDLER, O., SCHARFFETTER-KOCHANKE, K. & SOROKIN, L. M. 2001. Cell adhesion and migration properties of beta 2-integrin negative polymorphonuclear granulocytes on defined extracellular matrix molecules. Relevance for leukocyte extravasation. *J Biol Chem*, 276, 18878-87.
- SMOLENSKI, A. 2012. Novel roles of cAMP/cGMP-dependent signaling in platelets. *J Thromb Haemost*, 10, 167-76.
- SONG, X., YANG, J., HIRBAWI, J., YE, S., PERERA, H. D., GOKSOY, E., DWIVEDI, P., PLOW, E. F., ZHANG, R. & QIN, J. 2012. A novel membrane-dependent on/off switch mechanism of talin FERM domain at sites of cell adhesion. *Cell Res*, 22, 1533-45.
- SOSSEY-ALAOUI, K., PLUSKOTA, E., DAVULURI, G., BIALKOWSKA, K., DAS, M., SZPAK, D., LINDNER, D. J., DOWNS-KELLY, E., THOMPSON, C. L. & PLOW, E. F. 2014. Kindlin-3 enhances breast cancer progression and metastasis by activating Twist-mediated angiogenesis. *FASEB J*, 28, 2260-71.
- SRINIVASAN, S., SCHIEMER, J., ZHANG, X., CHISHTI, A. H. & LE BRETON, G. C. 2015. Galpha13 Switch Region 2 Binds to the Talin Head Domain and Activates alphaIIb beta3 Integrin in Human Platelets. *J Biol Chem*, 290, 25129-39.
- STADTMANN, A., BRINKHAUS, L., MUELLER, H., ROSSAINT, J., BOLOMINI-VITTORI, M., BERGMEIER, W., VAN AKEN, H., WAGNER, D. D., LAUDANNA, C., LEY, K. & ZARBOCK, A. 2011. Rap1a activation by CalDAG-GEFI and p38 MAPK is involved in E-selectin-dependent slow leukocyte rolling. *Eur J Immunol*, 41, 2074-85.
- STANCHI, F., GRASHOFF, C., YONGA, C. F. N., GRALL, D., FASSLER, R. & VAN OBBERGHEN-SCHILLING, E. 2009. Molecular dissection of the ILK-PINCH-parvin triad reveals a fundamental role for the ILK kinase domain in the late stages of focal-adhesion maturation. *Journal of Cell Science*, 122, 1800-1811.
- STEFANINI, L. & BERGMEIER, W. 2010. CalDAG-GEFI and platelet activation. *Platelets*, 21, 239-43.
- STEFANINI, L., LEE, R. H., PAUL, D. S., O'SHAUGHNESSY, E. C., GHALLOUSSI, D., JONES, C. I., BOULAFTALI, Y., POE, K. O., PIATT, R., KECELE, D. O., CARON, K. M., HAHN, K. M., GIBBINS, J. M. & BERGMEIER, W. 2018. Functional redundancy between RAP1 isoforms in murine platelet production and function. *Blood*, 132, 1951-1962.
- STEFANINI, L., PAUL, D. S., ROBLEDI, R. F., CHAN, E. R., GETZ, T. M., CAMPBELL, R. A., KECELE, D. O., CASARI, C., PIATT, R., CARON, K. M., MACKMAN, N., WEYRICH, A. S., PARROTT, M. C., BOULAFTALI, Y., ADAMS, M. D., PETERS, L. L. & BERGMEIER, W. 2015. RASA3 is a critical inhibitor of RAP1-dependent platelet activation. *J Clin Invest*, 125, 1419-32.



- STRITT, S., WOLF, K., LORENZ, V., VOGTLE, T., GUPTA, S., BOSL, M. R. & NIESWANDT, B. 2015. Rap1-GTP-interacting adaptor molecule (RIAM) is dispensable for platelet integrin activation and function in mice. *Blood*, 125, 219-22.
- SU, W., WYNNE, J., PINHEIRO, E. M., STRAZZA, M., MOR, A., MONTENONT, E., BERGER, J., PAUL, D. S., BERGMEIER, W., GERTLER, F. B. & PHILIPS, M. R. 2015. Rap1 and its effector RIAM are required for lymphocyte trafficking. *Blood*, 126, 2695-703.
- SUN, N., CRITCHLEY, D. R., PAULIN, D., LI, Z. & ROBSON, R. M. 2008. Identification of a repeated domain within mammalian alpha-synemin that interacts directly with talin. *Exp Cell Res*, 314, 1839-49.
- SUN, Z., COSTELL, M. & FASSLER, R. 2019. Integrin activation by talin, kindlin and mechanical forces. *Nat Cell Biol*, 21, 25-31.
- SUN, Z., LAMBACHER, A. & FASSLER, R. 2014. Nascent adhesions: from fluctuations to a hierarchical organization. *Curr Biol*, 24, R801-3.
- SUN, Z., TSENG, H. Y., TAN, S., SENER, F., KURZAWA, L., DEDDEN, D., MIZUNO, N., WASIK, A. A., THERY, M., DUNN, A. R. & FASSLER, R. 2016. Kank2 activates talin, reduces force transduction across integrins and induces central adhesion formation. *Nat Cell Biol*, 18, 941-53.
- SVENSSON, L., HOWARTH, K., MCDOWALL, A., PATZAK, I., EVANS, R., USSAR, S., MOSER, M., METIN, A., FRIED, M., TOMLINSON, I. & HOGG, N. 2009. Leukocyte adhesion deficiency-III is caused by mutations in KINDLIN3 affecting integrin activation. *Nat Med*, 15, 306-12.
- TANENTZAPF, G. & BROWN, N. H. 2006. An interaction between integrin and the talin FERM domain mediates integrin activation but not linkage to the cytoskeleton. *Nat Cell Biol*, 8, 601-6.
- TANENTZAPF, G., MARTIN-BERMUDO, M. D., HICKS, M. S. & BROWN, N. H. 2006. Multiple factors contribute to integrin-talin interactions in vivo. *J Cell Sci*, 119, 1632-44.
- TEHRANI, S., FACCIO, R., CHANDRASEKAR, I., ROSS, F. P. & COOPER, J. A. 2006. Cortactin has an essential and specific role in osteoclast actin assembly. *Mol Biol Cell*, 17, 2882-95.
- TENG, T. S., JI, A. L., JI, X. Y. & LI, Y. Z. 2017. Neutrophils and Immunity: From Bactericidal Action to Being Conquered. *Journal of Immunology Research*.
- THEODOSIOU, M., WIDMAIER, M., BOTTCHE, R. T., ROGNONI, E., VEELDERS, M., BHARADWAJ, M., LAMBACHER, A., AUSTEN, K., MULLER, D. J., ZENT, R. & FASSLER, R. 2016. Kindlin-2 cooperates with talin to activate integrins and induces cell spreading by directly binding paxillin. *Elife*, 5, e10130.
- TOFTS, P. S., CHEVASSUT, T., CUTAJAR, M., DOWELL, N. G. & PETERS, A. M. 2011. Doubts concerning the recently reported human neutrophil lifespan of 5.4 days. *Blood*, 117, 6050-2; author reply 6053-4.
- TRONIK-LE ROUX, D., ROULLOT, V., POIJOL, C., KORTULEWSKI, T., NURDEN, P. & MARGUERIE, G. 2000. Thrombasthenic mice generated by replacement of the integrin alpha(IIb) gene: demonstration that transcriptional activation of this megakaryocytic locus precedes lineage commitment. *Blood*, 96, 1399-408.
- TSUJIOKA, M., MACHESKY, L. M., COLE, S. L., YAHATA, K. & INOUE, K. 1999. A unique talin homologue with a villin headpiece-like domain is required for multicellular morphogenesis in Dictyostelium. *Current Biology*, 9, 389-392.
- TSUJIOKA, M., YOSHIDA, K. & INOUE, K. 2004. Talin B is required for force transmission in morphogenesis of Dictyostelium. *Embo Journal*, 23, 2216-2225.
- TSUJIOKA, M., YOSHIDA, K., NAGASAKI, A., YONEMURA, S., MULLER-TAUBENBERGER, A. & UYEDA, T. Q. 2008. Overlapping functions of the two talin homologues in Dictyostelium. *Eukaryot Cell*, 7, 906-16.
- TU, Y., WU, S., SHI, X., CHEN, K. & WU, C. 2003. Migfilin and Mig-2 link focal adhesions to filamin and the actin cytoskeleton and function in cell shape modulation. *Cell*, 113, 37-47.



- ULMER, T. S. 2010. Structural basis of transmembrane domain interactions in integrin signaling. *Cell Adh Migr*, 4, 243-8.
- ULUCAN, C., WANG, X., BALJINNYAM, E., BAI, Y., OKUMURA, S., SATO, M., MINAMISAWA, S., HIROTANI, S. & ISHIKAWA, Y. 2007. Developmental changes in gene expression of Epac and its upregulation in myocardial hypertrophy. *Am J Physiol Heart Circ Physiol*, 293, H1662-72.
- USSAR, S., MOSER, M., WIDMAIER, M., ROGNONI, E., HARRER, C., GENZEL-BOROVICZENY, O. & FASSLER, R. 2008. Loss of Kindlin-1 causes skin atrophy and lethal neonatal intestinal epithelial dysfunction. *PLoS Genet*, 4, e1000289.
- USSAR, S., WANG, H. V., LINDER, S., FASSLER, R. & MOSER, M. 2006. The Kindlins: subcellular localization and expression during murine development. *Exp Cell Res*, 312, 3142-51.
- VALDIVIA, M., VEGA-MACAYA, F. & OLGUIN, P. 2017. Mechanical Control of Myotendinous Junction Formation and Tendon Differentiation during Development. *Front Cell Dev Biol*, 5, 26.
- VAN AUDENHOVE, I., DEBEUF, N., BOUCHERIE, C. & GETTEMANS, J. 2015. Fascin actin bundling controls podosome turnover and disassembly while cortactin is involved in podosome assembly by its SH3 domain in THP-1 macrophages and dendritic cells. *Biochim Biophys Acta*, 1853, 940-52.
- VAN DEN BOUT, I. & DIVECHA, N. 2009. PIP5K-driven PtdIns(4,5)P<sub>2</sub> synthesis: regulation and cellular functions. *J Cell Sci*, 122, 3837-50.
- VAN DER FLIER, A. & SONNENBERG, A. 2001. Function and interactions of integrins. *Cell Tissue Res*, 305, 285-98.
- VANDERPLOEG, J. & JACOBS, J. R. 2015. Talin is required to position and expand the luminal domain of the Drosophila heart tube. *Dev Biol*, 405, 189-201.
- VARGA-SZABO, D., PLEINES, I. & NIESWANDT, B. 2008. Cell adhesion mechanisms in platelets. *Arterioscler Thromb Vasc Biol*, 28, 403-12.
- VEILLAT, V., SPUUL, P., DAUBON, T., EGANA, I., KRAMER, I. & GENOT, E. 2015. Podosomes: Multipurpose organelles? *Int J Biochem Cell Biol*, 65, 52-60.
- VERSTEEG, H. H., HEEMSKERK, J. W., LEVI, M. & REITSMA, P. H. 2013. New fundamentals in hemostasis. *Physiol Rev*, 93, 327-58.
- WALCHECK, B., MOORE, K. L., MCEVER, R. P. & KISHIMOTO, T. K. 1996. Neutrophil-neutrophil interactions under hydrodynamic shear stress involve L-selectin and PSGL-1. A mechanism that amplifies initial leukocyte accumulation of P-selectin in vitro. *J Clin Invest*, 98, 1081-7.
- WALKER, J. L., FOURNIER, A. K. & ASSOIAN, R. K. 2005. Regulation of growth factor signaling and cell cycle progression by cell adhesion and adhesion-dependent changes in cellular tension. *Cytokine Growth Factor Rev*, 16, 395-405.
- WANG, L., SHEN, W., LEI, S., MATUS, D., SHERWOOD, D. & WANG, Z. 2014. MIG-10 (Lamellipodin) stabilizes invading cell adhesion to basement membrane and is a negative transcriptional target of EGL-43 in *C. elegans*. *Biochem Biophys Res Commun*, 452, 328-33.
- WANG, S., VOISIN, M. B., LARBI, K. Y., DANGERFIELD, J., SCHEIERMANN, C., TRAN, M., MAXWELL, P. H., SOROKIN, L. & NOURSHARGH, S. 2006. Venular basement membranes contain specific matrix protein low expression regions that act as exit points for emigrating neutrophils. *J Exp Med*, 203, 1519-32.
- WANG, S., WATANABE, T., MATSUZAWA, K., KATSUMI, A., KAKENO, M., MATSUI, T., YE, F., SATO, K., MURASE, K., SUGIYAMA, I., KIMURA, K., MIZOGUCHI, A., GINSBERG, M. H., COLLARD, J. G. & KAIBUCHI, K. 2012. Tiam1 interaction with the PAR complex promotes talin-mediated Rac1 activation during polarized cell migration. *J Cell Biol*, 199, 331-45.



- WANG, Y., LIAN, L., GOLDEN, J. A., MORRISEY, E. E. & ABRAMS, C. S. 2007. PIP5KI gamma is required for cardiovascular and neuronal development. *Proc Natl Acad Sci U S A*, 104, 11748-53.
- WATANABE, N., BODIN, L., PANDEY, M., KRAUSE, M., COUGHLIN, S., BOUSSIOTIS, V. A., GINSBERG, M. H. & SHATTIL, S. J. 2008. Mechanisms and consequences of agonist-induced talin recruitment to platelet integrin  $\alpha\text{IIb}\beta\text{3}$ . *J Cell Biol*, 181, 1211-22.
- WEBB, D. J., DONAIS, K., WHITMORE, L. A., THOMAS, S. M., TURNER, C. E., PARSONS, J. T. & HORWITZ, A. F. 2004. FAK-Src signalling through paxillin, ERK and MLCK regulates adhesion disassembly. *Nat Cell Biol*, 6, 154-61.
- WEHRLE-HALLER, B. 2012. Structure and function of focal adhesions. *Curr Opin Cell Biol*, 24, 116-24.
- WEI, X., WANG, X., XIA, Y., TANG, Y., LI, F., FANG, W. & ZHANG, H. 2014. Kindlin-2 regulates renal tubular cell plasticity by activation of Ras and its downstream signaling. *Am J Physiol Renal Physiol*, 306, F271-8.
- WEINSTEIN, E. J., BOURNER, M., HEAD, R., ZAKERI, H., BAUER, C. & MAZZARELLA, R. 2003. URP1: a member of a novel family of PH and FERM domain-containing membrane-associated proteins is significantly over-expressed in lung and colon carcinomas. *Biochim Biophys Acta*, 1637, 207-16.
- WERNIMONT, S. A., LEGATE, K. R., SIMONSON, W. T., FASSLER, R. & HUTTENLOCHER, A. 2010. PIPKI gamma 90 negatively regulates LFA-1-mediated adhesion and activation in antigen-induced CD4<sup>+</sup> T cells. *J Immunol*, 185, 4714-23.
- WERNIMONT, S. A., WIEMER, A. J., BENNIN, D. A., MONKLEY, S. J., LUDWIG, T., CRITCHLEY, D. R. & HUTTENLOCHER, A. 2011. Contact-dependent T cell activation and T cell stopping require talin1. *J Immunol*, 187, 6256-67.
- WESSEL, F., WINDERLICH, M., HOLM, M., FRYE, M., RIVERA-GALDOS, R., VOCKEL, M., LINNEPE, R., IPE, U., STADTMANN, A., ZARBOCK, A., NOTTEBAUM, A. F. & VESTWEBER, D. 2014. Leukocyte extravasation and vascular permeability are each controlled in vivo by different tyrosine residues of VE-cadherin. *Nat Immunol*, 15, 223-30.
- WHITEHEART, S. W. 2011. Platelet granules: surprise packages. *Blood*, 118, 1190-1.
- WICK, M., BURGER, C., BRUSSELBACH, S., LUCIBELLO, F. C. & MULLER, R. 1994. Identification of serum-inducible genes: different patterns of gene regulation during G0-->S and G1-->S progression. *J Cell Sci*, 107 ( Pt 3), preceding table of contents.
- WIESNER, C., FAIX, J., HIMMEL, M., BENTZIEN, F. & LINDER, S. 2010. KIF5B and KIF3A/KIF3B kinesins drive MT1-MMP surface exposure, CD44 shedding, and extracellular matrix degradation in primary macrophages. *Blood*, 116, 1559-69.
- WINKLER, J., LUNSDORF, H. & JOCKUSCH, B. M. 1997. Energy-filtered electron microscopy reveals that talin is a highly flexible protein composed of a series of globular domains. *Eur J Biochem*, 243, 430-6.
- WITKO-SARSAT, V., RIEU, P., DESCAMPS-LATSCHA, B., LESAVRE, P. & HALBWACHS-MECARELLI, L. 2000. Neutrophils: molecules, functions and pathophysiological aspects. *Lab Invest*, 80, 617-53.
- WU, L. & LIU, Y. J. 2007. Development of dendritic-cell lineages. *Immunity*, 26, 741-50.
- WYNNE, J. P., WU, J., SU, W., MOR, A., PATSOUKIS, N., BOUSSIOTIS, V. A., HUBBARD, S. R. & PHILIPS, M. R. 2012. Rap1-interacting adapter molecule (RIAM) associates with the plasma membrane via a proximity detector. *J Cell Biol*, 199, 317-30.
- XIONG, J. P., STEHLE, T., ZHANG, R., JOACHIMIAK, A., FRECH, M., GOODMAN, S. L. & ARNAOUT, M. A. 2002. Crystal structure of the extracellular segment of integrin  $\alpha\text{V}\beta\text{3}$  in complex with an Arg-Gly-Asp ligand. *Science*, 296, 151-5.
- XU, Z., NI, B., CAO, Z., ZIELONKA, J., GAO, J., CHEN, F., KALYANARAMAN, B., WHITE, G. C. & MA, Y. Q. 2018. Kindlin-3 negatively regulates the release of neutrophil extracellular traps. *J Leukoc Biol*, 104, 597-602.



- YAKUBENKO, V. P., BELEVYCH, N., MISHCHUK, D., SCHURIN, A., LAM, S. C. & UGAROVA, T. P. 2008. The role of integrin alpha D beta2 (CD11d/CD18) in monocyte/macrophage migration. *Exp Cell Res*, 314, 2569-78.
- YAN, J., LI, F., INGRAM, D. A. & QUILLIAM, L. A. 2008. Rap1a is a key regulator of fibroblast growth factor 2-induced angiogenesis and together with Rap1b controls human endothelial cell functions. *Mol Cell Biol*, 28, 5803-10.
- YANG, J., ZHU, L., ZHANG, H., HIRBAWI, J., FUKUDA, K., DWIVEDI, P., LIU, J., BYZOVA, T., PLOW, E. F., WU, J. & QIN, J. 2014. Conformational activation of talin by RIAM triggers integrin-mediated cell adhesion. *Nat Commun*, 5, 5880.
- YATES, L. A., FUZERY, A. K., BONET, R., CAMPBELL, I. D. & GILBERT, R. J. C. 2012a. Biophysical Analysis of Kindlin-3 Reveals an Elongated Conformation and Maps Integrin Binding to the Membrane-distal beta-Subunit NPXY Motif. *Journal of Biological Chemistry*, 287.
- YATES, L. A., LUMB, C. N., BRAHME, N. N., ZALYTE, R., BIRD, L. E., DE COLIBUS, L., OWENS, R. J., CALDERWOOD, D. A., SANSOM, M. S. P. & GILBERT, R. J. C. 2012b. Structural and Functional Characterization of the Kindlin-1 Pleckstrin Homology Domain. *Journal of Biological Chemistry*, 287, 43246-43261.
- YE, F., PETRICH, B. G., ANEKAL, P., LEFORT, C. T., KASIRER-FRIEDE, A., SHATTIL, S. J., RUPPERT, R., MOSER, M., FASSLER, R. & GINSBERG, M. H. 2013a. The mechanism of kindlin-mediated activation of integrin alphaIIb beta3. *Curr Biol*, 23, 2288-2295.
- YE, F., PETRICH, B. G., ANEKAL, P., LEFORT, C. T., KASIRER-FRIEDE, A., SHATTIL, S. J., RUPPERT, R., MOSER, M., FASSLER, R. & GINSBERG, M. H. 2013b. The mechanism of kindlin-mediated activation of integrin alphaIIb beta3. *Curr Biol*, 23, 2288-95.
- YE, X., MCLEAN, M. A. & SLIGAR, S. G. 2016. Phosphatidylinositol 4,5-Bisphosphate Modulates the Affinity of Talin-1 for Phospholipid Bilayers and Activates Its Autoinhibited Form. *Biochemistry*, 55, 5038-48.
- YU, Y., WU, J., WANG, Y., ZHAO, T., MA, B., LIU, Y., FANG, W., ZHU, W. G. & ZHANG, H. 2012. Kindlin 2 forms a transcriptional complex with beta-catenin and TCF4 to enhance Wnt signalling. *EMBO Rep*, 13, 750-8.
- ZAMBONIN-ZALLONE, A., TETI, A., GRANO, M., RUBINACCI, A., ABBADINI, M., GABOLI, M. & MARCHISIO, P. C. 1989. Immunocytochemical distribution of extracellular matrix receptors in human osteoclasts: a beta 3 integrin is colocalized with vinculin and talin in the podosomes of osteoclastoma giant cells. *Exp Cell Res*, 182, 645-52.
- ZARBOCK, A., LOWELL, C. A. & LEY, K. 2007. Spleen tyrosine kinase syk is necessary for E-Selectin-induced alpha(L)beta 2 integrin-mediated rolling on intercellular adhesion molecule-1. *Immunity*, 26, 773-783.
- ZEILER, M., MOSER, M. & MANN, M. 2014. Copy number analysis of the murine platelet proteome spanning the complete abundance range. *Mol Cell Proteomics*, 13, 3435-45.
- ZHANG, G., XIANG, B., YE, S., CHRZANOWSKA-WODNICKA, M., MORRIS, A. J., GARTNER, T. K., WHITEHEART, S. W., WHITE, G. C., 2ND, SMYTH, S. S. & LI, Z. 2011. Distinct roles for Rap1b protein in platelet secretion and integrin alphaIIb beta3 outside-in signaling. *J Biol Chem*, 286, 39466-77.
- ZHANG, H., CHANG, Y. C., HUANG, Q., BRENNAN, M. L. & WU, J. 2016a. Structural and Functional Analysis of a Talin Triple-Domain Module Suggests an Alternative Talin Autoinhibitory Configuration. *Structure*, 24, 721-729.
- ZHANG, K. & CHEN, J. 2012. The regulation of integrin function by divalent cations. *Cell Adh Migr*, 6, 20-9.
- ZHANG, Z., MU, Y., VEEVERS, J., PETER, A. K., MANSO, A. M., BRADFORD, W. H., DALTON, N. D., PETERSON, K. L., KNOWLTON, K. U., ROSS, R. S., ZHOU, X. & CHEN, J. 2016b. Postnatal Loss of Kindlin-2 Leads to Progressive Heart Failure. *Circ Heart Fail*, 9.



- ZHU, J., LUO, B. H., XIAO, T., ZHANG, C., NISHIDA, N. & SPRINGER, T. A. 2008. Structure of a complete integrin ectodomain in a physiologic resting state and activation and deactivation by applied forces. *Mol Cell*, 32, 849-61.
- ZHU, J., ZHU, J. & SPRINGER, T. A. 2013. Complete integrin headpiece opening in eight steps. *J Cell Biol*, 201, 1053-68.
- ZHU, L., LIU, H., LU, F., YANG, J., BYZOVA, T. V. & QIN, J. 2019. Structural Basis of Paxillin Recruitment by Kindlin-2 in Regulating Cell Adhesion. *Structure*.
- ZHU, L., YANG, J., BROMBERGER, T., HOLLY, A., LU, F., LIU, H., SUN, K., KLAPPROTH, S., HIRBAWI, J., BYZOVA, T. V., PLOW, E. F., MOSER, M. & QIN, J. 2017. Structure of Rap1b bound to talin reveals a pathway for triggering integrin activation. *Nat Commun*, 8, 1744.

## ACKNOWLEDGEMENT

Finally, I would like to take the opportunity to express my gratitude to all the people, who accompanied me through the time of my PhD and contributed to the success of this work. First, I want to thank my supervisor Dr. Markus Moser for the possibility to work on this interesting project, for his invaluable support during the whole time and for always being available for any kind of problems, shortly said for an excellent supervision. Furthermore, I am deeply grateful to Dr. Sarah Klapproth for all her advice and support as well as constant encouragement, especially during the more stressful phases of my PhD. I always appreciated the highly collaborative working environment in our group.

I would like to thank Prof. Reinhard Fässler for the opportunity to work in his department under such excellent conditions, providing access to all microscopes and equipment and agreeing to be my official supervisor and first referee of this work.

I also would like to thank Prof. Markus Sperandio for evaluating my work as second referee and Prof. Martin Biel, Prof. Klaus Förstemann, Prof. Veit Hornung and Prof. Karl-Peter Hopfner for agreeing to be part of my thesis committee.

I appreciate the great collaborations that were important for the success of this project: Thanks to Dr. Ina Rohwedder, Laura Mittmann, Prof. Markus Sperandio and PD Dr. Christoph Reichel from the Walter Brendel Centre of Experimental Medicine, LMU, Munich and Dr. Liang Zhu and Prof. Jun Qin from the Lerner Research Institute, Cleveland.

Furthermore, I want to mention the members of my thesis advisory committee Prof. Carsten Grashoff and Prof. Oliver Söhnlein. I would like to thank them for taking the time to attend our annual meetings and for their feedback and suggestions on my project.

Thanks to all colleagues from the department of Molecular Medicine for support and availability in case of questions and a nice working atmosphere, especially Maria, Johannes, Irene, Peter and Raquel. A big thank also goes to Michal and Alicja for their help during their time as technicians in our group. Additionally, I want to thank Klaus Weber and Ines Lach-Kusevic for all the administrative support.

Finally, I would like to thank my family and friends for their continuous support and encouragement during the whole time.



# Curriculum vitae

## Personal data

Name: Thomas Bromberger  
Born: May 16<sup>th</sup>, 1991 in Starnberg  
Nationality: German  
E-mail: bromberger@biochem.mpg.de

## Education

Since 2016: **Max-Planck-Institute of Biochemistry, Martinsried, Germany**  
Department Molecular Medicine, Prof. Dr. Reinhard Fässler  
PhD thesis in the group of Dr. Markus Moser

2013-2015: **Technical University of Munich, Munich, Germany**  
Master studies in Molecular Biotechnology  
Master thesis at the Chair of Livestock Biotechnology, Prof. Dr. Angelika Schnieke; Title of the thesis: "Analysis of Colorectal Cancer associated genes: transition from low-grade to high-grade intraepithelial neoplasia"

2010-2013: **Technical University of Munich, Munich, Germany**  
Bachelor studies in Molecular Biotechnology  
Bachelor thesis at the Chair of Livestock Biotechnology, Prof. Dr. Angelika Schnieke; Title of the thesis: "Construction and comparison of different FokI domains for usage in TALENs"

2001-2010: Gymnasium Geretsried, Germany

1996-2001: Elementary school in Eurasburg, Germany

## **APPENDIX**

In the following, papers 1-4 including supplementary information are reprinted.





## ARTICLE

DOI: 10.1038/s41467-017-01822-8

OPEN

# Structure of Rap1b bound to talin reveals a pathway for triggering integrin activation

Liang Zhu<sup>1,2</sup>, Jun Yang<sup>1</sup>, Thomas Bromberger<sup>3</sup>, Ashley Holly<sup>1</sup>, Fan Lu<sup>1,2</sup>, Huan Liu<sup>1</sup>, Kevin Sun<sup>1</sup>, Sarah Klapproth<sup>3</sup>, Jamila Hirbawi<sup>1</sup>, Tatiana V. Byzova<sup>1</sup>, Edward F. Plow<sup>1</sup>, Markus Moser<sup>3</sup> & Jun Qin<sup>1,2</sup>

Activation of transmembrane receptor integrin by talin is essential for inducing cell adhesion. However, the pathway that recruits talin to the membrane, which critically controls talin's action, remains elusive. Membrane-anchored mammalian small GTPase Rap1 is known to bind talin-FO domain but the binding was shown to be weak and thus hardly studied. Here we show structurally that talin-FO binds to human Rap1b like canonical Rap1 effectors despite little sequence homology, and disruption of the binding strongly impairs integrin activation, cell adhesion, and cell spreading. Furthermore, while being weak in conventional binary binding conditions, the Rap1b/talin interaction becomes strong upon attachment of activated Rap1b to vesicular membranes that mimic the agonist-induced microenvironment. These data identify a crucial Rap1-mediated membrane-targeting mechanism for talin to activate integrin. They further broadly caution the analyses of weak protein-protein interactions that may be pivotal for function but neglected in the absence of specific cellular microenvironments.

<sup>1</sup>Department of Molecular Cardiology, Lerner Research Institute, Cleveland Clinic, 9500 Euclid Avenue, Cleveland, OH 44195, USA. <sup>2</sup>Department of Biochemistry, Case Western Reserve University, Cleveland, OH 44106, USA. <sup>3</sup>Max-Planck-Institute of Biochemistry, Department of Molecular Medicine, 82152 Martinsried, Germany. Liang Zhu, Jun Yang and Thomas Bromberger contributed equally to this work. Correspondence and requests for materials should be addressed to M.M. (email: [moser@biochem.mpg.de](mailto:moser@biochem.mpg.de)) or to J.Q. (email: [qinj@ccf.org](mailto:qinj@ccf.org))



The adhesion of cells to the extracellular matrix (ECM) is essential for regulating a variety of physiological or pathological responses such as platelet aggregation, blood clotting, stroke, wound-healing, and cancer metastasis. Such adhesion critically depends upon integrins, a class of cell surface receptors that are ( $\alpha/\beta$ ) heterodimers with each subunit containing a small cytoplasmic tail (CT), a transmembrane segment, and a large extracellular domain. In unstimulated cells, integrin adopts an inactive conformation with low affinity for ECM ligands but, upon agonist stimulation, integrin CT is bound by intracellular proteins, in particular talin and/or kindlin, which trigger global conformational change of the extracellular domain to acquire high affinity for ECM ligand and initiate firm adhesion. This process, widely regarded as inside-out signaling or integrin activation, has been the central topic of cell adhesion research for nearly three decades<sup>1–6</sup>. Extensive efforts have been focused on investigating the mechanism of integrin activation by talin—a major cytoskeletal protein comprising an N-terminal head domain (talin-H) and a C-terminal rod domain (talin-R). Talin-H contains four subdomains F0, F1, F2, and F3 in which F1–F3 constitutes a so-called FERM (4.1/ezrin/radixin/moesin)-like domain. Talin-R is made up of 13 consecutive helical bundles followed by a C-terminal dimerization domain (Fig. 1). Intact talin adopts an inactive conformation where the major integrin-binding site located in talin-H F3 domain is masked by talin-R (autoinhibition)<sup>7–10</sup>. Talin may be unmasked via multiple mechanisms to bind integrin  $\beta$  CT<sup>7, 8, 11–13</sup> and trigger the receptor activation<sup>14–17</sup>.

While a great deal has been learned about talin, a fundamental issue still remains unresolved: how is cytoplasmic talin recruited to plasma membrane—a crucial step for talin to bind and activate integrin? A previous dogma, largely derived from studying prototypic integrin  $\alpha_{IIb}\beta_3$  from platelets, is that agonist stimulation activates small GTPase Rap1 on the membrane to recruit an effector called RIAM that in turn recruits talin<sup>5, 18</sup>. However, while both Rap1 and talin are highly abundant<sup>19</sup>, RIAM is present at very low levels in platelets with no other homologs detected<sup>20</sup>. More importantly, mice lacking RIAM are viable and the platelet functions including the  $\alpha_{IIb}\beta_3$  activation are totally normal<sup>20–22</sup>. By contrast, Rap1 and talin are both essential for integrin activation<sup>4, 5, 18</sup>. For example, ablation of the Rap1 isoform Rap1b severely impairs  $\alpha_{IIb}\beta_3$  activation and platelet aggregation<sup>23</sup>—defects that were also observed in talin knockout mice<sup>24, 25</sup>. These

observations strongly suggest a RIAM-independent engagement between Rap1 and talin to regulate integrin activation. Interestingly, previous studies reported a direct interaction between Rap1 and talin in mammals<sup>26</sup> and in *Dictyostelium*<sup>27</sup>, but the affinity of the interaction was found to be low especially for that in mammals ( $K_d \sim 0.14$  mM)<sup>26</sup>. Since weak protein–protein interactions (PPIs) are typically assumed to be nonspecific and RIAM was widely regarded as a key bridge between Rap1 and talin, the Rap1/talin interaction was hardly studied at the mechanistic level. Through comprehensive structural, biochemical, and cell biological analyses, we discovered that talin is actually a distinct effector of Rap1 that recruits talin to membrane and triggers integrin activation. We further found that, while being weak in conventional binary binding assays, Rap1/talin interaction became strong when activated Rap1 was anchored to membrane that mimics the cellular condition. Our results thus uncover a mechanism of membrane-targeting of talin by Rap1 and also highlight the importance of weak PPIs that may be neglected in the absence of specific cellular microenvironments.

## Results

**Rap1 recognizes talin-F0 domain in a GTP-dependent manner.** Rap1 is known to contain two highly homologous isoforms called Rap1a and Rap1b<sup>28–31</sup>. In this study, we choose to focus on examining the interaction between the platelet-rich Rap1b and talin-F0. Like other small GTPases, Rap1b exists in inactive (GDP-bound) and active (GTP-bound) states. We first used a highly sensitive NMR technique called heteronuclear single quantum coherence (HSQC)<sup>32</sup> to examine the Rap1b/talin-F0 interaction. Figure 2a and Supplementary Fig. 1a show that Rap1b loaded with GTP analog GMP-PNP induced residue-specific chemical shift changes of <sup>15</sup>N-talin-F0. Inactive Rap1b loaded with GDP also binds to talin-F0 but at weaker affinity as evidenced by smaller chemical shift changes than those with GMP-PNP (Fig. 2b). Thus, talin-F0 binds favorably to the active form of Rap1b but, as shown in Fig. 2c, the binding affinity is quite low ( $K_d \sim 162$   $\mu$ M) as previously concluded<sup>26</sup>. On the other hand, talin-F0 does not bind H-Ras (Supplementary Fig. 1b) that is near 90% homologous in terms of binding interface (overall similarity is  $\sim 76\%$ ) to Rap1b (see also Supplementary Fig. 1c), suggesting that despite being weak, the talin-F0/Rap1b interaction is specific. To further investigate the specificity of Rap1b/talin-F0

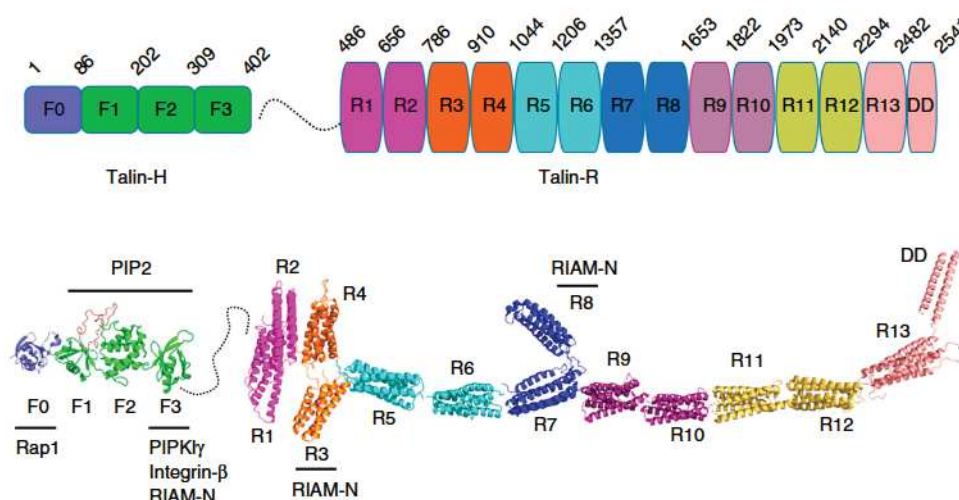


**Fig. 1** Domain organization and a linear structural model of talin. The model was generated from known crystal and NMR structures of talin fragments and shown in cartoon representation. Critical talin-binding partners involved in talin membrane recruitment and activation are indicated in the figure. PIP2 phosphatidylinositol-4,5-bisphosphate, RIAM-N the N terminus of RIAM, PIPK1 $\gamma$  type I phosphatidylinositol phosphate kinase isoform- $\gamma$



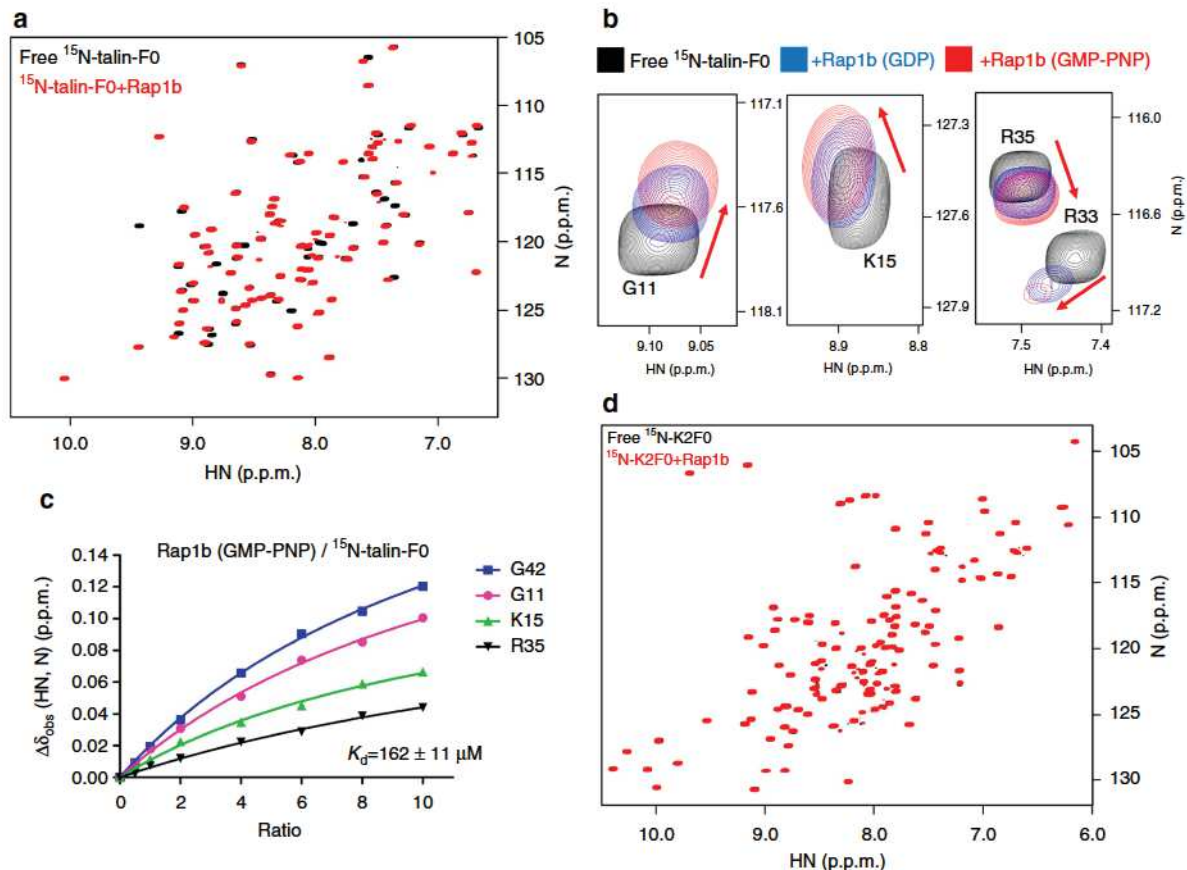


**Fig. 2** Rap1b/talin-F0 interaction is GTP-dependent and specific but is of weak affinity. **a** The HSQC spectra of 50  $\mu\text{M}$   $^{15}\text{N}$ -labeled talin-F0 in the absence (black) and presence of 125  $\mu\text{M}$  GMP-PNP loaded Rap1b (red). **b** The HSQC spectra (four representative residues were shown) of 50  $\mu\text{M}$   $^{15}\text{N}$ -labeled talin-F0 in the absence (black) and presence of 125  $\mu\text{M}$  GDP loaded Rap1b (blue) or GMP-PNP loaded Rap1b (red). Note that Rap1b-GDP induced the same overall pattern of chemical shift changes of  $^{15}\text{N}$ -labeled talin-F0 as Rap1b-GMP-PNP does but with less peak shifts and broadenings, indicating a weaker affinity. **c** The affinity of Rap1b (GMP-PNP)/talin-F0 interaction measured by HSQC titration. **d** The HSQC spectra of 50  $\mu\text{M}$   $^{15}\text{N}$ -labeled kindlin2-F0 in the absence (black) and presence of 125  $\mu\text{M}$  GMP-PNP loaded Rap1b (red)

interaction, we examined the Rap1b binding to F0 domain of another integrin activator kindlin2 that is homologous to talin-H (Supplementary Fig. 2a)<sup>33</sup>, but no interaction was detected (Fig. 2d). Since talin-H contains FERM domain (F1–F3) prior to F0 and F1–F2 of KRIT1 FERM domain was shown to bind Rap1b<sup>34</sup>, we also wondered whether F1–F2 of talin FERM would be involved in binding to Rap1b. However, Supplementary Fig. 2b shows that Rap1b does not interact with talin FERM F1–F2. Overall, these data suggest that Rap1b engages with talin-F0 in a highly specific manner. Interestingly, NMR (Fig. 3a, Supplementary Figs. 1a and 2c) and Glutathione S-transferase (GST) pull-down (Fig. 3b) experiments revealed that active Rap1b also binds talin-H and full-length talin in the same manner as to talin-F0. Given that full-length talin is autoinhibited with F0 being unmasked<sup>7</sup>, these data suggest that active Rap1b specifically recognizes the F0 domain of resting talin.

**Rap1b/talin interface exhibits distinct features.** To understand how Rap1b recognizes talin, we decided to pursue the total structure of active human Rap1b (~20 kDa) in complex with talin-F0 (~10 kDa). Solution NMR is particularly suitable for structure determination of weak protein complexes<sup>32</sup>. By performing a series of three-dimensional (3D) heteronuclear experiments using a combination of  $^1\text{H}/^{15}\text{N}/^{13}\text{C}$ -labeled and  $^2\text{H}/^{15}\text{N}$ -labeled samples, we were able to obtain nearly complete resonance assignment, 3422 intramolecular NOEs, and 78 intermolecular NOEs (Supplementary Fig. 3), which allowed

determination of the complex structure (Fig. 4a and Supplementary Table 1). Figure 4b displays the cartoon diagram of the overall complex in which individual subunits, Rap1b and talin-F0, adopt a Ras family GTPase fold and an ubiquitin-like fold, respectively, as expected. The ubiquitin-like fold of talin-F0 has similarity to Ras-association (RA) domain present in known Rap1 effectors such as KRIT1, RIAM, and c-Raf1 (Fig. 4c). However, despite this similar fold, talin-F0 has little sequence homology with these Rap1b RAs (Fig. 4d) with only three positively charged residues being relatively conserved (highlighted in red in Fig. 4d). The detailed Rap1b/talin-F0 interface is summarized in Fig. 4e and Supplementary Fig. 4a and compared with other Rap1b effectors (Supplementary Table 2). Majority of the contacts in the Rap1b/talin-F0 complex are different from other Rap1b/effector complexes (Supplementary Table 2) apparently due to the scant sequence homology of talin-F0 with other Rap1b effectors (Fig. 4d). A particularly distinct feature in the Rap1b/talin-F0 complex is the existence of a hydrophobic core between I36/P37 of talin-F0 and V21/I27/V29 of Rap1b (Fig. 4e and Supplementary Fig. 4b). Such core was not observed in other Rap1b/effector complexes. To understand how Rap1b but not the highly homologous H-Ras binds talin-F0 (Supplementary Fig. 1b), we mutated I27 and K31 of Rap1b, which closely contact with talin-F0, into corresponding H-Ras residues, Histidine and Glutamate, respectively. Both mutations showed reduced binding to talin-F0 (Supplementary Fig. 4c). By contrast, both Rap1b and H-Ras bind equally well to RIAM as shown before<sup>35</sup> as also confirmed in



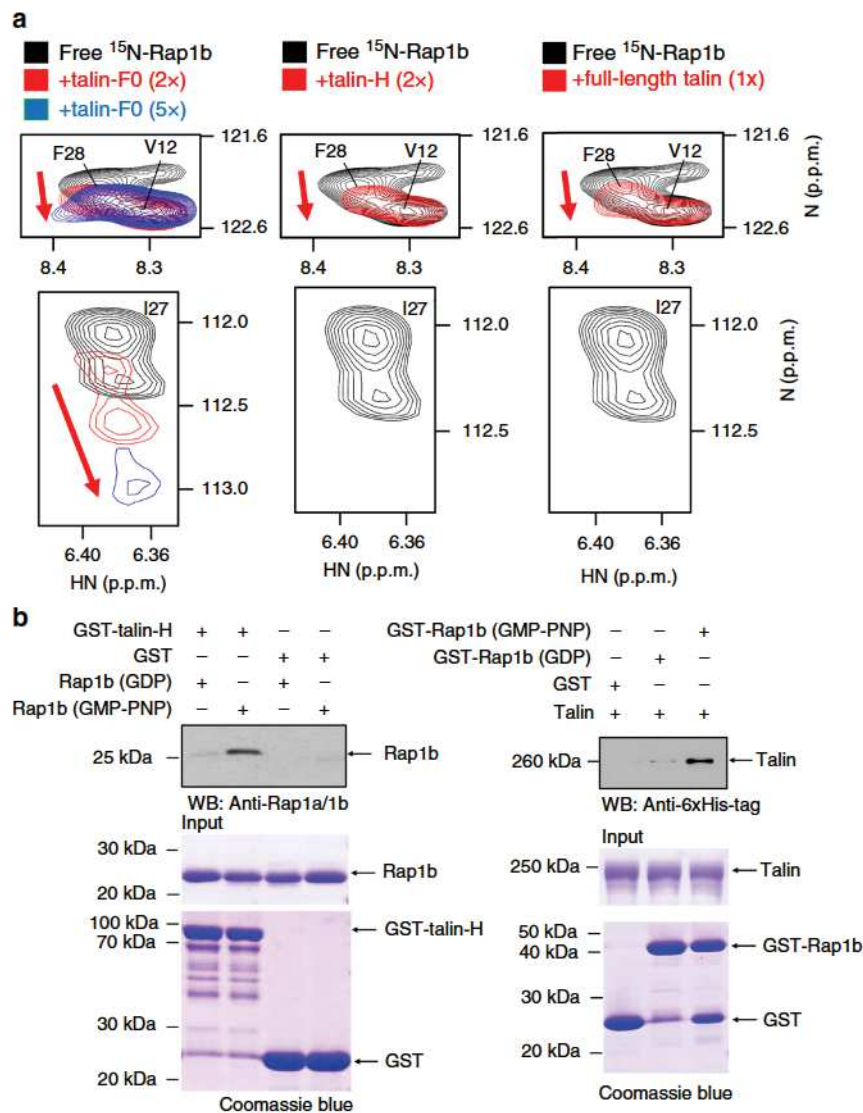


**Fig. 3** Rap1b recognizes F0 domain of talin in a GTP-dependent manner. **a** The HSQC spectra (representative regions were shown) of 45  $\mu\text{M}$  GMP-PNP loaded  $^{15}\text{N}$ -labeled Rap1b (1–167) in the absence (black) and presence of 90  $\mu\text{M}$  talin-F0 (red), 225  $\mu\text{M}$  talin-F0 (blue), 90  $\mu\text{M}$  talin-H (red), or 45  $\mu\text{M}$  full-length talin (red). Note that the peak of I27 was broadened in the presence of talin-H or full-length talin. **b** GST pull-down assays to show that Rap1b interacts with both talin-H and full-length talin in a GTP-dependent manner. Full blot/gel images are shown in Supplementary Figs. 11 and 12

Supplementary Fig. 4d and Supplementary Fig. 16. These data provide insight into the high specificity of the talin binding to Rap1b despite the weaker affinity than that between talin and RIAM (Supplementary Fig. 4e).

Further analysis revealed that, while the Rap1b/talin-F0 interface exhibits distinct features (Fig. 4e, Supplementary Fig. 4a, and Supplementary Table 2), the overall topology of the complex shares similarity with other Rap1b/effector complexes (Fig. 4b, c). A key determinant for this similarity appears to be the antiparallel  $\beta$ -sheet between Rap1b  $\beta$ 2 strand and talin-F0  $\beta$ 2 strand (Fig. 4b and Supplementary Fig. 4a), as also present in other Rap1b/effector complexes (Fig. 4c). In addition, charge–charge interactions in the talin-F0/Rap1b complex, which involve talin-F0 K7 with Rap1b E37 and talin-F0 K15/R35 with Rap1b D33, are relatively conserved in other Rap1b/effector complexes (Fig. 4d and Supplementary Table 2). By contrast, kindlin2-F0, which is not a Rap1b effector (Fig. 2d) but is highly homologous to talin-F0 (Supplementary Fig. 2a), lacks two positively charged residues in the corresponding positions (Fig. 4d).

In summary, the Rap1b/talin-F0 interface is quite unique yet resembles other Rap1b/effector complexes in overall topology. These structural and binding data suggest that talin is a direct effector of Rap1. Interestingly, the interface residues are highly conserved in both talin/Rap1 isoforms and in different species (Supplementary Fig. 5a, b), suggesting that Rap1/talin recognition is evolutionally conserved.

**Rap1b binding to talin is crucial for integrin activation.** To further evaluate the importance of the Rap1b/talin interaction, we performed the structure-based analysis and mutated two critical interface residues K15 and R35 of talin-F0 (Fig. 4e and Supplementary Fig. 4a) into alanines. Figure 5a and Supplementary Fig. 6 show that K15A/R35A double mutations (DM) drastically reduced the Rap1b interaction to talin-F0 as well as talin-H. Since talin-H is the unit responsible for binding and activating integrin<sup>5, 36</sup>, we next tested the impact of the Rap1b-binding defective mutations on its ability to activate  $\alpha_{\text{IIb}}\beta_3$ —the prototypic integrin widely used to study integrin activation. To this end, we



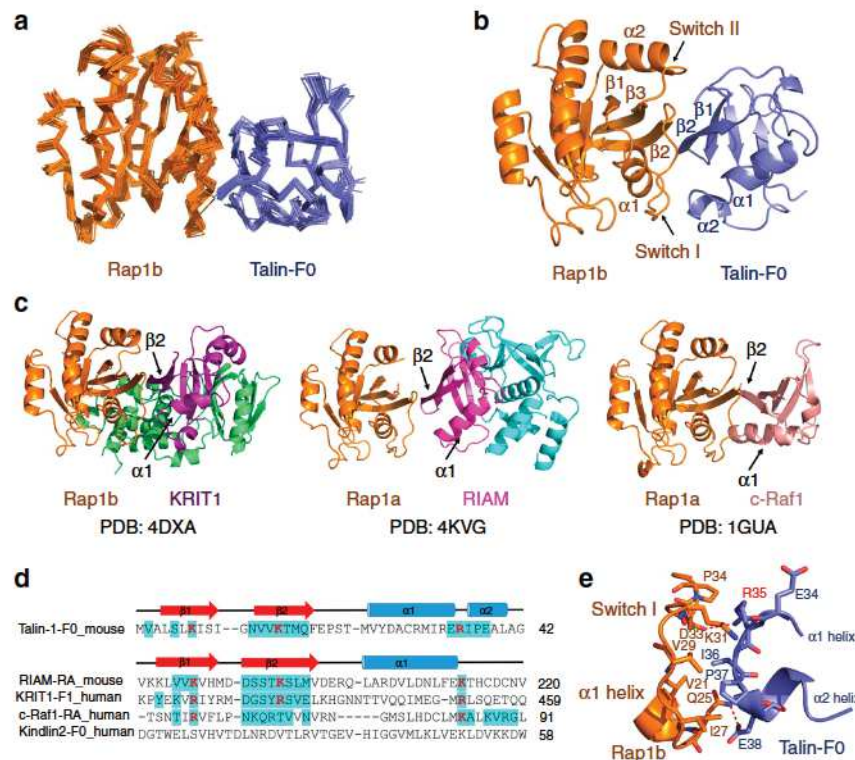


**Fig. 4** Solution structure of Rap1b/talin-F0 complex by NMR. **a** Superposition of 20 calculated Rap1b/talin-F0 complex structures with lowest energies (shown in ribbon representation). **b** Cartoon representation of the Rap1b/talin-F0 complex structure with the lowest energy. **c** Current solved complex structures of Rap1 and its effector proteins (shown in cartoon representation). **d** Structure-based sequence alignment of talin-F0 and RA domain containing Rap1b effector proteins or kindlin2-F0 (only binding interfaces were shown). Residues involved in the binding interface with a cutoff of 4 Å are highlighted in cyan. Conserved residues are colored in red. **e** Detailed interaction diagram between the  $\alpha 1$  helix and switch I of Rap1b and the  $\alpha 2$  helix of talin-F0. Hydrogen bond or salt bridge is represented by red dashed line

transfected wild-type (WT) talin-H or talin-H DM into Chinese hamster ovary (CHO) A5 cells stably expressing  $\alpha_{IIb}\beta_3$  (Supplementary Fig. 7a). Figure 5b shows that, as compared to the WT talin-H, the talin-H mutant-induced  $\alpha_{IIb}\beta_3$  activation was substantially reduced. These results provide strong evidence that the interaction of talin-H with Rap1b is crucial for the talin-H-mediated integrin activation. They also explain a previously reported phenomenon where deletion of F0 domain in talin-H significantly impaired the integrin activation<sup>37</sup>. To further demonstrate that the impaired interaction between talin DM and Rap1 has an impact on integrin-mediated functions, we retrovirally transduced talin-null fibroblasts (talin<sup>1/2dko</sup>), which show a strong defect in cell adhesion and spreading<sup>38</sup>, with C terminally ypet-tagged talin WT as well as talin DM. The transduced cells were FACS-sorted for equal talin and talin DM expression as confirmed by flow cytometry and western blotting (Supplementary Figs. 7b and 17). Re-expression of both WT talin and talin DM induced cell spreading of talin<sup>1/2dko</sup> cells with WT and mutant talin localizing to paxillin-positive focal adhesions (FAs; Supplementary Figs. 7c, d). We then performed adhesion assays on various integrin ligands and observed that talin DM only partially rescued cell adhesion of talin<sup>1/2dko</sup> cells to fibronectin (FN), laminin-111 (LN), and vitronectin (VN) compared to WT talin, whereas integrin-independent adhesion to poly-L-lysine was unchanged (Fig. 5c). As expected, talin<sup>1/2dko</sup> cells expressing ypet as a control hardly adhered to any integrin ligand (Fig. 5c). Importantly, expression of mutant talin did not alter the expression levels of surface integrins nor those of RIAM and Rap1 (Supplementary Figs. 7b, e). Next, we plated the cells on FN and measured cell spreading for 4 h. While ypet-transduced talin<sup>1/2dko</sup> cells remained roundish and did not spread, talin DM cells

displayed a significant spreading defect compared to talin WT-transduced cells (Fig. 5d).

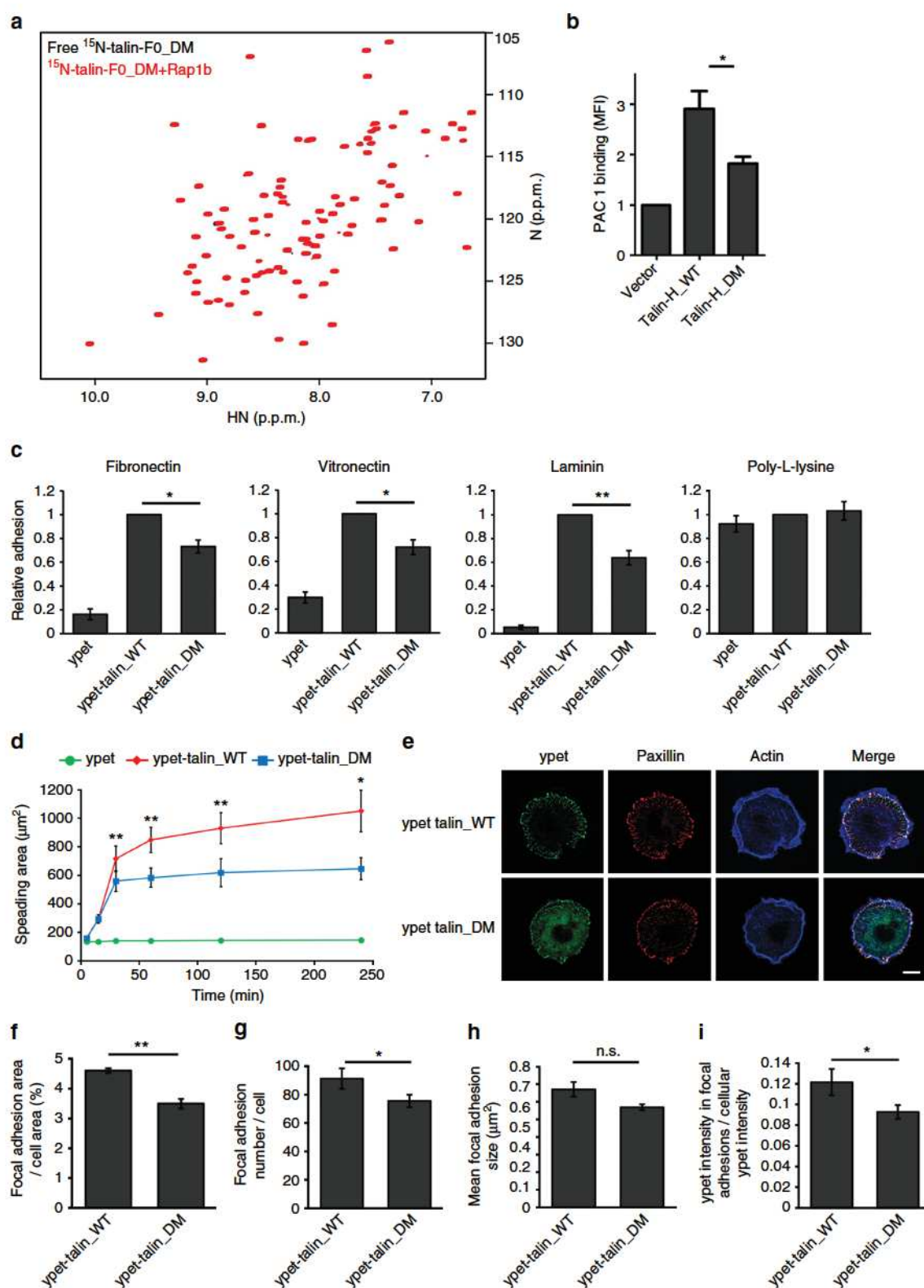
We hypothesize that the reduced PAC1 binding, cell adhesion, and spreading of talin DM-expressing cells are due to impaired integrin activation caused by deficient talin recruitment to the integrin site at the plasma membrane. To test this hypothesis experimentally, we seeded WT talin and talin DM-expressing cells on FN-coated micropatterns for 4 h and measured the number and size of paxillin-positive FAs. This analysis reveals that indeed the FA area and number per cell are significantly reduced in cells expressing talin DM compared to those expressing WT talin (Figs. 5e–g). The mean FA size (Fig. 5h) was also reduced by talin DM, although with a *p* value of 0.09. To further test whether impaired talin/Rap1 interaction affects the recruitment of talin DM to FAs, we measured the intensity of ypet fluorescence within FAs and correlated it to the total cellular ypet fluorescence intensity. We observed a significantly reduced relative intensity of ypet signal within FAs in talin DM-transduced cells, which suggests that the talin/Rap1b interaction is important for talin recruitment to FAs (Fig. 5i). Collectively, our data provide strong evidence for the physiological importance of direct Rap1/talin interaction in integrin regulation.

**Membrane-anchored Rap1b shows enhanced binding to talin.** While the foregoing data demonstrated the unique specificity of Rap1b/talin interaction and its importance in regulating integrin-mediated functions, a key issue still remains: how can such interaction with  $\sim 0.16$  mM affinity be effective since protein concentration in cells is typically much lower than 0.16 mM? We attempted to address this issue from two angles. First, both Rap1



and talin are highly abundant in cells. For example, recent proteomic studies showed that Rap1b and talin belong to the top most abundant proteins in platelets with copy numbers of ~200,000, which are nearly 1/4 of the most abundant platelet protein actin<sup>19</sup>. The high levels of Rap1 and talin in platelets are consistent with our protein expression analysis (Fig. 6a). Given that the average concentration of actin is above 200  $\mu$ M in

platelets<sup>39</sup>, the estimated concentration of Rap1b or talin in platelets should be at least 50  $\mu$ M. By contrast, the RIAM level is very low in both human and murine platelets (Fig. 6a), which was also confirmed by quantitative mass spectrometry with a copy number of only 162<sup>19</sup>. Thus, the high concentrations of Rap1 and talin increase the chance for their direct interaction to occur. Second, given that Ras family GTPases including Rap1 are all





known to be attached to membrane via Cys prenylation of their C-terminal CAAX motif<sup>29</sup> and talin-H also binds to membrane via a large positively charged surface on F1, F2, and F3 domains<sup>8, 40</sup>, we reasoned that Rap1 and talin-H might be more tightly associated if Rap1 were prenylated with membrane to mimic the true cellular microenvironment (Fig. 6b). Our Rap1b/talin-F0 structure superimposed with the structure of talin-H supports this possibility in that the CAAX containing C terminus of Rap1b and the positively charged surface of talin-H align well to all face toward the membrane surface (Fig. 6b). To address this possibility experimentally, we prepared membrane vesicles with anchored Rap1b using the well-established thiol-maleimide crosslinking method<sup>41</sup> (Supplementary Fig. 8a). As shown in Fig. 6c, membrane-anchored Rap1b indeed bound much more robustly to talin-H than Rap1b unanchored to membrane. Isothermal titration calorimetry (ITC) experiments revealed a  $K_d$  of  $\sim 1.52$   $\mu$ M for membrane-anchored active Rap1b to bind to talin-H (Supplementary Fig. 8b), which indicates a more than two orders of magnitude stronger binding than that measured without membrane (Fig. 2c and Supplementary Fig. 4e). Consistently, the membrane-binding capacity of talin-H was also substantially enhanced by Rap1 anchored to the membrane, but such enhancement was diminished for talin-H DM that is defective for binding to Rap1 (Fig. 6d). Importantly, the binding of membrane-anchored Rap1b to talin-H is GTP-dependent as shown by two independent methods: GST pull-down assay (Supplementary Figs. 8c and 18) and co-sedimentation assay (Supplementary Figs. 9a and 19). Such GTP dependence indicates that the effective membrane targeting of talin requires active Rap1b. These findings provide key evidence for talin being a bona fide Rap1 effector and suggest how agonist-activated and membrane-anchored Rap1 can effectively recruit talin to the membrane surface. Although full-length talin binds to membrane more weakly than talin-H possibly due to some degree of autoinhibition for the former, membrane with anchored Rap1b clearly binds more potently to full-length talin contrasting to the scenario where Rap1b was not attached to the membrane (Fig. 6e). Similar to membrane-mediated Rap1b/talin-H binding (Supplementary Fig. 9a), membrane-anchored Rap1b also interacts with full-length talin in a GTP-dependent manner (Supplementary Fig. 9b). Importantly, since full-length talin adopts an autoinhibited conformation<sup>7, 10</sup>, which may be unmasked through a pull-push mechanism by binding to the membrane<sup>8</sup>, our data further suggest that Rap1 not only promotes the membrane targeting but also leads to activation of talin via this mechanism (Fig. 6b). In order to test this hypothesis, we performed NMR-based competition experiments by examining the interaction of  $^{15}\text{N}/^2\text{H}$ -labeled inhibitory talin rod domain 9 (talin-R9) with talin-H in the absence and presence of membrane-anchored Rap1b. Supplementary Fig. 9c shows that, while talin-H induces residue-specific chemical shift changes of talin-R9 as the signature of the autoinhibition<sup>8</sup>, such chemical shift changes were

suppressed by membrane-anchored Rap1b, thus demonstrating the talin-unmasking process.

## Discussion

Rap1 was discovered nearly three decades ago<sup>42</sup>, and its two isoforms Rap1a and Rap1b (with  $\sim 95\%$  identity, see also Supplementary Fig. 5b) are regarded as the key membrane-associated small GTPases to target proteins to the plasma membrane to regulate diverse cellular responses<sup>28–31</sup>. A large body of data have indicated that Rap1 is critically involved in activation of integrins<sup>5, 18, 43</sup>, but the immediate downstream effector of Rap1 has been highly elusive. Our studies have now obtained an important clue on this longstanding mystery. We found that the activated Rap1b interacts with the F0 domain of talin—the key mediator of integrin activation, and we determined the NMR structure of the Rap1b/talin-F0 complex. Despite little sequence homology between talin-F0 and other Rap1 effectors, the overall topology of the complex was found to resemble those known Rap1/effector complexes. Moreover, disruption of the Rap1b/talin interface substantially impaired the integrin  $\alpha_{\text{IIb}}\beta_3$  activation, cell adhesion, and cell spreading. Interestingly, we found that, while being weak measured in conventional binary conditions<sup>26</sup>, the Rap1b/talin interaction became quite strong when Rap1b was anchored to membrane—a condition mimicking the cellular microenvironment of Ras family GTPases<sup>41</sup> and also favoring talin unmasking as indicated previously<sup>8</sup>. Overall, our data suggest a crucial pathway by which agonist-activated Rap1 directly promotes the membrane recruitment of talin, which further leads to the talin unmasking and integrin activation (Fig. 6b). Our data also provide an explanation of why Rap1 and talin are essential for integrin activation, whereas RIAM is dispensable for activation of most integrins expressed on many cell types as indicated by the recent series of genetic studies<sup>20–22</sup>. On the other hand, RIAM, which is highly abundant in leukocytes, was shown to play an important role in regulating leukocyte integrin function<sup>21, 22</sup> by possibly forming the so-called “MIT complex” with talin and integrin<sup>44</sup>, indicating that the direct Rap1/talin pathway plays a minor role in regulating the leukocyte  $\beta_2$  integrins. The fact that talin DM still partially supports cell adhesion and spreading of talin<sup>1/2dko</sup> cells (Fig. 5c, d) further indicates the existence of other compensatory pathways including “Rap1-RIAM-talin” and “PIPKI $\gamma$ /PIP2-talin”<sup>7, 8, 11</sup>. More detailed investigations are needed to understand how these different pathways are turned on or cooperated in a spatiotemporal manner. Nevertheless, our data, combined with the genetic evidence of Rap1 and talin in integrin activation, suggest that direct Rap1–talin interaction critically regulates integrin activity.

In addition to uncovering the physiological role of the Rap1b/talin interaction, our findings also bear broad implications in the analyses of PPIs. Tens of thousands of PPIs in cells form a web of intricate communication networks for regulating diverse

**Fig. 5** The Rap1b binding to talin is crucial for integrin activation. **a** The HSQC spectra of 50  $\mu$ M  $^{15}\text{N}$ -labeled talin-F0\_DM (K15A, R35A) in the absence (black) and presence of 125  $\mu$ M GMP-PNP loaded Rap1b (red). **b** Integrin activation assay in CHO A5 cells, which stably express integrin  $\alpha_{\text{IIb}}\beta_3$ . Double mutations (K15A, R35A) in talin-H substantially decreases integrin activation. The data are shown as means  $\pm$  S.E.M. from four independent experiments.  $*p < 0.05$ . **c** Static adhesion of talin<sup>1/2dko</sup> fibroblasts, expressing either ypet alone, ypet-tagged talin WT, or ypet-tagged talin DM (K15A, R35A). Number of adherent cells was quantified by measuring absorbance of crystal violet staining. Values measured for talin WT-transduced cells were set to one in each of six independent experiments. Values are given as mean  $\pm$  S.E.M.  $*p < 0.05$  and  $**p < 0.01$ . **d** Spreading of talin<sup>1/2dko</sup> fibroblasts expressing ypet (green), ypet-tagged talin WT (red), or ypet-tagged talin DM (blue) on a fibronectin-coated surface, measured 5, 15, 30 min, 1, 2 and 4 h after plating.  $N = 5$ . **e** Confocal images of ypet-tagged talin WT or ypet-tagged talin DM cells on FN-coated round micropatterns stained for paxillin (red) and F-actin (blue). Ypet signal is shown in green. Scale bar 10  $\mu$ m. Focal adhesion area per cell area (**f**), focal adhesion number per cell (**g**), and focal adhesion size (**h**) of ypet-tagged talin WT and ypet-tagged talin DM cells on FN-coated micropatterns. **i** Ypet fluorescence intensity within paxillin-positive focal adhesion area in relation to the cellular ypet fluorescence.  $N = 5$ ; 10–15 talin WT and talin DM-expressing cells in each measurement were analyzed. All values are given as mean  $\pm$  S.E.M.  $*p < 0.05$  and  $**p < 0.01$ .



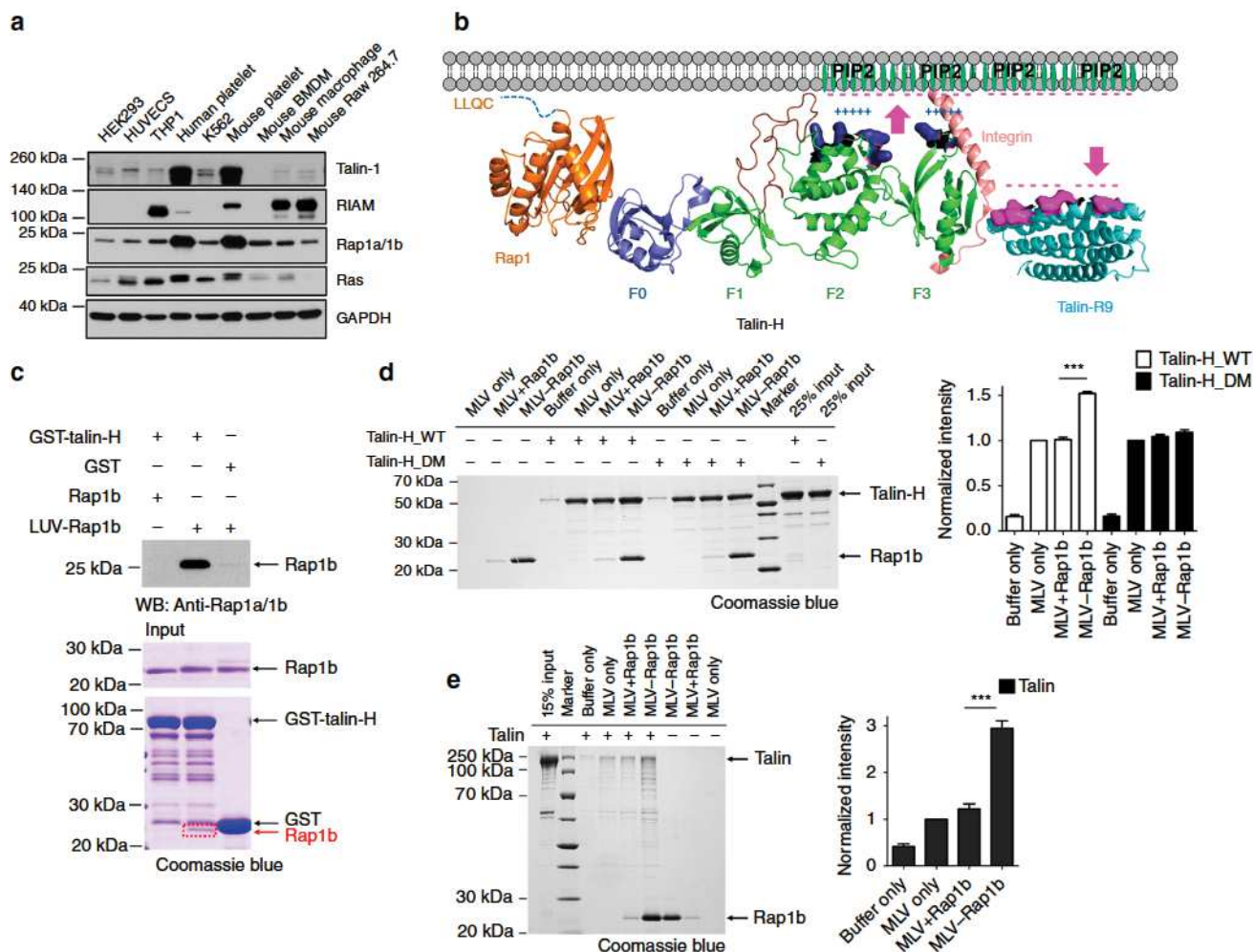


**Fig. 6** Mechanism of talin recruitment by Rap1. **a** Protein expression levels of talin, RIAM, Rap1, Ras GTPases, and GAPDH in various types of cell lines indicated in the figure. Full blots are shown in Supplementary Fig. 13. **b** A model of membrane-associated Rap1b recruiting talin for integrin activation. Proteins are shown in cartoon representation. Talin F1 loop is colored in maroon, the positively charged residues of talin-F2F3 domains (green), which interact with PIP2, are colored in deep blue and shown in surface representation, and the negatively charged residues of talin-R9 (cyan) are colored in magenta and shown in surface representation. **c** GST pull-down assay to show the robustly enhanced interaction between membrane-anchored Rap1b and talin-H. Rap1b was loaded with GMP-PNP in this assay and “LUV-Rap1b” represents that Rap1b was anchored to large unilamellar vesicles (LUVs). LUV-Rap1b could be easily pulled down by GST-talin-H and the band was visible in Coomassie blue staining gel (boxed in red) and intense in WB analysis, while free Rap1b pulled down by GST-talin-H was hardly seen in the same condition. Full blot/gel images are shown in Supplementary Fig. 14. **d** Left, a representative vesicle co-sedimentation assay showing that the interaction between talin-H<sub>WT</sub> and membrane is enhanced by around 1.5-folds when Rap1b (GMP-PNP) is attached to membrane but not for talin-H<sub>DM</sub>. “MLV + Rap1b” represents that Rap1b remained as free form in solution without being attached to multilamellar vesicles (MLVs), which were pre-incubated with  $\beta$ -mercaptoethanol. “MLV-Rap1b” represents that Rap1b was anchored to MLVs. Right, the quantification of four independent experiments. The intensity of talin-H<sub>WT</sub> or talin-H<sub>DM</sub> band was normalized to that of corresponding “MLV only” group and the data are shown in means  $\pm$  S.E.M. \*\*\* $p$  < 0.0001. Full gel image is shown in Supplementary Fig. 15. **e** Left, a representative vesicle co-sedimentation assay showing that the interaction between full-length talin and membrane is significantly enhanced by around 3-folds when Rap1b (GMP-PNP) is attached to membrane. Right, the quantification of four independent experiments. The intensity of talin band was normalized to that of the “MLV only” group and the data are shown as means  $\pm$  S.E.M. \*\*\* $p$  < 0.0001. Full gel image is shown in Supplementary Fig. 15

biological processes<sup>45</sup>. Interestingly, recent proteomic analyses have suggested that weak PPIs dominate in these cellular PPI networks<sup>46</sup>. However, because cellular protein concentrations, which are typically estimated on whole-cell volumes, are low (e.g., nM), weak binary PPIs, as detected by conventional *in vitro* methods, were commonly treated to be nonspecific and therefore disregarded for further investigations. Nevertheless, these weak PPIs may be enhanced and they exert crucial functions at specific microenvironments, which is strongly demonstrated in our study. Specifically, while isolated Rap1b and talin-F0 binds at sub-mM affinity, the binding became very strong in the presence of membrane that mimics the cellular microenvironment. As

illustrated in Fig. 6b, the membrane-anchoring ability of both Rap1b and talin may increase the local concentration of both proteins, thereby markedly strengthening their association. Other types of cellular strategies may also exist to enhance the association of otherwise weak binary interactions, which remain to be further investigated. With the completion of human genome and rapidly growing data of weak PPIs<sup>46</sup>, our study emphasizes cautious treatment of a wide variety of weak PPIs by including specific microenvironments. In this regard, NMR is particularly valuable for deciphering the detailed structural basis of weak PPIs<sup>32</sup> in vitro, laying down the foundation for further analysis of the interaction in certain networks both in vitro and in vivo, as



exemplified in our study. Such approach would complement with other techniques such as crystallography and CryoEM that are advantageous for elucidating large high-affinity complexes, together, facilitating a thorough and unbiased view of how proteins function in cells.

## Methods

**Plasmid constructs and mutagenesis.** The following constructs for bacterial expression were used in this study: mouse talin-F0 (1–86) subcloned into a pHis-1 vector, mouse full-length talin subcloned into a pET28t vector, human kindlin2-F0 (1–105) subcloned into a pGST-1 vector, mouse talin-H (1–429) subcloned into a pET28t, and a pGST-1 vector, mouse RIAM-RAPH (149–438) subcloned into a pGST-1 vector, human full-length Rap1b subcloned into a pGST-1 vector, and C-terminal truncated Rap1b (1–167) subcloned into a pET28t vector. Human wild-type Rap1b and H-Ras (G12V) subcloned into pET28a vectors (6xHis tag) were kind gifts from Dr. Matthias Buck at Case Western Reserve University. Construct mutagenesis was conducted by using QuickChange lightning site-directed mutagenesis Kit (Agilent Technologies). Mutated constructs generated in this study include talin-F0\_DM (K15A, R35A), talin-H\_DM (K15A, R35A), Rap1b (G12V), Rap1b (1–167, G12V), Rap1b (G12V, I27H), Rap1b (G12V, K31E), Rap1b\_TM1 (C51S, C118S, C141S), and Rap1b\_TM2 (G12V, C51S, C118S, C141S). Note that pET28t is a modified pET28a vector where the thrombin cleavage site is substituted with a TEV protease cleavage site. Primers used in this study are listed in Supplementary Table 3.

**Protein expression and purification.** Recombinant proteins with fusion tag (6xHis tag or GST tag) were expressed in *Escherichia coli* BL21 (DE3) strain (New England Biolabs). Typically, bacteria was initially grown in 50 ml lysogeny broth (LB) medium and then amplified in 1 ~ 2 l LB at 37 °C. The culture was induced by 0.4 mM Isopropyl β-D-1-thiogalactopyranoside (IPTG) at 20 °C or room temperature (RT) for overnight when it reached an  $A_{600}$  of 0.7. The pellet was then collected and suspended in buffer and frozen at –80 °C. For protein purification, the pellet was lysed by incubation with lysozyme and sonication. After high-speed centrifugation, the supernatant was subjected to affinity column purification by using either nickel or GST gravity column. Ion exchange chromatography was an optional purification step depending on protein purity (in this study, full-length Rap1b was purified by anion exchange method using Hi-trap Q column). Gel filtration was always performed in the final step by using either Superdex-75 (16/60) or Superdex-200 (16/60; GE Healthcare). Note that Superose-6 (10/300) was used for full-length talin purification. Purified protein was checked by SDS-PAGE. Proteins with 90% purity or above were used in this study. According to experimental requirement, fusion tag (either His-tag or GST tag) was removed by TEV protease during protein purification if necessary. Isotope-labeled ( $^{15}\text{N}$  and/or  $^{13}\text{C}$ ) proteins were achieved by employing minimal medium with  $^{15}\text{NH}_4\text{Cl}$  and/or  $^{13}\text{C}$ -glucose as the sole nitrogen and carbon sources.  $^2\text{H}$ -labeled protein was achieved by using the minimal medium prepared in 99.8%  $\text{D}_2\text{O}$  with  $^2\text{H}$ -glucose as the carbon source. Protein concentration was measured by absorbance at 280 nm or Pierce 660 nm protein assay reagent (Thermo Fisher Scientific).

**GTPase nucleotide exchange.** Non-hydrolyzable analogs of GDP and GTP, named Guanosine 5'-[β-thio] diphosphate trilithium salt (GDP-β-S) and Guanosine 5'-[β, γ-imido] triphosphate trisodium salt (GMP-PNP), respectively, were purchased from Sigma-Aldrich. In this study, wild-type Rap1b loaded with GDP-β-S was used as an inactive form, and Rap1b (G12V) or H-Ras (G12V) loaded with GMP-PNP was used as an active form. Purified wild-type Rap1b (50 μM), Rap1b (G12V) or H-Ras (G12V) was first incubated with 2 mM EDTA and 2 mM GDP-β-S or GMP-PNP at RT for 35 min,  $\text{MgCl}_2$  was then added in to reach a final concentration of 7 mM and incubated for another 30 min. After that, they were kept on ice and concentrated into a high concentration for experimental use.

**NMR 2D-HSQC and HSQC titration.** 2D-HSQC experiments were performed on Bruker 600 MHz NMR spectrometer, and samples containing 50 μM  $^{15}\text{N}$ -labeled protein were studied. For  $^{15}\text{N}$ -labeled talin-F0 or kindlin2-F0, experiments were performed at 25 °C in buffer containing 20 mM  $\text{NaH}_2\text{PO}_4/\text{Na}_2\text{HPO}_4$  (pH 6.6), 50 mM NaCl, 5 mM  $\text{MgCl}_2$ , 2 mM dithiothreitol (DTT), and 5%  $\text{D}_2\text{O}$ . For  $^{15}\text{N}$ -labeled Rap1b (1–167), experiments were performed at 25 °C in buffer containing 25 mM  $\text{NaH}_2\text{PO}_4/\text{Na}_2\text{HPO}_4$  (pH 6.8), 150 mM NaCl, 5 mM  $\text{MgCl}_2$ , 2 mM DTT, and 5%  $\text{D}_2\text{O}$ . Chemical shift change ( $\Delta\delta_{\text{obs}}^{\text{[HN,N]}}$ ) was calculated with the equation  $\Delta\delta_{\text{obs}}^{\text{[HN,N]}} = [(\Delta\delta_{\text{HN}}W_{\text{HN}})^2 + (\Delta\delta_{\text{N}}W_{\text{N}})^2]^{1/2}$ , where  $W_{\text{HN}}$  and  $W_{\text{N}}$  are weighting factors based on the gyromagnetic ratios of  $^1\text{H}$  and  $^{15}\text{N}$  ( $W_{\text{HN}} = 1$  and  $W_{\text{N}} = 0.154$ ) and  $\Delta\delta$  (p.p.m.) =  $\delta_{\text{bound}} - \delta_{\text{free}}$ . For HSQC titration, samples containing 45 μM  $^{15}\text{N}$ -labeled talin-F0 with increasing amount of GMP-PNP-loaded Rap1b (G12V) were used to collect 2D-HSQC spectra. Dissociation constant ( $K_d$ ) was achieved by fitting the chemical shift changes into the equation as shown below<sup>47</sup>. Four independent well-resolved residues were selected for fitting and an average  $K_d$  was obtained.

$$\Delta\delta_{\text{obs}} = \Delta\delta_{\text{max}} \left( \frac{[K_d + [P]_t + [L]_t]}{[K_d + [P]_t + [L]_t]^2 - 4 \times [P]_t \times [L]_t} \right)^{1/2} / 2[P]_t$$

( $\Delta\delta_{\text{max}}$  maximum chemical shift change;  $[P]_t$ , labeled protein concentration;  $[L]_t$ , ligand or titrant concentration).

**GST pull-down.** A volume of ~25 μg purified GST or GST-fused protein was immobilized on 15 μl glutathione-Sepharose 4B resin (beads) via incubation on a rotator for 1.5 h at 4 °C in the binding buffer containing 25 mM Tris-HCl (pH 7.5), 150 mM NaCl, 5 mM  $\text{MgCl}_2$ , 1 mM DTT, 0.01% Nondiet P-40, and supplemented with Complete EDTA-free Protease Inhibitor (Roche, Indianapolis, IN). Desired amount of prey protein was then added in and incubated with beads for another 2 h at 4 °C. After that, the beads were washed by 600 μl binding buffer twice and subjected to be denatured by adding 35 μl 2 × SDS loading buffer and boiling for 5 min. After centrifuging down, supernatants were resolved by SDS-PAGE or western blotting. All the pull-down experiments were performed in triplicate independently.

**Western blotting and antibodies.** After SDS-PAGE, samples were transferred onto a 0.45 μm polyvinylidene fluoride (PVDF) membrane (Millipore, Billerica, MA). The membrane was blocked with 5% non-fat milk in TBST buffer overnight at 4 °C. After that, the membrane was incubated with primary antibody at RT for 3 h and then incubated with horseradish peroxidase (HRP)-conjugated secondary antibody at RT for 1 h. The blots were detected by Pierce ECL Western Blotting Substrate (Thermo Fisher Scientific). The following primary antibodies were used in this study: 6xHis epitope tag antibody (Catalog# MA1-21315, Thermo Fisher Scientific), Rap1a/Rap1b (26B4) Rabbit mAb (Catalog# 2399, Cell Signaling Technology), Ras (27H5) Rabbit mAb (Catalog# 3339, Cell Signaling Technology), GAPDH (D16H11) Rabbit mAb (Catalog# 5174, Cell Signaling Technology), Anti-Talin-1 antibody (Catalog# ab57758, Abcam Inc.), and Anti-RIAM antibody (EPR2806; Catalog# ab92537, Abcam Inc.). The following secondary antibodies were used in this study: anti-mouse IgG, HRP-linked antibody (Catalog# 7076, Cell Signaling Technology), and anti-rabbit IgG, HRP-linked antibody (Catalog# 7074, Cell Signaling Technology). Primary antibodies were used at 1:1000 dilution, and secondary antibodies were used at 1:3000 dilution.

**Assignment of Rap1b and talin-F0 and their bound forms.** C-terminal truncated Rap1b (1–167) with G12V mutation was used in all the following structure determination studies. For assignment of Rap1b,  $^{15}\text{N}/^{13}\text{C}$ -labeled Rap1b was purified and the N-terminal 6xHis tag was removed during purification. Standard triple-resonance experiments were conducted with 0.6 mM GMP-PNP-loaded Rap1b. Rap1b sequential assignment was performed using PASA software<sup>48</sup>. For assignment of talin-F0, the complete chemical shift-assignment table of talin-F0 from Biological Magnetic Resonance Data Bank (accession code 15458) was downloaded and used in this study<sup>26</sup>. Amide proton to nitrogen to α-carbon correlation (HNCA) experiment was performed on 1.0 mM  $^{15}\text{N}/^{13}\text{C}$ -labeled talin-F0 to confirm the assigned resonances. All these experiments were performed on Bruker 600 MHz NMR spectrometer, and at 25 °C in the buffer that contained 20 mM  $\text{NaH}_2\text{PO}_4/\text{Na}_2\text{HPO}_4$  (pH 6.6), 50 mM NaCl, 5 mM  $\text{MgCl}_2$ , 2 mM d-DTT, and 5%  $\text{D}_2\text{O}$ . For assignments of the bound Rap1b and talin-F0 forms, the chemical shifts of majority of residues were readily transferred from the free forms with slight adjustments as they are similar to those of the free forms. A few residues (e.g., I27, R41) exhibited duplex peaks in the free form of Rap1 likely due to local conformational flexibility, and most of these peaks were merged into single peaks in the complex. All assignments were also verified by through-bond NOESY experiments of the complex.

**3D-NOESY experiments.** The following samples were prepared: (1) 0.6 mM  $^{15}\text{N}/^{13}\text{C}$ -labeled Rap1b in the presence of 0.9 mM unlabeled talin-F0, (2) 0.5 mM  $^{15}\text{N}/^{13}\text{C}$ -labeled talin-F0 in the presence of 0.7 mM unlabeled Rap1b, (3) 0.5 mM  $^{15}\text{N}/^{100\%}\text{D}_2\text{O}$ -labeled talin-F0 in the presence of 0.7 mM unlabeled Rap1b, and (4) 0.5 mM  $^{15}\text{N}/^{13}\text{C}$ -labeled talin-F0 in the presence of 0.7 mM unlabeled Rap1b prepared in 99.8%  $\text{D}_2\text{O}$ . The following NOESY experiments were performed using the above samples: (i) 3D  $^{15}\text{N}/^{13}\text{C}$ -edited NOESY experiment (120 ms mixing time) with sample 1, (ii) 3D  $^{15}\text{N}/^{13}\text{C}$ -edited NOESY experiment (120 ms mixing time) with sample 2, (iii) 3D  $^{15}\text{N}$ -edited NOESY experiment (300 ms mixing time) with sample 3, and (iv) 3D  $^{15}\text{N}/^{13}\text{C}$ -filtered NOESY experiment (120 ms mixing time) with sample 4. All these experiments were performed on Bruker 850 or 900 MHz spectrometers at the same condition as mentioned above.

**Structure determination.** All NMR data were processed and analyzed using nmrPipe<sup>49</sup>, PIPP<sup>50</sup>, and Sparky<sup>51</sup>. Distance restraints (NOE constraints) were obtained from 3D-NOESY experiments mentioned above, and Xplor-NIH<sup>52</sup> was used to calculate the complex structure. In brief, the individual structures of Rap1b and talin-F0 in complex form were calculated first based on the NOEs collected from sample 1 (2308 NOEs) and sample 2 (1114 NOEs), respectively. 302 dihedral-angle restraints for Rap1b derived from TALOS<sup>53</sup> were applied during Rap1b structure calculation. The initial templates for Rap1b and talin-F0 were derived from PDB database with PDB codes of 4DXA and 3IVF, respectively. A total of 78 unambiguous intermolecular NOEs collected from sample 3 and sample 4 were used to calculate complex structure (also see Supplementary Table 1 for structural



statistics). After refinements, a total of 50 final structures were calculated and the 20 lowest-energy structures were selected for analysis. The quality of structure was evaluated with PROCHECK<sup>54</sup>. Structures are visualized by PyMOL 1.3 (Schrödinger LLC.).

**Membrane-anchored Rap1b preparation.** To prepare large unilamellar vesicles (LUVs), 1-palmitoyl-2-oleoyl-sn-glycero-3-phosphocholine (POPC), L- $\alpha$ -phosphatidylinositol-4,5-bisphosphate (PI(4,5)P<sub>2</sub>), and 1,2-dipalmitoyl-sn-glycero-3-phosphoethanolamine-N-[4-(p-maleimidomethyl)cyclohexane-carboxamide] (16:0 PE MCC) were purchased from Avanti Polar Lipids. LUVs, which consist of 96% POPC, 1% PIP<sub>2</sub>, and 3% PE MCC, were prepared by extrusion. In brief, lipids were first dissolved together in chloroform, and then the chloroform was removed under a stream of nitrogen followed by overnight vacuum pumping. The lipid film was suspended in buffer containing 25 mM NaH<sub>2</sub>PO<sub>4</sub>/Na<sub>2</sub>HPO<sub>4</sub> (pH 6.8), 100 mM NaCl, and 5 mM MgCl<sub>2</sub>, and subjected to homogenization with a few freeze-thaw cycles. LUVs were finally formed by extruding the lipid suspension ~20 times through two stacked 0.1 mm polycarbonate filters. Rap1b was tethered to LUVs via Michael addition between the thiol group of Cys 180 and the maleimide group of PE MCC<sup>41,55</sup>. To mimic the physiological condition that only the C-terminal Cys 180 of Rap1b is attached to membrane and meanwhile to avoid nonspecific chemical interactions, all the cysteines of Rap1b except Cys 180 were mutated to serines. Rap1b\_TM1 (C51S, C118S, and C141S) and Rap1b\_TM2 (G12V, C51S, C118S, and C141S) were generated, purified, and loaded with GDP- $\beta$ -S and GMP-PNP, respectively, as described above. Rap1b\_TM2 was first confirmed to interact with <sup>15</sup>N-talin-F0 by HSQC (Supplementary Fig. 10a). To make Rap1b-anchored LUVs, Rap1b\_TM1 or Rap1b\_TM2 was incubated with freshly prepared LUVs in 1:6 molar ratio overnight at RT in the same buffer. The reaction was terminated by adding  $\beta$ -mercaptoethanol to a final concentration of 5 mM. The achievement of membrane-anchored Rap1b was confirmed by Native-PAGE combined with SDS-PAGE (Supplementary Figs. 10b and 20). Unanchored Rap1b was dialyzed out in the same buffer using a dialyzer with 100 kDa cutoff membrane (Harvard Apparatus) before use.

**Vesicle co-sedimentation.** Multilamellar vesicles (MLVs) rather than LUVs are used in this study since MLVs are larger in size and could be pelleted down easily. MLVs, which consist of 87% POPC, 10% PIP<sub>2</sub>, and 3% PE MCC were prepared similarly to LUVs as described above but without extrusion. MLVs with anchored Rap1b (either GDP- $\beta$ -S or GMP-PNP) were also prepared similarly as described above. Talin-H (10  $\mu$ M) or full-length talin was incubated with 10  $\mu$ M “MLV-Rap1b (Rap1b-anchored MLVs)”, “MLV only”, and “MLV + Rap1b (MLVs with unanchored Rap1b)” separately in a “7 × 21 mm” Polycarbonate tube (Beckman Coulter Inc.) with a total volume of 30  $\mu$ l at RT for 15 min. Samples were then centrifuged down at 22,000 r.p.m. for 35 min. Membrane pellet was dissolved in 2 × SDS loading buffer and subjected to SDS-PAGE analysis. Gels were stained with Coomassie blue, and then scanned and quantified with an Odyssey CLx Imaging System (LI-COR Inc.). The intensities of protein bands were quantified by the fluorescent signal detected from the 700 nm channel according to the manufacturer's protocol. Experiments were performed in quadruplets. Statistical significance was tested by two-tailed unpaired *t*-test.

**Isothermal titration calorimetry.** ITC experiments were performed using a Microcal iTC 200 system (GE Healthcare Life Sciences) at 25 °C. Before experiments, all samples were dialyzed into the same buffer that contained 25 mM NaH<sub>2</sub>PO<sub>4</sub>/Na<sub>2</sub>HPO<sub>4</sub> (pH 6.8), 100 mM NaCl, and 5 mM MgCl<sub>2</sub> overnight at 4 °C. Talin-H (200  $\mu$ M) in the syringe (~40  $\mu$ l) was injected 20 times in 2.0  $\mu$ l aliquots into the sample-cell (~220  $\mu$ l) containing 15  $\mu$ M LUV-Rap1b (GMP-PNP). As controls (Supplementary Fig. 10c), talin-H was titrated into LUV only, Rap1b only, or buffer only, and talin-H\_DM was titrated into LUV-Rap1b (GMP-PNP) using the same condition. ITC Data were analyzed by fitting to a single-site binding model with Origin Software.

**Microscale thermophoresis analysis.** The affinity of the interaction between GMP-PNP-loaded GFP-Rap1b (G12V) and RIAM-RAPH, talin-F0 or talin-H was measured by using a Monolith NT.115 instrument (NanoTemper Technologies). Rap1b (G12V) was subcloned into a pRSET vector (Thermo Fisher Scientific), which expresses an N-terminal 6xHis tag and a C-terminal GFP fusion tag. RIAM-RAPH, talin-F0, or talin-H was prepared at different concentrations through 1:1 serial dilution and then mixed with 100 nM GFP-Rap1b (G12V) in buffer containing 50 mM Tris-HCl (pH 7.5), 100 mM NaCl, 5 mM MgCl<sub>2</sub>, 2 mM DTT, and 0.05% Tween 20. The samples were incubated at RT for 10 min and then loaded into microscale thermophoresis (MST) standard or premium capillary tubes. The fluorescent signal of GFP fusion tag was detected by the blue channel of the instrument according to the manufacturer's protocol, and the data were collected using 20% LED power and 40% MST powder at RT. Three independent experiments were performed, and the collected MST data were used to fit the dissociation constant (*K*<sub>d</sub>) by using the MO. Affinity Analysis software (NanoTemper Technologies).

**Integrin activation assay.** Wild-type talin-H or talin-H\_DM (K15A, R35A) was subcloned into a pEGFP-C1 vector. CHO A5 cells stably expressing integrin  $\alpha_{\text{IIb}}\beta_3$  were transfected with empty vector, wild-type talin-H, or talin-H\_DM using Lipofectamine 2000 reagent (Life Technologies). After 24 h, cells were stained with anti- $\alpha_{\text{IIb}}\beta_3$  activation-specific mAb PAC1 (1:100 dilution; Catalog# 340535, BD Biosciences) at RT for 40 min, and later incubated with Alexa Fluor 647 Goat Anti-Mouse IgM (Catalog# 115-607-020, Jackson ImmunoResearch Laboratories; 1:3000 dilution) on ice for 30 min. After wash, cells were fixed and subjected to flow cytometry analysis. Values for PAC1 binding were reported as median fluorescent intensities and the data were normalized to control with empty vector only and are presented by the means  $\pm$  S.E.M. The two-tailed unpaired *t*-test was performed to calculate the *p* value using GraphPad software.

**Generation of cell lines and cell culture conditions.** Murine talin1 and 2 double-knockout fibroblasts (talin1<sup>1/2dko</sup>)<sup>38</sup> were retrovirally transduced with pLPCX expression construct containing YPET alone, C terminally YPET-tagged talin-1 cDNA (talin WT), or YPET-tagged double-mutant talin-1 (talin DM; K15A, R35A) using the Phoenix retroviral expression system. Phoenix cells were transfected using a conventional calcium phosphate protocol and five infection cycles were performed by transferring the phoenix cell culture supernatant supplemented with 5  $\mu$ g ml<sup>-1</sup> polybrene to talin1<sup>1/2dko</sup> cells<sup>56,57</sup>. Cells were FACS-sorted using a FACSaria™ IIu cell sorter (BD Biosciences, Heidelberg, Germany) to isolate cells with comparable expression levels. Cells were characterized by western blotting using mouse  $\alpha$ -GFP (home-made), rabbit anti-talin-1 (Catalog# sc-15336, Santa Cruz Biotechnology Inc.), rabbit anti-Rap1 (Catalog# sc-65, Santa Cruz Biotechnology Inc.), rabbit anti-RIAM (Catalog# ab92537, Abcam Inc.), mouse anti-GAPDH (Catalog# CB1001-500UG, Millipore), goat anti-rabbit-HRP (Catalog# 111-035-144, Jackson ImmunoResearch Laboratories), and goat anti-mouse-HRP (Catalog# 115-035-003, Jackson ImmunoResearch Laboratories Inc.) antibodies following standard protocols. Rabbit anti-talin-1, rabbit anti-Rap1, and rabbit anti-RIAM antibodies were used at a dilution of 1:1000. Mouse anti-GAPDH, goat anti-rabbit-HRP, and goat anti-mouse-HRP antibodies were used at a dilution of 1:20,000. Cells were cultured under standard conditions in DMEM GlutaMAX™ (Thermo Fisher Scientific) supplemented with 10% fetal bovine serum, 100 U ml<sup>-1</sup> penicillin, 100  $\mu$ g ml<sup>-1</sup> streptomycin, and non-essential amino acids (all from Thermo Fisher Scientific).

**Adhesion and spreading assays.** For adhesion assays, polystyrol flat-bottom 96-well microplates (Greiner Bio-One, Frickenhausen, Germany) were coated with 10  $\mu$ g ml<sup>-1</sup> laminin (Sigma) in HBSS (Thermo Fisher Scientific), 5  $\mu$ g ml<sup>-1</sup> FN, 0.01 % poly-L-lysine (both Sigma), or 5  $\mu$ g ml<sup>-1</sup> VN (STEMCELL Technologies, Köln, Germany) in coating buffer (20 mM Tris-HCl pH 9.0, 150 mM NaCl, 2 mM MgCl<sub>2</sub>) overnight at 4 °C. After blocking with 3% bovine serum albumin in PBS for 30 min at room temperature, 4 × 10<sup>4</sup> cells in DMEM containing 0.1 % FBS, and 25 mM HEPES were seeded per well, incubated for 1 h, and washed with PBS. Adherent cells were fixed with 4% paraformaldehyde (PFA) for 15 min and stained with 5 mg ml<sup>-1</sup> crystal violet in 2% ethanol for 30 min. After washing, remaining crystal violet was dissolved in 2% SDS and quantified by measuring absorbance at 595 nm using a microplate reader (Tecan, Männedorf, Switzerland). All experiments were performed in quadruplets. For spreading analysis, cells were plated on FN (5  $\mu$ g ml<sup>-1</sup>)-coated dishes and phase contrast pictures were taken using an EVOS™ FL Auto live cell microscope (Thermo Fisher Scientific) 5, 15, 30, 60, 120, and 240 min after seeding the cells. Cell spreading area of 30 cells per group at each time point were measured using ImageJ software (US National Institutes of Health). Statistical significance was tested by two-tailed paired *t*-test.

**Flow cytometry.** Integrin surface expression was determined by FACS using a LSRFortessa™ X-20 flow cytometer (BD Biosciences). Staining and measurement were performed in PBS supplemented with 2% FBS and 2 mM EDTA. Cells were incubated with biotinylated anti-integrin antibodies and subsequently with Cy5-labeled streptavidin (Catalog# 016-170-084, Jackson ImmunoResearch Laboratories). Data were analyzed using FlowJo software. The following antibodies were used for flow cytometry: hamster IgM anti-integrin  $\beta_1$  (Catalog# 13-0291-82, eBioscience), rat IgG2a anti-integrin  $\alpha_6$  (Catalog# 13-0495-82, eBioscience), rat IgG1 isotype control (Thermo Fisher Scientific), hamster IgG isotype control (Thermo Fisher Scientific), hamster IgG anti-integrin  $\beta_3$  (Catalog# 553345, BD Pharmingen), rat IgG2a anti-integrin  $\alpha_5$  (Catalog# 557446, BD Pharmingen™), rat IgG1 anti-integrin  $\alpha_V$  (Catalog #104104, BioLegend), hamster IgM isotype control (BioLegend), and rat IgG2a isotype control (BioLegend). All listed antibodies were biotinylated and used at 1:200 dilution.

**Immunostaining and FA analysis.** Cells were cultured on FN-coated glass coverslips (Thermo Fisher Scientific) overnight or on FN-coated micropatterns (disc-shaped with 1100  $\mu$ m<sup>2</sup> area; Cytoo, Grenoble, France) for 5 h and fixed for 10 min with 4% PFA. Mouse anti-paxillin with a dilution of 1:300 (Catalog# 610051, BD Transduction Laboratories, Heidelberg, Germany), goat anti-mouse-Cy3 with a dilution of 1:400 (Catalog# 115-165-146, Jackson ImmunoResearch Laboratories), and Phalloidin-Alexa Fluor 647 with a dilution of 1:100 (Catalog# A22287, Thermo Fisher Scientific) were used for immunostainings. Images were acquired using a



Leica TCS SP5 X confocal microscope (Leica Microsystems, Wetzlar, Germany) equipped with  $\times 63$  numerical aperture (NA) 1.40 oil objective lenses and Leica Confocal Software (LAS AF). All pictures were processed with Photoshop (Adobe Systems, San José, CA, USA). FA area was defined by paxillin staining and quantified using ImageJ software. For quantitative analysis of talin recruitment to FAs, the total ypet signal intensity within the FA area was normalized to the total ypet fluorescence of the whole cell. Statistical significance was tested by two-tailed paired *t*-test.

**Cell lysate preparations.** Various types of cells indicated in Fig. 6a were isolated from blood or cultured cells. Cells were washed once with cold PBS, and lysed by adding buffer that contained 50 mM Tris-HCl (pH 6.8) and 1% SDS. The cell lysates were boiled for 5 min, and the concentration of total protein in each cell lysate was quantified with Pierce BCA Protein Assay Kit (Thermo Fisher Scientific). Approximately 8  $\mu$ g total protein for each lysate was loaded onto SDS-PAGE gels for western blotting analysis.

**Data availability.** Accession codes: The complete chemical shift-assignment tables of free Rap1b, bound Rap1b, and bound talin-F0 have been deposited in the Biological Magnetic Resonance Bank (BMRB) with the accession code 30353. The coordinates of Rap1b/talin-F0 complex structure have been deposited in the Protein Data Bank (PDB) with the code 6BA6. Other data are available from the corresponding authors upon reasonable request.

Received: 11 April 2017 Accepted: 18 October 2017

Published online: 23 November 2017

## References

- Springer, T. A. Adhesion receptors of the immune system. *Nature* **346**, 425–434 (1990).
- Hynes, R. O. Integrins: bidirectional, allosteric signaling machines. *Cell* **110**, 673–687 (2002).
- Qin, J., Vinogradova, O. & Plow, E. F. Integrin bidirectional signaling: a molecular view. *PLoS Biol.* **2**, e169 (2004).
- Moser, M., Legate, K. R., Zent, R. & Fassler, R. The tail of integrins, talin, and kindlins. *Science* **324**, 895–899 (2009).
- Calderwood, D. A., Campbell, I. D. & Critchley, D. R. Talins and kindlins: partners in integrin-mediated adhesion. *Nat. Rev. Mol. Cell Biol.* **14**, 503–517 (2013).
- Arnaout, M. A. Biology and structure of leukocyte beta 2 integrins and their role in inflammation. *F1000Res* **5**, 2433 (2016).
- Goksoy, E. et al. Structural basis for the autoinhibition of talin in regulating integrin activation. *Mol. Cell* **31**, 124–133 (2008).
- Song, X. et al. A novel membrane-dependent on/off switch mechanism of talin FERM domain at sites of cell adhesion. *Cell Res.* **22**, 1533–1545 (2012).
- Goult, B. T. et al. The structure of an interdomain complex that regulates talin activity. *J. Biol. Chem.* **284**, 15097–15106 (2009).
- Goult, B. T. et al. Structural studies on full-length talin1 reveal a compact auto-inhibited dimer: implications for talin activation. *J. Struct. Biol.* **184**, 21–32 (2013).
- Martel, V. et al. Conformation, localization, and integrin binding of talin depend on its interaction with phosphoinositides. *J. Biol. Chem.* **276**, 21217–21227 (2001).
- Yang, J. et al. Conformational activation of talin by RIAM triggers integrin-mediated cell adhesion. *Nat. Commun.* **5**, 5880 (2014).
- Schiemer, J. et al. Galpha13 switch region 2 relieves talin autoinhibition to activate alphaIIb beta3 integrin. *J. Biol. Chem.* **291**, 26598–26612 (2016).
- Vinogradova, O. et al. A structural mechanism of integrin alpha(IIb)beta(3) “inside-out” activation as regulated by its cytoplasmic face. *Cell* **110**, 587–597 (2002).
- Kim, M., Carman, C. V. & Springer, T. A. Bidirectional transmembrane signaling by cytoplasmic domain separation in integrins. *Science* **301**, 1720–1725 (2003).
- Wegener, K. L. et al. Structural basis of integrin activation by talin. *Cell* **128**, 171–182 (2007).
- Xu, X. P. et al. Three-dimensional structures of full-length, membrane-embedded human alpha(IIb)beta(3) integrin complexes. *Biophys. J.* **110**, 798–809 (2016).
- Shattil, S. J., Kim, C. & Ginsberg, M. H. The final steps of integrin activation: the end game. *Nat. Rev. Mol. Cell Biol.* **11**, 288–300 (2010).
- Zeiler, M., Moser, M. & Mann, M. Copy number analysis of the murine platelet proteome spanning the complete abundance range. *Mol. Cell Proteomics* **13**, 3435–3445 (2014).
- Stritt, S. et al. Rap1-GTP-interacting adaptor molecule (RIAM) is dispensable for platelet integrin activation and function in mice. *Blood* **125**, 219–222 (2015).
- Klapproth, S. et al. Loss of the Rap1 effector RIAM results in leukocyte adhesion deficiency due to impaired beta2 integrin function in mice. *Blood* **126**, 2704–2712 (2015).
- Su, W. et al. Rap1 and its effector RIAM are required for lymphocyte trafficking. *Blood* **126**, 2695–2703 (2015).
- Chrzanowska-Wodnicka, M., Smyth, S. S., Schoenwaelder, S. M., Fischer, T. H. & White, G. C. 2nd Rap1b is required for normal platelet function and hemostasis in mice. *J. Clin. Invest.* **115**, 680–687 (2005).
- Nieswandt, B. et al. Loss of talin1 in platelets abrogates integrin activation, platelet aggregation, and thrombus formation in vitro and in vivo. *J. Exp. Med.* **204**, 3113–3118 (2007).
- Petrich, B. G. et al. Talin is required for integrin-mediated platelet function in hemostasis and thrombosis. *J. Exp. Med.* **204**, 3103–3111 (2007).
- Goult, B. T. et al. Structure of a double ubiquitin-like domain in the talin head: a role in integrin activation. *EMBO J.* **29**, 1069–1080 (2010).
- Plak, K., Pots, H., Van Haastert, P. J. & Kortholt, A. Direct interaction between TalinB and Rap1 is necessary for adhesion of dictyostelium cells. *BMC Cell Biol.* **17**, 1 (2016).
- White, G. C. 2nd, Crawford, N. & Fischer, T. H. Cytoskeletal interactions of Rap1b in platelets. *Adv. Exp. Med. Biol.* **344**, 187–194 (1993).
- Hancock, J. F. Ras proteins: different signals from different locations. *Nat. Rev. Mol. Cell Biol.* **4**, 373–384 (2003).
- Gloerich, M. & Bos, J. L. Regulating rap small G-proteins in time and space. *Trends Cell Biol.* **21**, 615–623 (2011).
- Chrzanowska-Wodnicka, M. Rap1 in endothelial biology. *Curr Opin Hematol.* **24**, 248–255 (2017).
- Vaynberg, J. & Qin, J. Weak protein-protein interactions as probed by NMR spectroscopy. *Trends Biotechnol.* **24**, 22–27 (2006).
- Perera, H. D. et al. Membrane binding of the N-terminal ubiquitin-like domain of kindlin-2 is crucial for its regulation of integrin activation. *Structure* **19**, 1664–1671 (2011).
- Li, X. et al. Structural basis for small G protein effector interaction of Ras-related protein 1 (Rap1) and adaptor protein Krev interaction trapped 1 (KRIT1). *J. Biol. Chem.* **287**, 22317–22327 (2012).
- Wynne, J. P. et al. Rap1-interacting adapter molecule (RIAM) associates with the plasma membrane via a proximity detector. *J. Cell Biol.* **199**, 317–330 (2012).
- Das, M., Subbayya Ithychanda, S., Qin, J. & Plow, E. F. Mechanisms of talin-dependent integrin signaling and crosstalk. *Biochim. Biophys. Acta* **1838**, 579–588 (2014).
- Bouaouina, M., Lad, Y. & Calderwood, D. A. The N-terminal domains of talin cooperate with the phosphotyrosine binding-like domain to activate beta1 and beta3 integrins. *J. Biol. Chem.* **283**, 6118–6125 (2008).
- Theodosiou, M. et al. Kindlin-2 cooperates with talin to activate integrins and induces cell spreading by directly binding paxillin. *Elife* **5**, e10130 (2016).
- Pollard, T. D., Blanchoin, L. & Mullins, R. D. Molecular mechanisms controlling actin filament dynamics in nonmuscle cells. *Annu. Rev. Biophys. Biomol. Struct.* **29**, 545–576 (2000).
- Elliott, P. R. et al. The Structure of the talin head reveals a novel extended conformation of the FERM domain. *Structure* **18**, 1289–1299 (2010).
- Gureasko, J. et al. Membrane-dependent signal integration by the Ras activator Son of sevenless. *Nat. Struct. Mol. Biol.* **15**, 452–461 (2008).
- Pizon, V., Leroisey, I., Chardin, P. & Tavittian, A. Nucleotide sequence of a human cDNA encoding a ras-related protein (rap1B). *Nucleic Acids Res.* **16**, 7719 (1988).
- Lilja, J. et al. SHANK proteins limit integrin activation by directly interacting with Rap1 and R-Ras. *Nat. Cell Biol.* **19**, 292–305 (2017).
- Lagarigue, F. et al. A RIAM/lamellipodin-talin-integrin complex forms the tip of sticky fingers that guide cell migration. *Nat. Commun.* **6**, 8492 (2015).
- Gavin, A. C. et al. Functional organization of the yeast proteome by systematic analysis of protein complexes. *Nature* **415**, 141–147 (2002).
- Hein, M. Y. et al. A human interactome in three quantitative dimensions organized by stoichiometries and abundances. *Cell* **163**, 712–723 (2015).
- Williamson, M. P. Using chemical shift perturbation to characterise ligand binding. *Prog. Nucl. Magn. Reson. Spectrosc.* **73**, 1–16 (2013).
- Xu, Y., Wang, X., Yang, J., Vaynberg, J. & Qin, J. PASA—a program for automated protein NMR backbone signal assignment by pattern-filtering approach. *J. Biomol. NMR* **34**, 41–56 (2006).
- Delaglio, F. et al. NMRPipe: a multidimensional spectral processing system based on UNIX pipes. *J. Biomol. NMR* **6**, 277–293 (1995).
- Garrett, D. S., Powers, R., Gronenborn, A. M. & Clore, G. M. A common sense approach to peak picking in two-, three-, and four-dimensional spectra using automatic computer analysis of contour diagrams. 1991. *J. Magn. Reson.* **213**, 357–363 (2011).



51. Goddard T. D. & Kneller D. G. SPARKY 3 (University of California, San Francisco). <http://www.cgl.ucsf.edu/home/sparky/>.
52. Schwieters, C. D., Kuszewski, J. J., Tjandra, N. & Clore, G. M. The Xplor-NIH NMR molecular structure determination package. *J. Magn. Reson.* **160**, 65–73 (2003).
53. Shen, Y., Delaglio, F., Cornilescu, G. & Bax, A. TALOS+: a hybrid method for predicting protein backbone torsion angles from NMR chemical shifts. *J. Biomol. NMR* **44**, 213–223 (2009).
54. Laskowski, R. A., Rullmann, J. A., MacArthur, M. W., Kaptein, R. & Thornton, J. M. AQUA and PROCHECK-NMR: programs for checking the quality of protein structures solved by NMR. *J. Biomol. NMR* **8**, 477–486 (1996).
55. Moore, D. T. et al. Affinity of talin-1 for the beta3-integrin cytosolic domain is modulated by its phospholipid bilayer environment. *Proc. Natl Acad. Sci. USA* **109**, 793–798 (2012).
56. Austen, K. et al. Extracellular rigidity sensing by talin isoform-specific mechanical linkages. *Nat. Cell Biol.* **17**, 1597–1606 (2015).
57. Austen, K., Kluger, C., Freikamp, A., Chrostek-Grashoff, A. & Grashoff, C. Generation and analysis of biosensors to measure mechanical forces within cells. *Methods Mol. Biol.* **1066**, 169–184 (2013).

## Acknowledgements

We thank Reinhard Fässler for providing us with talin1/2 double-knockout fibroblasts. This work was supported by NIH grants R01HL58758, R01GM62823 to J.Q., P01HL073311 to E.F.P., the Max-Planck-Society, and the SFB1123 TP A08 to M.M. We thank Jianmin Liu, Koichi Fukuda, Sujay Ithychanda, and Xi-An Mao for assistance and useful discussions.

## Author contributions

L.Z., M.M. and J.Q. conceived this study. L.Z. performed all biochemical/biophysical studies including NMR 2D-HSQC experiments, GST pull-down assays, ITC experiments, and MST assay. L.Z. and J.Y. performed all 3D-NMR studies and determined the solution structure of Rap1b/talin-F0 complex. T.B. and S.K. performed the functional experiments showing that the double mutations of talin resulted in defective cell adhesion and

spreading, and T.B., S.K. and M.M. analyzed the data. A.H. and J.H. performed the integrin activation assay in CHO A5 cells. L.Z., F.L. and J.Y. designed and performed vesicle co-sedimentation assays. L.Z. and H.L. prepared various types of cell lysates and analyzed the expression levels of desired proteins. L.Z. and K.S. prepared  $^{15}\text{N}/^{13}\text{C}$ -labeled Rap1 and  $^{15}\text{N}/^{13}\text{C}$ -labeled talin-F0 for 3D-NMR studies. T.B. and E.F.P. participated in the interpretation and preparation of the manuscript. L.Z., M.M. and J.Q. wrote the manuscript with contributions from all other co-authors.

## Additional information

Supplementary Information accompanies this paper at doi:10.1038/s41467-017-01822-8.

**Competing interests:** The authors declare no competing financial interests.

**Reprints and permission information** is available online at <http://npg.nature.com/reprintsandpermissions/>

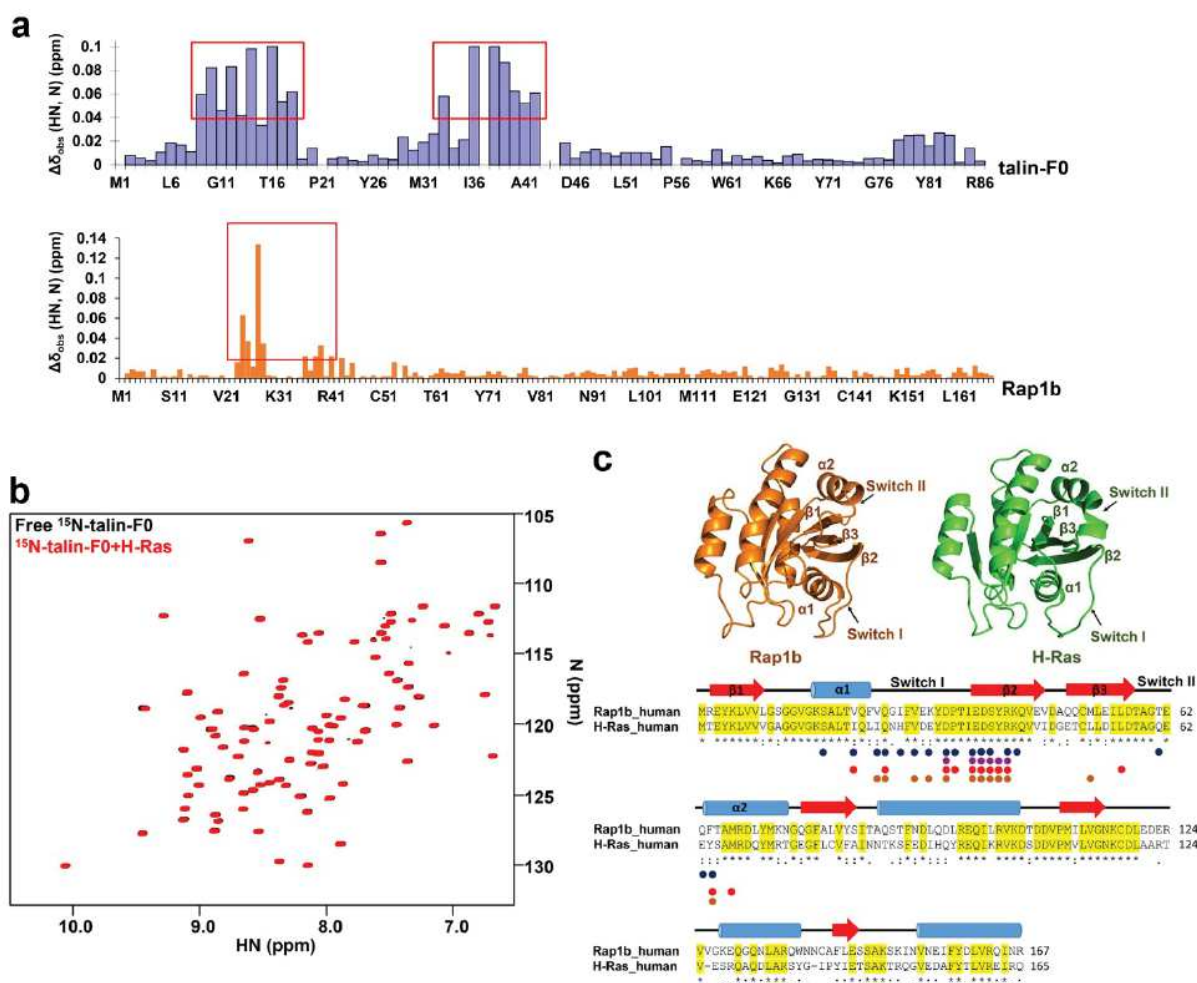
**Publisher's note:** Springer Nature remains neutral with regard to jurisdictional claims in published maps and institutional affiliations.



**Open Access** This article is licensed under a Creative Commons Attribution 4.0 International License, which permits use, sharing, adaptation, distribution and reproduction in any medium or format, as long as you give appropriate credit to the original author(s) and the source, provide a link to the Creative Commons license, and indicate if changes were made. The images or other third party material in this article are included in the article's Creative Commons license, unless indicated otherwise in a credit line to the material. If material is not included in the article's Creative Commons license and your intended use is not permitted by statutory regulation or exceeds the permitted use, you will need to obtain permission directly from the copyright holder. To view a copy of this license, visit <http://creativecommons.org/licenses/by/4.0/>.

© The Author(s) 2017

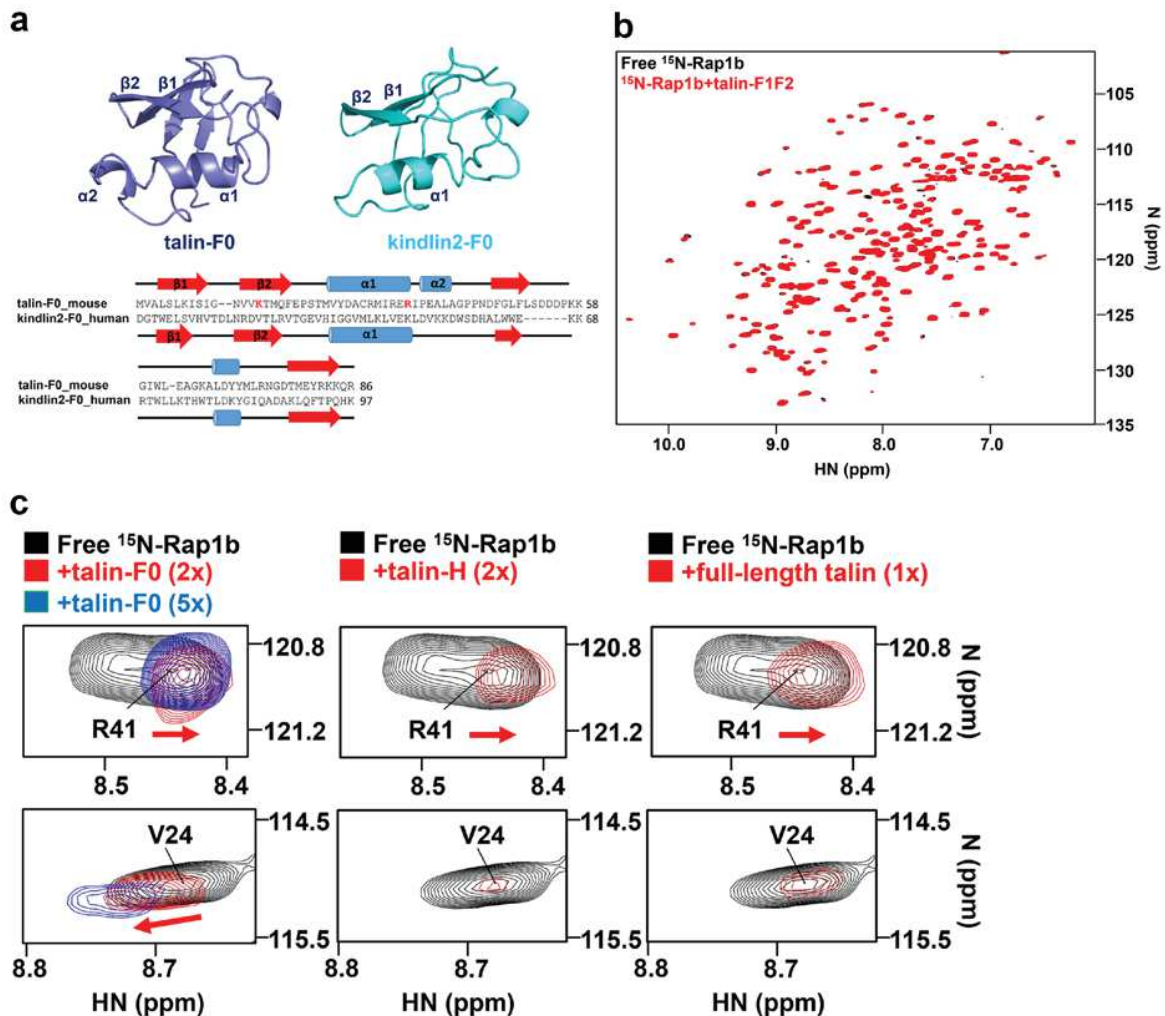
## Supplementary Figure 1



**Supplementary Figure 1. Rap1b but not H-Ras interacts with talin-F0** (a) Upper panel, the profile of chemical shift changes of 50  $\mu\text{M}$   $^{15}\text{N}$ -talin-F0 induced by 125  $\mu\text{M}$  GMP-PNP loaded Rap1b. The chemical shift changes of completely broadened residues (T16, I36 and E38) were set to 0.1 ppm. The most perturbed regions are boxed in red. Lower panel, the profile of chemical shift changes of 45  $\mu\text{M}$  GMP-PNP loaded  $^{15}\text{N}$ -labeled Rap1b (1-167) induced by 225  $\mu\text{M}$  talin-F0. The most perturbed region is boxed in red. (b) The HSQC spectra of 50  $\mu\text{M}$   $^{15}\text{N}$ -labeled talin-F0 in the absence (black) and presence of 125  $\mu\text{M}$  GMP-PNP loaded H-Ras (red). (c) Sequence alignment of Rap1b and H-Ras. Identical residues are highlighted in yellow. (\*) indicates fully conserved residue, (.) indicates residues with strongly similar properties, and (.) indicates residues with weakly similar properties. Residues of Rap1b involved in the binding interface (cut-off of 4 Å) with talin-F0, RIAM-RA, KRIT1-F1, and c-Raf1-RA are indicated in the figure with blue, purple, red and brown solid circles respectively.

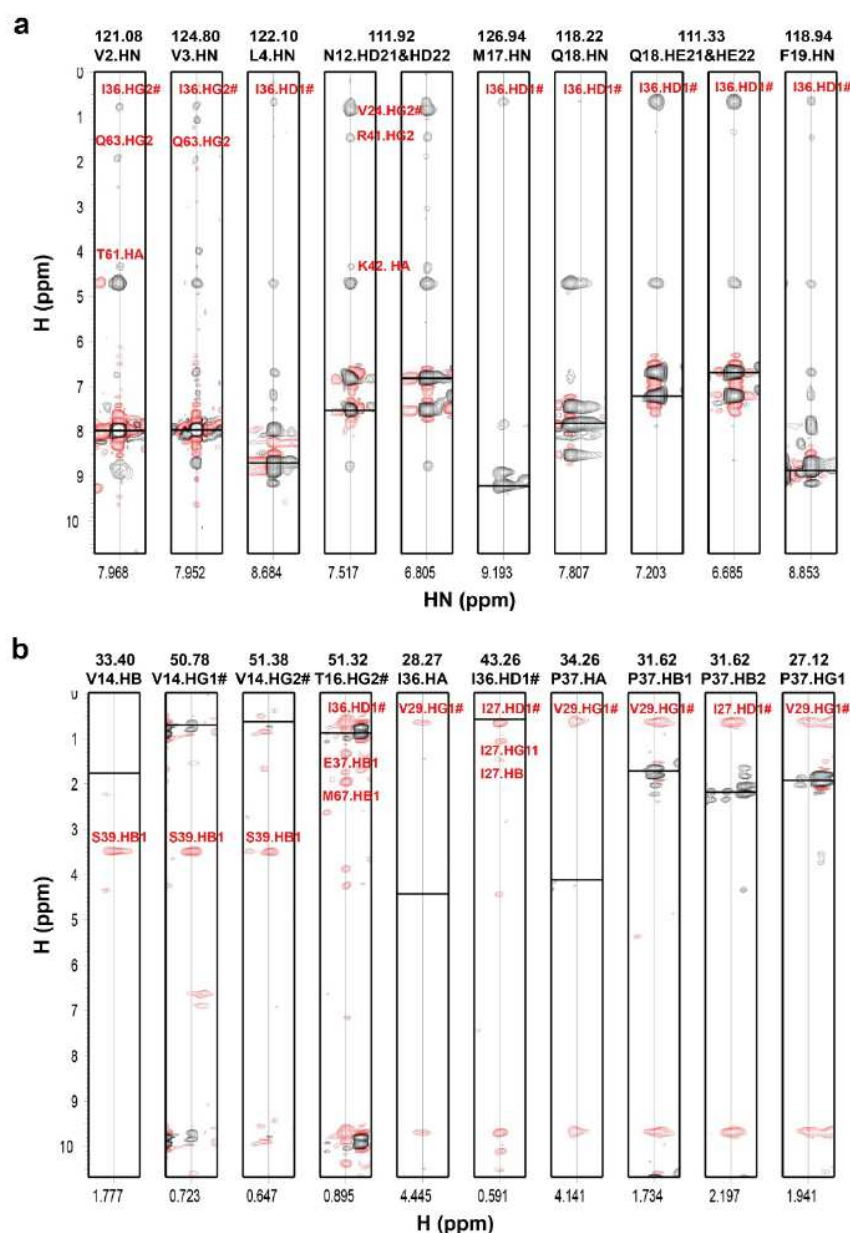


## Supplementary Figure 2



**Supplementary Figure 2. Neither talin-F1F2 nor kindlin2-F0 interacts with Rap1b** (a) Structure-based sequence alignment of talin-F0 and kindlin2-F0. (b) The HSQC spectra of 45  $\mu$ M GMP-PNP loaded  $^{15}$ N-labeled Rap1b (1-167) in the absence (black) and presence of 90  $\mu$ M talin-F1F2 (red). (c) The HSQC spectra (representative regions were shown) of 45  $\mu$ M GMP-PNP loaded  $^{15}$ N-labeled Rap1b (1-167) in the absence (black) and presence of 90  $\mu$ M talin-F0 (red), 225  $\mu$ M talin-F0 (blue), 90  $\mu$ M talin-H (red), or 45  $\mu$ M full-length talin (red). Note that the peak of V24 was broadened in the presence of talin-H or full-length talin.

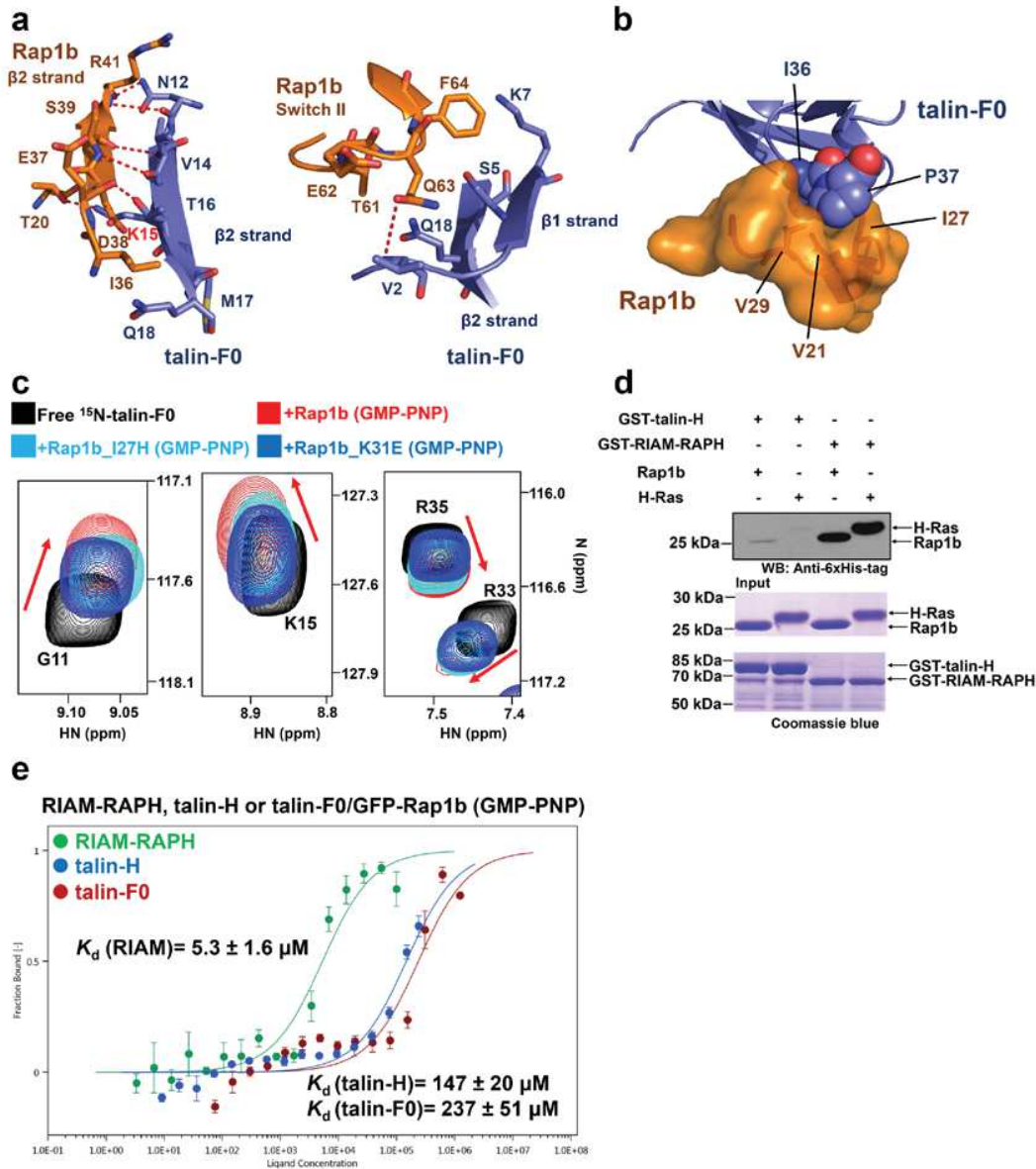
### Supplementary Figure 3



**Supplementary Figure 3. Representative intermolecular NOEs for the structure calculation of Rap1b/talin-F0 complex** (a) Representative intermolecular NOEs obtained from 3D  $^{15}\text{N}$ -edited NOESY experiment (300 ms mixing time) with sample 3: 0.5 mM  $^{15}\text{N}/100\%$   $^2\text{H}$ -labeled talin-F0 in the presence of 0.7 mM unlabeled Rap1b. Selected residues of talin-F0 were indicated on top of each strip. (b) Representative intermolecular NOEs obtained from 3D  $^{15}\text{N}/^{13}\text{C}$ -filtered NOESY experiment (120 ms mixing time) with sample 4: 0.5 mM  $^{15}\text{N}/^{13}\text{C}$ -labeled talin-F0 in the presence of 0.7 mM unlabeled Rap1b prepared in 99.8%  $\text{D}_2\text{O}$ . Selected residues of talin-F0 were indicated on top of each strip. Cross-peaks shown in both (a) and (b) which were unambiguously assigned to the specific proton of unlabeled Rap1b residues are labeled in red. The horizontal black line of each strip is diagonal line whose position indicates the chemical shift of the specific proton labeled on top of each strip.



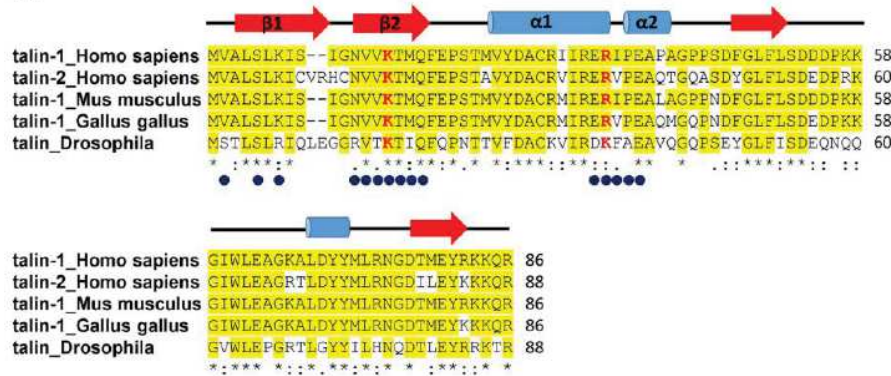
## Supplementary Figure 4



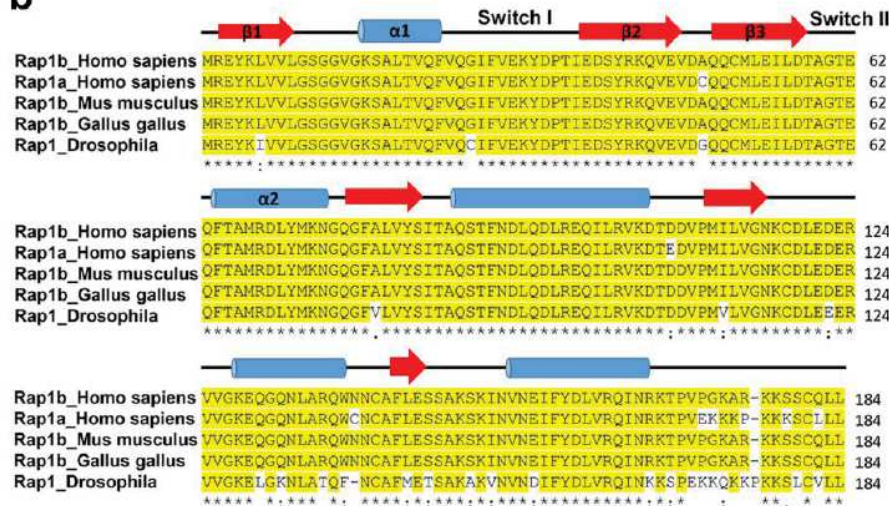
**Supplementary Figure 4. Rap1b/talin-F0 interaction in the absence of membrane is modest but highly specific**  
**(a)** Detailed binding interface between  $\beta 2$  strand or switch II region of Rap1b and talin-F0. Hydrogen bonds are represented in red dashed lines. **(b)** A distinct hydrophobic core formed between I36/P37 (shown in spheres representation) of talin-F0 and V21/I27/V29 of Rap1b (shown in surface representation). **(c)** The HSQC spectra (four representative residues were shown) of  $50 \mu\text{M}$   $^{15}\text{N}$ -labeled talin-F0 in the absence (black) and presence of  $125 \mu\text{M}$  GMP-PNP loaded Rap1b (red), K31E mutant (blue) or I27H mutant (cyan). Note that all Rap1b variants also bear a G12V mutation. K31E and I27H mutations resulted in overall less chemical shift changes and less extent of line broadening. **(d)** GST pull down assay to show that talin-H interacts specifically with Rap1b while RIAM interacts with both Rap1b and H-Ras equally. Full blot/gel images are shown in **Supplementary Fig. 16**. **(e)** The affinity between GMP-PNP loaded GFP-Rap1b and RIAM-RAPH, talin-F0 or talin-H measured by Nanotemper. Experiments were done in triplicates. The affinity of GFP-Rap1b/talin-H shown here is an estimated value because the saturation step was not reached due to the aggregation issue of talin-H at high concentration.

## Supplementary Figure 5

**a**



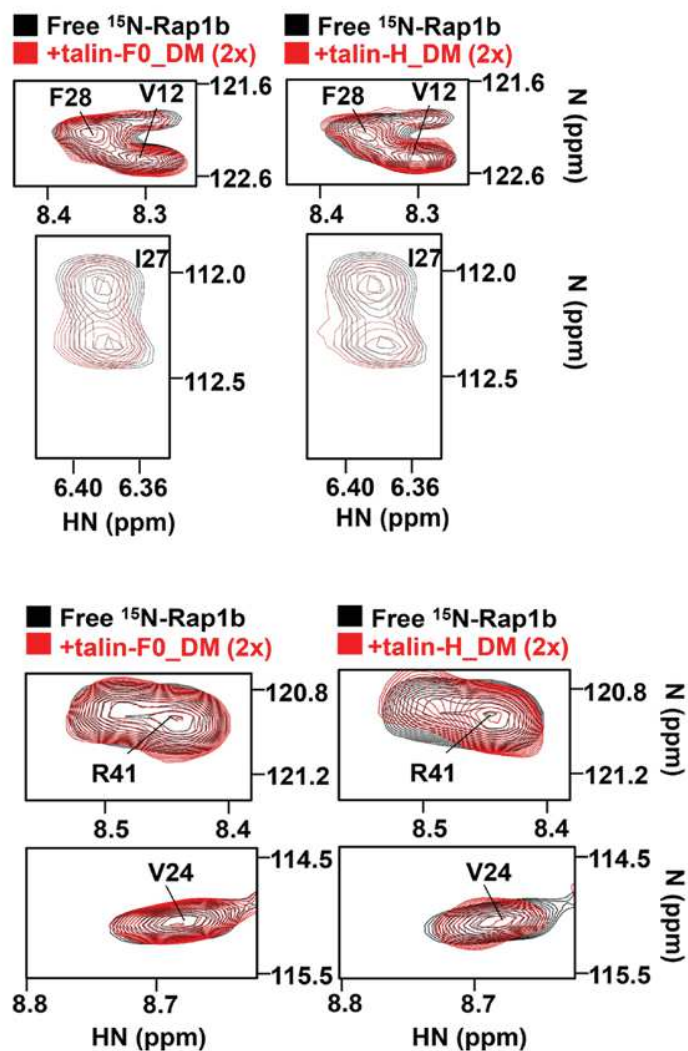
**b**



**Supplementary Figure 5. Rap1/talin interaction is evolutionally conserved** (a) Sequence alignment of talin-F0 from different species. Residues of talin-F0 involved in the binding interface (cut-off of 4 Å) with Rap1b are indicated in the figure with blue solid circles. (b) Sequence alignment of Rap1 from different species. (Residues identical to human talin-1 or Rap1b are highlighted in yellow. '\*' indicates fully conserved residue, ':' indicates residues with strongly similar properties, and '.' indicates residues with weakly similar properties).

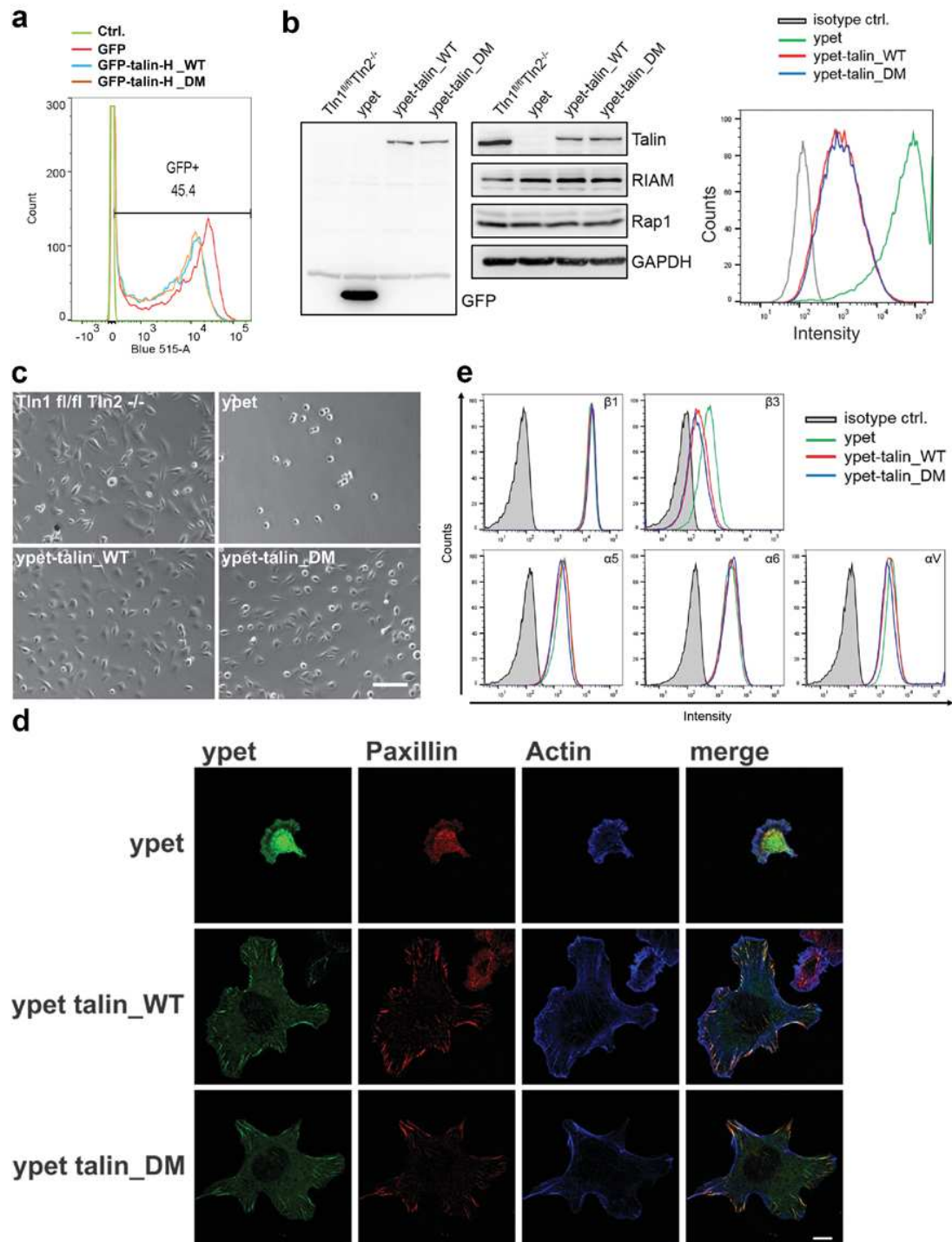


## Supplementary Figure 6



**Supplementary Figure 6. Rap1b/talin interaction is drastically reduced by double mutations (K15A, R35A) in talin-F0 domain** The HSQC spectra (representative regions were shown) of 45  $\mu\text{M}$  GMP-PNP loaded  $^{15}\text{N}$ -labeled Rap1b (1-167) in the absence (black) and presence of 90  $\mu\text{M}$  talin-F0\_DM or talin-H\_DM (red).

## Supplementary Figure 7

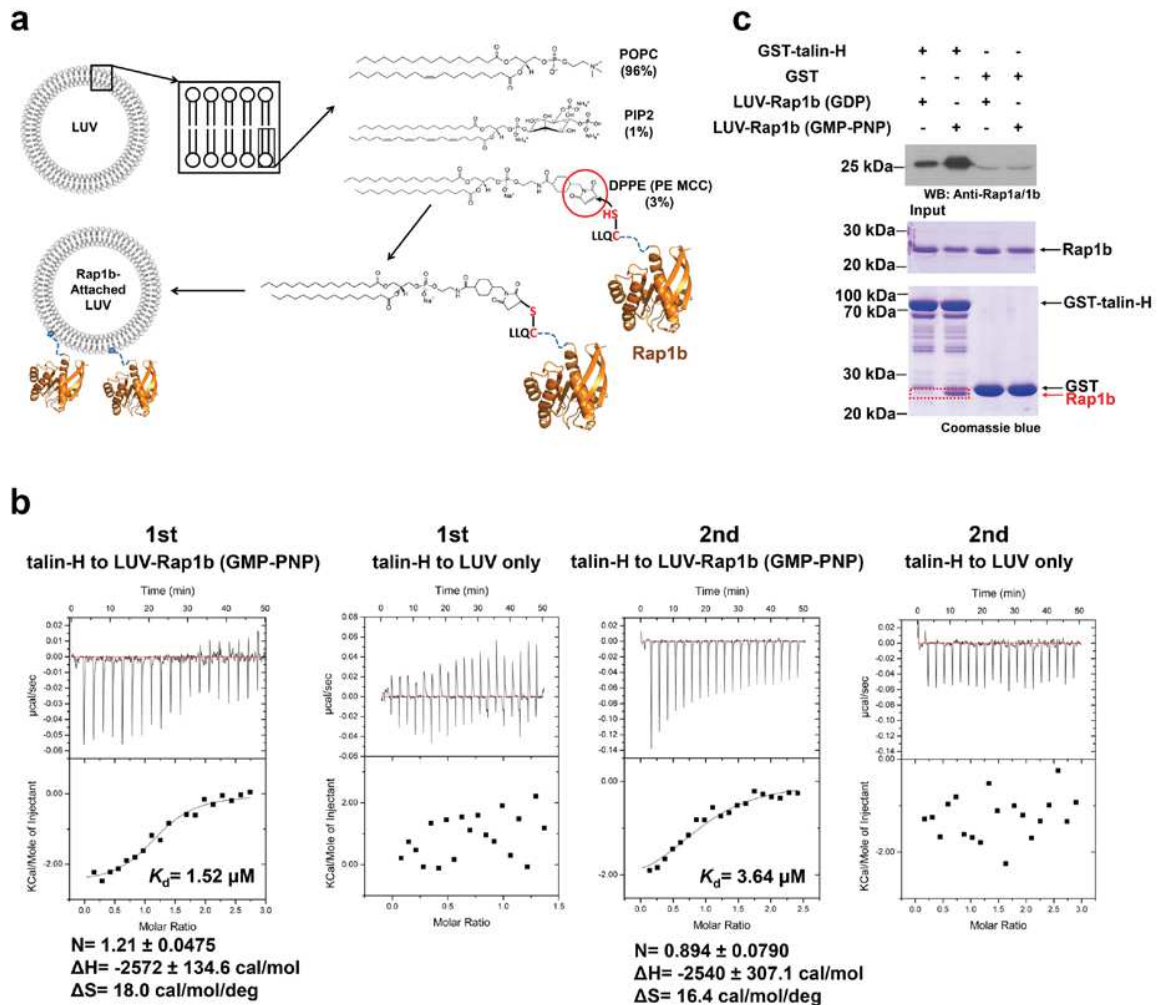


**Supplementary Figure 7. Impaired Rap1/talin interaction results in defective integrin activation (a)** Expression levels of GFP (red), GFP-tagged talin-H WT (cyan) and GFP-tagged talin-H double mutant (DM) (orange) in transfected CHO A5 cells analyzed by flow cytometry. **(b)** Left, western blot analyses of talin control (talin-1<sup>fl/fl</sup>/talin-2<sup>-/-</sup>) and talin1/2 double knockout (talin1<sup>fl/fl</sup>/talin2<sup>-/-</sup>) fibroblasts which were retrovirally transduced with either ypet alone, ypet-tagged



talín WT or ypet-tagged talín DM (K15A, R35A) to show expression levels of ypet and ypet-tagged talín (recognized by GFP antibody), talín, RIAM and Rap1. GAPDH served as loading control. Right, flow cytometric analysis of talín control (talín-1<sup>fl/fl</sup>/talín-2<sup>-/-</sup>) (grey) and talín<sup>1/2dko</sup> fibroblasts retrovirally transduced with ypet alone (green), ypet-tagged talín WT (red) or ypet-tagged talín DM (blue) to quantify expression levels of the transduced proteins. Full blots are shown in **Supplementary Fig. 17**. (c) Phase contrast images of talín-1<sup>fl/fl</sup>/talín-2<sup>-/-</sup> control cells and talín<sup>1/2dko</sup> cells expressing ypet, ypet-talín WT or ypet-talín DM plated on fibronectin. Scale bar 100µm. (d) Confocal images of the ventral side of talín<sup>1/2dko</sup>, ypet-talín WT or ypet-talín DM cells stained for paxillin (red) and F-actin (blue). Ypet-signal is shown in green. Scale bar 10µm. (e) Surface expression levels of integrin β1, β3, α5, α6 and αV on talín control (grey) and talín<sup>1/2dko</sup> fibroblasts expressing ypet (green), ypet-tagged talín WT (red) or ypet-tagged talín double mutant (DM) (blue) analyzed by flow cytometry.

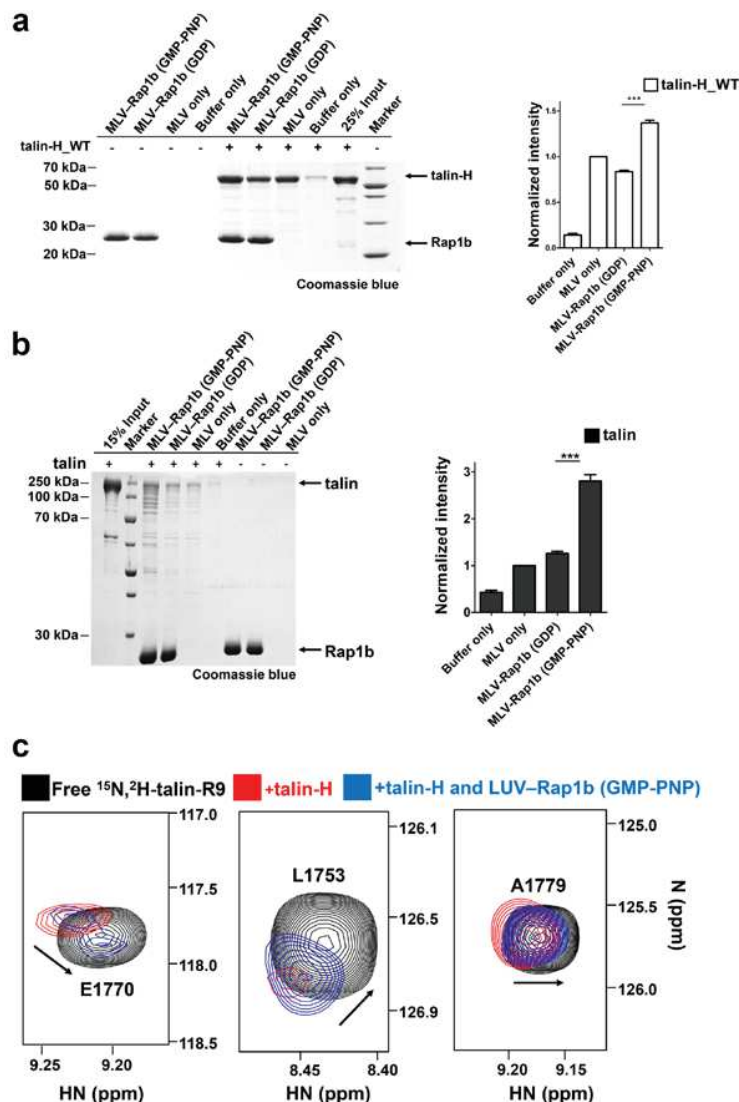
## Supplementary Figure 8



**Supplementary Figure 8. Membrane anchored Rap1b robustly enhances its binding to talin (a)** The diagram procedure of generating Rap1b-anchored LUVs. **(b)** Binding affinity between membrane-anchored Rap1b and talin-H measured by isothermal titration calorimetry (ITC). The titrations of talin-H to LUV-only showed different background heats due to different batches of LUVs, but the enthalpy changes and affinities of talin-H/LUV-Rap1b were consistent after subtraction. N, the number of binding sites.  $\Delta H$ , enthalpy change.  $\Delta S$ , entropy change. **(c)** GST pull down assay to show that the interaction between membrane-anchored Rap1b and talin-H is also in a GTP dependent manner. Full blot/gel images are shown in Supplementary Fig. 18.

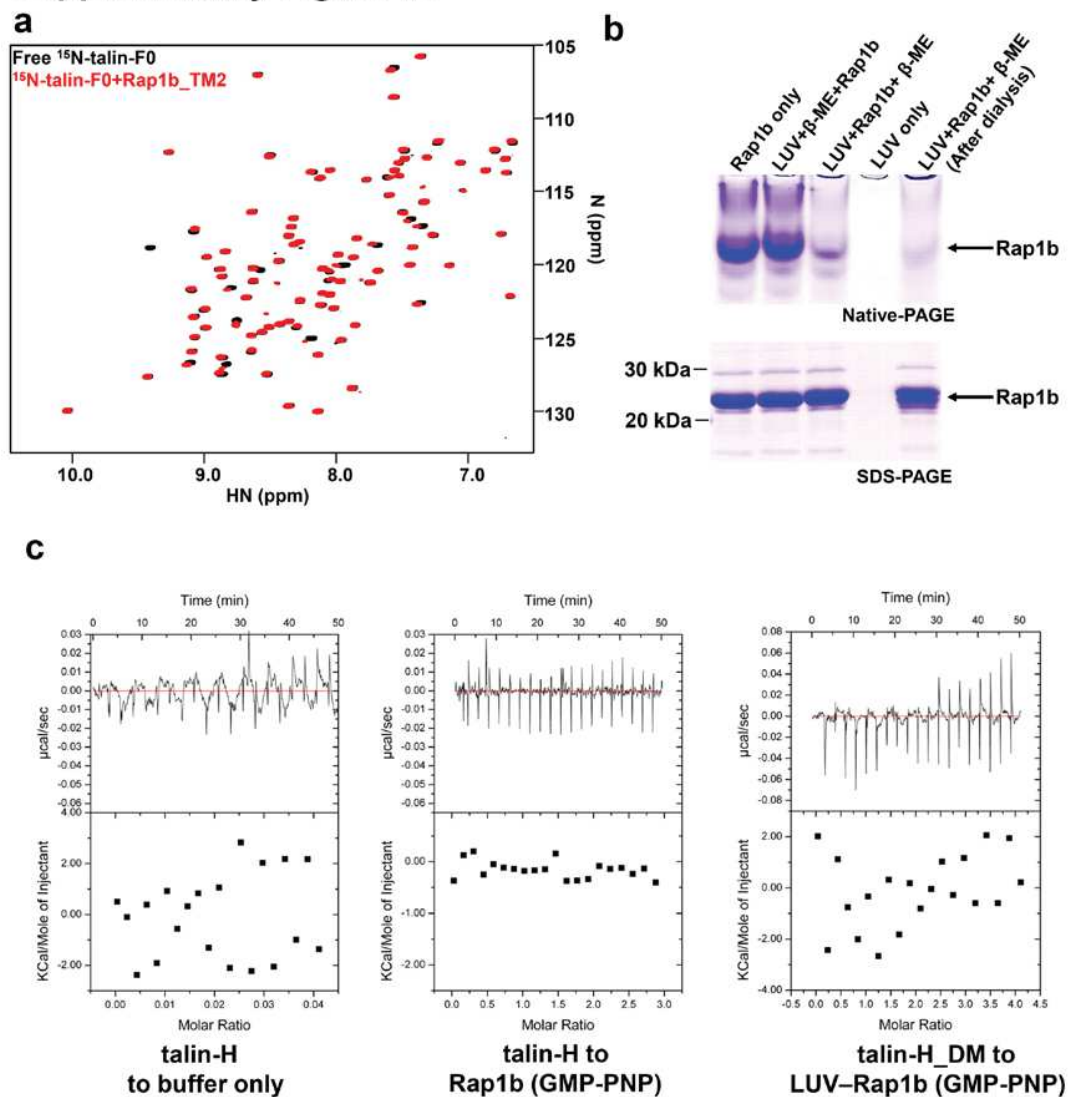


## Supplementary Figure 9



**Supplementary Figure 9. Membrane anchored Rap1b interacts with talin in a GTP dependent manner and promotes talin unmasking** (a) Left, a representative vesicle co-sedimentation assay showing that the interaction between talin-H and membrane-anchored Rap1b is GTP dependent. Right, the quantification of four independent experiments. The intensity of talin-H\_WT band was normalized to that of “MLV only” group and the data are shown in means  $\pm$  S.E.M. \*\*\* denotes  $p < 0.0001$ . Full gel image is shown in **Supplementary Fig. 19**. (b) Left, a representative vesicle co-sedimentation assay showing that the interaction between full-length talin and membrane-anchored Rap1b is GTP dependent. Right, the quantification of four independent experiments. The intensity of talin band was normalized to that of “MLV only” group and the data are shown as means  $\pm$  S.E.M. \*\*\* denotes  $p < 0.0001$ . Full gel image is shown in **Supplementary Fig. 19**. (c) HSQC-based spectral changes (three representative residues were shown) of 30  $\mu$ M  $^{15}\text{N}/80\%$   $^2\text{H}$ -labeled talin-R9 in the absence (black) and presence of 22  $\mu$ M talin-H (red) showing the talin-H masking by the autoinhibitory talin-R9 as reported before (Song et al., 2012). Addition of 11  $\mu$ M membrane-anchored Rap1b shifts the peaks towards the free form of talin-R9 (blue) indicating the talin unmasking. Note that the concentrations of the proteins were kept low, which cause less pronounced chemical shift changes but to avoid precipitation. The peak intensity for each dataset was set to the same scale. These experiments were performed at 28.5  $^{\circ}\text{C}$  on Bruker 900 MHz NMR spectrometer. The buffer contained 25 mM  $\text{NaH}_2\text{PO}_4/\text{Na}_2\text{HPO}_4$  (pH 6.8), 100 mM NaCl, 5 mM  $\text{MgCl}_2$ , 5 mM  $\beta$ -mercaptoethanol ( $\beta$ -ME) and 5%  $\text{D}_2\text{O}$ .

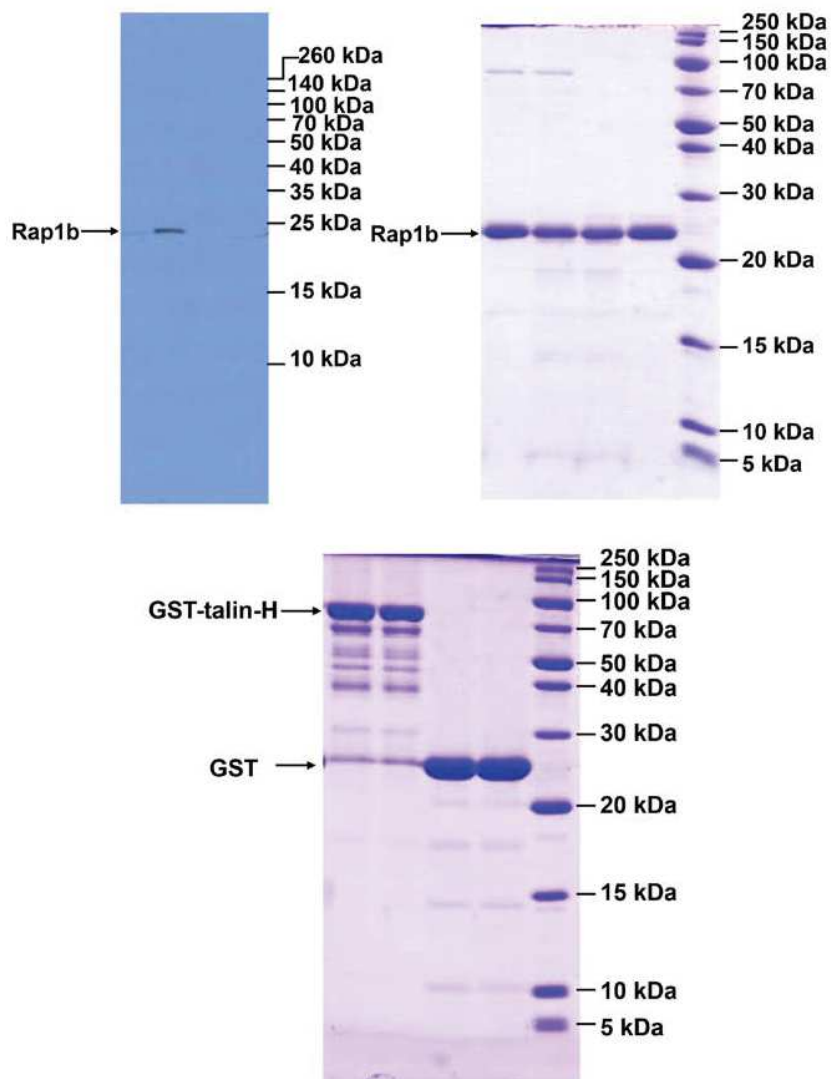
## Supplementary Figure 10



**Supplementary Figure 10. The anchorage of Rap1b to membrane vesicles and isothermal titration calorimetry (ITC) control experiments** (a) The HSQC spectra of 45  $\mu\text{M}$   $^{15}\text{N}$ -labeled talin-F0 in the absence (black) and presence of 90  $\mu\text{M}$  GMP-PNP loaded Rap1b\_TM2 (red). (b) A combination of Native-PAGE and SDS-PAGE analysis to confirm that Rap1b was anchored to large unilamellar vesicles (LUVs) efficiently. Upper panel, free undenatured Rap1b migrated into a native-gel, but LUVs anchored Rap1b couldn't due to the increasing size of the whole molecule, shown as "LUV+Rap1b+β-ME" in which the intensity of Rap1b band was significantly reduced. As a control, LUVs pre-incubated with β-ME failed to anchor Rap1b (shown as "LUV+β-ME+Rap1b") and the intensity of Rap1b band remained unchanged. Lower panel, SDS-PAGE to confirm that the total amount of Rap1b remained the same. Full gel images are shown in **Supplementary Fig.18**. (c) ITC control experiments as indicated in the figure.

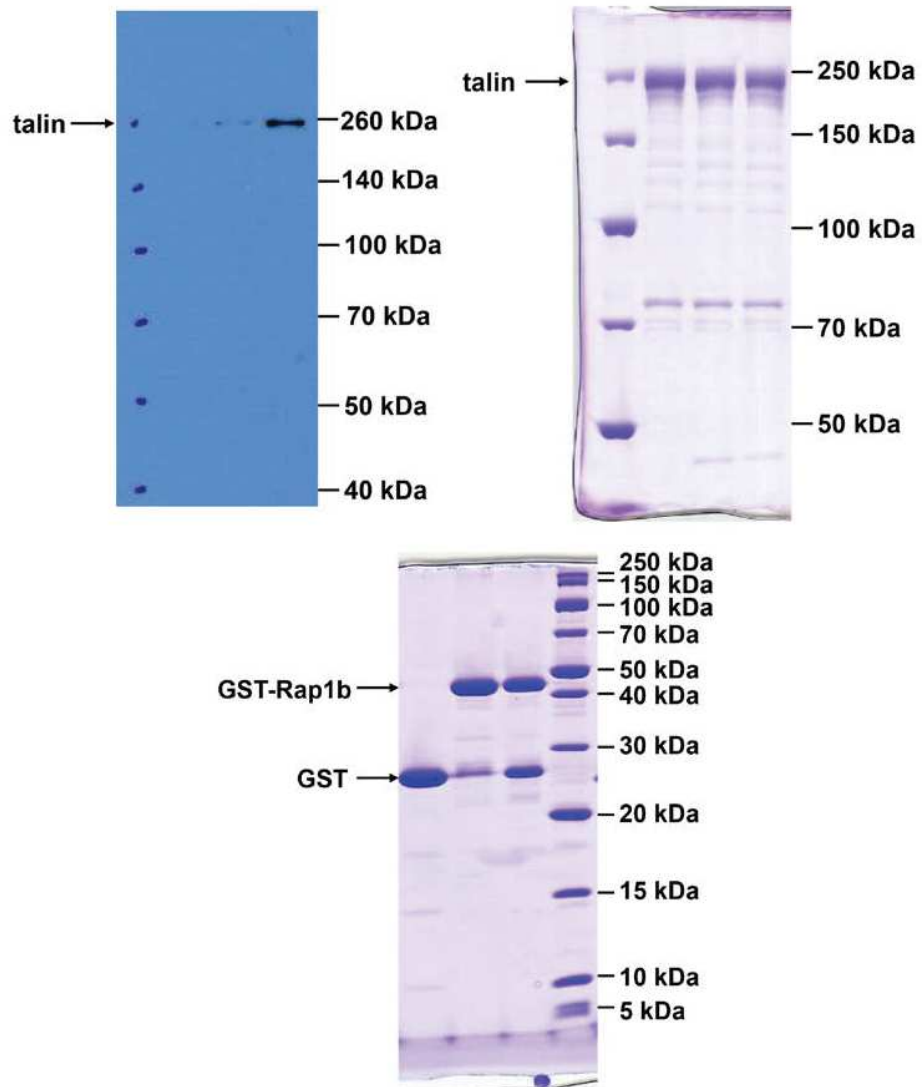


## Supplementary Figure 11



Supplementary Figure 11. Full blot/gel images for Fig. 3b (left panel)

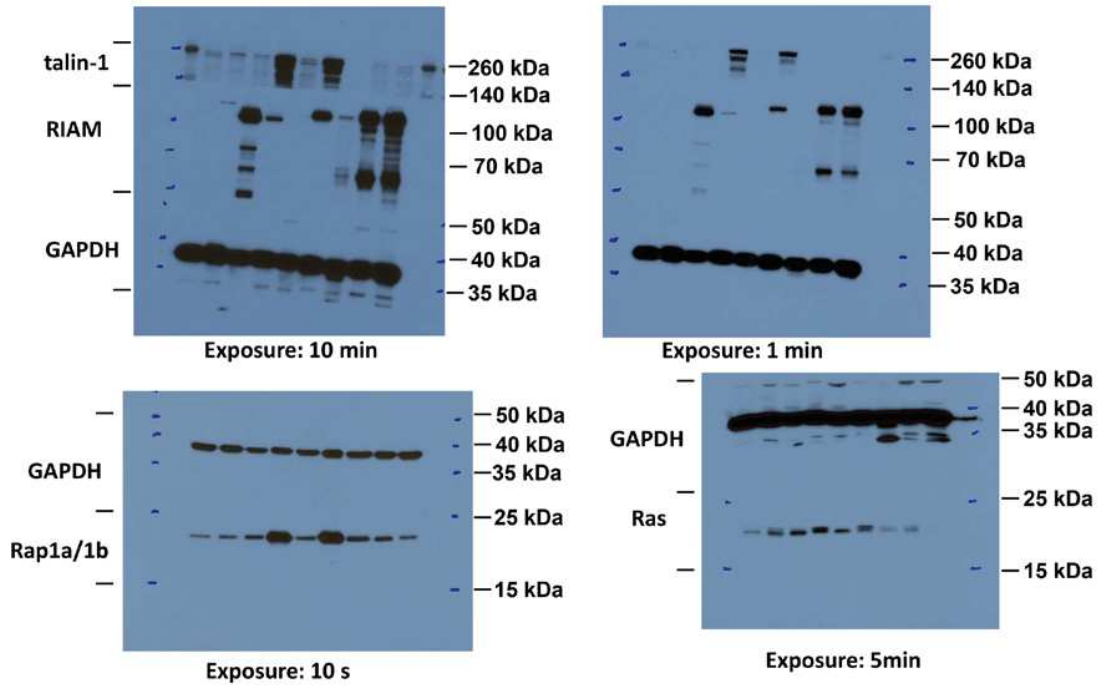
## Supplementary Figure 12



Supplementary Figure 12. Full blot/gel images for Fig. 3b (right panel)

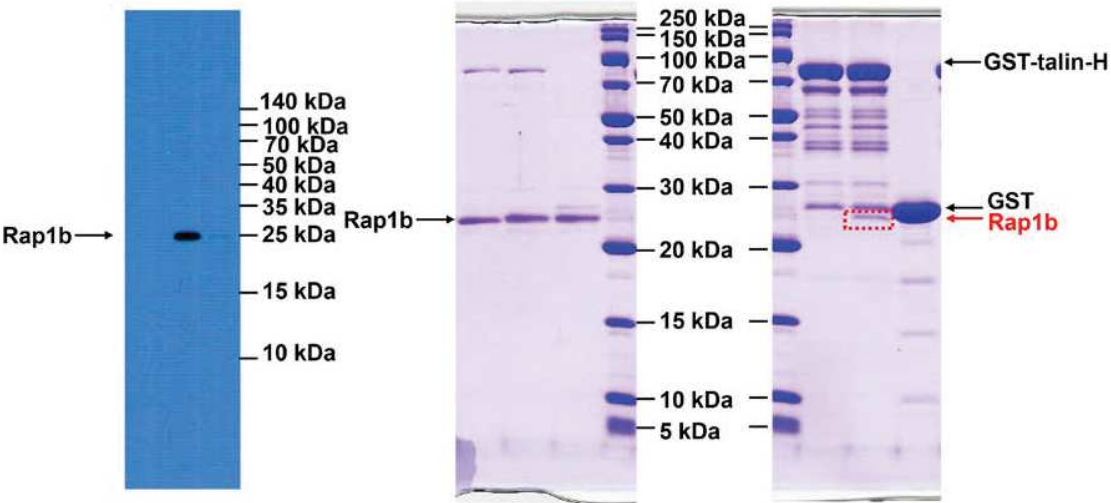


## Supplementary Figure 13



Supplementary Figure 13. Full western-blot images for Fig. 6a

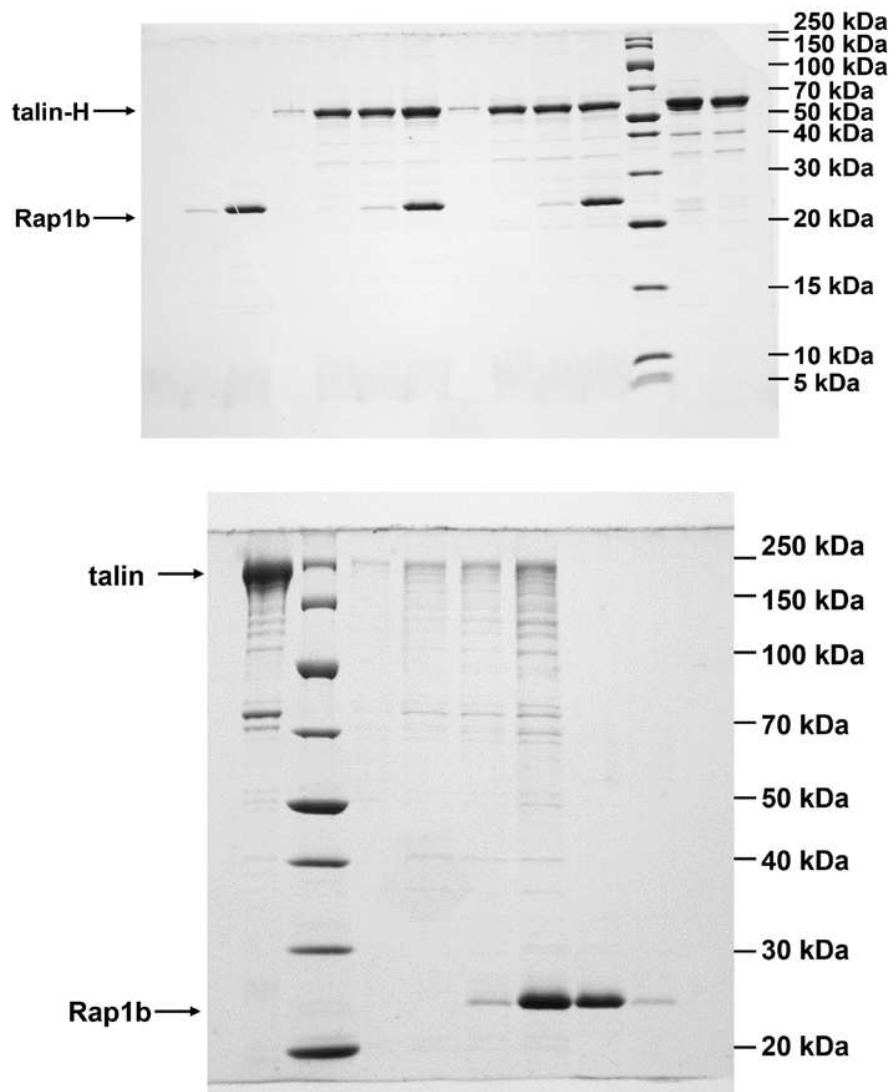
Supplementary Figure 14



Supplementary Figure 14. Full blot/gel images for Fig. 6c

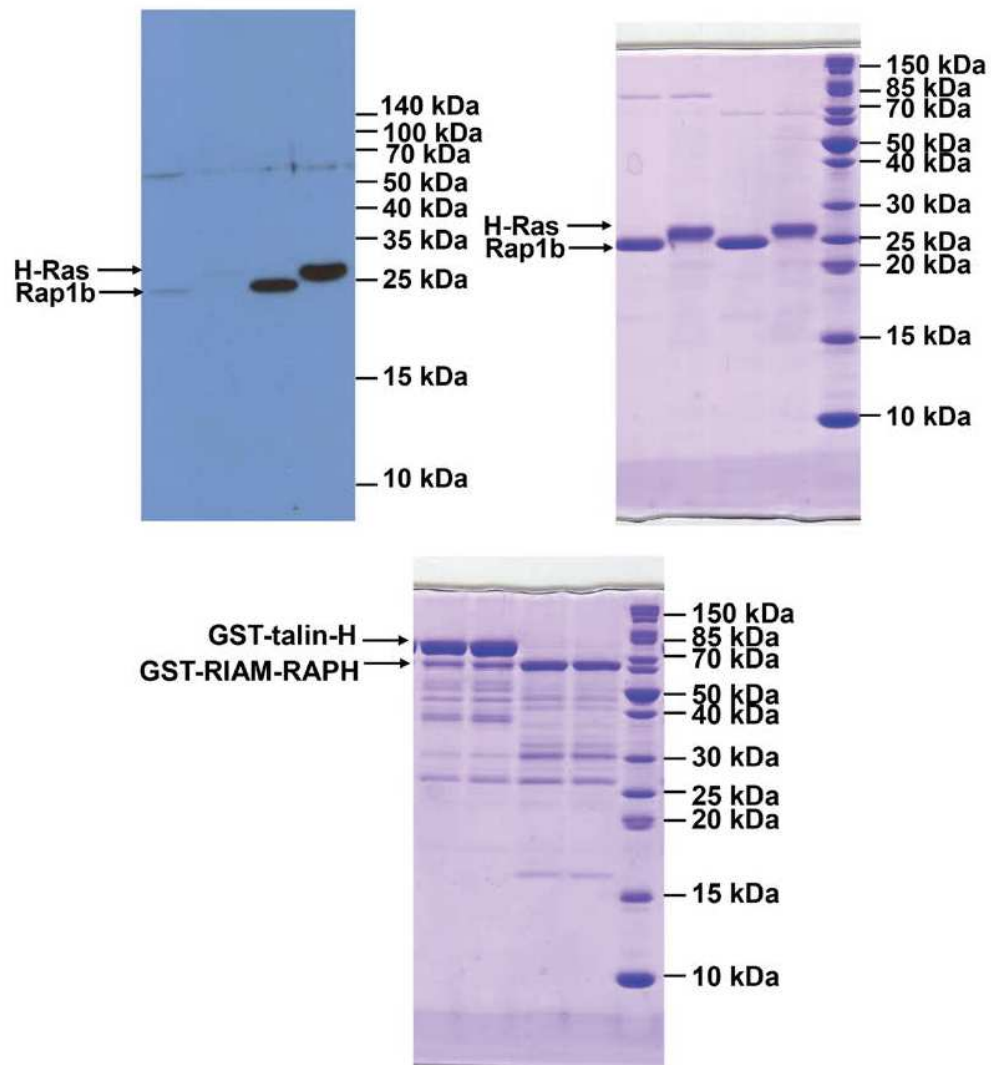


## Supplementary Figure 15



Supplementary Figure 15. Full gel images for Fig. 6d, e

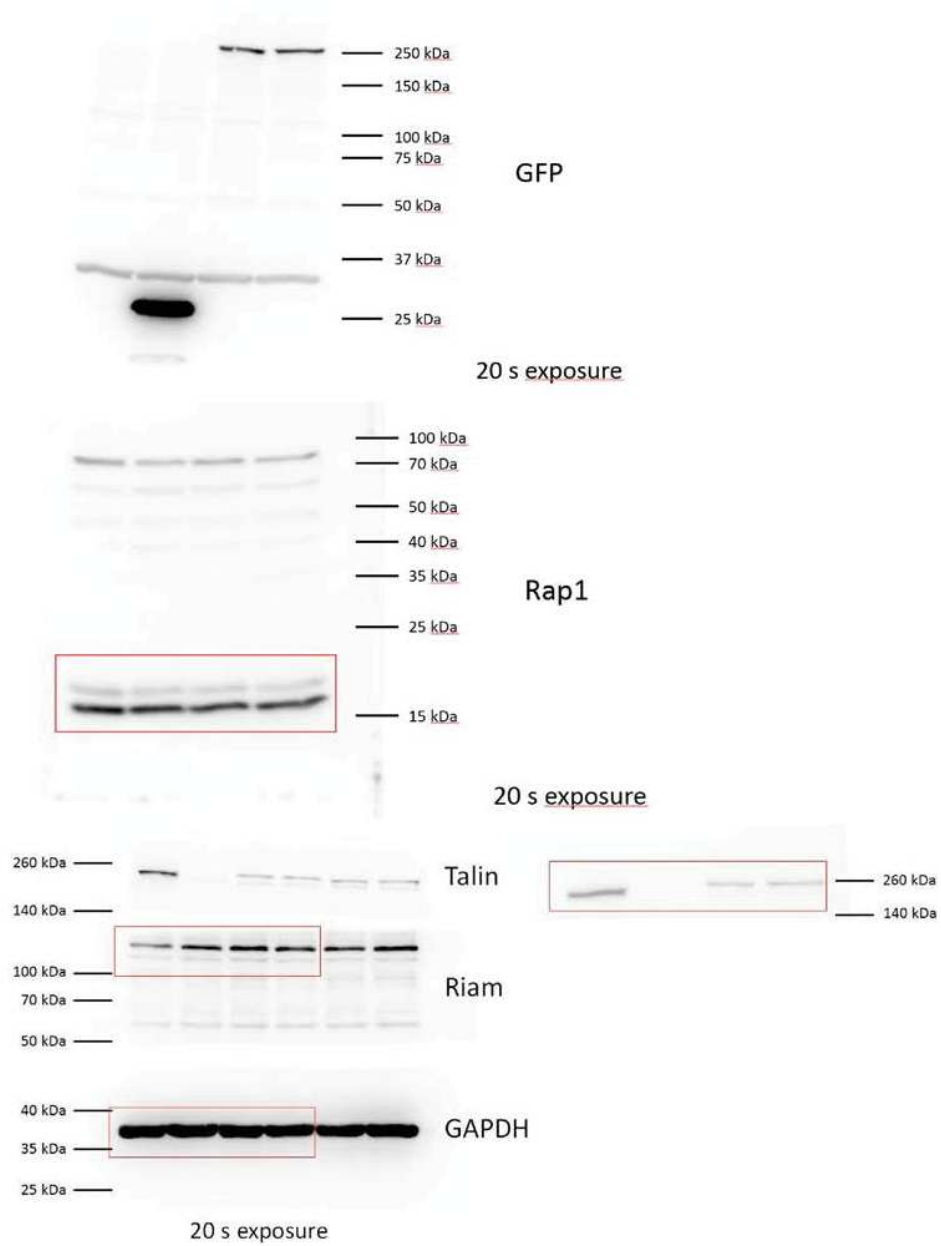
## Supplementary Figure 16



Supplementary Figure 16. Full blot/gel images for Supplementary Fig. 4d

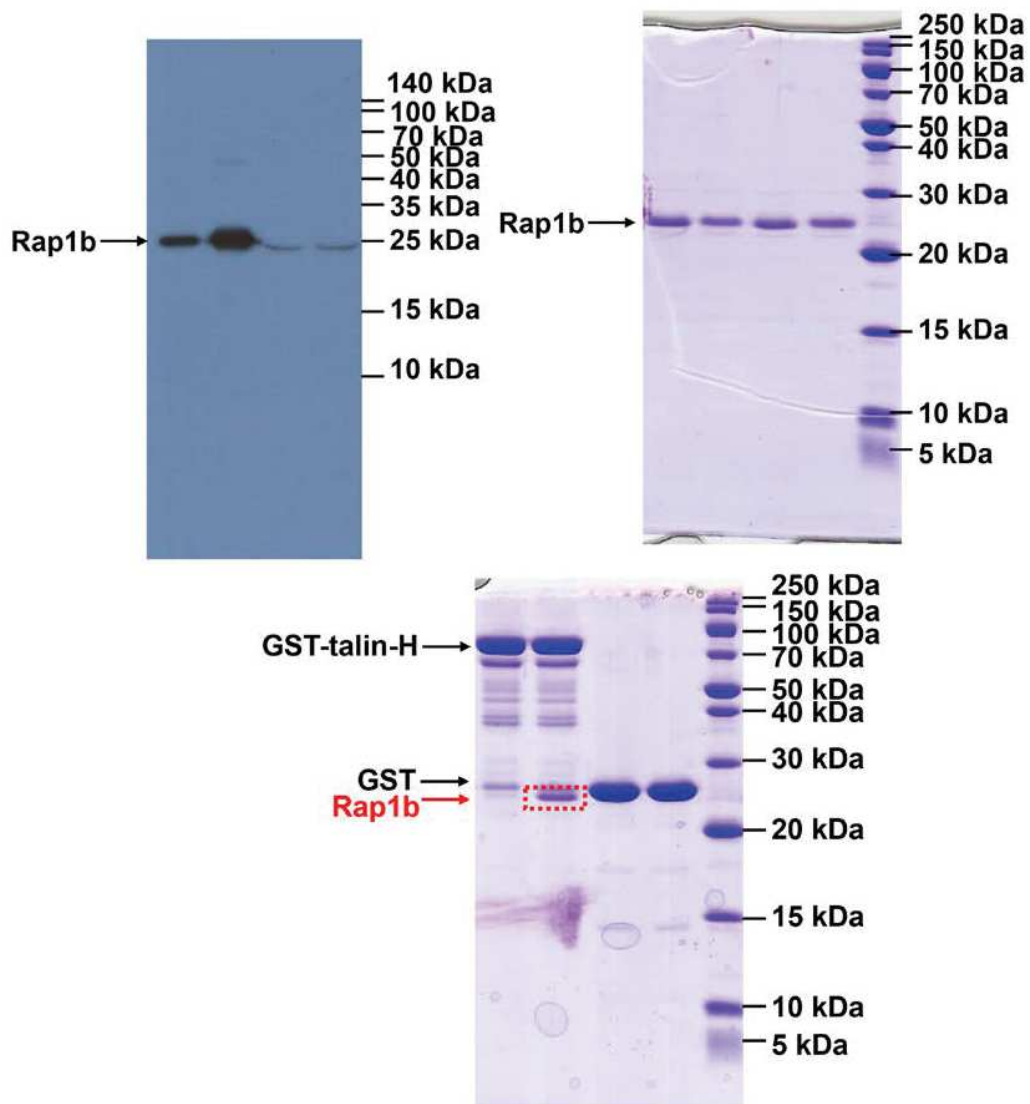


## Supplementary Figure 17



Supplementary Figure 17. Full blot/gel images for Supplementary Fig. 7b

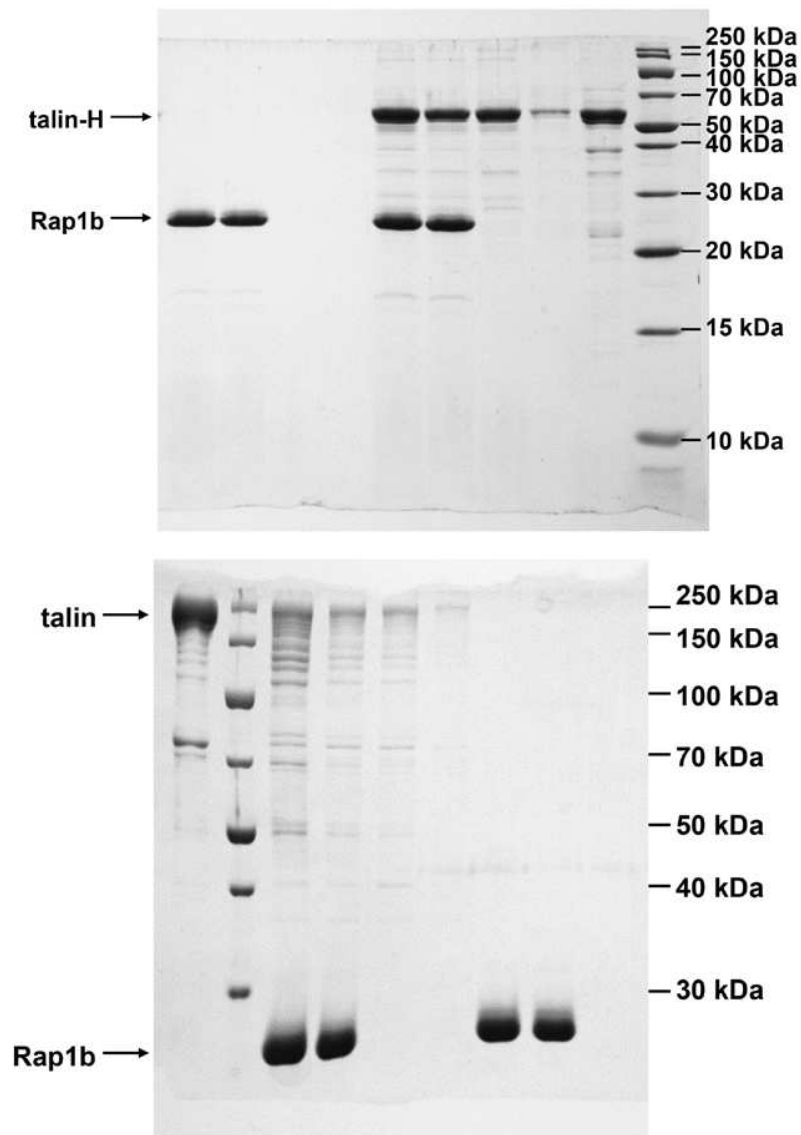
## Supplementary Figure 18



Supplementary Figure 18. Full blot/gel images for Supplementary Fig. 8c

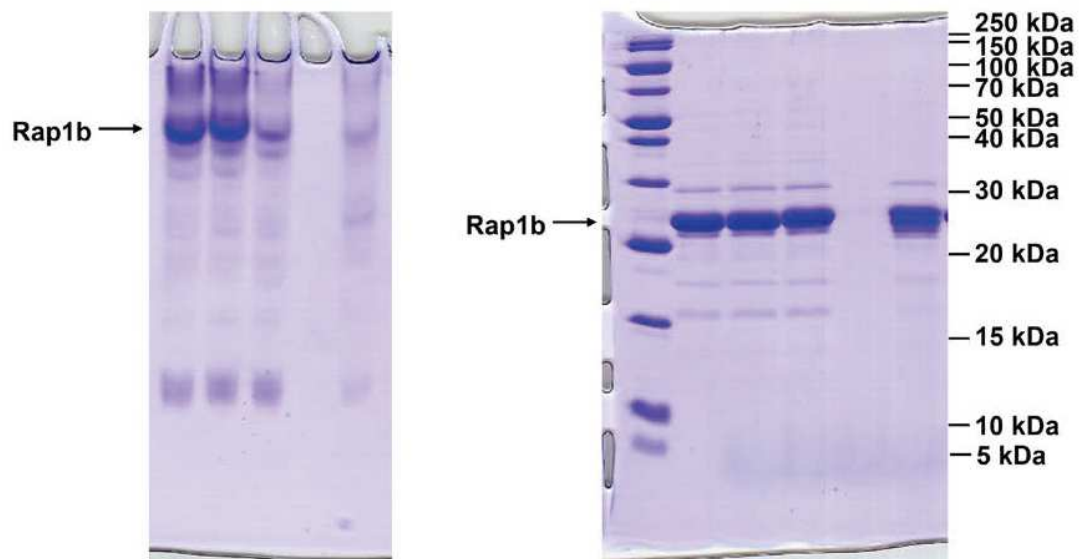


## Supplementary Figure 19



Supplementary Figure 19. Full gel images for Supplementary Fig. 9a, b

## Supplementary Figure 20



Supplementary Figure 20. Full gel images for Supplementary Fig. 10b



**Supplementary Table 1. Structural Statistics of the Rap1b/talin-F0 complex**

	Complex
<b>NMR distance &amp; dihedral constraints</b>	3802
Distance constraints	3500
Total NOE	3500
Intra-residue	894
Inter-residue	
Sequential ( $ i-j  = 1$ )	1158
Medium-range ( $ i-j  < 5$ )	620
Long-range ( $ i-j  \geq 5$ )	750
Intermolecular	78
Hydrogen bonds <sup>a</sup>	
Total dihedral angle restraints	302
phi	151
psi	151
<b>Structure Statistics</b>	
Violations (mean $\pm$ s.d.) <sup>a</sup>	
Distance constraints (Å)	0.12780 $\pm$ 0.00229
Dihedral angle constraints (°)	2.47094 $\pm$ 0.31544
Max. dihedral angle violation (°)	5
Max. distance constraint violation (Å)	0.5
Deviations from idealized geometry	
Bond lengths (Å)	0.00796 $\pm$ 0.00014
Bond angles (°)	0.94224 $\pm$ 0.01034
Impropers (°)	0.73831 $\pm$ 0.01966
Average pairwise r.m.s.d. (Å)	
Backbone atoms	0.584 $\pm$ 0.106
All heavy atoms	1.177 $\pm$ 0.097
Ramachandran Plot	
Residues in allowed region (%)	98.8
Residues in disallowed regions (%)	1.2

<sup>a</sup> Statistics were calculated over 20 structures with lowest energies.

**Supplementary Table 2. Comparison of binding interface between Rap1 and its effector proteins<sup>a,b,c</sup>**

	Rap1	F0	RIAM-RA PDB: 4DXA	KRIT1-F1 PDB: 4KVG	cRaf-1 PDB: 1GUA
$\alpha$ 1 helix	S17	<b>K15</b>			
	V21	<b>K15</b> , I36		<b>R452</b>	
	V24	N12, V13			V88
Switch I	Q25	V13, I36, E38		<b>R452</b>	K87, V88, R89, G90
	I27	P37, E38			
	V29	P37			<b>K84</b>
	K31	E34, <b>R35</b>			<b>K84</b>
	D33	<b>K15</b> , <b>R35</b>	<b>K213</b>	<b>R432</b> , <b>R452</b>	<b>K84</b>
	P34	T16, <b>R35</b>		<b>R432</b>	
	I36	S5, T16, M17, Q18	V182, S194, L195, M196	S433, V434, E435	I57, V69, N71
$\beta$ 2 strand	E37	<b>K7</b> , T16	<b>K193</b> , S194	<b>R423</b> , Y431, S433	<b>R59</b> , R67, T68, V69
	D38	V14	T192, <b>K193</b> , S194	Y431, <b>R432</b> , S433	R67, T68, R89
	S39	V14	S191, T192	S430, Y431	Q66, R67, R89
	Y40		<b>K193</b>	<b>R452</b>	Q66, R89
	R41	N12, V13, V14	S190	D428, G429	N64, K65, Q66
	K42	N12			
$\beta$ 3 strand	M52				N64
	L56			Y431	
Switch II	T61	Q18			
	Q63	V2, Q18			
	F64	S5, <b>K7</b> , G76		F419	
	M67			K421	

<sup>a</sup> A cut-off of 4 Å was used to define the interface. The residues were identified in PyMOL 1.3 (Schrödinger, LLC.) and then manually organized into the table.

<sup>b</sup> Conserved residues are highlighted in red.

<sup>c</sup> The Rap1b/talin-F0 complex with the lowest energy was analyzed in this table.



**Supplementary Table 3. Primer sequence information<sup>a</sup>**

Plasmid construct	Primer sequence (5'-3')
pGST1-RIAM-RAPH (149-438)	Forward (EcoR I): ATTCCG <b><u>GAATTC</u></b> CCCTGAACTTCTCTCTAAAGAAG Reverse (Xho I): TATCCG <b><u>CTCGAGT</u></b> TATCCAGCTCTTGCCACAGCCC
pGST1-Rap1b	Forward (EcoR I): ATTCCG <b><u>GAATTC</u></b> ATGCGTGAGTATAAGCTTGTCG Reverse (Xho I): TATCCG <b><u>CTCGAGT</u></b> TAAAGCAGCTGACCTGATGACTT
pET28t-Rap1b (1-167)	Forward (Nde I): GGCATTCC <b><u>CATATG</u></b> CGTGAGTATAAGCTTGTCG Reverse (Xho I): TATCCG <b><u>CTCGAGT</u></b> TATCTGTTGATTGCGCGACTAG
talin (K15A, R35A)	Forward (K15A): TAGCATTGGGAATGTGGTGGCGACGATGCAATTTGAGCCA Reverse (K15A): TGGCTCAAATTGCATCGTCGCCACCACATTCCCAATGCTA Forward (R35A): GCATGATTTCGTGAGGCGATCCCAGAGGCCC Reverse (R35A): GGGCCTCTGGGATCGCCTCACGAATCATGC
Rap1b (G12V)	Forward: GTCGTTCTTGGCTCAGTAGGCGTTGGAAAGTCT Reverse: AGACTTTCCAACGCCTACTGAGCCAAGAACGAC
Rap1b (I27H)	Forward: CAATTTGTTCAAGGACACTTTGTAGAAAAATACG Reverse: CGTATTTTCTACAAAGTGCCTTGAACAAATTG
Rap1b (K31E)	Forward: GGAATTTTTGTAGAAGAGTACGATCCTACGATAG Reverse: CTATCGTAGGATCGTACTCTTCTACAAAAATTCC
Rap1b (C51S, C118S, C141S)	Forward (C51S): GTAGATGCACAACAGAGTATGCTTGAAATCTTGG Forward (C118S): CTTGTTGGTAATAAGAGTGAAGTGGAAAGATG Forward (C141S): GCAAGACAATGGAACAACAGTGCATTCTTAGAATC

<sup>a</sup> Restriction sites are in bold and underlined.



## PLATELETS AND THROMBOPOIESIS

## Direct Rap1/Talin1 interaction regulates platelet and neutrophil integrin activity in mice

Thomas Bromberger,<sup>1</sup> Sarah Klapproth,<sup>1</sup> Ina Rohwedder,<sup>2</sup> Liang Zhu,<sup>3</sup> Laura Mittmann,<sup>2,4</sup> Christoph A. Reichel,<sup>2,4</sup> Markus Sperandio,<sup>2,5</sup> Jun Qin,<sup>3</sup> and Markus Moser<sup>1</sup>

<sup>1</sup>Department Molecular Medicine, Max Planck Institute of Biochemistry, Martinsried, Germany; <sup>2</sup>Walter Brendel Centre of Experimental Medicine, Klinikum der Universität München, Ludwig Maximilians University Munich, Martinsried, Germany; <sup>3</sup>Department of Molecular Cardiology, Lerner Research Institute, Cleveland Clinic, Cleveland, OH; <sup>4</sup>Department of Otorhinolaryngology, Ludwig Maximilians University Munich, Munich, Germany; and <sup>5</sup>German Centre for Cardiovascular Research, Munich Heart Alliance, Munich, Germany

## KEY POINTS

- Direct Rap1/Talin1 interaction controls platelet and neutrophil integrin functions.
- Rap1/Talin1 interaction is important in blood cells, which depend on rapid integrin-mediated processes.

Targeting Talin1 to the plasma membrane is a crucial step in integrin activation, which in leukocytes is mediated by a Rap1/RIAM/Talin1 pathway, whereas in platelets, it is RIAM independent. Recent structural, biochemical, and cell biological studies have suggested direct Rap1/Talin1 interaction as an alternative mechanism to recruit Talin1 to the membrane and induce integrin activation. To test whether this pathway is of relevance in vivo, we generated Rap1 binding-deficient Talin1 knockin (Tln1<sup>3mut</sup>) mice. Although Tln1<sup>3mut</sup> mice showed no obvious abnormalities, their platelets exhibited reduced integrin activation, aggregation, adhesion, and spreading, resulting in prolonged tail-bleeding times and delayed thrombus formation and vessel occlusion in vivo. Surprisingly, neutrophil adhesion to different integrin ligands and  $\beta 2$  integrin-dependent phagocytosis were also significantly impaired, which caused profound leukocyte adhesion and extravasation defects in Tln1<sup>3mut</sup> mice. In contrast, macrophages exhibited no defect in adhesion or spreading

despite reduced integrin activation. Taken together, our findings suggest that direct Rap1/Talin1 interaction is of particular importance in regulating the activity of different integrin classes expressed on platelets and neutrophils, which both depend on fast and dynamic integrin-mediated responses. (*Blood*. 2018;132(26):2754-2762)

## Introduction

Integrins can adopt different conformations with different affinities for their ligands. Blood cell integrins become activated upon direct binding of the 2 adapter proteins Talin1 and Kindlin-3 to the cytoplasmic domain of integrin  $\beta$  subunit. Rapid regulation of integrin activity is particularly important for integrins expressed on platelets, which control thrombosis and hemostasis at sites of vascular injury, and for leukocyte integrins, which are essential for leukocyte adhesion and extravasation at sites of inflammation. A critical but as yet incompletely understood process during integrin activation is the recruitment of these activators from the cytoplasm to the plasma membrane. A series of in vitro studies on the prototypic integrin  $\alpha IIb\beta 3$  from platelets suggested that membrane-bound, guanosine triphosphate (GTP)-loaded Rap1 binds its effector protein Rap1 GTP-interacting adapter molecule (RIAM), which in turn binds Talin1 and thereby recruits it to the plasma membrane to activate integrins.<sup>1-4</sup> However, although leukocyte  $\beta 2$  integrin activation is dependent on the Rap1/RIAM/Talin1 pathway, platelet integrins become normally activated in RIAM knockout mice, suggesting the existence of a RIAM-independent Talin1 recruitment pathway.<sup>5-10</sup> On the basis of previous studies, which showed that the F0 domain of Talin1 can interact with Rap1 weakly and is required for maximal integrin

activation,<sup>11-13</sup> we recently provided strong evidence that the direct Rap1/Talin1 interaction becomes stabilized when Rap1 is membrane anchored and that the disruption of such an interaction diminishes Talin1 recruitment to the plasma membrane, resulting in reduced integrin activation and signaling in vitro.<sup>14</sup> Here we report a thorough analysis of Rap1 binding-deficient Talin1 knockin mice and demonstrate the importance of such interactions for both platelet and neutrophil functions in vivo.

## Materials and methods

## Mice

Tln1<sup>3mut</sup> mice were generated by injection of correctly targeted R1 embryonic stem cells into C57BL/6 blastocysts. The resulting chimeric mice were crossed with deleter-Cre mice to remove the loxP-flanked neomycin cassette.<sup>15</sup> Mouse experiments were performed with approval of the District Government of Bavaria.

## Platelet in vitro assays

Integrin activation and platelet aggregation,<sup>16</sup> platelet spreading,<sup>17</sup> and platelet filamentous actin content measurement<sup>18</sup> were in essence carried out as previously described. Platelet adhesion under flow was measured using fibrillar collagen-coated



(10  $\mu\text{g/mL}$ ; Horm, Takeda Austria GmbH, Linz, Austria) Ibidi  $\mu$ -Slides VI 0.1, uncoated (Ibidi, Martinsried, Germany). Chambers were perfused with heparinized blood for 4 minutes and subsequently washed with Tyrode's solution at a shear rate of 1000/s. Images were taken with a Zeiss Axio Imager Z1 microscope equipped with a 20 $\times$  NA 0.75 objective and an AxioCam MRm (Carl Zeiss, Inc., Oberkochen, Germany) after staining with a CellTrace CFSE Cell Proliferation Kit (Thermo Fisher Scientific). Pictures were processed and surface coverage was measured using ImageJ software (US National Institutes of Health) and normalized against platelet counts.

### Microvascular thrombosis and tail bleeding

The surgical preparation of the mouse cremaster muscle was performed as described previously by Baez<sup>19</sup> with minor modifications. Mice were anesthetized by intraperitoneal administration of a mixture of 100 mg/kg of ketamine and 10 mg/kg of xylazine. The left femoral artery was cannulated in a retrograde manner for the administration of fluorescein isothiocyanate-labeled dextran (molecular weight, 150 kDa; Sigma Aldrich) as well as of DyLight 649-labeled antibodies directed against GPIIb/IIIa for the visualization of platelets (EMFRET, Eibelstadt, Germany). The right cremaster muscle was exposed through a ventral incision of the scrotum, then opened and spread over the pedestal of a custom-made microscopy stage. Epididymis and testicle were detached from the cremaster muscle and placed back into the abdominal cavity. Throughout the surgical procedure and during in vivo microscopy measurements, the cremaster muscle was continuously perfused with warm buffered saline. Microvascular thrombus formation was induced by photochemical injury as described previously.<sup>20</sup> Briefly, a 2.5% solution of fluorescein isothiocyanate-dextran was infused intraarterially, and the exposed vessel segment under investigation was continuously epi-illuminated with a wavelength of 488 nm. An Axio Scope.A1 microscope (Carl Zeiss Microscopy GmbH, Goettingen, Germany), equipped with a Colibri 2 LED light source (Carl Zeiss Microscopy GmbH) for fluorescence epi-illumination microscopy, was used to visualize microvascular thrombogenesis. Thrombus formation was induced in 3 venules and 1 arteriole (inner diameter, 20–30  $\mu\text{m}$ ) per experiment. Time until the first platelet adhesion to the vessel wall (defined as the onset of thrombus formation) and time until blood flow ceased (defined as the complete occlusion of the vessel) were analyzed.

To study thrombus formation in larger vessels, the tails of anesthetized mice were transected at a 5-mm distance from the tail tip using a sterile surgical scalpel blade. Subsequently, the tail was immersed in warm buffered saline (37°C), and tail bleeding was monitored until bleeding ceased. The end point was the arrest of bleeding lasting >6 seconds. Bleeding was recorded for a maximum of 15 minutes.

### Leukocyte in vitro assays

Neutrophils were isolated from bone marrow using an EasySep Mouse Neutrophil Enrichment Kit (STEMCELL Technologies) following the manufacturer's instructions.

Bone marrow-derived macrophages for in vitro assays were differentiated by culturing bone marrow cells in RPMI 1640 supplemented with 10% fetal bovine serum, 100 U/mL of penicillin, 100  $\mu\text{g/mL}$  of streptomycin (all Thermo Fisher Scientific), 50  $\mu\text{M}$  of  $\beta$ -mercaptoethanol, and macrophage colony-stimulating factor

for 6 days. Neutrophil and macrophage adhesion and spreading assays were performed as previously described.<sup>10</sup>

Polymorphonuclear leukocyte (PMN) adhesion strengthening was analyzed using ibidi  $\mu$ -Slides VI 0.4, uncoated (Ibidi), coated with 12.5  $\mu\text{g/mL}$  of recombinant human intercellular cell adhesion molecule 1 (ICAM-1; R&D Systems). A neutrophil suspension of  $3 \times 10^6$  cells per mL isolated from bone marrow using an EasySep Mouse Neutrophil Enrichment Kit (STEMCELL Technologies) was stained using a CellTrace CFSE Cell Proliferation Kit (Thermo Fisher Scientific). PMNs were stimulated with 2  $\mu\text{g/mL}$  of tumor necrosis factor  $\alpha$  (TNF- $\alpha$ ; R&D Systems), placed into flow chambers, and allowed to adhere for 10 minutes. Subsequently, shear stress of 0.5, 1, 2, 4, 6, and 9 dyn/cm<sup>2</sup> was applied, gradually increasing every 90 seconds, and time-lapse movies were recorded using an Epos FL Auto 2 life cell microscope (Thermo Fisher Scientific) equipped with an Epos FL 10 $\times$  NA 0.30 objective. The number of adherent cells was counted and normalized to the number of initially adherent cells for all applied shear rates using Photoshop CS6 (Adobe).

### Intravital microscopy of TNF- $\alpha$ -stimulated mouse cremaster muscle venules

Mice were treated by intrascrotal injection of 500 ng of TNF- $\alpha$  (R&D Systems) 2 hours before microscopy, anesthetized, and prepared for intravital microscopy as described.<sup>21</sup> Movies from cremasteric postcapillary venules ranging from 20 to 40  $\mu\text{m}$  in diameter were recorded using a BX51WI microscope with a water immersion objective of 40 $\times$  0.80 NA and an Olympus CCD camera (CF8/1,  $\kappa$ ). Blood samples were taken after the experiment. White blood cell and neutrophil counts were determined using ProCyt Dx Hematology Analyzer (IDEXX, Westbrook, ME). Leukocyte rolling flux fraction (percentage of rolling leukocytes in all leukocytes passing through the vessel), rolling velocity, adhesion, and adhesion efficiency (number of adherent cells per mm<sup>2</sup> divided by the systemic neutrophil count) were calculated based on the recorded movies using Fiji software.<sup>22</sup> Afterward, cremaster muscles were fixed with 4% paraformaldehyde (AppliChem GmbH, Darmstadt, Germany) and stained using Giemsa (Merck Millipore, Darmstadt, Germany). The number of perivascular cells per mm<sup>2</sup> was assessed with a Leica DM2500 microscope equipped with a DMC2900 CMOS camera and an HCX PL APO 100 $\times$ /1.40 Oil Ph3 at the Ludwig Maximilians University Munich Biomedical Center BioImaging core facility.

### Statistical analysis

Data are presented as means  $\pm$  95% confidence intervals or standard errors of the mean. Paired or unpaired Student's *t* tests were used to compare data sets. A difference between data sets was considered to be significant if *P* < .05.

Additional methods and more detailed descriptions are provided in the supplemental Material and methods, available on the Blood Web site.

## Results

### Rap1-binding mutant Talin1 knockin mice are viable and appear healthy

To interfere with Rap1/Talin1 interaction in vivo, we generated a Talin1 knockin mouse strain (Tln1<sup>3mut</sup>) carrying mutations within



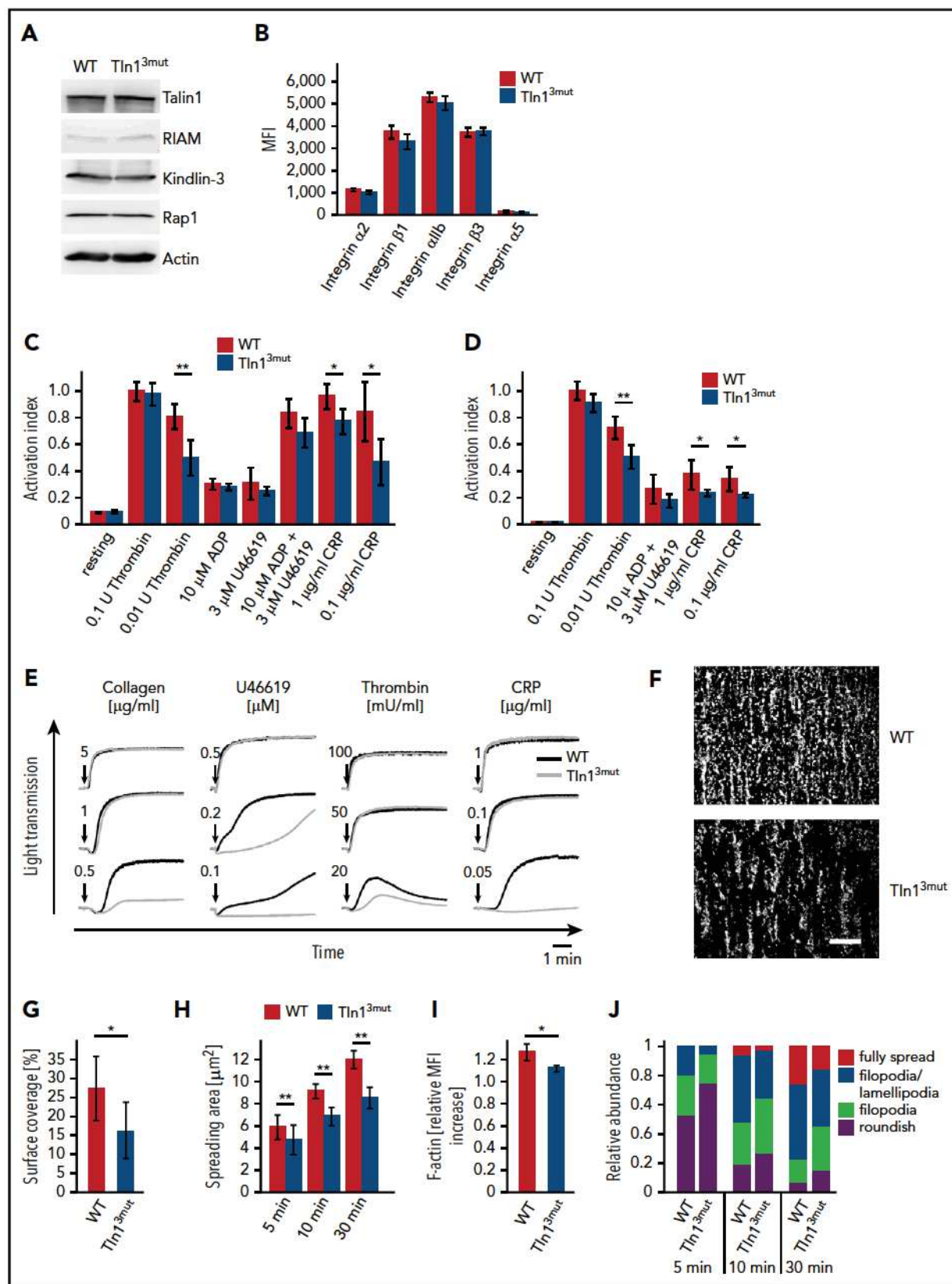


**Figure 1. Platelet function is impaired in Tln1<sup>3mut</sup> mice.** (A) Western blots showing Talin1, RIAM, Kindlin-3, and Rap1 levels in WT and Tln1<sup>3mut</sup> platelets. Actin served as loading control. (B) Surface levels of integrins  $\alpha 2$ ,  $\beta 1$ ,  $\alpha 1 \text{b}$ ,  $\beta 3$ , and  $\alpha 5$  assessed by flow cytometry (n = 4 mice). (C-D) Platelet integrin activation of control and Tln1<sup>3mut</sup> platelets analyzed by JON/A (C) and fibrinogen binding (D) upon stimulation with thrombin (n = 11 WT/12 Tln1<sup>3mut</sup>), ADP (n = 11 WT/12 Tln1<sup>3mut</sup>), U46619 (n = 5), a combination of ADP and U46619 (n = 5), or collagen-related peptide (CRP; n = 5). Activation index represents mean fluorescence intensity (MFI) values of JON/A-PE or fibrinogen-Alexa 647 normalized to integrin  $\beta 3$  levels. MFI values of WT platelets stimulated with 0.1 U of thrombin are set to 1; n represents the number of mice. (E) Representative platelet aggregation curves



exon 2, where K15, R30, and R35 in the Talin1-F0 domain were changed into alanines (supplemental Figure 1A). We chose to mutate these 3 basic residues based on the previous surface charge analysis that suggested their involvement in binding to Rap1.<sup>12</sup> While we generated Tln1<sup>3mut</sup> knockin mice, the complex structure of Rap1/Talin1-F0 was determined, which revealed that K15 and R35 are indeed part of the binding interface and their mutations into alanines (Talin1-F0\_DM) are sufficient to block Rap1 binding.<sup>14</sup> R30 is located near the binding interface; although not directly involved in Rap1 binding, its mutation into alanine should exert little effect on the folding of Talin1-F0.<sup>14</sup> By NMR-based experiments, we show that Talin1-F0 bearing K15A/R30A/R35A (Talin1-F0\_3mut) exhibit a similar NMR spectrum to that of wild-type (WT) Talin1-F0 domain (Talin1-F0\_WT) and the previously reported K15A/R35A (Talin1-F0\_DM) mutant<sup>14</sup> demonstrating no perturbation in the overall folding of mutant Talin1-F0 domains (supplemental Figure 2A-B). As expected, the Talin1-F0\_3mut, like the Talin1-F0\_DM, did not bind to Rap1b (supplemental Figure 2C). This is consistent with the cellular data, which show that Talin1 and Talin2 double-deficient (Talin<sup>1/2dko</sup>) fibroblasts with retroviral expression of full-length ypet-tagged Talin1\_3mut or Talin1\_DM exhibited identical defects in cell adhesion and spreading compared with those with Talin1\_WT (supplemental Figure 2D-E). Importantly, similar to Talin1\_DM, the Talin1\_3mut also showed significantly reduced recruitment to focal adhesions (FAs) (supplemental Figure 2F).

Lagarrigue et al<sup>23</sup> recently reported single point mutant Talin1 knockin (R35E) mice, which exhibited a significantly milder phenotype than ours. It remains unclear what caused the discrepancy, but a strong possibility is the weaker disruption of Rap1/Talin1 interaction by the single R35E mutation compared with our Talin1-F0\_3mut. This explanation is supported by the overall chemical shift changes of <sup>15</sup>N-labeled Talin1-F0 variants, including WT, K15A, R35A, R35E, DM, and 3mut, in the presence of GMP-PNP-loaded Rap1b, where single mutants, including R35E, of Talin1-F0 indeed showed much less reduced binding to Rap1 than Talin1-F0\_DM or 3mut (supplemental Figures 3A-D and 4A-F). That is, the residual interaction between Rap1 and Talin1 (R35E) may still play an important role in integrin signaling, thereby leading to the milder phenotype observed in Talin1 (R35E) knockin mice. Our Tln1<sup>3mut</sup> mice are clearly better suited to explore the physiological relevance of Rap1/Talin1 interaction in regulating integrin activity, even though a residual interaction between Rap1 and Talin1\_3mut may still exist in the cellular context, because we found that expression of Talin1 lacking the entire F0 domain led to more dramatic adhesion, spreading, and recruitment defects in Talin<sup>1/2dko</sup> fibroblasts than the DM or 3mut mutant (supplemental Figure 2D-F).

Heterozygous Tln1<sup>3mut</sup> mice were intercrossed to obtain homozygous Tln1<sup>3mut</sup> mice, and their mutations were confirmed by genomic polymerase chain reaction followed by sequencing

(supplemental Figure 1B). Tln1<sup>3mut</sup> mice were born at a normal Mendelian ratio (supplemental Table 1), were viable, and did not show any overt phenotype. The lack of any obvious phenotype was indeed surprising, given that our previous study revealed a robust integrin-signaling defect in Talin<sup>1/2dko</sup> fibroblasts expressing a Rap1 binding-deficient Talin1.<sup>14</sup> Our reasoning was that Talin2 might compensate for the integrin defect in Tln1<sup>3mut</sup> mice. Indeed, we found that mouse embryonic fibroblasts (MEFs) and endothelial cells isolated from WT and Tln1<sup>3mut</sup> mice expressed Talin2, which was not detectable in blood cells (supplemental Figure 5A). Consistently, MEFs from Tln1<sup>3mut</sup> mice showed no difference in adhesion to the integrin ligands fibronectin and vitronectin or in the number or size of FAs (supplemental Figure 5B-F) as compared with MEFs isolated from WT embryos. Our hypothesis was further supported by the localization of Talin2 to FAs in both WT and mutant MEFs (supplemental Figure 5G).

We then focused our study on blood cells, which exhibit negligible Talin2 expression (supplemental Figure 5F). To exclude the possibility that targeting the *Talin1* gene locus might alter Talin1 expression, we carefully measured Talin1 protein levels in platelets and macrophages from WT and Tln1<sup>3mut</sup> mice by western blotting and found them to be identical (supplemental Figure 6). Furthermore, platelet and white blood cell counts were indistinguishable between control and Tln1<sup>3mut</sup> mice (supplemental Table 2). Altogether, these data suggest that Tln1<sup>3mut</sup> is normally expressed in vivo, expression of Talin2 in non-hematopoietic cells might compensate for the defective Rap1/Talin1 interaction, and direct Rap1/Talin1 interaction is not essential for hematopoiesis.

### Impaired integrin activity and signaling in Tln1<sup>3mut</sup> platelets

Because Talin1 and Rap1 are highly expressed in platelets, whereas RIAM expression is much lower,<sup>24</sup> we hypothesized that direct Rap1/Talin1 interaction is of particular importance for platelet integrin activity. We first determined the expression of Kindlin-3, RIAM, and Rap1 and the surface levels of integrins and found them comparable between platelets from WT and Tln1<sup>3mut</sup> mice (Figure 1A-B). Next, we measured agonist-induced  $\alpha$ IIb $\beta$ 3 integrin activation using the conformation-specific JON/A-PE antibody.<sup>25</sup> We found that stimulation of WT and Tln1<sup>3mut</sup> platelets by high concentrations of thrombin or other agonists, such as ADP, U46619, and collagen-related peptide, results in a similar response. However, lower concentrations of thrombin or other agonists induced the activation of fewer integrins in Tln1<sup>3mut</sup> platelets compared with WT controls, suggesting a reduced susceptibility of Tln1<sup>3mut</sup> platelets in response to agonist stimulation (Figure 1C). Similar results were obtained in binding assays with Alexa Fluor 647-conjugated fibrinogen (Figure 1D). Consistently, Tln1<sup>3mut</sup> platelets revealed similar aggregation responses compared with WT platelets when activated by high concentrations of agonists but showed defective aggregation

**Figure 1 (continued)** measured upon stimulation with different concentrations of collagen, U46619, thrombin, and CRP. Quantification of the data is provided in supplemental Figure 5. (F-G) Heparinized whole blood was perfused through micro flow chambers coated with fibrillar collagen to assess adhesion under flow. (F) Representative images of adherent CFSE-stained platelets after perfusion. Scale bar, 80  $\mu$ m. (G) Quantification of platelet surface coverage normalized to platelet counts ( $n = 7$  mice). (H) Quantification of platelet spreading area on fibrinogen 5, 10, and 30 minutes after activation with 0.01 U of thrombin ( $n = 5$  experiments and mice). (I) Relative F-actin levels in resting vs thrombin-activated (0.01 U of thrombin) platelets quantified by phalloidin-Alexa Fluor 546 staining and subsequent fluorescence-activated cell sorter analysis ( $n = 4$  mice). (J) Relative distribution of WT and Tln1<sup>3mut</sup> platelets at different spreading stages 5, 10, and 30 minutes after plating on a fibrinogen-coated surface ( $n = 5$  experiments and mice). Values are given as means  $\pm$  95% confidence intervals. \* $P < .05$ , \*\* $P < .01$ .



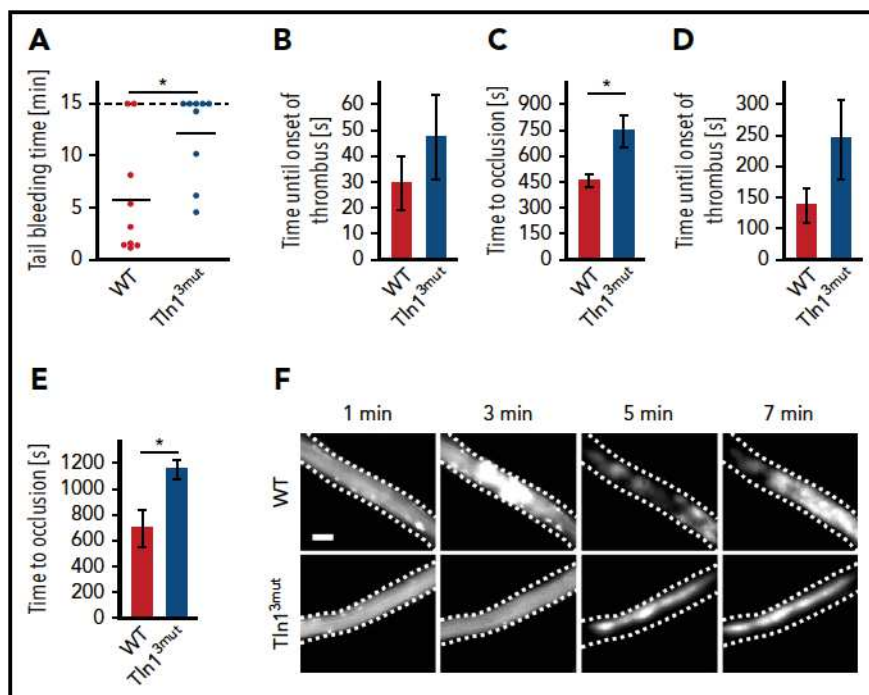


**Figure 2. Hemostasis and thrombosis are reduced in Tln1<sup>3mut</sup> mice.** (A) Tail-bleeding time of WT and Tln1<sup>3mut</sup> mice (cutoff at 15 minutes;  $n = 9$ ). (B-C) Onset of thrombus formation (B) and vessel occlusion (C) measured in cremaster muscle venules of WT and Tln1<sup>3mut</sup> mice after induction of phototoxic injury ( $n = 5$ ). (D-E) Thrombus onset (D) and occlusion time (E) in injured cremaster muscle arterioles of WT and Tln1<sup>3mut</sup> mice ( $n = 4$ ). (F) Representative images of WT and Tln1<sup>3mut</sup> cremaster muscle venules showing the progress of thrombus formation after 1, 3, 5, and 7 minutes. Scale bar, 25  $\mu$ m. Values are given as means  $\pm$  standard errors of the mean;  $n$  represents the number of mice. \* $P < .05$ .

upon stimulation with agonists at lower concentrations (Figure 1E; supplemental Figure 7). To test whether  $\alpha 2\beta 1$  integrin activation is also diminished in Tln1<sup>3mut</sup> platelets, we performed platelet adhesion assays on collagen under flow and observed significantly reduced adhesion (Figure 1F-G). We also allowed control and Tln1<sup>3mut</sup> platelets to adhere and spread on fibrinogen and analyzed the spreading kinetics by measuring the spreading area over time and found delayed spreading in Tln1<sup>3mut</sup> platelets (Figure 1H). A more detailed characterization revealed that the spreading defect is caused by delayed filopodia and lamellipodia formation resulting from reduced actin polymerization (Figure 1I-J), suggesting that integrin outside-in signaling is also significantly impaired in Tln1<sup>3mut</sup> platelets. Collectively, our data demonstrate an important role of direct Rap1/Talin1 interaction in regulating platelet aggregation, adhesion, and spreading.

### Rap1/Talin1 interaction is important for hemostasis and thrombosis

To investigate whether the loss of Rap1/Talin1 interaction in platelets is of any relevance *in vivo*, we first tested the hemostatic potential in Tln1<sup>3mut</sup> mice by performing tail-bleeding assays, which revealed significantly prolonged bleeding time in Tln1<sup>3mut</sup> mice compared with WT mice (Figure 2A). We also studied pathological thrombus formation at a phototoxic-induced vessel injury site in the cremaster muscle vasculature of WT and Tln1<sup>3mut</sup> mice. To this end, platelets were fluorescently labeled, and the time at which thrombi started to form and finally occluded the vessels was recorded by intravital microscopy. We found that while Tln1<sup>3mut</sup> platelets showed a tendency of delayed attachment to the injured vessel wall, Tln1<sup>3mut</sup> mice showed a significantly prolonged vessel occlusion time in both venules (Figure 2B-C) and arterioles (Figure 2D-E) compared with control mice (Figure 2F). Collectively, our observations clearly indicate a critical role for direct Rap1/Talin1 interaction in regulating platelet function *in vivo*.

### Rap1/Talin1 interaction controls integrin activity in neutrophils

Despite the important role of the Rap1/RIAM/Talin complex in leukocyte integrin activation, we still wondered whether the loss of Talin1/Rap1 interaction also impairs leukocyte integrin functions. Therefore, we isolated PMNs and performed adhesion assays in the presence and absence of TNF- $\alpha$  or phorbol-12-myristate-13-acetate (PMA). Unexpectedly, our assays revealed that adhesion of Tln1<sup>3mut</sup> PMNs to the  $\beta 2$  integrin ligand ICAM-1, the  $\alpha 4\beta 1$  integrin ligand vascular cell adhesion molecule 1 (VCAM-1), and fibronectin, which is bound by several integrins, was significantly reduced compared with WT controls (Figure 3A). Importantly, intracellular expression of Talin1 and other integrin regulatory proteins, such as Rap1, Kindlin-3, and RIAM, and surface integrin levels were comparable between WT and mutant PMNs (Figure 3B, D). To test whether the reduced adhesion of Tln1<sup>3mut</sup> PMNs was due to a defect in adhesion strengthening, we isolated PMNs from the bone marrow of control and Tln1<sup>3mut</sup> mice, seeded them on ICAM-1-coated flow chambers, activated them with TNF- $\alpha$ , and applied a stepwise increase in shear stress within the chamber (detachment assay). In line with the results of the static adhesion assay, we observed an initial drop in the number of adherent Tln1<sup>3mut</sup> cells when flow was started. However, increase in shear stress did not lead to further detachment of Tln1<sup>3mut</sup> cells, indicating that direct Rap1 binding to Talin1 is not required for adhesion strengthening (Figure 3C). To investigate whether the loss of Rap1/Talin1 interaction also impairs other  $\beta 2$  integrin-mediated functions besides adhesion, we measured phagocytosis of serum-opsonized bacteria and found a significantly reduced bacterial uptake by Tln1<sup>3mut</sup> PMNs compared with control PMNs (Figure 3E). Taken together, these data indicate that direct Rap1/Talin1 interaction is also critically involved in regulating neutrophil integrin functions.



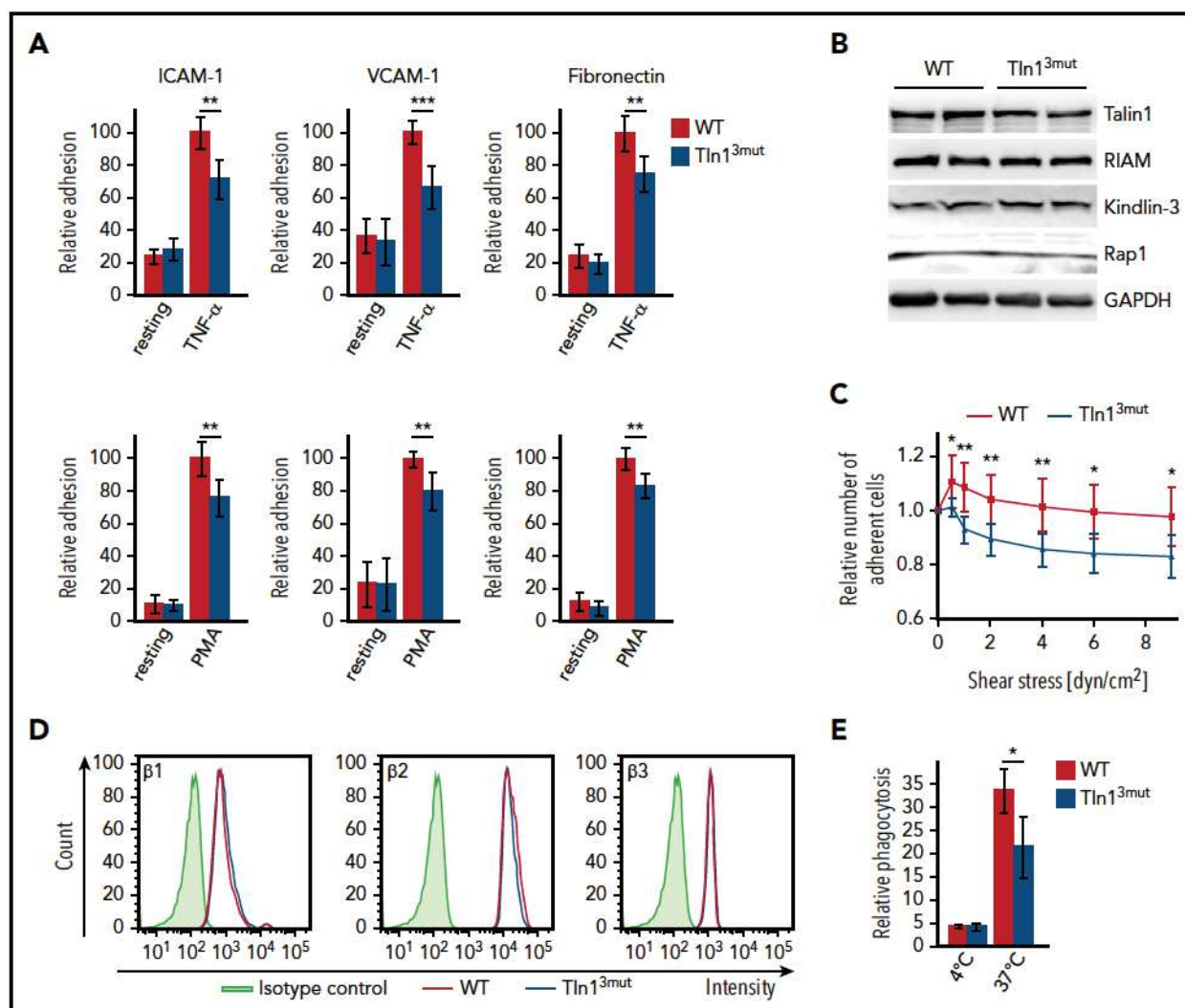


**Figure 3. Integrin-mediated functions are impaired in Tln1<sup>3mut</sup> PMNs.** (A) Static adhesion of WT and Tln1<sup>3mut</sup> PMNs on fibronectin, ICAM-1, and VCAM-1 upon stimulation with TNF-α or PMA compared with resting PMNs (n = 12 mice). (B) Analysis of Talin1, RIAM, Kindlin-3, and Rap1 expression in control and Tln1<sup>3mut</sup> PMNs by western blotting. Glyceraldehyde-3-phosphate dehydrogenase (GAPDH) served as loading control. (C) Adhesion strengthening of TNF-α-stimulated WT and Tln1<sup>3mut</sup> PMNs on ICAM-1 under increasing shear stress (0.5–9.0 dyn/cm²) measured as the number of adherent cells relative to initially adherent cells (n = 16 channels analyzed in 4 independent experiments). (D) Representative fluorescence-activated cell sorter blots illustrating surface levels of integrin β1, β2, and β3 on Gr-1<sup>+</sup> neutrophils isolated from bone marrow. (E) Relative amount of fluorescently labeled *Escherichia coli* particles phagocytosed by WT and Tln1<sup>3mut</sup> neutrophils (n = 3 mice). All values are given as means ± 95% confidence intervals. \*P < .05, \*\*P < .01, \*\*\*P < .001.

### Direct Rap1/Talin1 interaction is required for neutrophil adhesion and extravasation in vivo

Next, we tested whether Tln1<sup>3mut</sup> PMNs displayed a defect in response to inflammation in vivo. To do so, we investigated the adhesion and extravasation of PMNs on TNF-α-stimulated cremaster muscle venules using intravital microscopy. Although mean leukocyte rolling velocity was similar between control and Tln1<sup>3mut</sup> neutrophils (Figure 4A), the adhesion efficiency (calculated as number of adherent PMNs per mm² of vascular surface area divided by the systemic PMN count) of Tln1<sup>3mut</sup> PMNs was significantly reduced compared with controls (Figure 4B), which is consistent with the reduced adhesion observed in isolated Tln1<sup>3mut</sup> PMNs (Figure 3A). Importantly, we observed a strongly reduced number of extravasated PMNs in the perivascular cremaster muscle tissue of Tln1<sup>3mut</sup> mice, suggesting that neutrophil recruitment into inflamed tissue is significantly impaired in the absence of direct Rap1 binding to Talin1 (Figure 4C–D). Our data

therefore reveal a previously unappreciated role of the Rap1/Talin1 pathway in regulating leukocyte function in vivo.

### Direct Rap1/Talin1 interaction is not required for macrophage adhesion or spreading despite reduced integrin activation

The functional defects observed in platelets and neutrophils of Tln1<sup>3mut</sup> mice suggest that Rap1/Talin1 interaction is crucial for circulating blood cells, which require rapid and dynamic integrin-mediated responses. We then asked whether the adhesion and spreading of other blood cells such as macrophages are affected in Tln1<sup>3mut</sup> mice. In contrast to platelets and neutrophils, which respond immediately to vascular damage and infections, respectively, most macrophages differentiate within the tissue from extravasated monocytes and act as professional phagocytes and regulators of immune responses. We hypothesized that their functions are less dependent on fast integrin activation



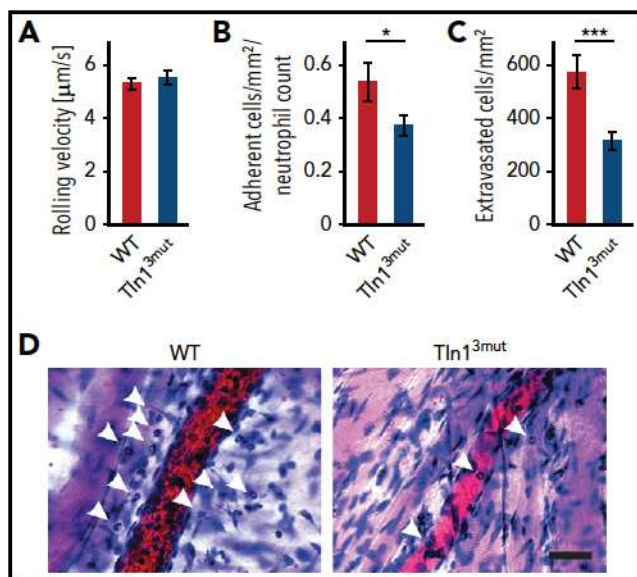


**Figure 4. Neutrophil recruitment is reduced in Tln1<sup>3mut</sup> mice.** (A-D) In vivo leukocyte rolling velocity, adhesion efficiency, and extravasation were analyzed in mouse cremaster muscle venules of WT and Tln1<sup>3mut</sup> mice 2 hours after intrascrotal injection of TNF- $\alpha$ . Rolling velocity (A) and adhesion efficiency (B) (adherent cells per mm<sup>2</sup> normalized to the total neutrophil count) were analyzed using intravital microscopy. (C) Leukocyte extravasation was assessed in the perivascular region upon Giemsa staining of cremaster muscle whole mounts (n = 17 vessels in 4 WT and 4 Tln1<sup>3mut</sup> mice). Values are given as means  $\pm$  standard errors of the mean. (D) Representative images of Giemsa-stained whole mounts of WT and Tln1<sup>3mut</sup> mice. Arrows point to extravasated neutrophils. Scale bar, 30  $\mu$ m. \**P* < .05, \*\*\**P* < .001.

regulated by Rap1/Talin1 interaction. Therefore, we generated bone marrow-derived macrophages from WT and Tln1<sup>3mut</sup> mice, which revealed normal expression of integrin regulatory proteins and similar levels of  $\beta$ 1,  $\beta$ 2, and  $\beta$ 3 integrins on their cell surfaces (Figure 5A-B). Interestingly, adhesion and spreading of Tln1<sup>3mut</sup> macrophages on  $\beta$ 1,  $\beta$ 2, and  $\beta$ 3 integrin ligands were not altered compared with WT macrophages (Figure 5C-D), even though 9EG7 staining on Tln1<sup>3mut</sup> macrophages revealed reduced levels of active  $\beta$ 1 integrins (Figure 5E-F). These data suggest that in macrophages, unlike platelets and neutrophils, the activation of a reduced number of integrins is still sufficient to promote efficient cell adhesion and spreading.

## Discussion

In this study, we generated Rap1 binding-deficient Talin1 knockin mice to investigate the physiological importance of direct Rap1/Talin1 interaction in integrin signaling. Tln1<sup>3mut</sup> mice develop normally and are viable and apparently healthy. Although MEFs isolated from Tln1<sup>3mut</sup> mice show normal integrin function, likely because of functional compensation by Talin2, hematopoietic cells such as platelets and neutrophils, which express no or low levels of Talin2, showed significant defects in integrin activation and integrin-dependent cell functions. Our study thus for the first time demonstrates the important role of Rap1/Talin1 interaction in vivo.

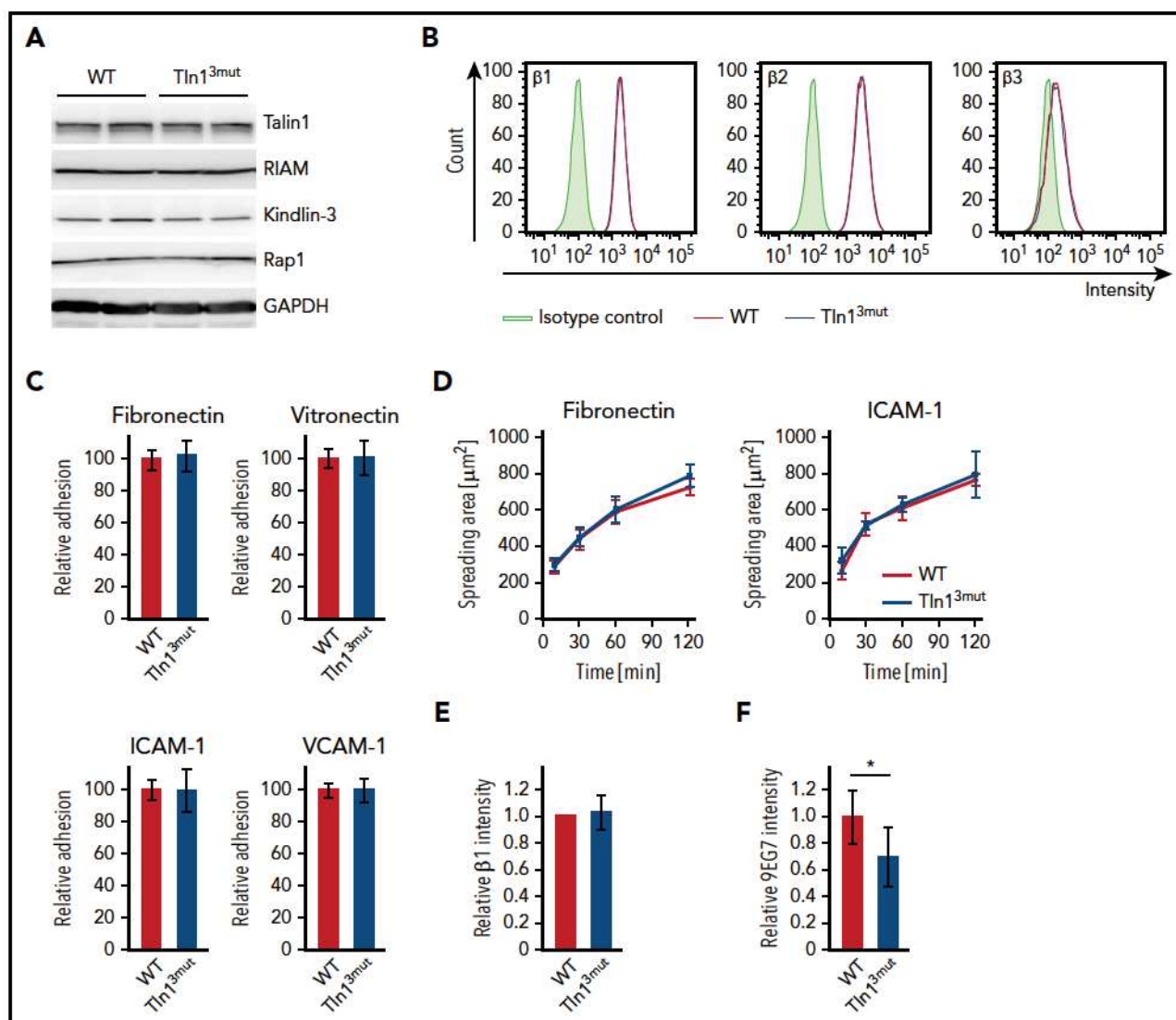
One important finding of our study is that platelet integrin activity, aggregation, and spreading as well as hemostasis and thrombosis are impaired in Rap1 binding-deficient Tln1<sup>3mut</sup> mice, demonstrating the critical physiological relevance of this interaction in vivo. The platelet defects and the resulting phenotype in Tln1<sup>3mut</sup> mice are similar to mice lacking the most

prominent Rap1 isoform (Rap1b) in platelets, which exhibit moderate integrin activation and signaling defects.<sup>7</sup> A recent elegant study showed that the deletion of both Rap1 genes (Rap1a and Rap1b) in the megakaryocyte lineage<sup>26</sup> led to a more severe defect in integrin activation, where ~80% of the platelet integrins remained inactive upon activation via different agonists. Although Talin1<sup>3mut</sup> protein likely fails to interact with both Rap1 proteins due to their high similarity,<sup>14</sup> Tln1<sup>3mut</sup> mice indeed showed a milder phenotype. There are several factors that may contribute to this difference. First, the interaction between Rap1 and mutant Talin1 is impaired but may not be completely abolished in cells. This possibility is supported by the rather moderate cell adhesion, spreading, and Talin1 recruitment defects in cells expressing double- or triple-mutant Talin1 proteins compared with Talin1 mutant lacking the complete F0 domain (supplemental Figure 2D-F). That is, residual interaction between Rap1 and Talin1 mutant may still support some Talin1 recruitment to regulate integrin activation and signaling, especially in platelets, which express high protein levels of Rap1b and Talin1.<sup>24</sup> Such a possibility is also consistent with the more severe phenotypes observed in our Tln1<sup>3mut</sup> mice compared with the recently reported Talin1 (R35E) knockin mice<sup>23</sup> because of the less disrupted Rap1/Talin1 interaction of the latter (supplemental Figures 3A-D and 4A-F). Second, abolishing Rap1/Talin1 interaction is fundamentally different from complete Rap1a/Rap1b double knockout. The former blocks only 1 of many Rap1 functions, in contrast to the latter. It is well known that the small GTPase Rap1 serves as a central signaling unit and regulates many integrin-dependent (Rap1 is involved in both integrin inside-out and outside-in signaling<sup>27</sup>) and -independent signaling pathways by interacting with a variety of effector proteins; complete loss of Rap1a/Rap1b expression has therefore much more dramatic functional consequences. Third, despite the low RIAM expression in platelets, the formation of some Rap1/RIAM/Talin1 complexes may partially compensate for deficient Rap1/Talin1 interaction to regulate Talin recruitment. Additional depletion of RIAM in Talin1 (R35E) knockin mice did not lead to a more obvious platelet phenotype.<sup>23</sup> However, functional compensation by RIAM might be dispensable, given that Talin1 (R35E) platelets alone have very mild defects. Therefore, generating Tln1<sup>3mut</sup> mice with further depletion of RIAM instead will clarify this.

We would also like to mention that residual (20%) platelet integrin activity was observed even in Rap1a/b double-mutant platelets,<sup>26</sup> suggesting the involvement of Rap1-independent pathways (eg, PIP2-mediated Talin recruitment)<sup>28,29</sup> in regulating basal platelet function. Nevertheless, our study clearly showed significant platelet defects when the direct Rap1/Talin1 pathway was impaired and demonstrated its important role in regulating platelet integrin activity and function in vivo.

A second important finding of our study is that the direct Rap1/Talin1 pathway is also used in neutrophils to regulate integrin activity. Tln1<sup>3mut</sup> neutrophils revealed impaired  $\beta$ 2 integrin-mediated adhesion and phagocytosis, indicating that direct Rap1/Talin1 interaction is indispensable for full  $\beta$ 2 integrin function. This observation is surprising, because we and others have shown that leukocyte  $\beta$ 2 integrin functions are critically dependent on the Rap1/RIAM/Talin1 complex.<sup>6,10</sup> Moreover, Tln1<sup>3mut</sup> neutrophils also exhibited defective adhesion to  $\beta$ 1 and  $\beta$ 3 integrin ligands, suggesting that direct Rap1/Talin1 interaction is of general importance to regulate the activity of all major integrin classes,





whereas Rap1/RIAM/Talin1 is mainly involved in  $\beta 2$  integrin activation. Notably, both *Tln1*<sup>3mut</sup> and RIAM knockout mice show defective  $\beta 2$  integrin-mediated neutrophil adhesion and extravasation into inflamed tissue, indicating the synergistic action of both Rap1/Talin1 and Rap1/RIAM/Talin1 pathways in regulating neutrophil integrin signaling. However, we did not observe clear leukocytosis in *Tln1*<sup>3mut</sup> mice, which is present in RIAM knockout mice, indicating that the RIAM-dependent pathway plays a major role in  $\beta 2$  integrin-mediated leukocyte extravasation. Moreover, *Tln1*<sup>3mut</sup> macrophages exhibited no adhesion or spreading defect despite reduced  $\beta 1$  integrin activity, suggesting that direct Rap1/Talin1 interaction is particularly important in circulating cells, like platelets and neutrophils, which require fast and dynamic integrin-mediated responses. Additional studies are required to address this point. Nevertheless, our data provide strong evidence that direct Rap1/

Talin1 interaction is important for regulating integrin signaling in the physiological context.

## Acknowledgments

The authors thank Soo Jin Min-Weißenhorn and members of the transgenic facility team of the Max Planck Institute of Biochemistry for help in generating the *Tln1*<sup>3mut</sup> mice. The authors also thank Reinhard Fässler for his support and Arnaud Sonnenberg for critically reading the manuscript.

The work was supported by the Deutsche Forschungsgemeinschaft (SFB914 TP A01, B01, B03), the Max Planck Society, and grant R01GM62823 from National Institute of General Medical Sciences, National Institutes of Health.

## Authorship

Contribution: T.B., S.K., I.R., L.Z., L.M., and M.M. designed and performed the experiments and analyzed data; C.A.R., M.S., and J.Q.



designed experiments and analyzed data; M.M. supervised the work; and J.Q. and M.M. wrote the paper with input from all other authors.

Conflict-of-interest disclosure: The authors declare no competing financial interests.

ORCID profiles: S.K., 0000-0003-4723-056X; L.Z., 0000-0002-6529-5706; M.S., 0000-0002-7689-3613; M.M., 0000-0001-8825-5566.

Correspondence: Markus Moser, Max Planck Institute of Biochemistry, Department of Molecular Medicine, Am Klopferspitz 18, D-82152 Martinsried, Germany; e-mail: moser@biochem.mpg.de.

## Footnotes

Submitted 23 April 2018; accepted 8 November 2018. Prepublished online as *Blood* First Edition paper, 15 November 2018; DOI 10.1182/blood-2018-04-846766.

The online version of this article contains a data supplement.

The publication costs of this article were defrayed in part by page charge payment. Therefore, and solely to indicate this fact, this article is hereby marked "advertisement" in accordance with 18 USC section 1734.

## REFERENCES

- Han J, Lim CJ, Watanabe N, et al. Reconstructing and deconstructing agonist-induced activation of integrin  $\alpha$ IIb $\beta$ 3. *Curr Biol*. 2006;16(18):1796-1806.
- Watanabe N, Bodin L, Pandey M, et al. Mechanisms and consequences of agonist-induced talin recruitment to platelet integrin  $\alpha$ IIb $\beta$ 3. *J Cell Biol*. 2008;181(7):1211-1222.
- Lee HS, Lim CJ, Puzon-McLaughlin W, Shattil SJ, Ginsberg MH. RIAM activates integrins by linking talin to ras GTPase membrane-targeting sequences. *J Biol Chem*. 2009;284(8):5119-5127.
- Lagarigue F, Vikas Anekal P, Lee HS, et al. A RIAM/lamellipodin-talin-integrin complex forms the tip of sticky fingers that guide cell migration. *Nat Commun*. 2015;6:8492.
- Stritt S, Wolf K, Lorenz V, et al. Rap1-GTP-interacting adaptor molecule (RIAM) is dispensable for platelet integrin activation and function in mice. *Blood*. 2015;125(2):219-222.
- Su W, Wynne J, Pinheiro EM, et al. Rap1 and its effector RIAM are required for lymphocyte trafficking. *Blood*. 2015;126(25):2695-2703.
- Chrzanowska-Wodnicka M, Smyth SS, Schoenwaelder SM, Fischer TH, White GC II. Rap1b is required for normal platelet function and hemostasis in mice. *J Clin Invest*. 2005;115(3):680-687.
- Bergmeier W, Goerge T, Wang HW, et al. Mice lacking the signaling molecule CalDAG-GEFI represent a model for leukocyte adhesion deficiency type III. *J Clin Invest*. 2007;117(6):1699-1707.
- Crittenden JR, Bergmeier W, Zhang Y, et al. CalDAG-GEFI integrates signaling for platelet aggregation and thrombus formation [published correction appears in *Nat Med*. 2004 Oct;10(10):1139]. *Nat Med*. 2004;10(9):982-986.
- Klapprath S, Sperandio M, Pinheiro EM, et al. Loss of the Rap1 effector RIAM results in leukocyte adhesion deficiency due to impaired  $\beta$ 2 integrin function in mice. *Blood*. 2015;126(25):2704-2712.
- Bouaouina M, Lad Y, Calderwood DA. The N-terminal domains of talin cooperate with the phosphotyrosine binding-like domain to activate  $\beta$ 1 and  $\beta$ 3 integrins. *J Biol Chem*. 2008;283(10):6118-6125.
- Goult BT, Bouaouina M, Elliott PR, et al. Structure of a double ubiquitin-like domain in the talin head: a role in integrin activation. *EMBO J*. 2010;29(6):1069-1080.
- Plak K, Pots H, Van Haastert PJ, Kortholt A. Direct Interaction between TalinB and Rap1 is necessary for adhesion of Dictyostelium cells. *BMC Cell Biol*. 2016;17:1.
- Zhu L, Yang J, Bromberger T, et al. Structure of Rap1b bound to talin reveals a pathway for triggering integrin activation. *Nat Commun*. 2017;8(1):1744.
- Betz UA, Vossenhilf CA, Rajewsky K, Müller W. Bypass of lethality with mosaic mice generated by Cre-loxP-mediated recombination. *Curr Biol*. 1996;6(10):1307-1316.
- Klapprath S, Moretti FA, Zeiler M, et al. Minimal amounts of kindlin-3 suffice for basal platelet and leukocyte functions in mice. *Blood*. 2015;126(24):2592-2600.
- Hofmann S, Braun A, Pozgaj R, Morowski M, Vögtle T, Nieswandt B. Mice lacking the SLAM family member CD84 display unaltered platelet function in hemostasis and thrombosis. *PLoS One*. 2014;9(12):e115306.
- Petzold T, Ruppert R, Pandey D, et al.  $\beta$ 1 integrin-mediated signals are required for platelet granule secretion and hemostasis in mouse. *Blood*. 2013;122(15):2723-2731.
- Baez S. An open cremaster muscle preparation for the study of blood vessels by in vivo microscopy. *Microvasc Res*. 1973;5(3):384-394.
- Rumbaut RE, Randhawa JK, Smith CW, Burns AR. Mouse cremaster venules are predisposed to light/dye-induced thrombosis independent of wall shear rate, CD18, ICAM-1, or P-selectin. *Microcirculation*. 2004;11(3):239-247.
- Pruenster M, Kurz AR, Chung KJ, et al. Extracellular MRP8/14 is a regulator of  $\beta$ 2 integrin-dependent neutrophil slow rolling and adhesion. *Nat Commun*. 2015;6:6915.
- Schindelin J, Arganda-Carreras I, Frise E, et al. Fiji: an open-source platform for biological-image analysis. *Nat Methods*. 2012;9(7):676-682.
- Lagarigue F, Gingras AR, Paul DS, et al. Rap1 binding to the talin 1 F0 domain makes a minimal contribution to murine platelet GPIIb-IIIa activation. *Blood Adv*. 2018;2(18):2358-2368.
- Zeiler M, Moser M, Mann M. Copy number analysis of the murine platelet proteome spanning the complete abundance range. *Mol Cell Proteomics*. 2014;13(12):3435-3445.
- Bergmeier W, Schulte V, Brockhoff G, Bier U, Zirngibl H, Nieswandt B. Flow cytometric detection of activated mouse integrin  $\alpha$ IIb $\beta$ 3 with a novel monoclonal antibody. *Cytometry*. 2002;48(2):80-86.
- Stefanini L, Lee RH, Paul DS, et al. Functional redundancy between RAP1 isoforms in murine platelet production and function. *Blood*. 2018;132(18):1951-1962.
- Zhang G, Xiang B, Ye S, et al. Distinct roles for Rap1b protein in platelet secretion and integrin  $\alpha$ IIb $\beta$ 3 outside-in signaling. *J Biol Chem*. 2011;286(45):39466-39477.
- Goksoy E, Ma YQ, Wang X, et al. Structural basis for the autoinhibition of talin in regulating integrin activation. *Mol Cell*. 2008;31(1):124-133.
- Legate KR, Takahashi S, Bonakdar N, et al. Integrin adhesion and force coupling are independently regulated by localized PtdIns (4,5)2 synthesis. *EMBO J*. 2011;30(22):4539-4553.



## Supplementary Material and Methods

### NMR Spectroscopy

Protein purification. Talin1-F0 (1-86) subcloned into a pHis-1 vector<sup>1</sup> was used as a template to generate Talin1-F0 single mutants including K15A, R35A and R35E by using QuickChange lightning site-directed mutagenesis Kit (Agilent Technologies). Talin1-F0\_DM (K15A, R35A) subcloned into a pHis-1 vector<sup>1</sup> was used as a template to generate Talin1-F0\_3mut (K15A, R30A, R35A) using the same mutagenesis Kit. Talin1-F0 (WT or mutant) was expressed in *E. coli* BL21 (DE3) strain and <sup>15</sup>N Isotope-labeled Talin1-F0 was achieved by growing bacteria in minimal medium with <sup>15</sup>NH<sub>4</sub>Cl as the sole nitrogen source. Talin1-F0 was first purified by nickel affinity column and then incubated with TEV protease to remove the recombinant N-terminal 6xHis-tag. By flowing through nickel affinity column, untagged Talin1-F0 was collected and subjected to gel filtration by using Superdex-75 (10/300, GE Healthcare), which was pre-equilibrated with buffer containing 20 mM NaH<sub>2</sub>PO<sub>4</sub>/Na<sub>2</sub>HPO<sub>4</sub> (pH 6.6), 50 mM NaCl and 2 mM Dithiothreitol (DTT). Protein concentration was measured by absorbance at 280 nm. Human full-length Rap1b (G12V) subcloned into a pET28a vector<sup>1</sup> was used to express active form of Rap1b. Rap1b (G12V) with N-terminal 6xHis tag was purified by nickel affinity column, followed by anion exchange using Hi-trap Q column (GE Healthcare). Gel filtration was performed in the final step by using Superdex-75 (16/60, GE Healthcare). Purified Rap1b (G12V) was then loaded with Guanosine 5'-[β, γ-imido] triphosphate trisodium salt (GMP-PNP)<sup>1</sup> for experiment use. Protein concentration of Rap1b (G12V) was measured by Pierce 660 nm protein assay reagent (Thermo Fisher Scientific).

NMR 2D-HSQC. HSQC experiments were performed on a Bruker 600 or 700 MHz NMR spectrometer. Samples containing <sup>15</sup>N-labeled Talin1-F0 (WT or mutant) in the absence or presence of GMP-PNP loaded Rap1b (G12V) were studied. Experiments were performed at 25 °C in buffer containing 20 mM NaH<sub>2</sub>PO<sub>4</sub>/Na<sub>2</sub>HPO<sub>4</sub> (pH 6.6), 50 mM NaCl, 5 mM MgCl<sub>2</sub>, 2 mM Dithiothreitol (DTT) and 5% D<sub>2</sub>O. Chemical shift change ( $\Delta\delta_{\text{obs}}[\text{HN},\text{N}]$ ) of each selected residue was calculated with the equation  $\Delta\delta_{\text{obs}}[\text{HN},\text{N}] = [(\Delta\delta_{\text{HN}}W_{\text{HN}})^2 + (\Delta\delta_{\text{N}}W_{\text{N}})^2]^{1/2}$  where  $\Delta\delta$  (ppm) =  $\delta_{\text{bound}} - \delta_{\text{free}}$ , and  $W_{\text{HN}}$  and  $W_{\text{N}}$  are weighting factors,  $W_{\text{HN}} = 1$ ,  $W_{\text{N}} = 0.154$ .

### Antibodies and reagents

The following antibodies were used for flow cytometry: FITC-labeled hamster IgM anti-CD29 (Biolegend, Uithoorn, Netherlands), rat IgG2a anti-CD18, hamster IgG anti-CD61, hamster IgG anti-CD49b, rat IgG2a anti-CD41, rat IgG2a anti-CD49e (BD Biosciences, Heidelberg, Germany),



isotype controls rat IgG (Thermo Fisher Scientific, Braunschweig, Germany) and hamster IgG (BD Biosciences, Heidelberg, Germany), PE-labeled rat IgG2b anti-activated integrin  $\alpha$ IIb  $\beta$ 3 clone JON/A (Emfret Analytics, Eibelstadt, Germany), fibrinogen-Alexa Fluor 647, Phalloidin-Alexa Fluor 546, eFluor450-labeled rat IgG2b anti-CD11b and biotinylated rat IgG2b anti-Ly-6G (Gr-1) (Thermo Fisher Scientific), Streptavidin-Cy5 (Jackson ImmunoResearch Laboratories, Inc.; Suffolk; UK). All flow cytometry based assays were carried out using an LSRFortessa™ X-20 flow cytometer (BD Biosciences). The following antibodies were used for Western blotting: mouse anti-Talin, mouse anti-Actin (Sigma-Aldrich, Deisenhofen, Germany), rabbit anti-RIAM (Abcam, Cambridge, UK), rabbit anti-Talin1 (Cell Signaling Technology, Frankfurt, Germany), mouse anti-Talin2 (Abcam plc, Cambridge, UK) rabbit anti-Rap1 (Santa Cruz Biotechnology, Inc., Heidelberg, Germany), rabbit anti-Kindlin-3 (homemade<sup>2</sup>), mouse anti-GAPDH (Merck-Millipore, Darmstadt, Germany), goat anti-rabbit-HRP and goat anti-mouse-HRP (Jackson ImmunoResearch Laboratories). Antibodies used for immunofluorescence stainings: mouse anti-Talin2, rabbit anti-Paxillin (both Abcam plc), rat anti-active  $\beta$ 1 integrin (9EG7; BD Pharmingen), rabbit anti- $\beta$ 1 integrin (homemade<sup>3</sup>), goat anti-mouse-Cy3 (Jackson ImmunoResearch Laboratories), goat anti-rabbit-Alexa Fluor 488, goat anti-rat-Alexa Fluor 546 and Phalloidin-Alexa Fluor 647 (Thermo Fisher Scientific).

The following agonists were used for platelet studies: Chrono-Par-Thrombin, Chrono-Par-ADP, Chrono-Par-Collagen (Probe & go Labordiagnostica GmbH, Lemgo, Germany), U46619 (Enzo Life Sciences GmbH, Lörrach, Germany) and Collagen-related peptide (CRP; kindly provided by Prof. Siess, LMU, Munich). The following ligands and agonists were used for leukocyte studies: recombinant human ICAM-1, recombinant human VCAM-1 (both R&D Systems, Abingdon, UK), fibronectin (Sigma-Aldrich), vitronectin (STEMCELL Technologies, Köln, Germany), PMA (Merck-Millipore), TNF- $\alpha$  (R&D Systems).

### **Platelet integrin activation, aggregation and spreading**

Platelet *in vitro* assays were either performed on isolated platelets or whole blood samples. Platelet preparation was performed by repeated centrifugation of heparinized blood at 50 g for 5 min and harvesting the upper platelet containing fraction. Platelets were washed in Tyrode's buffer (136 mM NaCl, 0.43 mM NaH<sub>2</sub>PO<sub>4</sub>, 2.7 mM KCl, 12mM NaHCO<sub>3</sub>, 5 mM HEPES, 0.1% glucose, 0.35% BSA; pH 7.35) containing apyrase and PGI<sub>2</sub> and kept at 37 °C. Platelet concentration was measured using a ProCyt Dx Hematology Analyzer (IDEXX, Westbrook, USA).

Integrin activation and platelet aggregation<sup>4</sup>, platelet spreading<sup>5</sup> and platelet filamentous actin content measurement<sup>6</sup> were in essence carried out as previously described.



Integrin activation was assessed on heparinized blood samples washed twice with Tyrode's buffer and resuspended in Tyrode's buffer containing 2 mM  $\text{CaCl}_2$  and 1 mM  $\text{MgCl}_2$ . Platelets were stimulated with indicated agonists and stained either with JON/A-PE antibody or AlexaFluor 647-labeled fibrinogen for 15 min at 37 °C. Active integrin level was measured by flow cytometry using an LSRFortessa™ X-20 flow cytometer (BD Biosciences). An activation index was calculated by normalizing active integrin staining intensity to total integrin  $\beta 3$  levels.

For platelet aggregation studies, washed platelets were treated with indicated agonists in the presence of fibrinogen and light transmission was measured using a Chrono-Log aggregometer for 15 min.

Spreading assays were carried out on glass bottom microwell dishes (MatTek Corporation, Ashland, USA) coated with 200  $\mu\text{g/ml}$  fibrinogen (Sigma-Aldrich) over night. After blocking with 1% BSA/PBS for 30 min,  $10^7$  platelets were seeded upon stimulation with 0.01 U/ml thrombin. Adherent platelets were fixed with 4% paraformaldehyde (PFA) at indicated time points and imaged using an Eclipse Ti live cell microscope equipped with a 100x NA 1.45 Plan Apo  $\lambda$  objective (Nikon Instruments, Amsterdam, Netherlands) and a ProEM EMCCD Camera (Princeton Instruments). Platelet spreading area and stage of spreading were analyzed using ImageJ software (US National Institutes of Health).

### **Leukocyte adhesion and spreading assays**

Neutrophil and macrophage adhesion and spreading assays were performed as previously described<sup>7</sup>. For adhesion assays, non-cell culture-treated 96-well plates were coated with recombinant human ICAM-1 (4  $\mu\text{g/ml}$ ), VCAM-1 (4  $\mu\text{g/ml}$ ), vitronectin (2.5  $\mu\text{g/ml}$ ) or fibronectin (5  $\mu\text{g/ml}$ ) in coating buffer (20 mM Tris-HCl pH 9.0, 150 mM NaCl, 2 mM  $\text{MgCl}_2$ ) at 4 °C overnight. Plates were washed with PBS and blocked with 3% BSA. PMNs were isolated from bone marrow and  $5 \times 10^4$  cells / well were seeded in adhesion medium (RPMI1640 containing 0.1% fetal bovine serum) in the absence or presence of PMA or TNF- $\alpha$ . For measurement of macrophage adhesion, an equal number of cells was seeded. After 30 min, plates were washed with PBS and adherent cells fixed with 4% PFA for 15 min. PMNs were stained with DAPI and imaged using an Evos FL Auto 2 life cell microscope (Thermo Fisher Scientific). Adherent cells were counted using ImageJ software. Adherent macrophages were stained with 5 mg/ml crystal violet in 2% ethanol. After washing the plates, remaining dye was solved in 2% SDS and quantified using a plate reader (Tecan, Männedorf, Switzerland).



Macrophage spreading was analyzed on fibronectin (5 µg/ml) or ICAM-1 (4 µg/ml) coated surfaces. Phase contrast images were taken 15, 30, 60 and 120 min after plating the cells using an Evos FL Auto 2 life cell microscope and spreading areas of 20 cells per time point, coating and group were measured using ImageJ software.

Macrophage  $\beta 1$  integrin activation was assessed by 9EG7 staining. Bone marrow derived macrophages were seeded on fibronectin-coated (5 µg/ml) glass coverslips (Thermo Fisher Scientific) in adhesion medium (RPMI 1640 containing 0.1% fetal bovine serum) for 2 h. Cells were washed with PBS, stained with active  $\beta 1$  integrin specific 9EG7 antibody for 30 min and fixed with 4% PFA. Cells were further stained using rabbit anti-integrin  $\beta 1$ , goat anti-rat-Alexa Fluor 546 and goat anti-rabbit-Alexa Fluor 488 and imaged using a Leica TCS SP5 X confocal microscope (Leica Microsystems, Wetzlar, Germany). Staining intensities of 9EG7 and total  $\beta 1$  staining were analyzed in areas of clustered integrins using ImageJ software.

#### **Neutrophil phagocytosis assay**

The neutrophil phagocytosis assay was performed using a pHrodo™ Red *E. coli* BioParticles™ Phagocytosis Kit for Flow Cytometry (Thermo Fisher Scientific) following the manufacturers' instructions. The relative amount of phagocytosed *Escherichia coli* particles was assessed by flow cytometry using an LSRFortessa™ X-20 flow cytometer (BD Biosciences).

#### **Adhesion, spreading and focal adhesion analysis of primary and Talin<sup>1/2dko</sup> fibroblasts**

Primary mouse embryonic fibroblasts derived from WT and *Tln1*<sup>3mut</sup> E14.5 embryos and Talin<sup>1/2dko</sup> fibroblasts were cultured in DMEM GlutaMAX™ supplemented with 10% fetal bovine serum, non-essential amino acids, 100 U/ml penicillin and 100 µg/ml streptomycin (all Thermo Fisher Scientific) under standard conditions.

To compare effects of a double (K15A, R35A; Talin DM) or triple (K15A, R30A, R35A; Talin 3mut) mutation in Talin1-F0, ypet-tagged WT Talin1, Talin1 DM, Talin1 3mut and Talin1  $\Delta$ F0 were expressed in murine Talin<sup>1/2dko</sup> fibroblasts and cell adhesion, spreading and Talin1 recruitment to focal adhesions were analyzed as previously described<sup>1</sup>.

To analyze focal adhesions in mouse embryonic fibroblasts, cells were cultured on fibronectin-coated (5 µg/ml) coverslips for 4 h and fixed with 4% PFA for 10 min. Cells were stained using mouse anti-Talin2, rabbit anti-Paxillin, goat anti-mouse-Cy3 and goat anti-rabbit-Alexa Fluor 488 and imaged using a Leica TCS SP5 X confocal microscope. Focal adhesions were quantified by measuring Paxillin positive areas using ImageJ software.



1. Zhu L, Yang J, Bromberger T, et al. Structure of Rap1b bound to talin reveals a pathway for triggering integrin activation. *Nat Commun*. 2017;8(1):1744.
2. Ussar S, Wang HV, Linder S, Fassler R, Moser M. The Kindlins: subcellular localization and expression during murine development. *Exp Cell Res*. 2006;312(16):3142-3151.
3. Azimifar SB, Bottcher RT, Zanivan S, et al. Induction of membrane circular dorsal ruffles requires co-signalling of integrin-ILK-complex and EGF receptor. *J Cell Sci*. 2012;125(Pt 2):435-448.
4. Klapproth S, Moretti FA, Zeiler M, et al. Minimal amounts of kindlin-3 suffice for basal platelet and leukocyte functions in mice. *Blood*. 2015;126(24):2592-2600.
5. Hofmann S, Braun A, Pozgaj R, Morowski M, Vogtle T, Nieswandt B. Mice lacking the SLAM family member CD84 display unaltered platelet function in hemostasis and thrombosis. *PLoS One*. 2014;9(12):e115306.
6. Petzold T, Ruppert R, Pandey D, et al. beta1 integrin-mediated signals are required for platelet granule secretion and hemostasis in mouse. *Blood*. 2013;122(15):2723-2731.
7. Klapproth S, Sperandio M, Pinheiro EM, et al. Loss of the Rap1 effector RIAM results in leukocyte adhesion deficiency due to impaired beta2 integrin function in mice. *Blood*. 2015;126(25):2704-2712.

**Supplementary Table 1:** Genotypes of offspring from heterozygous Tln1<sup>3mut</sup> intercrosses.

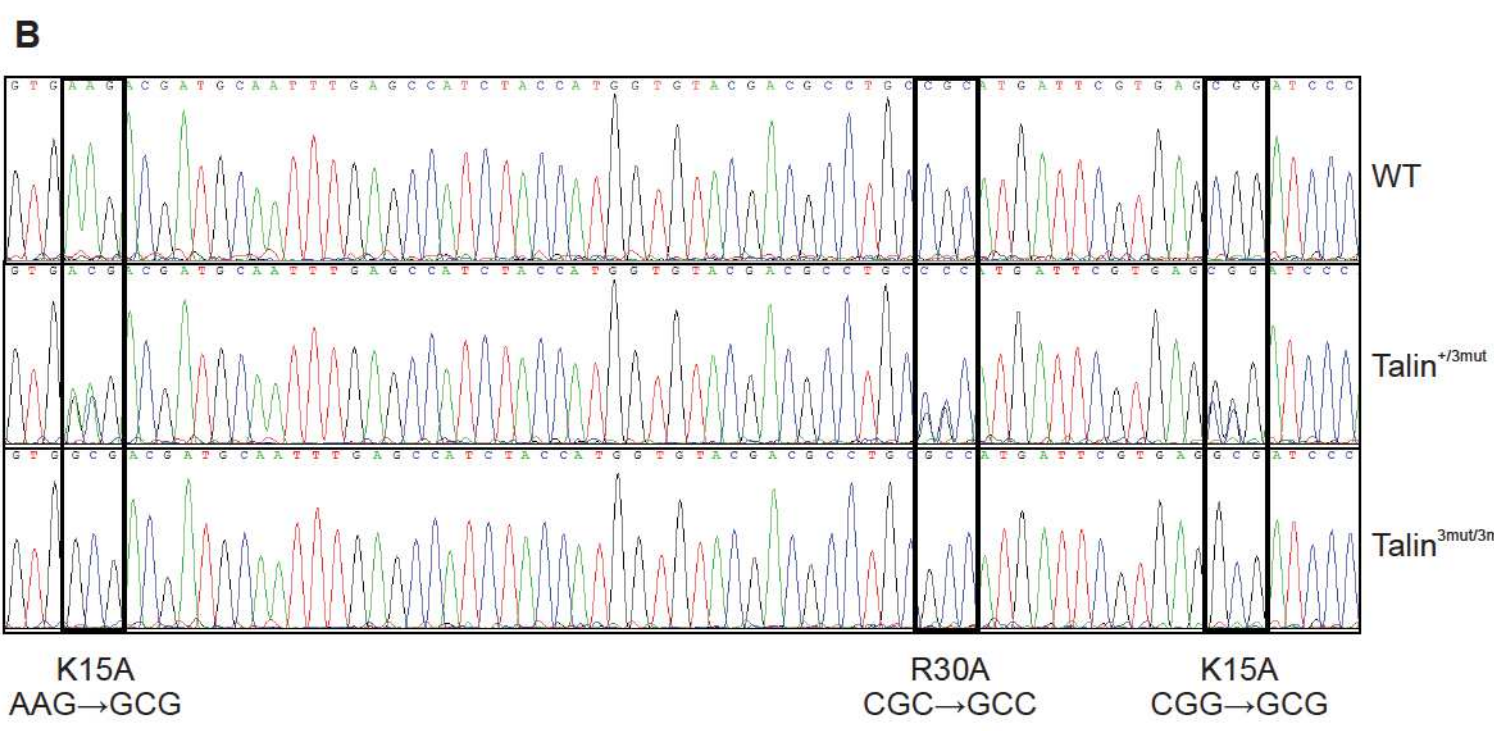
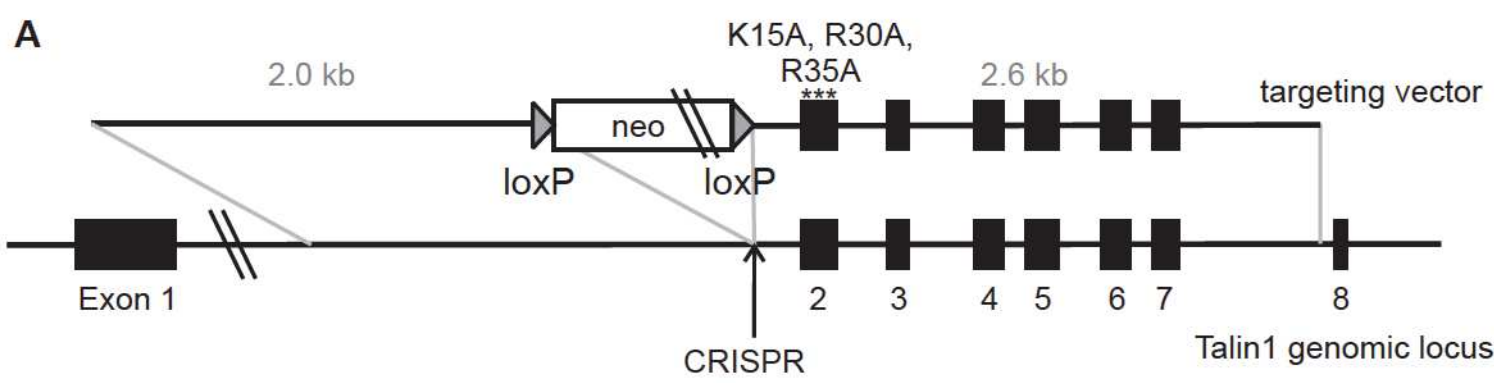
	Animal count	Ratio [%]
Talin <sup>+/+</sup>	62	26.2
Talin <sup>+/3mut</sup>	115	48.5
Talin <sup>3mut/3mut</sup>	60	25.3
Σ	237	100

**Supplementary Table 2:** Peripheral blood cell counts of WT and Tln1<sup>3mut</sup> mice (N=14/15). Values are given as mean ± 95% CI.

	WT (n=14)	Talin <sup>3mut</sup> (n=15)
Platelets [K/μL]	626 ± 58	577 ± 57
Mean platelet volume [fL]	5.77 ± 0.14	5.70 ± 0.25
White blood cells [K/μL]	8.46 ± 1.33	9.37 ± 1.73
Neutrophils [K/μL]	1.04 ± 0.26	1.20 ± 0.34
Lymphocytes [K/μL]	7.17 ± 1.19	7.90 ± 1.44
Monocytes [K/μL]	0.12 ± 0.05	0.13 ± 0.05
Eosinophils [K/μL]	0.12 ± 0.04	0.13 ± 0.07
Basophils [K/μL]	0.01 ± 0.01	0.01 ± 0.00
Red blood cells [M/μL]	10.02 ± 0.24	10.04 ± 0.26
Hemoglobin, [g/dL]	15.26 ± 0.24	15.29 ± 0.36
Hematocrit [%]	49.16 ± 0.99	49.05 ± 1.27

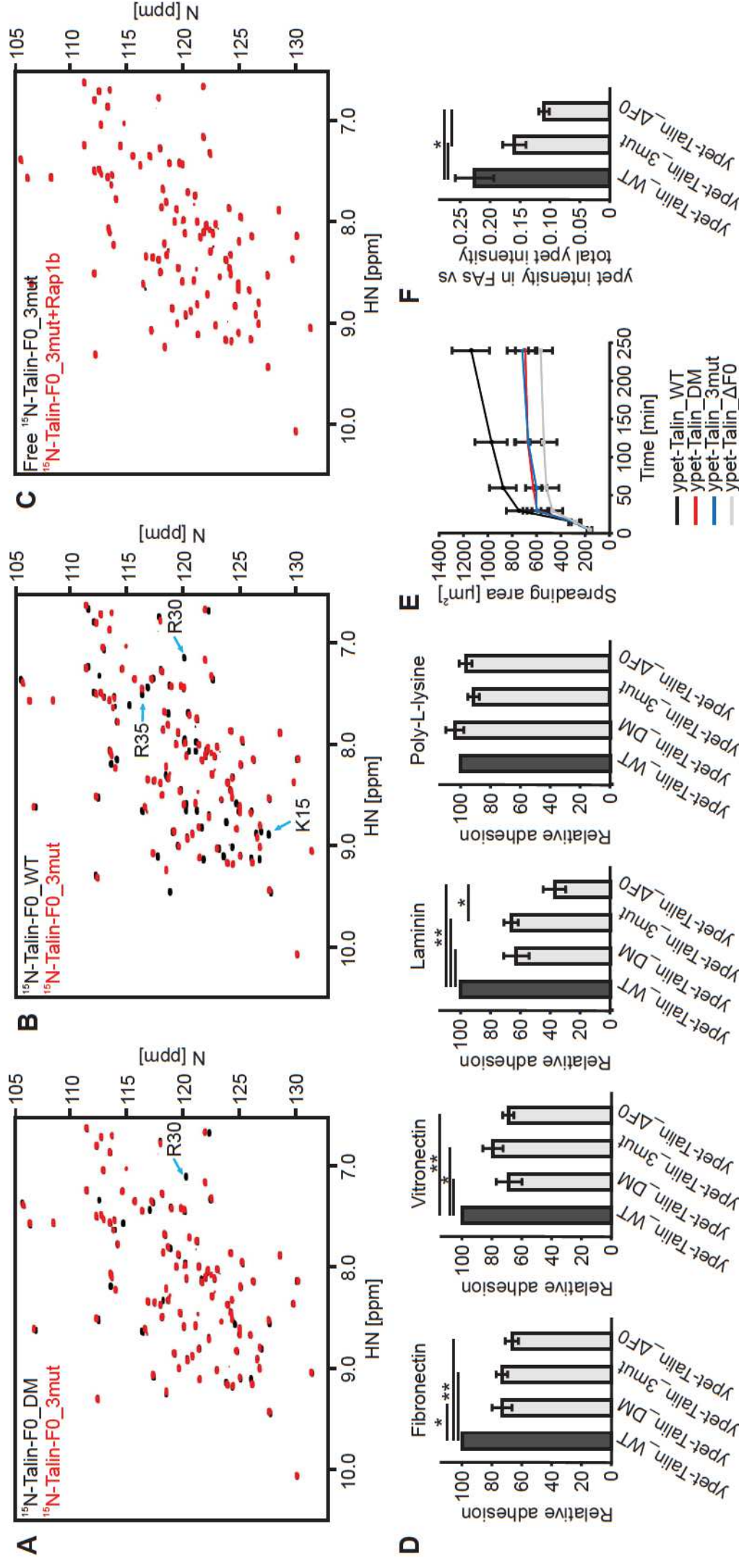


# Supplementary Figure 1



**Supplementary Figure 1: Generation of *Tln1*<sup>3mut</sup> mice.** (A) Targeting strategy of the Talin1 gene locus. Partial map of the Talin1 gene and the targeting vector, which carries mutations in exon 2 leading to the indicated amino acid substitutions. The targeting vector contains a neomycin-resistance cassette, which was later removed by breeding mice with a deleter-Cre strain. (B) Exon 2 from control, heterozygous and homozygous *Tln1*<sup>3mut</sup> mice was amplified by genomic PCR and sequenced. The three mutations are marked in the sequencing histograms.

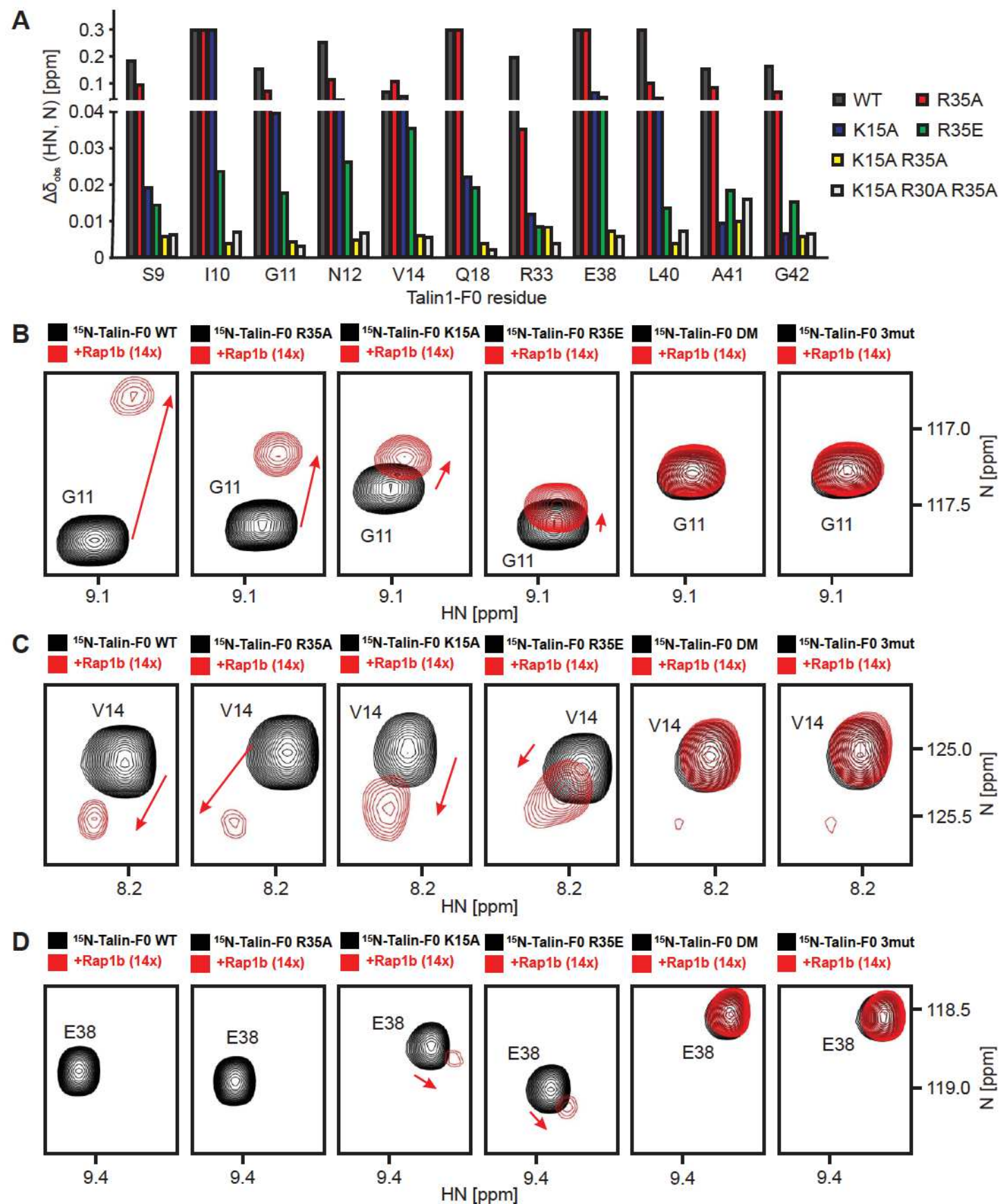
# Supplementary Figure 2



**Supplementary Figure 2: Triple mutation (3mut; K15A, R30A, R35A) in Talin1-F0/Rap1 interaction and generates equal effects as a double mutation (DM; K15A, R35A).** (A) HSQC spectral overlay of 50 μM <sup>15</sup>N-labeled Talin1-F0\_DM (black) and Talin1-F0\_3mut (red). (B) HSQC spectral overlay of 50 μM <sup>15</sup>N-labeled Talin1-F0\_WT (black) and Talin1-F0\_3mut (red). (C) The HSQC spectra of 50 μM <sup>15</sup>N-labeled Talin1-F0\_3mut in the absence (black) and presence of 125 μM GMP-PNP loaded Rap1b (red). (D) Static adhesion of Talin<sup>1/2dko</sup> fibroblasts expressing ypet-tagged Talin1\_DM, Talin1\_3mut or Talin1\_ΔF0 relative to cells expressing ypet-tagged WT Talin1 on fibronectin, vitronectin, laminin and poly-L-lysine coated surfaces (N=5 experiments). (E) Spreading of Talin<sup>1/2dko</sup> fibroblasts expressing ypet-tagged WT Talin1, Talin1\_DM, Talin1\_3mut or Talin1\_ΔF0 assessed 5, 15, 30, 60, 120 and 240 min after seeding the cells on a fibronectin coated surface (N=4 experiments). (F) Talin1 recruitment in Talin1\_WT, Talin1\_3mut and Talin1\_ΔF0 rescued Talin<sup>1/2dko</sup> fibroblasts assessed by measuring ypet intensity in focal adhesions normalized against ypet intensity of whole cells (N=3 experiments). All values are given as mean ± SEM, \* p<0.05, \*\* p<0.01.

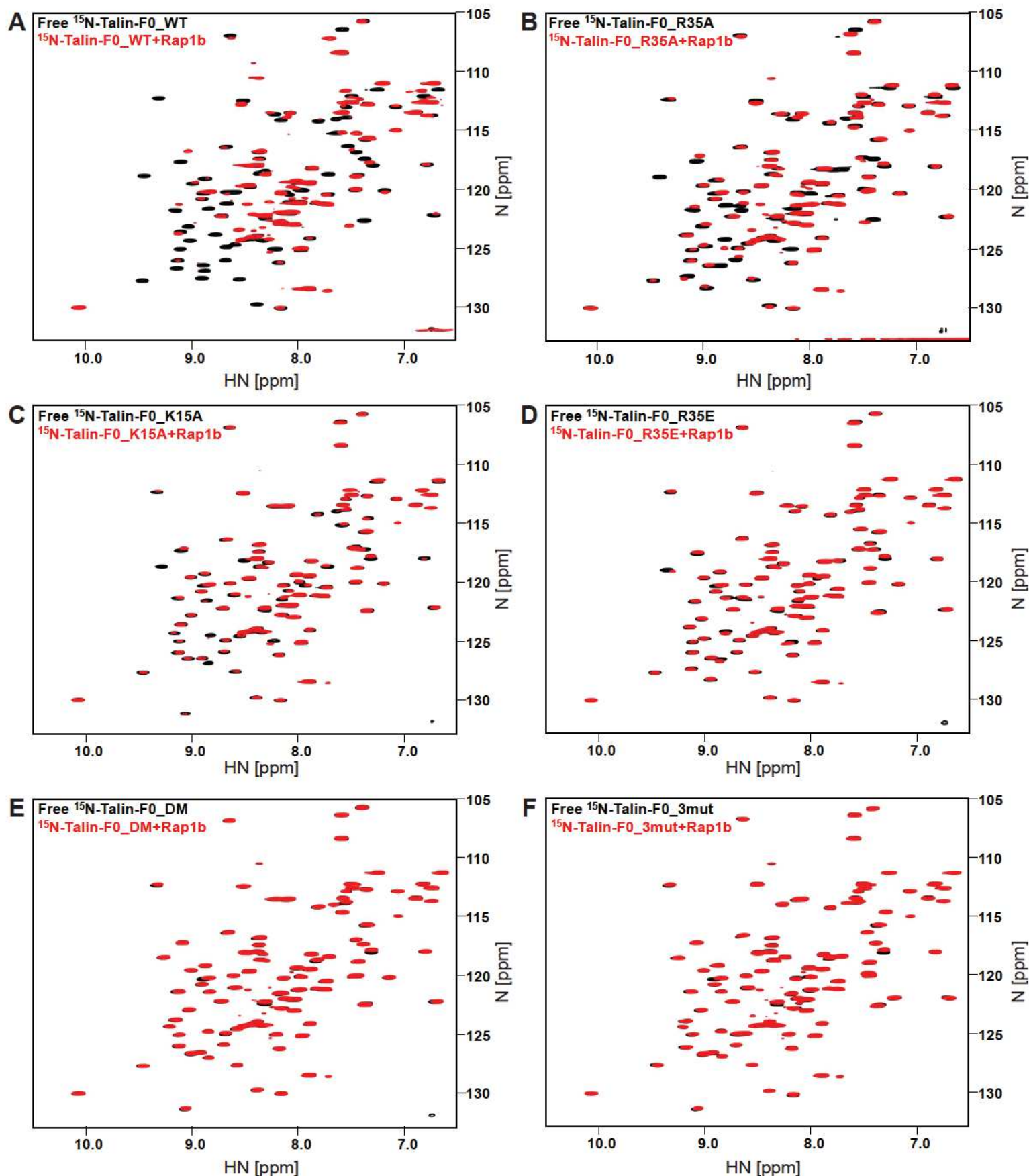


# Supplementary Figure 3



**Supplementary Figure 3: Talin1-F0 double (DM; K15A, R35A) or triple mutant (3mut; K15A, R30A, R35A) showed further reduced binding to Rap1b compared to single mutants.** (A) Chemical shift changes of 70  $\mu M$   $^{15}N$ -labeled Talin1-F0 WT and mutants including R35A, K15A, R35E, K15A/R35A (DM) and K15A/R30A/R35A (3mut) induced by the presence of 1 mM GMP-PNP loaded Rap1b (G12V). Interface residues indicated in the figure were analyzed. Chemical shift changes of broaden residues were set to 0.3. The data suggest that compared to Talin1-F0 single mutants, DM or 3mut are more potent in disrupting Talin1-F0/Rap1 interaction. (B-D) Spectra of representative residues, Glycine 11 (B), Valine 14 (C) and Glutamate 38 (D) of indicated Talin1-F0 variants in the absence (black) and presence (red) of GMP-PNP loaded Rap1b (G12V).

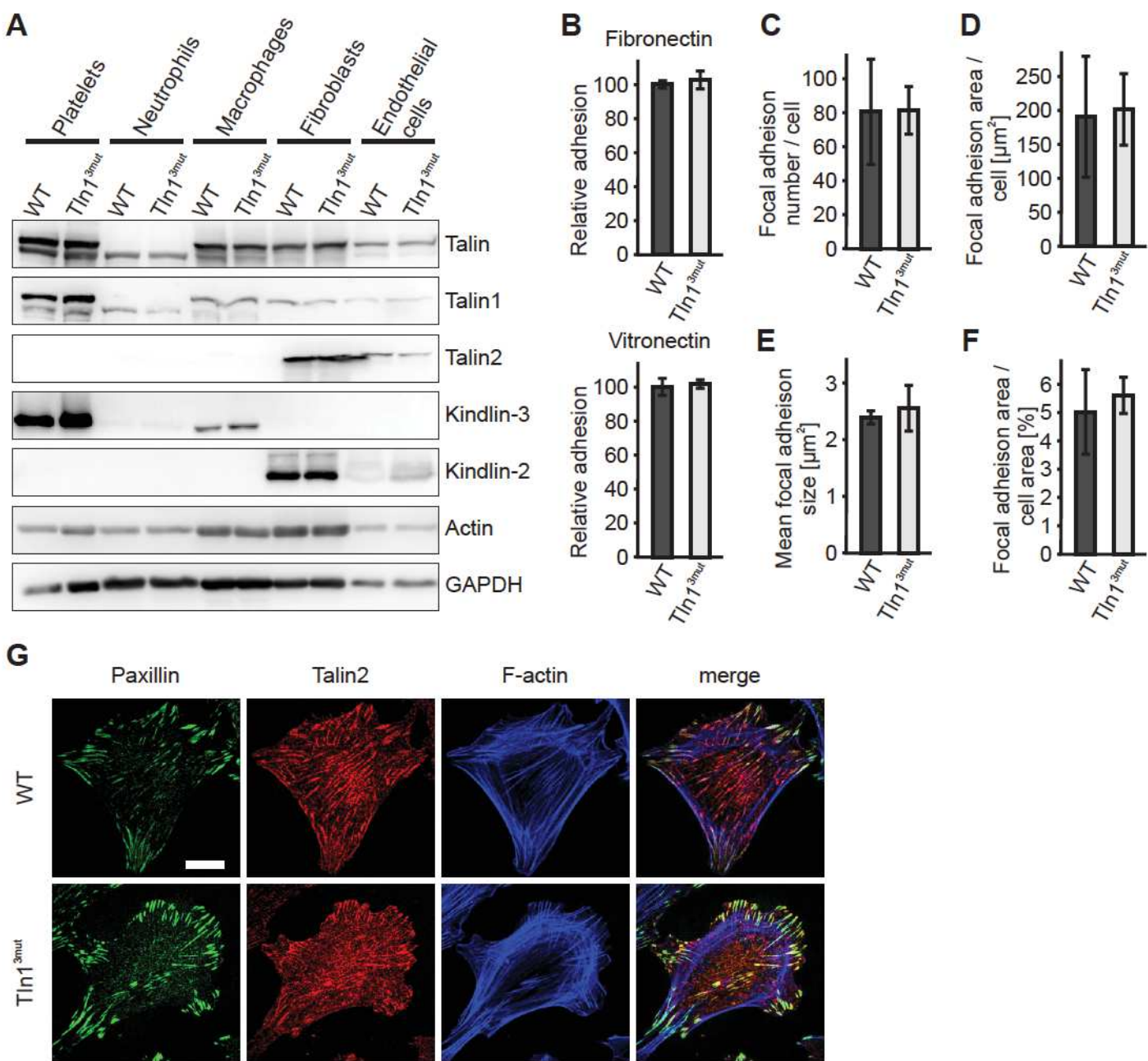
# Supplementary Figure 4



**Supplementary Figure 4: Comparison of Rap1b binding to different Talin1-F0 variants by NMR HSQC.** (A-F) Full HSQC spectra of 70  $\mu\text{M}$   $^{15}\text{N}$ -labeled Talin1-F0 WT (A), R35A (B), K15A (C), R35E (D), K15A/R35A (DM) (E) and K15A/R30A/R35A (3mut) (F) in the absence (black) and presence (red) of 1 mM GMP-PNP loaded Rap1b.

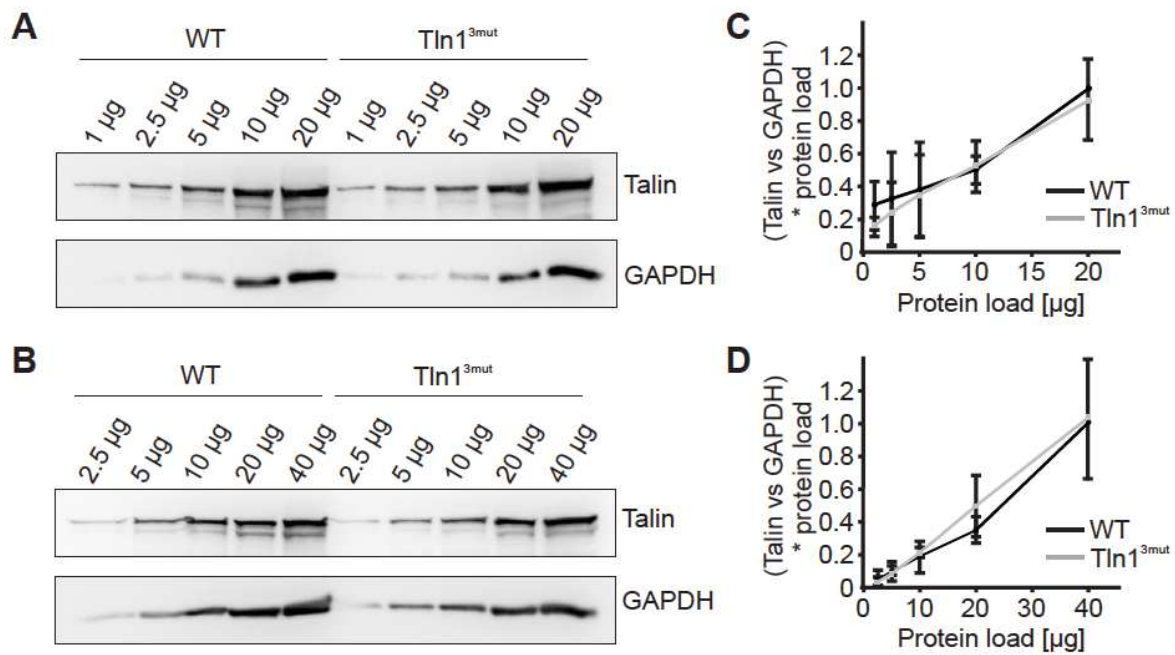


# Supplementary Figure 5



**Supplementary Figure 5: Adhesion and focal adhesion formation is not altered in Tln1<sup>3mut</sup> fibroblasts.** (A) Total Talin, Talin1, Talin2, Kindlin-2 and Kindlin-3 expression in platelets, neutrophils, macrophages, fibroblasts and endothelial cells analyzed by Western blotting. Actin and GAPDH served as loading controls. (B) Static adhesion of WT and Tln1<sup>3mut</sup> embryonic fibroblasts on fibronectin and vitronectin (N=6; cells isolated from 3 embryos per genotype). (C-F) Paxillin was immunofluorescently labeled in WT and Tln1<sup>3mut</sup> mouse embryonic fibroblasts plated on fibronectin-coated surfaces. Focal adhesion number (C), focal adhesion area per cell (D), mean focal adhesion size (E) and focal adhesion area relative to cell area (F) were quantified by counting and measuring Paxillin positive areas (N=5 experiments). (G) Immunofluorescence images of WT and Tln1<sup>3mut</sup> embryonic fibroblasts showing Paxillin (green) as a focal adhesion marker, Talin2 (red) and F-actin (blue). Scale bar: 20  $\mu\text{m}$ . All values are given as mean  $\pm$  95% CI.

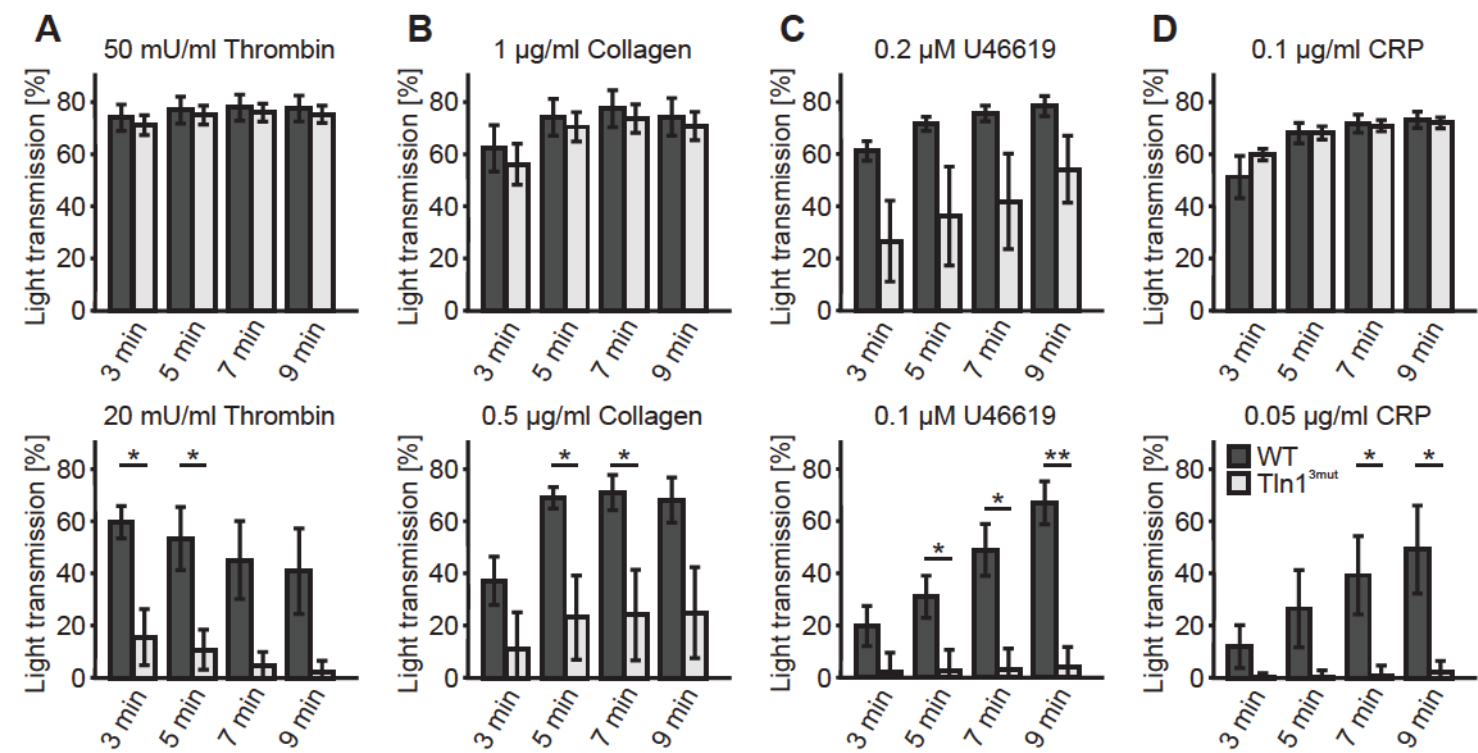
## Supplementary Figure 6



**Supplementary Figure 6: Comparable Talin1 expression in WT and Tln1<sup>3mut</sup> mice.** (A, B) Talin expression in WT and Tln1<sup>3mut</sup> platelets (A) and macrophages (B) analyzed by Western blotting. Increasing amounts of protein lysates were analyzed. GAPDH served as loading control. (C, D) Quantitative analysis of Western blots shown in (A) and (B) (value for highest amount of WT lysate set to 1). Values are given as mean  $\pm$  95% CI (N=3).




# Supplementary Figure 7



**Supplementary Figure 7: Aggregation of Tln1<sup>3mut</sup> platelets is affected at low agonist concentrations.** (A-D) Quantification of platelet aggregation by measuring light transmission 3, 5, 7 and 9 min after activation with 50 or 20 mU/ml thrombin (A), 1 or 0.5 µg/ml collagen (B), 0.2 or 0.1 µM U46619 (C) and 0.1 or 0.05 µg/ml CRP (D) (N=4-5 mice). All values are given as mean ± SEM, \* p<0.05, \*\* p<0.01.

ARTICLE

# A kindlin-3–leupaxin–paxillin signaling pathway regulates podosome stability

Sarah Klapproth<sup>1</sup> , Thomas Bromberger<sup>1</sup>, Clara Türk<sup>2</sup>, Marcus Krüger<sup>2</sup>, and Markus Moser<sup>1,3</sup> 

Binding of kindlins to integrins is required for integrin activation, stable ligand binding, and subsequent intracellular signaling. How hematopoietic kindlin-3 contributes to the assembly and stability of the adhesion complex is not known. Here we report that kindlin-3 recruits leupaxin into podosomes and thereby regulates paxillin phosphorylation and podosome turnover. We demonstrate that the activity of the protein tyrosine phosphatase PTP-PEST, which controls paxillin phosphorylation, requires leupaxin. In contrast, despite sharing the same binding mode with leupaxin, paxillin recruitment into podosomes is kindlin-3 independent. Instead, we found paxillin together with talin and vinculin in initial adhesion patches of kindlin-3–null cells. Surprisingly, despite its presence in these early adhesion patches, podosomes can form in the absence of paxillin or any paxillin member. In conclusion, our findings show that kindlin-3 not only activates and clusters integrins into podosomes but also regulates their lifetime by recruiting leupaxin, which controls PTP-PEST activity and thereby paxillin phosphorylation and downstream signaling.

## Introduction

Integrin-mediated cell-matrix adhesions anchor cells on or within extracellular matrices, sense the physical properties of the environment, and translate them into biochemical signals (Hynes, 2002). These signals are combined with those from other signaling pathways to regulate a variety of cellular functions such as cell proliferation, differentiation, and survival (Legate et al., 2009; Humphries et al., 2019). The ability of integrins to efficiently and stably bind to their extracellular ligands is regulated by changes in their affinity to ligands and the concentration of activated integrins into clusters (Iwamoto and Calderwood, 2015). Both aspects of integrin regulation require the binding of two intracellular adapter proteins, talin and kindlin, to the integrin  $\beta$  subunit cytoplasmic domain (Moser et al., 2009; Sun et al., 2019). These initial events are followed by a complex assembly of a multitude of adapter and signaling molecules, which define the biochemical and physical properties of the adhesion complex (Harburger and Calderwood, 2009).

Different integrin-mediated cell adhesion complexes exist depending on the cell type, integrin expression, or matrix composition (Block et al., 2008). Here we focus on podosomes, which are adhesion structures that show distinct morphological characteristics compared with focal adhesions, although they are composed of almost the same components (Marchisio et al.,

1988; Destaing et al., 2003; Calle et al., 2006). Podosomes have been observed in myeloid, endothelial, and some c-Src-transformed tumor cells. Each podosome is organized into two domains: a dense actin core, which contains actin-regulatory proteins, and a ring of signaling and adaptor proteins embedded in an actin cloud, which surrounds the actin core and is connected to the extracellular matrix via integrins (Linder and Kopp, 2005; Murphy and Courtneidge, 2011). Podosomes are more dynamic than focal adhesions with lifetimes within the minute scale and are involved in matrix degradation and cell invasion (Block et al., 2008). Talin-1 and kindlin-3 are both required for proper podosome assembly (Schmidt et al., 2011; Zou et al., 2013), most likely due to their essential role in integrin activation, clustering, and linkage to the actin cytoskeleton. But how these two proteins orchestrate the complex assembly of podosomes and regulate their stability and turnover, which are important for processes such as cell adhesion, migration, matrix degradation, transmigration, and tumor invasion, has not been investigated at the molecular level.

The adapter protein paxillin is one of the earliest proteins to be detected in nascent adhesions at the leading edge of the cell (Digman et al., 2008), and accumulation of paxillin is the first visible step in podosome assembly (Luxenburg et al., 2012). In

<sup>1</sup>Department of Molecular Medicine, Max Planck Institute of Biochemistry, Martinsried, Germany; <sup>2</sup>Institute for Genetics, Cologne Excellence Cluster on Cellular Stress Responses in Aging-Associated Diseases, Cologne, Germany; <sup>3</sup>Institute of Experimental Hematology, Center for Translational Cancer Research (TranslaTUM), Klinikum rechts der Isar der Technischen Universität München, Munich, Germany.

Correspondence to Markus Moser: [m.moser@tum.de](mailto:m.moser@tum.de).

© 2019 Klapproth et al. This article is distributed under the terms of an Attribution–Noncommercial–Share Alike–No Mirror Sites license for the first six months after the publication date (see <http://www.rupress.org/terms/>). After six months it is available under a Creative Commons License (Attribution–Noncommercial–Share Alike 4.0 International license, as described at <https://creativecommons.org/licenses/by-nc-sa/4.0/>).



addition to its role in the assembly of adhesion structures, paxillin regulates focal adhesion and podosome disassembly. Phosphorylation of paxillin at Y31 and Y118 is involved in focal adhesion turnover and dissolving podosomal belts (Laukaitis et al., 2001; Ballestrem et al., 2006; Badowski et al., 2008). Mutation of both tyrosines into non-phosphorylated amino acids impairs the disassembly of adhesion structures (Webb et al., 2004). Recently, a direct interaction between kindlin-2 and paxillin has been reported, which is crucial for paxillin recruitment to newly formed adhesion sites and induction of cell spreading in fibroblasts (Theodosiou et al., 2016; Böttcher et al., 2017). Moreover, interaction of paxillin with kindlin-3, the hematopoietic member of the kindlin family, was shown to promote platelet integrin activation (Gao et al., 2017).

In the present study, we aimed to elucidate a signaling pathway downstream of kindlin-3, which is involved in podosome assembly and stability regulation and identified leupaxin, a member of the paxillin gene family, as a new kindlin-3 interactor. Overall our study shows that kindlin-3 has a dual function in podosome regulation: besides its essential role in integrin regulation and proper podosome assembly, it also regulates podosome turnover by recruiting leupaxin into podosomes to control phospho-paxillin levels and thereby increasing the podosome lifetime.

## Results

### Low kindlin-3 expression results in reduced podosome lifetime

We have previously shown that kindlin-3-deficient cells fail to assemble definitive podosomes because of their inability to activate, cluster, and recruit integrins (Schmidt et al., 2011). Since the adhesion structures are not properly formed in the absence of kindlin-3, the role of kindlin-3 in integrin-mediated outside-in signaling could not be studied yet. We overcame this problem by strongly reducing kindlin-3 levels rather than eliminating it. We achieved this by generating preosteoclasts from kindlin-3 hypomorphic mice ( $K3^{n/n}$ ), which express only 5% of normal kindlin-3 levels due to the presence of a neomycin resistance cassette within the kindlin-3 gene locus (Klapproth et al., 2015). Despite the very low kindlin-3 expression,  $K3^{n/n}$  cells formed podosomal clusters, in which plaque proteins such as vinculin and paxillin, as well as  $\alpha V$  integrins, are correctly targeted to the podosomal ring (Fig. 1, A and B). Their actin core diameter, however, was reduced (Fig. 1 C). Although fewer  $K3^{n/n}$  cells formed podosomal clusters (Fig. 1 D), their cluster size was similar to that of control preosteoclasts (Fig. 1 E). Importantly and consistent with its strongly reduced expression, kindlin-3 is hardly detectable by immunofluorescence (IF) in podosomal clusters of  $K3^{n/n}$  (10% kindlin-3) and below detection level in  $K3^{n/n}$  preosteoclasts (Fig. 1 F). To further characterize the podosomes of  $K3^{n/n}$  cells, we determined their turnover by tracking individual podosomes of control and  $K3^{n/n}$  cells by life cell imaging. We transfected the cells with LifeAct-GFP, which binds to F-actin and labels the central podosomal actin core (Riedl et al., 2008). Whereas 50% of WT podosomes could be imaged for 260 s or longer, half of the podosomes in  $K3^{n/n}$  cells were already disassembled after 200 s (Fig. 1 G and Videos 1 and 2).

These data suggest two distinct functions of kindlin-3: (1) the assembly of podosomes, which requires just a small amount of kindlin-3 and is presumably due to kindlin-3-mediated integrin activation (inside-out signaling), and (2) stabilizing podosomes, which requires high kindlin-3 levels and is probably controlled by kindlin-3-mediated integrin outside-in signaling. The second mechanism is unexplored and was the focus of the following studies.

### Identification of leupaxin as a new kindlin-3 interactor

To elucidate the molecular mechanism of kindlin-3-mediated integrin outside-in signaling, we performed yeast-two-hybrid assays with kindlin-3 as bait using a mouse spleen cDNA library. In two screens, five cDNAs were isolated. One encoded the C terminus (CT) of leupaxin, a cytoskeleton adapter protein belonging to the paxillin protein family (Brown and Turner, 2004). Leupaxin is preferentially expressed in hematopoietic cells and consists of four leucine-aspartic acid (LD)-rich motifs in the N terminus (NT) and four Lin11, Isl-1, and Mec-3 (LIM) domains in the CT (Fig. 2 A).

To verify the interaction between kindlin-3 and leupaxin in hematopoietic cells, we used Flag-kindlin-3 knockin mice, in which a triple Flag sequence was inserted after the start codon of the kindlin-3 gene (Fig. S1, A and B). Flag-tagged kindlin-3 was expressed at normal levels (Fig. S1 C) and localized indistinguishably from kindlin-3 in the podosomal ring structure of macrophages (Fig. S1 D; Ussar et al., 2006). We differentiated macrophages from bone marrow of WT and Flag-kindlin-3 knockin mice and immunoprecipitated Flag-tagged kindlin-3 (Fig. 2 B). These immunoprecipitates contained leupaxin, supporting the direct binding between the two proteins suggested by the yeast-two-hybrid interaction.

To further map the leupaxin binding site within kindlin-3 we used RAW 246.7 (RAW) cells, a murine macrophage/monocyte-like cell line, in which we deleted the kindlin-3 gene by CRISPR/Cas9 technology. Kindlin-3-deficient RAW cells expressed normal levels of leupaxin, talin, and paxillin in all analyzed clones (Fig. 2 C) and were used for reexpression of various kindlin-3 mutants and domains (Fig. 2 D). We then transfected EGFP-tagged WT kindlin-3 and an integrin-binding mutant kindlin-3 (K3 QA; Moser et al., 2008) into these cells, performed a GFP immunoprecipitation, and again confirmed the interaction between WT kindlin-3 and leupaxin. Since the kindlin-3 integrin-binding mutant precipitated similar amounts of leupaxin as the WT kindlin-3 (Fig. 2 E), this indicates that association of kindlin-3 with leupaxin does not require kindlin-3 to be bound to the integrin tail. Furthermore, the interaction between kindlin-3 and integrin-linked kinase (ILK), which is mediated via the F2 domain (Fukuda et al., 2014; Huet-Calderwood et al., 2014), had no impact on kindlin-3/leupaxin interaction, as ILK-binding mutant kindlin-3 (K3 LA) showed normal leupaxin binding (Fig. 2 F). Additionally, we conducted immunoprecipitation experiments with truncated kindlin-3 constructs, which mapped the leupaxin binding site to the F0 domain. Binding of the F0 domain to leupaxin was rather weak but was enhanced in the presence of the F1 and F2 domains, indicating that these domains stabilize either the F0 domain or its interaction with leupaxin. On the contrary, all kindlin-3



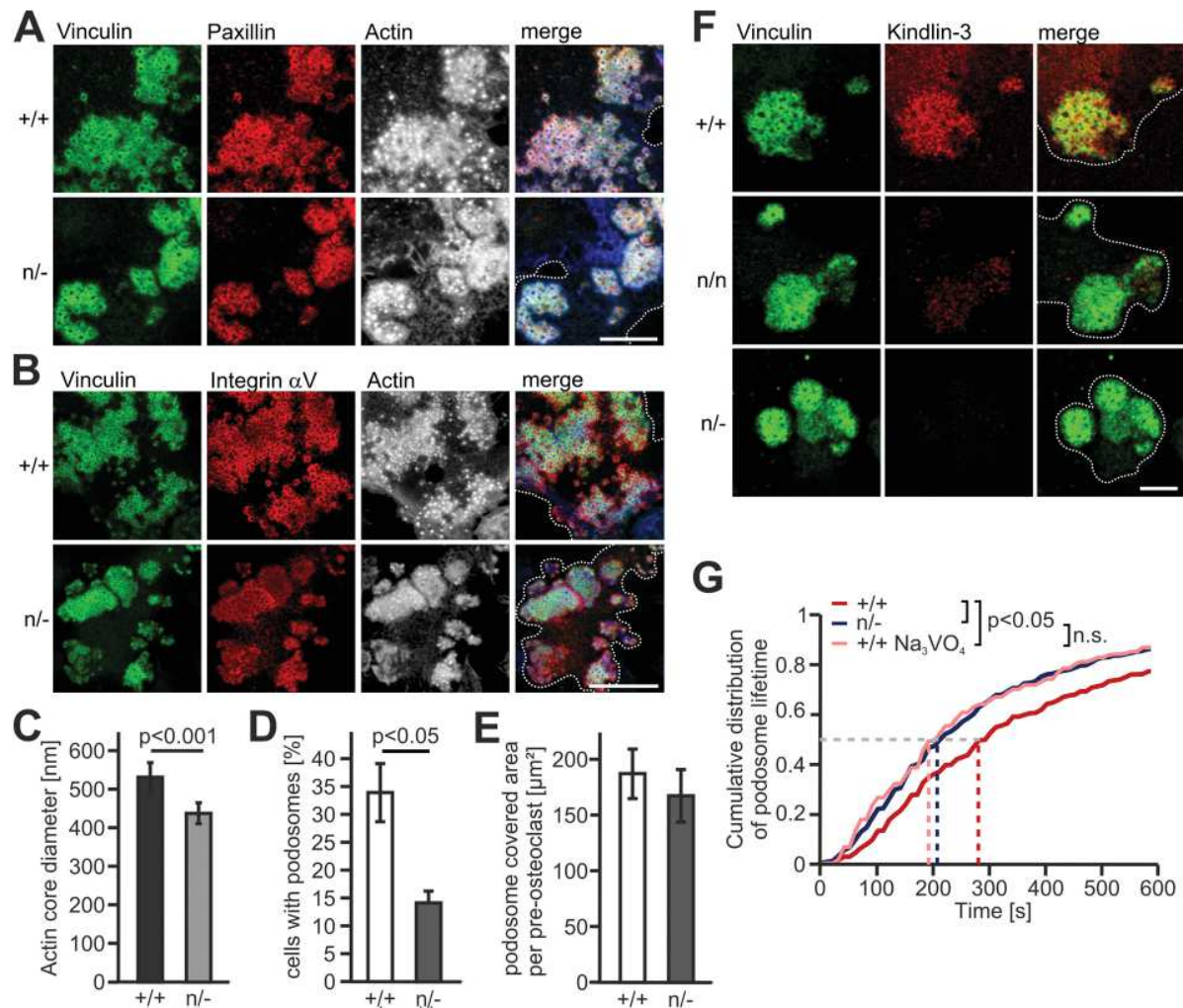


**Figure 1. Low kindlin-3 expression results in reduced podosome lifetime.** (A) IF stainings of WT (+/+) and K3<sup>-/-</sup> (n/-) preosteoclasts for vinculin (green), paxillin (red) and actin (white/blue in merge). Scale bar, 10  $\mu m$ . (B) IF stainings for vinculin (green), integrin  $\alpha V$  (red), and actin (white/blue in merge) in podosomes of +/+ and n/- preosteoclasts. Scale bar, 20  $\mu m$ . (C) Diameter of the podosomal actin cores in +/+ and n/- cells. 10 actin cores in two regions of three cells were measured per experiment.  $n = 5$ . (D) Percentage of podosome forming +/+ and n/- preosteoclasts.  $n = 4$ . (E) Quantification of the basal cell surface area that podosomal clusters cover in +/+ and n/- preosteoclasts.  $n = 48/50$  from five different preparations. (F) Vinculin (green) and kindlin-3 (red) IF stainings of +/+ and n/- preosteoclasts. Scale bar, 5  $\mu m$ . (G) Cumulative distribution of podosome lifetimes in +/+ untreated or treated with orthovanadate and n/- preosteoclasts. 15–20 podosomes were measured per cell. Two to five cells were analyzed in each of six different dishes per genotype. See also Videos 1 and 2. Dotted white lines mark cell borders.

constructs that lacked the F0 domain did not bind (Fig. 2 F). The strong binding of a kindlin-3 construct lacking the integrin-binding F3 domain confirmed that association of kindlin-3 with integrins was not required for leupaxin binding.

It has been shown recently that an exposed loop within the N-terminal F0 domain of kindlins mediates direct interaction with paxillin (Gao et al., 2017). To investigate whether the same motif (called the M3 cluster) conveys leupaxin binding, we substituted the M3 residues of kindlin-3 for alanines (K3 M3) and compared leupaxin and paxillin binding to WT kindlin-3, the kindlin-3 M3 mutant, and kindlin-3 lacking the F0 domain (K3 F1-3). After retroviral transduction into kindlin-3-deficient RAW cells, immunoprecipitation experiments revealed that when the F0 domain of kindlin-3 is mutated or absent, binding of both leupaxin and paxillin is strongly diminished (Fig. 2 G).

To map the kindlin-3 binding site within leupaxin, we generated leupaxin-deficient RAW cells using the CRISPR/Cas9 system. Loss of leupaxin had no effect on kindlin-3, paxillin, Hic-5, protein tyrosine phosphatase PEST (PTP-PEST), and talin expression (Fig. 2 H). Reconstitution of these cells with EGFP-tagged full-length (FL) leupaxin, its NT or CT, followed by GFP-immunoprecipitations revealed that endogenous kindlin-3 was precipitated with the FL and the C-terminal LIM domain-containing region of leupaxin, confirming the result of the yeast-two-hybrid assay (Fig. 2 I). Moreover, a specific mutation within the LIM3 domain of leupaxin (C293R), which disrupts the Zn finger motif and thereby the structural folding of this domain (Chen and Kroog, 2010; Robertson and Ostergaard, 2011), abolished kindlin-3/leupaxin interaction (Fig. 2 J). Finally, we proved direct kindlin-3/leupaxin interaction by GST-pulldown



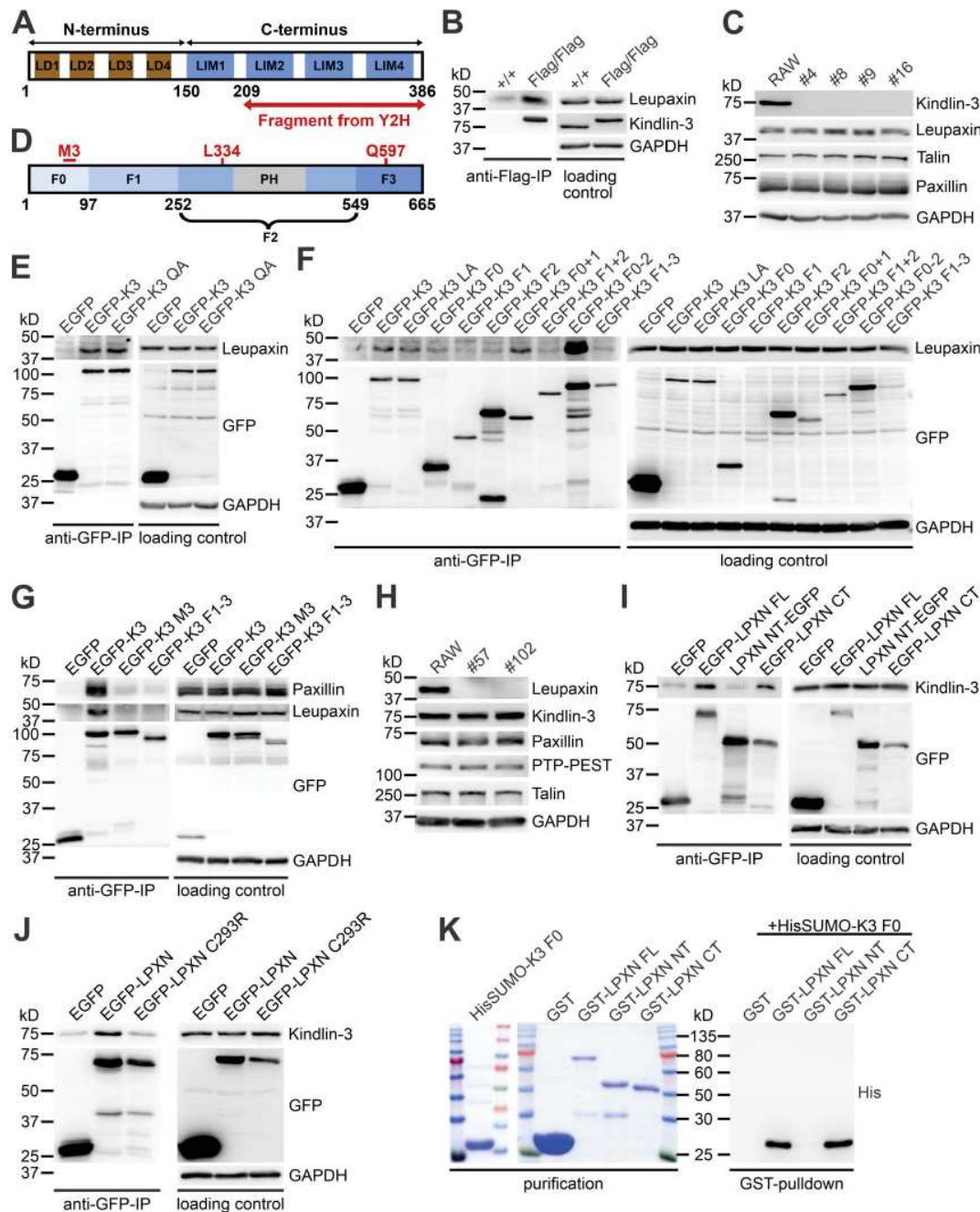


**Figure 2. Identification and characterization of leupaxin as new kindlin-3 interactor.** (A) Domain structure of leupaxin. A C-terminal leupaxin fragment bound to kindlin-3 in a yeast-two-hybrid screen. (B) Flag-immunoprecipitation (IP) from lysates of +/+ and Flag-tagged kindlin-3 expressing (Flag/Flag) bone marrow-derived macrophages to verify interaction with endogenous leupaxin. (C) Western blot analyses of leupaxin, talin, and paxillin expression in +/+ RAW cells and four different K3<sup>-/-</sup> RAW cell clones. (D) Domain structure of kindlin-3. (E) GFP-IP from lysates of K3<sup>-/-</sup> RAW cells expressing EGFP, EGFP-K3, or the EGFP-tagged K3 QA mutant analyzed for leupaxin. (F) GFP-IP from lysates of K3<sup>-/-</sup> RAW cells expressing different EGFP-K3 fragments to identify the leupaxin-interacting domain. (G) GFP-IP from lysates of K3<sup>-/-</sup> RAW cells expressing EGFP, EGFP-K3, EGFP-K3 M3 mutant, or EGFP-K3 F1-3 to investigate the interaction with leupaxin and paxillin. (H) Western blot analyses of +/+ RAW cells and two leupaxin<sup>-/-</sup> RAW cell clones for their expression of kindlin-3, paxillin, PTP-PEST, and talin. (I) GFP-IP from lysates of leupaxin<sup>-/-</sup> RAW cells reconstituted with EGFP-tagged FL leupaxin (LPXN), a N-terminal fragment (NT), or its CT to determine interaction with kindlin-3. (J) GFP-IP from lysates of leupaxin<sup>-/-</sup> RAW cells reconstituted either with EGFP-tagged WT leupaxin or a leupaxin mutant (C293R) analyzed for kindlin-3 binding. (K) GST-pulldown with GST, GST-leupaxin FL, GST-leupaxin NT, and GST-leupaxin CT incubated with His-SUMO-tagged K3 F0.



experiments with bacterially expressed HisSumo-tagged kindlin-3 F0 domain incubated with GST-FL leupaxin or the N- and C-terminal leupaxin LD and LIM domains, respectively (Fig. 2 K). Altogether, these results indicate that the M3 loop in the F0 domain of kindlin-3 interacts with the LIM domains of leupaxin, and this interaction is impaired by disrupting LIM3.

#### Kindlin-3-mediated leupaxin recruitment into podosomes reduces paxillin phosphorylation and increases podosome stability

Leupaxin is a cytoskeleton adapter protein, which localizes in focal adhesions of cancer cells, podosomes of macrophages, and sealing zones of osteoclasts (Gupta et al., 2003; Chen and Kroog, 2010; Tanaka et al., 2010). IF staining of preosteoclasts, differentiated from bone marrow cells and retrovirally transduced with EGFP-K3, revealed colocalization of leupaxin and kindlin-3 in the podosomal ring (Fig. 3 A). We then analyzed whether low kindlin-3 expression impacts on leupaxin localization and found strongly reduced leupaxin levels in podosomes of  $K3^{n/-}$  cells. In contrast, paxillin was found at comparable levels, indicating that leupaxin but not its paralog paxillin requires kindlin-3 for podosomal targeting (Fig. 3 B). In support of this observation, we detected a slight reduction in total cellular leupaxin levels to ~70% in  $K3^{n/-}$  cells, suggesting that the interaction with kindlin-3 stabilizes cellular leupaxin, whereas paxillin levels remained unchanged (Fig. 3, C and D).

Next, we investigated whether the interaction between kindlin-3 and leupaxin is involved in podosome lifetime regulation. Previous studies suggested that leupaxin is a central component of the osteoclast podosomal signaling complex and functions as a paxillin counterpart by suppressing the tyrosine phosphorylation of paxillin in focal adhesions (Lipsky et al., 1998; Gupta et al., 2003; Sahu et al., 2007a; Tanaka et al., 2010). Nevertheless, leupaxin-null RAW cells formed podosome clusters, which were comparable to control cells (Fig. 4 A). We quantified the fluorescence intensity of vinculin, paxillin, and phospho-paxillin Y31 and Y118 within podosomal units of control and leupaxin-null RAW cells by confocal microscopy and analyzed paxillin phosphorylation upon adhesion by Western blotting. Whereas vinculin and paxillin showed normal expression in podosomes, we measured an increase in phospho-paxillin Y31 and Y118 signal in leupaxin-null cells (Fig. 4, B and C; and Fig. S2, A and B). As paxillin phosphorylation at Y31 and Y118 is known to promote adhesion turnover, podosome disassembly, and reorganization (Badowski et al., 2008), we also determined the podosome lifetime in leupaxin-null and control cells like we did for  $K3^{n/-}$  cells. Whereas 50% of the podosomes in WT RAW cells can be imaged for ~250 s or longer, the mean lifetime of podosomes in leupaxin-null RAW cells was reduced to ~180 s (Fig. 4 D). To confirm that this reduction is due to elevated paxillin phosphorylation on tyrosines Y31 and Y118, we transfected the cells with mCherry-tagged WT or non-phosphorylatable paxillin (paxillin-2YF) and indeed measured an extension of the podosomal lifetime of paxillin-2YF expressing WT and leupaxin-null RAW cells compared with cells transfected with WT paxillin (Fig. 4 E).

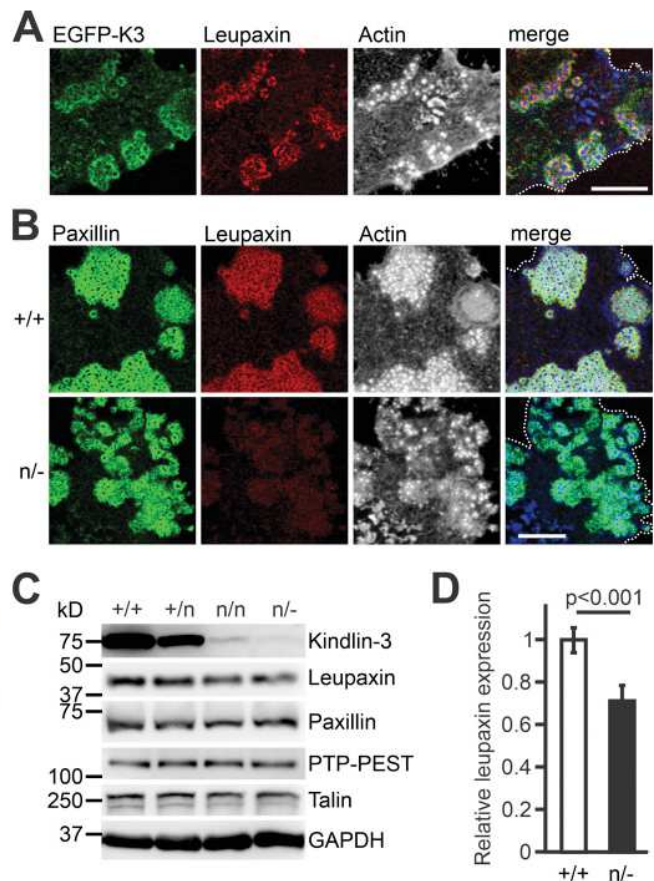


**Figure 3. Reduced kindlin-3 expression impairs leupaxin recruitment to podosomes.** (A) IF staining of a  $K3^{-/-}$  preosteoclast retrovirally transduced with EGFP-K3 (green), for leupaxin (red) and F-actin (white/blue in merge). (B) IF stainings of  $K3^{+/+}$  and  $K3^{n/-}$  preosteoclasts for paxillin (green), leupaxin (red), and actin (white/blue in merge). (C) Western blot analyses on lysates of  $K3^{+/+}$ ,  $K3^{+/n}$ ,  $K3^{n/n}$ , and  $K3^{n/-}$  macrophages for leupaxin, paxillin, PTP-PEST, and talin expression. (D) Densitometric quantification of leupaxin expression in  $K3^{n/-}$  macrophages relative to WT cells. All values were normalized to the corresponding GAPDH signal.  $n = 6$ . Scale bars, 10  $\mu$ m. Dotted white lines mark cell borders.

We then investigated whether the reduced podosomal lifetime of  $K3^{n/-}$  cells is also due to increased paxillin phosphorylation. In fact, we measured strongly increased phospho-paxillin levels in  $K3^{n/-}$  podosomes of preosteoclasts (Fig. 4, F and G; and Fig. S2 C), which could be stabilized again by expression of a phospho-dead paxillin mutant (paxillin 2YF; Fig. 4 H). To further confirm our hypothesis that adhesion-mediated paxillin de-phosphorylation stabilizes podosomes, which is impaired at low kindlin-3 levels, we directly interfered with protein phosphorylation experimentally. We treated WT cells with orthovanadate, a general tyrosine phosphatase inhibitor. Orthovanadate treatment of WT preosteoclasts resulted in an increase in paxillin phosphorylation (Fig. 4, F and G) and a decrease in podosome lifetime to a similar extent as in  $K3^{n/-}$  cells (Fig. 1 G).

Finally, we tested whether a retroviral overexpression of leupaxin rescues paxillin phosphorylation in  $K3^{n/-}$  cells. Notably, although overexpressed leupaxin localized to podosomes of  $K3^{n/-}$



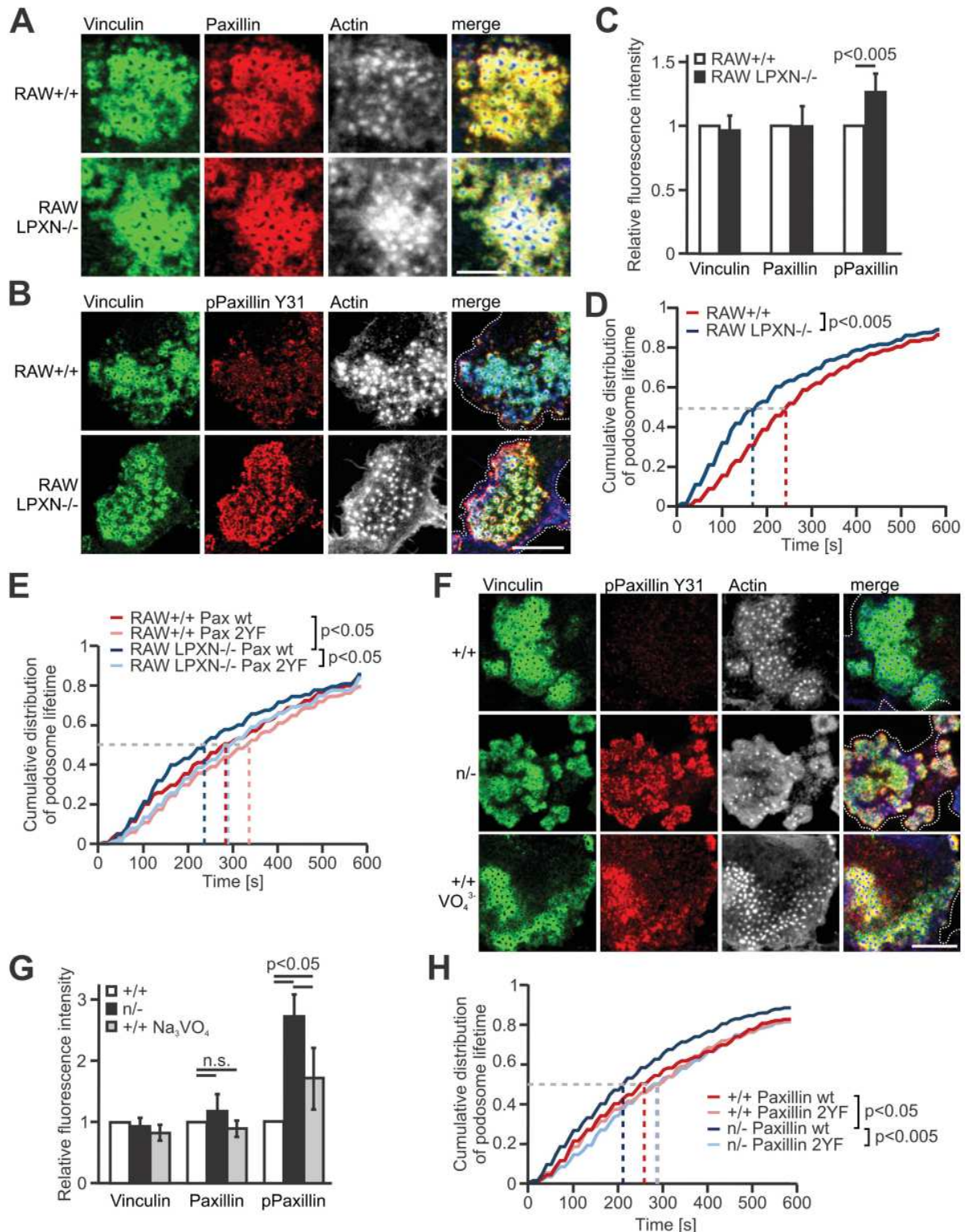


**Figure 4. Loss of leupaxin and reduced kindlin-3 expression result in increased podosomal paxillin phosphorylation and decreased podosome lifetime.** (A) IF stainings of +/+ RAW cells and leupaxin<sup>-/-</sup> RAW cells for vinculin (green), paxillin (red), and actin (white/blue in merge). Scale bar, 10  $\mu$ m. (B) IF stainings of +/+ and leupaxin<sup>-/-</sup> RAW cells for vinculin (green), phospho-paxillin Y31 (red), and actin (white/blue in merge). Scale bar, 5  $\mu$ m. (C) Quantification of vinculin, total paxillin, and phospho-paxillin Y31 recruitment to podosome clusters assessed by measuring fluorescence intensity (MFI) of confocal images. MFIs of +/+ cells were set to 1. In each independent experiment, five podosome regions in each of at least 10 cells were measured.  $n \geq 6$ . (D) Cumulative distribution of podosome lifetime in +/+ and leupaxin<sup>-/-</sup> RAW cells. 10–30 podosomes were measured per cell. At least two cells were analyzed in each of eight independent experiments. (E) Control RAW cells and different clones of leupaxin<sup>-/-</sup> RAW cells were cotransfected with WT paxillin-Cherry or a



non-phosphorylatable mutant paxillin-Cherry (paxillin 2YF) and LifeAct-GFP. Podosome lifetime was assessed and blotted as cumulative distribution. 10–30 podosomes were measured per cell. At least 2 cells were analyzed in each of 5 different dishes. **(F)** IF stainings of  $+/+$  preosteoclasts untreated or treated with  $\text{Na}_3\text{VO}_4$  and  $\text{K}^{3n/-}$  preosteoclasts for phosphorylated paxillin (red). Vinculin (green) and actin (white/blue in merge) served as control stainings. Scale bar, 10  $\mu\text{m}$ . **(G)** Quantification of the recruitment of vinculin, paxillin and phospho-paxillin Y31 to podosome clusters of  $+/+$  preosteoclasts untreated or treated with  $\text{Na}_3\text{VO}_4$  and  $\text{K}^{3n/-}$  preosteoclasts by measuring MFI of confocal images. MFIs of untreated  $+/+$  cells were set to 1. At least five podosome regions in each of at least 10 cells were measured per experiment.  $n \geq 5$ . **(H)** Control and  $\text{K}^{3n/-}$  preosteoclasts were transfected with LifeAct-GFP, left untreated or treated with  $\text{Na}_3\text{VO}_4$ , or cotransfected with WT paxillin-Cherry or a nonphosphorylatable mutant paxillin-Cherry (paxillin 2YF). The cells were imaged for 10 min with a 15-s time interval. Podosome lifetime was assessed and blotted as cumulative distribution. 10–30 podosomes were measured per cell. Two to five cells were analyzed per condition in each of six different dishes. Dotted white lines mark cell borders.

cells, it failed to reduce paxillin phosphorylation, suggesting that kindlin-3 not only recruits leupaxin into podosomes but also facilitates leupaxin-mediated paxillin dephosphorylation (Fig. S2, D and E). In sum, these experiments indicate that low kindlin-3 expression results in impaired leupaxin podosomal targeting, increased paxillin phosphorylation, and high podosomal turnover.

#### Paxillin dephosphorylation by PTP-PEST depends on kindlin-3-mediated recruitment of leupaxin into podosomes

How does the reduced recruitment of leupaxin in kindlin-3 hypomorphic cells control paxillin dephosphorylation? We speculated that the protein tyrosine phosphatase PTP-PEST, which interacts with both paxillin and leupaxin (Shen et al., 1998; Gupta et al., 2003), might be involved in this process. In support of this hypothesis, an anti-GFP immunoprecipitation with lysates from kindlin-3-deficient RAW cells expressing GFP-tagged kindlin-3 showed PTP-PEST in association with kindlin-3, leupaxin, and paxillin (Fig. 5 A). Unexpectedly, we detected more PTP-PEST in podosomal clusters of  $\text{K}^{3n/-}$  preosteoclasts and leupaxin-null RAW cells (Fig. 5, B–D), probably due to the increased binding of PTP-PEST to phosphorylated paxillin. This hypothesis was supported by anti-paxillin coimmunoprecipitation experiments showing more PTP-PEST associated with paxillin in leupaxin-null cells compared with control cells (Fig. 5 E). This experiment and an EGFP-leupaxin immunoprecipitation also showed leupaxin and kindlin-3 in association with paxillin and PTP-PEST (Fig. 5, E and F). The finding that both phospho-paxillin Y31 and PTP-PEST levels were elevated in  $\text{K}^{3n/-}$  and leupaxin-null podosomal clusters suggests that either PTP-PEST does not dephosphorylate paxillin or its enzymatic activity requires leupaxin. To address these possibilities, we lentivirally transduced WT and  $\text{K}^{3n/-}$  preosteoclasts with constructs expressing EGFP as a control, an EGFP-tagged constitutive active PTP-PEST mutant (S39A), or a dominant-negative form of the phosphatase (D199A; Garton et al., 1996; Motohashi et al., 2014) and measured paxillin Y31 phosphorylation levels by confocal microscopy. Constitutive active PTP-PEST reduced Y31 phosphorylation in podosome clusters of WT and  $\text{K}^{3n/-}$  cells, and dominant-negative PTP-PEST increased phosphorylation (Fig. 5, G and H). These data suggest that in the absence of leupaxin, PTP-PEST can still bind phospho-paxillin but does not dephosphorylate it.

#### Paxillin recruitment to primitive adhesion patches of actin cores precedes podosome maturation and is kindlin-3-independent

A striking observation of our study was that in contrast to leupaxin, paxillin is normally targeted to podosomes at very low

kindlin-3 levels. This suggests that either paxillin recruitment to podosomes is kindlin-3 independent, or very low kindlin-3 levels are sufficient for paxillin podosomal targeting. To address this point, we differentiated preosteoclasts from the fetal liver of kindlin-3 knockout embryos and transduced them with WT and kindlin-3 M3 retroviral constructs. Both WT kindlin-3 and kindlin-3 M3 mutant rescued podosome formation, which is also indicated by the restored podosomal actin core diameter (Fig. 6, A and B). Moreover, they showed colocalization with paxillin in the podosomal ring structure, demonstrating that paxillin binding to the kindlin-3 F0 domain is not needed for podosome targeting (Fig. 6 A). In contrast, leupaxin recruitment depends on this interaction, and hence kindlin-3 M3 transduced cells exhibited increased phospho-paxillin levels (Fig. 6, C and D). However, their podosomes appeared more diffuse, with kindlin-3 and paxillin aberrantly extending into the actin cores, suggesting that the individual podosomes are less organized (Fig. 6, E and F). Moreover, consistent with a kindlin-3-independent paxillin localization to podosomes, we found paxillin already strongly accumulated in actin-rich adhesion patches of kindlin-3-null cells (Fig. 6 A). These adhesion patches were also enriched for vinculin and talin, but lack  $\alpha 4$  and  $\beta 1$  integrins, indicating that paxillin is not recruited via binding to  $\alpha 4$  integrin (Fig. S3, A–D). The lack of kindlin-3 probably explains the absence of leupaxin within these adhesion patches and the higher phospho-paxillin levels compared with that within podosomal clusters of cells expressing WT kindlin-3 (Fig. 6 D). These data on the one hand show that paxillin recruitment to podosomes does not depend on interaction with kindlin-3 and on the other hand imply that during podosome formation, initial, actin-rich adhesion patches, which contain actin cores surrounded by the adapter proteins talin, vinculin, and paxillin, are formed independently of kindlin-3. Kindlin-3 is subsequently needed to recruit and cluster integrins as well as to induce integrin-mediated signaling leading to leupaxin-dependent regulation of phospho-paxillin levels.

#### Paxillin family proteins are not crucial for podosome formation but for their signaling

Based on the described interaction of paxillin with all members of the kindlin family and its early presence in forming podosomes (Luxenburg et al., 2012; Gao et al., 2017), we wondered whether paxillin instead recruits kindlin-3 to podosomes and how its deficiency affects podosome formation and dynamics. To this end, we mutated the paxillin gene by CRISPR/Cas9 in RAW cells. Paxillin-deficient RAW cells expressed normal levels of kindlin-3, leupaxin, and PTP-PEST (Fig. 7 A), and showed no



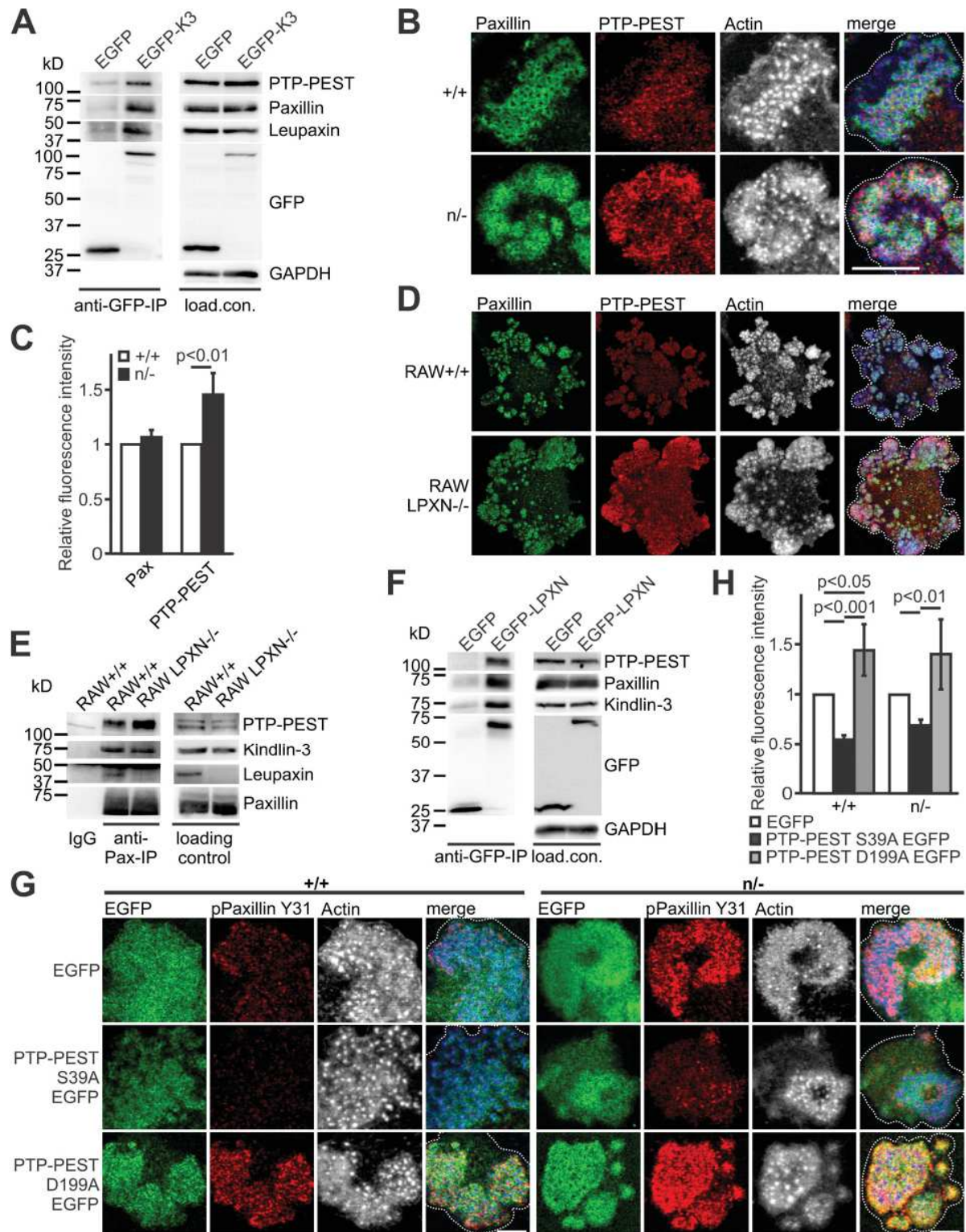


**Figure 5. Dephosphorylation of paxillin by PTP-PEST depends on kindlin-3-mediated recruitment of leupaxin into podosomes.** (A) GFP-IP from K3<sup>-/-</sup> RAW cells, retrovirally transduced with GFP alone or a N-terminally GFP-tagged kindlin-3 analyzed for leupaxin, paxillin, and PTP-PEST. (B) IF staining of +/+ and n/- preosteoclasts for paxillin (green), PTP-PEST (red), and actin (white/blue in merge). Scale bar, 10  $\mu$ m. (C) IF stainings shown in B were quantified by measuring fluorescence intensity. Values from WT cells were set to 1. In each independent experiment, five podosome regions in each of at least 10 cells were measured.  $n = 5$ . (D) Control and leupaxin<sup>-/-</sup> RAW cells stained for paxillin (green), PTP-PEST (red), and actin (white/blue in merge). Scale bar, 20  $\mu$ m. (E) IP using a mouse anti-paxillin antibody or an IgG control with lysates from +/+ and leupaxin<sup>-/-</sup> RAW cells. Binding of PTP-PEST, kindlin-3, and leupaxin was tested. (F) GFP-IP from lysates of leupaxin<sup>-/-</sup> RAW cells, retrovirally transduced with GFP alone or a N-terminally GFP-tagged leupaxin analyzed for kindlin-3,



paxillin, and PTP-PEST. (G) Control and *n/-* preosteoclasts lentivirally transduced with EGFP, PTP-PEST S39A EGFP, or PTP-PEST D199A EGFP and stained for paxillin phosphorylated at Y31 (red) and actin (white/blue in merge). Scale bars, 5  $\mu$ m. (H) Quantification of paxillin phosphorylation levels observed in G. *n* = 5. Dotted white lines mark cell borders.

induction of the third paxillin family member, Hic-5 (Fig. S4 A). Surprisingly, paxillin-null RAW cells did form podosomes, which were organized into kindlin-3-, talin-, and vinculin-positive rings surrounding an ~10% smaller actin core compared with control podosomes (Fig. 7, B–E). We often noticed a more diffuse staining of the plaque proteins, indicating a mild defect in podosomal organization similar to cells expressing the kindlin-3 M3 mutant. In addition, we measured a strongly reduced podosomal lifetime in paxillin-null cells; while 50% of control podosomes dissolved after 260 s, paxillin-null cells had a half-life of only 150 s (Fig. 7 F). Of note, PTP-PEST was virtually absent from the adhesion patches of paxillin-null cells, consistent with the coselevation of PTP-PEST and phospho-paxillin when kindlin-3 activity is reduced, and suggesting that phospho-paxillin is responsible for recruiting PTP-PEST to podosomes (Fig. 7 E). These data indicate that paxillin is dispensable for podosome formation, but podosomal organization and stability depend on the adapter protein paxillin.

The rather mild podosome defect in paxillin-null cells suggested partial functional compensation by leupaxin, which was indeed found at higher levels in podosomal rings of paxillin-null cells (Fig. 7, G and H). To further investigate the relationship between kindlin-3, leupaxin, and paxillin, we retrovirally transduced paxillin and leupaxin-deficient RAW cells with EGFP-K3 and performed EGFP-coimmunoprecipitation experiments. In both experiments, loss of one paxillin family member did not result in increased binding of the other member to kindlin-3, suggesting a lack of competitive binding (Fig. S4, B and C). This may be explained by an excess of kindlin-3 relative to the levels of paxillin and leupaxin, which we confirmed by a whole proteome analysis of WT RAW cells (Fig. S4 D).

To directly address the potential compensatory effects between paxillin and leupaxin, we generated paxillin and leupaxin double knockout (dKO) cells, which showed normal kindlin-3 and talin expression (Fig. 8 A). To our surprise, the dKO cells were also able to form podosomes and podosome clusters, in which kindlin-3, talin, vinculin, and  $\beta$ 1-integrin localized to the podosomal ring surrounding an actin core with a similarly reduced size like in paxillin-null cells (Fig. 8, B–D and F). Podosome lifetime was decreased to a similar extent as in paxillin<sup>-/-</sup> cells (Fig. 8 E). Notably, these cells showed no induction of Hic-5 expression at either the mRNA or the protein level (Fig. S4, E and F). We then expressed GFP-Hic-5 in dKO cells, which showed correct localization in the podosomal ring, however, it failed to rescue the reduced actin core size of dKO cells, again showing specific functions for the different paxillin family members (Pignatelli et al., 2012; Petropoulos et al., 2016; Fig. S4, G and H). Thus, recruitment of kindlin-3 and talin into podosomal rings as well as general organization of podosomes can occur in the absence of paxillin family members.

We then studied whether paxillin family members are critically involved in podosome/integrin signaling and function.

Consistent with previous studies (Luxenburg et al., 2006, 2007), strong phospho-tyrosine signals were detected in the podosomal ring of control cells, and also present in paxillin- and leupaxin-null cells (Fig. 8 F). In contrast, dKO cells revealed a dotted distribution of phospho-tyrosine signals colocalizing with the actin core, which was also illustrated by fluorescence intensity profiles across actin cores (Fig. 8, F and G). In addition, we investigated protein phosphorylation upon adhesion-mediated signaling to fibronectin by Western blot analyses (Fig. 8 H). Consistent with the IF stainings, we measured strong induction of paxillin phosphorylation at Y31 in leupaxin-null cells and only a weak increase in kindlin-3 knockout cells, which was probably due to the low number of adhesion complexes formed by kindlin-3-null cells. Phosphorylation of the actin core marker cortactin was comparable between the different cell lines. We detected a reduction in Pyk2 phosphorylation in leupaxin-null cells and virtually no Pyk2 phosphorylation at Y402 in dKO and kindlin-3-null cells, while FAK phosphorylation at Y397 was not reduced.

Finally, we tested whether these changes in podosome dynamics and adhesion signaling affect cell migration and matrix degradation and found reduced gelatin degradation of paxillin<sup>-/-</sup> and leupaxin<sup>-/-</sup> cells, which was further exacerbated in dKO cells (Fig. 9, A and B). Cell migration was assessed by Transwell assays showing reduced transmigration in paxillin<sup>-/-</sup> and dKO cells, whereas loss of leupaxin increased migration (Fig. 9 C).

## Discussion

The role of kindlin-3 in regulating integrin activity in cooperation with talin is well established in hematopoietic cells. The central aim of this study was to investigate how kindlin-3 regulates integrin signaling and adhesion structure formation in hematopoietic cells, which is far less understood. To this end, we performed a Y2H screen and identified leupaxin as a new kindlin-3 interactor. Leupaxin is primarily expressed in hematopoietic cells and belongs to the paxillin gene family of adapter proteins, which also includes paxillin and Hic-5 (Lipsky et al., 1998). We show that recruitment of leupaxin into podosomes depends on the interaction between a loop within the F0 domain of kindlin-3 and leupaxin LIM domains. The same loop also mediates binding to paxillin, indicating a conserved binding mode between kindlin and paxillin members (Gao et al., 2017). The finding that leupaxin binding to kindlin-3 is enhanced by removal of the F3 domain of kindlin-3 suggests that the F3 domain exerts an inhibitory effect via steric hindrance. Such a model is consistent with the fact that in the cloverleaf domain structure of kindlins, the C-terminal F3 domain and the N-terminal F0 domain are in proximity with each other (Li et al., 2017). Notably, leupaxin binds equally well to WT kindlin-3 and an integrin binding-defective mutant of kindlin-3 (QA), suggesting that their interaction occurs outside of the adhesion site



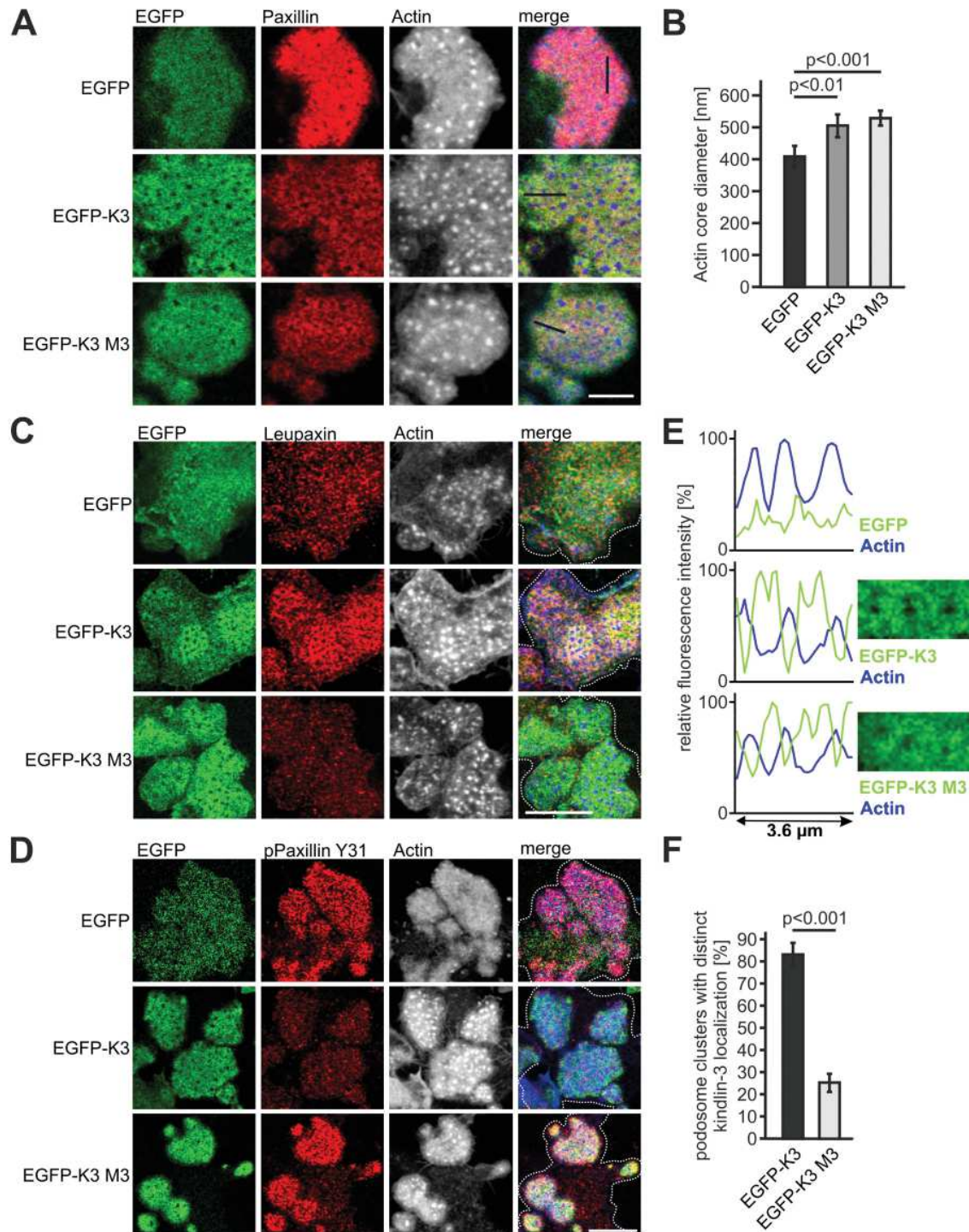


**Figure 6. Leupaxin-binding mutant kindlin-3 fails to recruit leupaxin to podosomes and to reduce paxillin phosphorylation. (A, C, and D)** IF staining and confocal imaging of  $K3^{-/-}$  preosteoclasts retrovirally transduced with EGFP, WT EGFP-K3, or the EGFP-K3 M3 mutant (green) for paxillin (red, A), leupaxin (red, C), and phospho-paxillin Y31 (red, D) and actin (white/blue in merge). Scale bars, 5  $\mu$ m (A) and 10  $\mu$ m (C and D). **(B)** Actin core diameter of  $K3^{-/-}$  preosteoclasts expressing EGFP, EGFP-K3, or the EGFP-K3 M3 mutant. 10 actin cores in two regions of three to five cells were measured per experiment.  $n = 5$ . **(E)** Fluorescence intensity profile through three actin-cores (indicated by the black lines in A) of  $K3^{-/-}$  preosteoclasts expressing EGFP, WT EGFP-K3, or the EGFP-K3 M3 mutant. **(F)** Percentage of cells with podosome clusters, which reveal discrete localization of EGFP-K3 and EGFP-K3 M3 in the podosomal ring. 50 cells were evaluated per condition in each of three independent experiments. Dotted white lines mark cell borders.



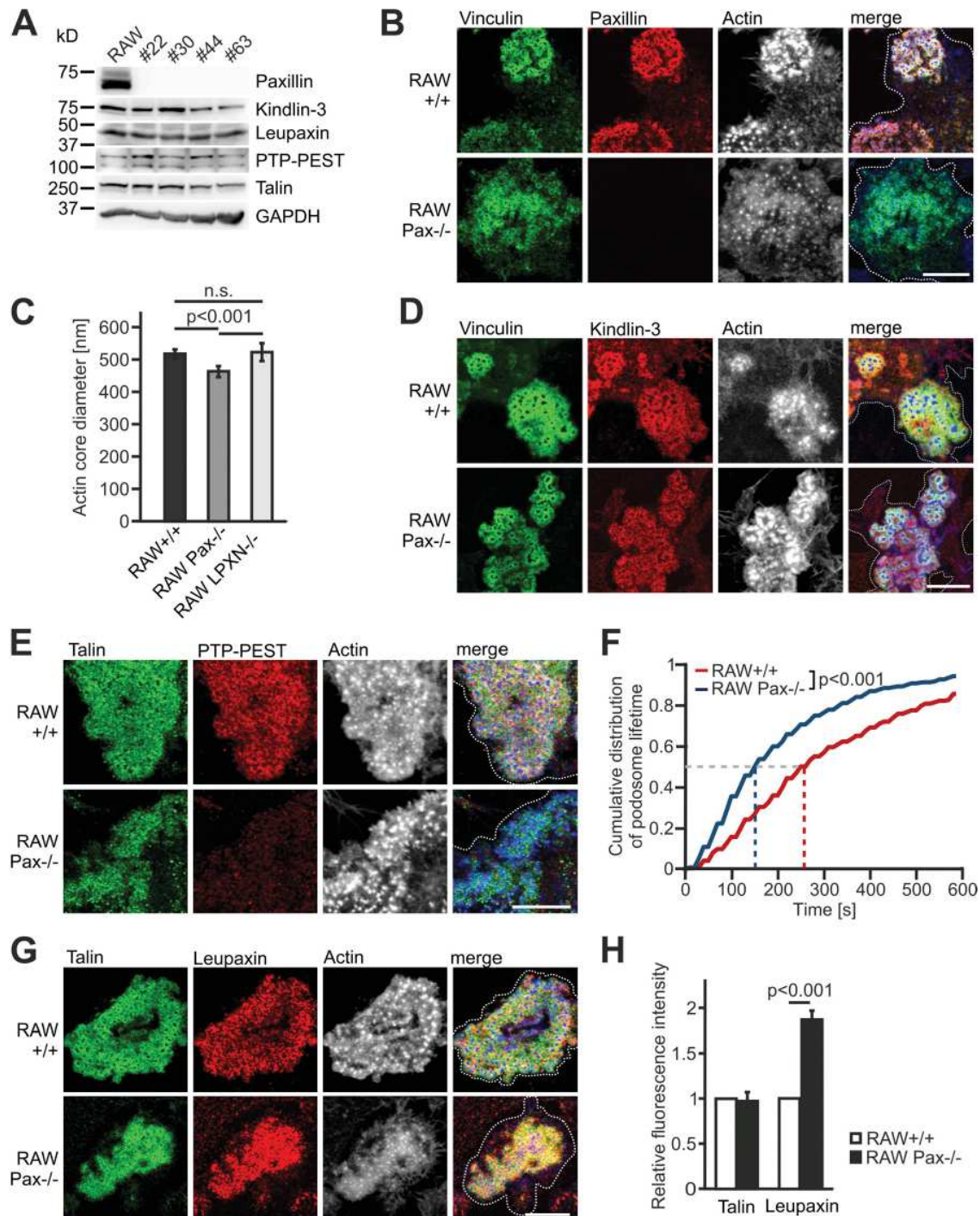


**Figure 7. Paxillin-deficient cells form podosomes with smaller actin cores and strongly reduced lifetime.** (A) Kindlin-3, leupaxin, PTP-PEST, and talin expression in  $+/+$  RAW cells and four different paxillin $^{-/-}$  RAW cell clones analyzed by Western blotting. (B) IF stainings of  $+/+$  and paxillin $^{-/-}$  RAW cells for vinculin (green), paxillin (red), and actin (white/blue in merge). (C) Diameter of the podosome actin cores in  $+/+$ , paxillin $^{-/-}$ , and leupaxin $^{-/-}$  RAW cells. 10 actin cores in two regions of five to eight cells were measured in each experiment.  $n = 10/6/7$ . (D) IF stainings for vinculin (green), kindlin-3 (red), and actin (white/blue in merge) on  $+/+$  and paxillin $^{-/-}$  RAW cells. (E) IF stainings for talin (green), PTP-PEST (red) and actin (white/blue in merge) on  $+/+$  and paxillin $^{-/-}$  RAW cells. (F) Control RAW cells and different clones of paxillin $^{-/-}$  RAW cells were transfected with LifeAct-GFP and imaged at a spinning disc microscope for 10 min with a 15-s time interval. The cumulative distribution of these measurements is shown. 10–30 podosomes were measured per cell. At least four cells were analyzed in each of six independent experiments. (G) Confocal images of talin (green), leupaxin (red), and actin (white/blue in merge) IF stainings of  $+/+$  and paxillin $^{-/-}$  RAW cells. (H) IF stainings shown in G were quantified by measuring fluorescence intensity. Values from WT cells were set to 1. In each independent experiment, five podosome regions in each of at least 10 cells were measured.  $n = 4$ . Scale bars, 10  $\mu\text{m}$ . Dotted white lines mark cell borders.



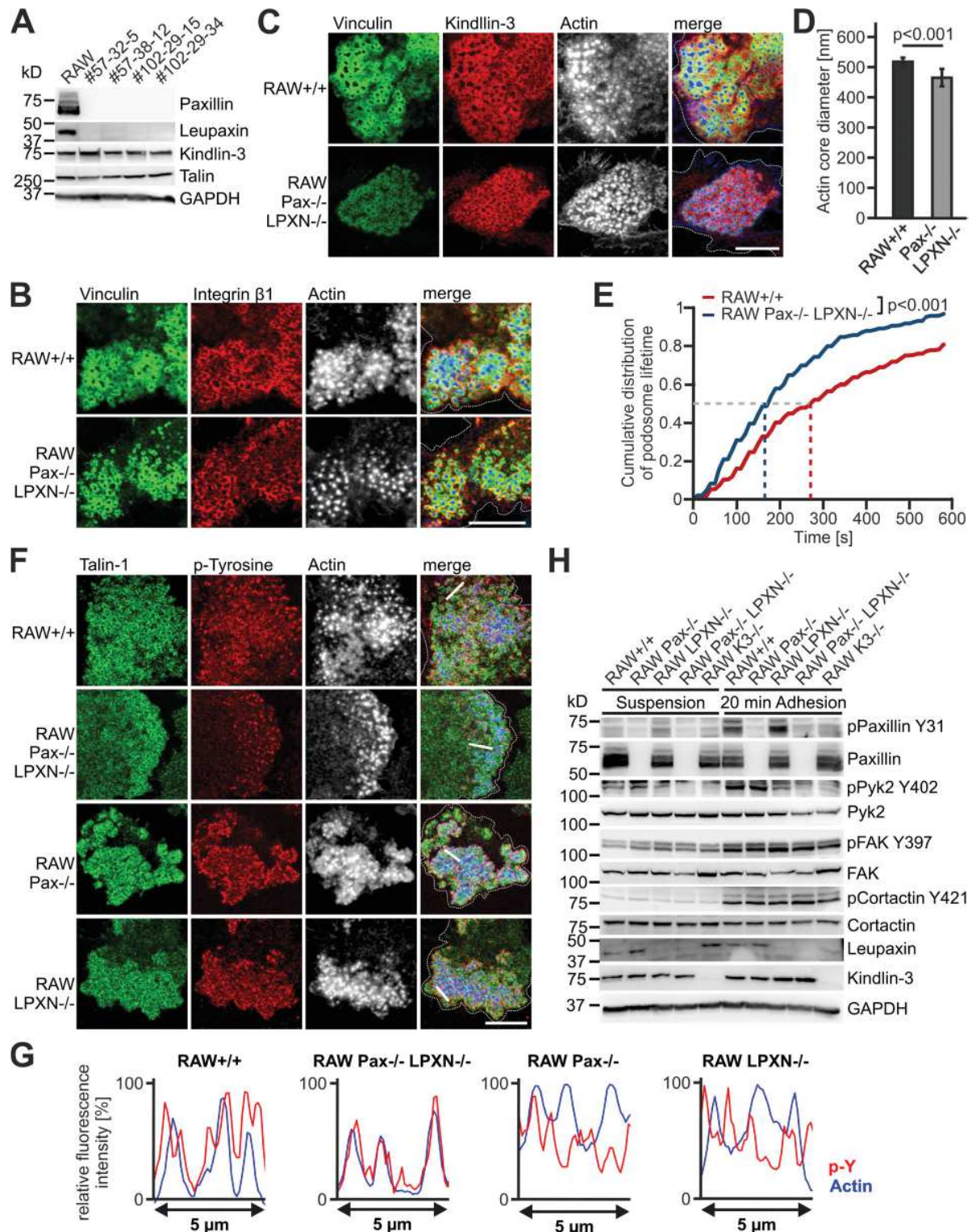


**Figure 8. Characterization of podosomes from paxillin/leupaxin double deficient RAW cells.** (A) Western blot analyses of RAW cells and four different clones of paxillin/leupaxin dKO RAW cells for their expression of kindlin-3 and talin. (B and C) IF stainings of RAW+/+ and paxillin/leupaxin dKO RAW cells for vinculin (green), integrin  $\beta 1$  (red, B), kindlin-3 (red, C) and actin (white/blue in merge). (D) Diameter of the podosome actin cores in RAW+/+ and paxillin/leupaxin dKO RAW cells. 10 actin cores in two regions of five to eight cells were measured in each experiment.  $n = 9/7$ . (E) Control RAW cells and different clones of paxillin/leupaxin dKO RAW cells were transfected with LifeAct-GFP and imaged at a spinning disc microscope for 10 min with a 15-s time interval. The cumulative distribution of these measurements is shown. 20 podosomes were measured per cell. At least four cells were analyzed in each of six dishes. (F) IF stainings for talin (green), tyrosine-phosphorylated proteins (red) and actin (white/blue in merge) on RAW+/+, paxillin/leupaxin dKO, paxillin $^{-/-}$  and leupaxin $^{-/-}$  RAW cells.



(G) Fluorescence intensity profiles of actin (blue) and phospho-tyrosine (p-Y; red) through three actin cores (indicated by the white lines in E) of  $+/+$ , paxillin/leupaxin dKO, paxillin $^{-/-}$ , and leupaxin $^{-/-}$  RAW cells. (H) Western blot analyses of the phosphorylation status of paxillin, Pyk2, FAK and cortactin in  $+/+$ , paxillin $^{-/-}$ , leupaxin $^{-/-}$ , K3 $^{-/-}$  and paxillin/leupaxin dKO RAW cells kept in suspension or adherent to fibronectin. Scale bars, 10  $\mu$ m. Dotted white lines mark cell borders.

and thus that kindlin-3/leupaxin interaction may also have functions other than regulating adhesion stability (Fig. 10). Which signals modulate their interaction or whether this interaction is of constitutive nature is unclear yet and requires further studies.

An important finding of our study is that although leupaxin and paxillin bind kindlin-3 in a similar manner and have multiple binding partners such as FAK, Pyk2, and PTP-PEST in common (Brown et al., 1996; Lipsky et al., 1998; Gupta et al., 2003; Brown and Turner, 2004; Vanarotti et al., 2016), only leupaxin recruitment to podosomes is kindlin-3 dependent. While both paxillin and leupaxin act as scaffolds within adhesion complexes, leupaxin also regulates paxillin activity by suppressing its tyrosine phosphorylation (Tanaka et al., 2010). Phosphorylation of paxillin on Y31 and Y118, which occurs in response to integrin-mediated adhesion signaling, creates new SH2 docking sites for other signaling proteins such as FAK, Crk, and p120RasGAP and thereby functions as a molecular switch, which changes the adhesive and signaling properties of the adhesion complex (Zaidel-Bar et al., 2007; Deakin and Turner, 2008). One important function of paxillin tyrosine phosphorylation is to enhance adhesion disassembly (Nakamura et al., 2000; Webb et al., 2004; Badowski et al., 2008). So kindlin-3 not only is essential for the assembly of podosomes by activating and clustering integrins within podosomes (Schmidt et al., 2011) but also stabilizes and prolongs the lifetime of these adhesions through recruitment of leupaxin.

How leupaxin regulates paxillin phosphorylation is not clear. Based on the reported interaction between the phosphatase

PTP-PEST with leupaxin and paxillin (Shen et al., 1998; Sahu et al., 2007b) and the higher phospho-paxillin levels in PTP-PEST-null cells (Angers-Loustau et al., 1999), we hypothesized that PTP-PEST might be critically involved in that process. Several findings supported this hypothesis. First, we found more PTP-PEST in podosomes of kindlin-3 hypomorphic and leupaxin-null cells, which have higher levels of phospho-paxillin, and PTP-PEST does not localize to podosomes in paxillin-null cells. Second, immunoprecipitation experiments revealed more PTP-PEST in association with paxillin in leupaxin-null cells compared with WT cells, indicating that PTP-PEST primarily associates with phosphorylated paxillin. Third, overexpression of a constitutive active form of PTP-PEST reduced paxillin phosphorylation. In sum, these findings suggest an impaired tyrosine phosphatase activity of PTP-PEST in cells where leupaxin is not efficiently recruited to podosomes. However, the molecular details of how leupaxin regulates PTP-PEST activity, e.g., by direct interaction or by recruiting a kinase or phosphatase that acts on PTP-PEST, require further investigations.

Another interesting aspect of our study concerns the role of paxillin family members in podosome formation and signaling. The first evidence for a direct interaction between paxillin and kindlin family members came from recent studies in fibroblasts, which showed that recruitment of paxillin by kindlin-2 to small, peripheral forming adhesion sites, also known as nascent adhesions, precedes focal adhesion maturation and is required for lamellipodia formation and cell spreading (Theodosiou et al., 2016; Böttcher et al., 2017). Another study reported that paxillin binding to both kindlin and talin stabilizes talin binding to

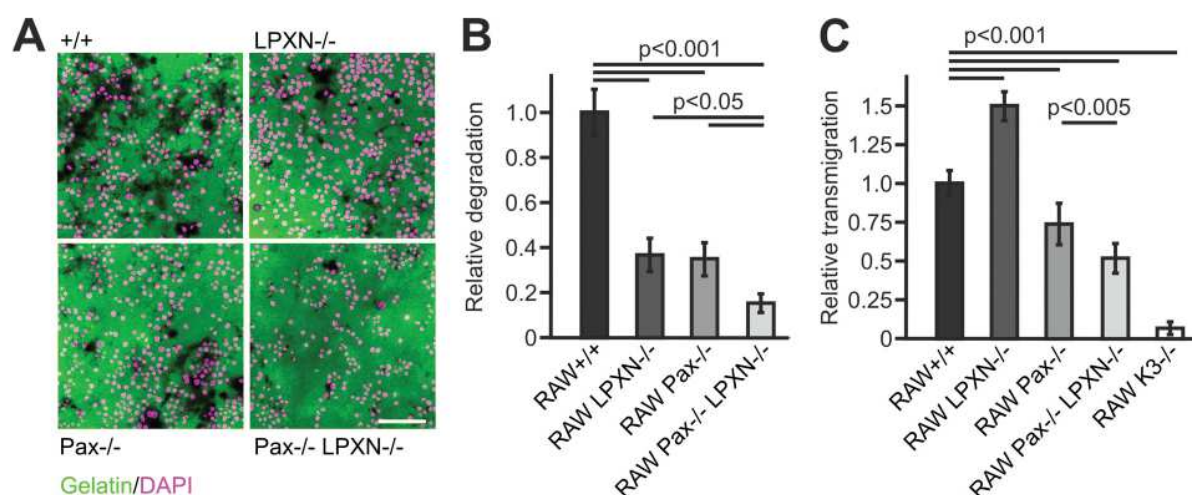
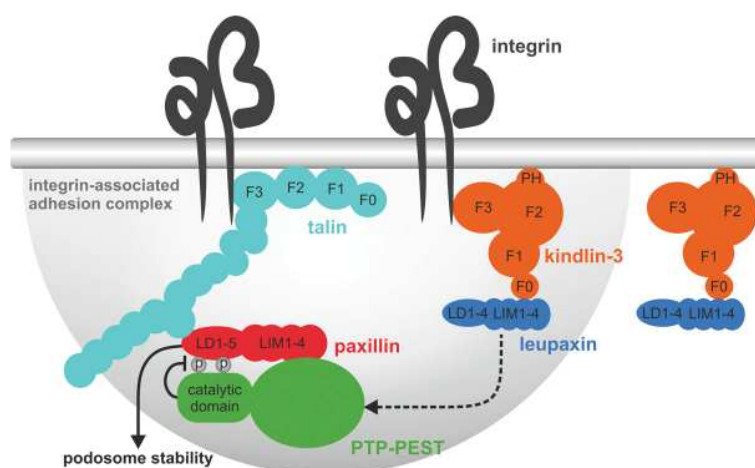


Figure 9. Loss of leupaxin and/or paxillin affect matrix degradation and cell migration. (A) IF images of DAPI-stained (magenta)  $+/+$ , leupaxin $^{-/-}$ , paxillin $^{-/-}$ , and paxillin/leupaxin dKO RAW cells seeded on Oregon Green 488-labeled gelatin (green) for 24 h. Scale bar, 100  $\mu$ m. (B) Relative degradation capacity (area of degraded collagen normalized by number of nuclei) quantified from images shown in A. (C) Migration of these and K3 $^{-/-}$  RAW cells in relation to  $+/+$  cells assessed by Transwell assays.





**Figure 10. A kindlin-3/leupaxin complex regulates paxillin tyrosine phosphorylation and podosome stability.** Kindlin-3/leupaxin interaction is independent of integrin binding. However, kindlin-3 targets leupaxin into the podosome adhesion complex. In contrast, paxillin recruitment to podosomes occurs independent of kindlin-3. The recruitment of leupaxin into podosomes enables the tyrosine phosphatase PTP-PEST to dephosphorylate paxillin at Y31 and Y118, resulting in increased podosome lifetime and stability. PH, pleckstrin homology domain.

the integrin cytoplasmic domain, thereby promoting integrin activation in CHO cells and platelets (Gao et al., 2017). These studies suggested that interactions between kindlins and paxillin are particularly important during the initial phases of adhesion formation by stabilizing the activation state of talin-bound integrin and establishing signaling platforms that further promote cell adhesion and spreading. Consistent with this idea is the observation of very early local accumulation of paxillin at sites where podosomes assemble (Luxenburg et al., 2012). However, in contrast to the kindlin-2-dependent paxillin recruitment to focal complexes, paxillin accumulation at sites where podosomes form is kindlin-3 independent, as shown by normal paxillin localization in podosomes of cells expressing a paxillin-binding mutant kindlin-3 or in adhesion patches of kindlin-3-deficient cells. Notably, paxillin together with talin and vinculin are already present within these initial adhesion sites of kindlin-3-null cells and surround small, less interconnected actin cores that lack a ring of integrins. It is important to note here that hematopoietic cells only express kindlin-3 (Ussar et al., 2006; Moser et al., 2008), which was also confirmed by the whole proteome analysis of RAW cells. Thus, paxillin in complex with vinculin and talin may already form a preassembled complex within immature adhesion patches before kindlin-3 and integrins are recruited to finally assemble podosomes (Deakin and Turner, 2008). The kindlin-independent mechanism of paxillin targeting to podosomes is also consistent with the recent finding that paxillin recruitment to invadosomes, which share many similarities to podosomes, is mediated via the N-terminal LD domains, whereas targeting to focal adhesions is mediated via the LIM2 and LIM3 domains (Brown et al., 1996). Thus, targeting paxillin family members during formation of podosomes and nascent adhesions occurs via different mechanisms.

Finally, our study shows that podosomes can be formed in the absence of any paxillin family member. Although paxillin-deficient podosomes appear less organized and higher leupaxin levels suggest compensation, the overall organization of podosomes does not further deteriorate when both paxillin and leupaxin are absent. Since Hic-5 is not expressed in RAW cells, these cells obviously find a way by which other adapter proteins help out to organize the

adhesion structure. Nevertheless, podosomes from dKO cells may exhibit more subtle defects such as an altered equilibrium between the podosome actin core and the actin cloud, which may impact on the mechanical properties of the podosome. These unapparent defects become evident in functional assays such as cell migration and matrix degradation, which are affected when one or more paxillin family members are absent, or at the molecular level when specific signaling pathways such as Pyk2 phosphorylation are investigated. In this context, the role of paxillin family members in the formation and function of invadosomes, which are similar to podosomes, has recently been investigated in src-transformed fibroblasts (Petropoulos et al., 2016). While paxillin deficiency also affected invadosome assembly, loss of both paxillin and Hic-5 abolished invadosome formation. This contrasts with our study and might be explained by differences in cell type or the src-driven process of invadosome assembly, which depends on the presence of either paxillin or Hic-5. Unfortunately, the role of leupaxin was not addressed in this study (Petropoulos et al., 2016).

In sum, our study shows that kindlin-3 regulates the turnover and lifetime of podosomes in myeloid cells by recruiting leupaxin to the adhesion complex, which in turn controls PTP-PEST enzymatic activity and paxillin phosphorylation (Fig. 10); that initial adhesion patches containing talin, vinculin, and paxillin form in the absence of kindlin-3; and that podosomes can form independent of paxillin family proteins.

## Materials and methods

### Mice

Kindlin-3-deficient ( $K3^{-/-}$ ) and kindlin-3 hypomorphic ( $K3^{n/+}$ ;  $K3^{n/n}$ ;  $K3^{n/-}$ ) mice were described previously (Moser et al., 2008; Klapproth et al., 2015). To generate Flag-tagged kindlin-3 knockin mice, a targeting vector was cloned in which a triple Flag sequence was inserted into exon 2 after the codon for methionine at position 4. In addition, we introduced a loxP-flanked neomycin resistance cassette into intron 2 of the *Kindlin-3* gene. Correctly targeted R1 embryonic stem cells were injected into C57BL/6 blastocysts and the resulting chimeric mice were crossed with deleter-Cre mice to remove the loxP-flanked neomycin cassette (Betz et al., 1996).



Mouse experiments were performed with the approval of the District Government of Bavaria.

## Reagents

Recombinant murine macrophage colony-stimulating factor (M-CSF) and receptor activator of NF- $\kappa$ B ligand (RANKL) were obtained from Peprotech. Bovine plasma fibronectin was purchased from Merck Millipore and murine TNF- $\alpha$  from R&D Systems. A list of key resources is shown in Table S1.

## Antibodies

The following antibodies were used for immunostaining of cells: mouse anti-vinculin antibody, mouse anti-Flag M2-Cy3 antibody (Sigma-Aldrich); rat anti-integrin  $\alpha$ V-PE (Millipore); integrin  $\alpha$ 4-PE (BD PharMingen); mouse anti-cathepsin K (Calbiochem); rabbit anti-paxillin and mouse anti-leupaxin (Abcam); rabbit anti-paxillin Y31, rabbit anti-paxillin Y118, and mouse anti-PTP-PEST (Thermo Fisher Scientific); rabbit anti-kindlin-3 antibody (homemade [Ussar et al., 2006]); rabbit anti-integrin  $\beta$ 1 (homemade [Azimifar et al., 2012]); rabbit anti-talin-1 (Abcam); and mouse anti p-tyrosine (pY99, Santa Cruz Biotechnology). Phalloidin dyes and secondary antibodies were obtained from Invitrogen (Thermo Fisher Scientific).

The following antibodies were used for Western blotting: mouse anti-GAPDH (Merck); mouse anti-talin (Sigma-Aldrich); mouse anti-paxillin, rabbit anti-paxillin Y118 (Thermo Fisher Scientific); mouse anti-leupaxin (Abcam); mouse anti-PTP-PEST, rabbit anti-paxillin Y31 (Thermo Fisher Scientific); mouse anti-Hic-5 (BD Biosciences); rabbit anti-Pyk2, rabbit anti-phospho-Pyk2 Y402, rabbit anti-FAK, rabbit anti-phospho-FAK Y397, rabbit anti-cortactin, rabbit anti-phospho-cortactin Y421, rabbit anti-His-tag (all from Cell Signaling Technology); mouse anti-GFP (homemade cell culture supernatant); and rabbit anti-kindlin-3 antibody (homemade [Ussar et al., 2006]). HRP-labeled secondary antibodies were purchased from Jackson ImmunoResearch Laboratories.

## Cell culture

Preosteoclasts were differentiated from bone marrow ( $K3^{+/+}$  and  $K3^{n/-}$ ) or from embryonic day 14.5 fetal liver cells ( $K3^{-/-}$ ). Cells were kept in complete  $\alpha$ -MEM supplemented with 20 ng/ml M-CSF overnight. Non-adherent cells were collected after 24 h. Leukocytes were isolated from the interface after centrifugation at 1,000  $g$  for 20 min in leukocyte separation medium (Laboratories Eurobio), and then washed with  $\alpha$ -MEM medium and seeded at a concentration of 2,000–2,500 cells/mm<sup>2</sup> in osteoclast differentiation medium ( $\alpha$ -MEM [Gibco] containing 10% FCS, 100 U/ml penicillin, 100  $\mu$ g/ml streptomycin, 60 ng/ml M-CSF, and 40 ng/ml RANKL). Cells were cultured at 37°C in 5% CO<sub>2</sub> for 3–5 d, and medium was changed every second day. Preosteoclasts were defined as adherent cells that were treated with osteoclast differentiation medium for at least 3 d but had not yet rearranged their cytoskeleton and translocated the nuclei to the cell periphery.

RAW cells (RAW 264.7) were cultured in D10 medium (DMEM containing 10% FCS, 100 U/ml penicillin, 100  $\mu$ g/ml streptomycin, 2 mM L-Glu, and nonessential amino acids; all

from Gibco/Thermo Fisher Scientific). For differentiation into preosteoclasts, RAW cells were treated with osteoclast differentiation medium for ~5 d.

Bone marrow-derived macrophages were generated by treating bone marrow cells with R10 medium (RPMI 1640 [Gibco] containing 10% FCS, 25 mM Hepes, 100 U/ml penicillin, 100  $\mu$ g/ml streptomycin, 2 mM L-Glu, nonessential amino acids, and 50  $\mu$ M  $\beta$ -mercaptoethanol) supplemented with M-CSF for 6 d.

For transient transfection of RAW cells, Lipofectamine 3000 (Invitrogen) was used according to the manufacturer's protocol. Primary preosteoclasts were transfected using the Mouse Macrophage Nucleofector Kit from Lonza.

## Plasmids and viral infections

All kindlin-3 constructs were cloned into pEGFP-C1 to express EGFP-tagged proteins. The subdomains were defined according to Huet-Calderwood et al. (2014): the F0 domain from aa 1–97, the F1 domain from aa 98–252, the F2 from aa 253–549, and the F3 domain from aa 550–665. Point mutations (Q597 to A, L334A, Q57A, D58A, W59A, S60A, and D61A) were generated by site-directed mutagenesis.

EGFP, EGFP-kindlin-3, EGFP-kindlin-3 M3 mutant, and EGFP-leupaxin were directionally cloned into the pCLMFG retroviral vector (Naviaux et al., 1996) using the XhoI and NotI restriction sites. Vesicular stomatitis virus G-pseudotyped retroviral vectors were produced in 293T (human embryonic kidney) cells. Viral particles were concentrated from cell culture supernatant as described previously (Pfeifer et al., 2000) and used for infection of preosteoclasts at day three of differentiation.

Murine FL leupaxin and the C-terminal part (aa 150–386) were cloned into pEGFP-C1, and the N-terminal part (1–149) into pEGFP-N1. The C293R mutation was introduced by site-directed mutagenesis. Murine Hic-5 was cloned into pEGFP-C1.

LifeAct-GFP vector (Riedl et al., 2008) was provided by M. Sixt (Institute of Science and Technology, Klosterneuburg, Austria). Mouse paxillin cDNA was cloned into pCherry-C1. Mutations (Y31 to F and Y118 to F) were introduced by site-directed mutagenesis (pCherry-C1 paxillin 2YF).

Human PTP-PEST cDNA was subcloned into pjet to introduce mutations (S39 to A and D199 to A) and then cloned into a lentiviral vector (rrl-CMV-GFP; provided by A. Pfeifer, University of Bonn, Bonn, Germany).

## CRISPR/Cas9 mediated gene ablation

The CRISPR/Cas9 guiding sequence was designed with the help of the CRISPR design webpage of the Zhang laboratory. The sequence for the single guide RNA was cloned into the GFP-expressing vector pX458 (for kindlin-3 targeting: 5'-GGTGGC ACCCACTTTATTCAG-3', for leupaxin targeting: 5'-GTCCAA AGACCTTGTCATCGC-3'), and RAW cells were transfected using Lipofectamine LTX.

For paxillin ablation, gRNA was generated with a GeneArt Precision gRNA Synthesis Kit (Thermo Fisher Scientific) according to the manufacturer's instructions (paxillin target sequence: 5'-TGAACCTGACCGGCTGTTAC-3'). 10  $\mu$ g Cas9 protein



(Thermo Fisher Scientific) were combined with 2.5  $\mu$ g gRNA and incubated for 5 min. The complexes together with a GFP-encoding plasmid were electroporated into  $10^6$  RAW cells using the NEON transfection system (Thermo Fisher Scientific; conditions: resuspension buffer R, 1,680 V, 20 ms, 1 pulse,  $10^7$  cells/ml).

After 2 d, GFP-positive cells were FACS-sorted and seeded at very low concentrations to allow picking of single cell clones. Clones were checked by Western blot for the presence or absence of kindlin-3, leupaxin, and paxillin, respectively.

### Immunoprecipitation

For immunoprecipitations, cells were washed twice with PBS, and 0.5 mM dithiobis(succinimidyl propionate) (Thermo Fisher Scientific) dissolved in PBS was added for 30 min at RT to cross-link proximal proteins. The reaction was stopped by incubation with 50 mM Tris, pH 7.5, for 10 min. Cells were washed with cold PBS and lysed in mammalian protein extraction reagent (Thermo Fisher Scientific) supplemented with protease inhibitors (Roche Diagnostics) and phosphatase inhibitor cocktails (Sigma-Aldrich).  $\mu$ MACS GFP and DYKDDDDK (to recognize the Flag-tag) Isolation kits (Miltenyi) were used according to the manufacturer's protocol using 1–2 mg protein lysate. Endogenous paxillin immunoprecipitation was performed using 5  $\mu$ g mouse anti-paxillin antibody (BD Biosciences) and Pierce Protein A/G Magnetic Beads following the user's guide. Mouse IgG1 (Sigma-Aldrich) was used as control. Immunoprecipitations and 40  $\mu$ g per loading control were subjected to 10% SDS-PAGE and subsequent Western blotting.

### IF microscopy

Preosteoclasts were stained as previously described (Schmidt et al., 2011). For most antibody stainings, cells were fixed with 4% PFA for 10 min. For kindlin-3 labeling, cells were fixed with 1% PFA for 10 min followed by a 10-min incubation with ice-cold acetone. Leupaxin was stained in cells fixed with 1.5% PFA for 12 min. Cells were imaged at RT with a Leica TCS SP5 X confocal microscope (Leica Microsystems) using 63 $\times$  NA 1.40 oil objective lenses and Leica Confocal Software (LAS AF). Single channels were imaged sequentially. All pictures were processed with Photoshop (Adobe Systems).

Protein recruitment to podosome clusters was quantified using ImageJ software (US National Institutes of Health). Fluorescence intensities were assessed in five randomly chosen areas ( $\sim 10 \mu\text{m}^2$ ) within podosome clusters per cell. All values were corrected by background fluorescence. Intensities of control stainings were measured at the identical areas in the corresponding channels (vinculin/paxillin, vinculin/phospho-paxillin Y31, and paxillin/PTP-PEST).

To assess podosome lifetime, preosteoclasts transfected with LifeAct-GFP (Riedl et al., 2008) were imaged with a custom-made spinning disc confocal microscope (Visitron System) based on a Zeiss Observer Z1 and a Yokogawa spinning disk, equipped with a 100 $\times$  NA 1.45 oil objective and an EVOLVE EM512 digital camera (Photometrics). Where stated, the cells were additionally transfected with pCherry-C1 paxillin WT or pCherry-C1 paxillin 2YF. The cells were either left untreated or

treated with 5 mM  $\text{Na}_3\text{VO}_4$  and imaged at the spinning disc microscope for 10 min with a 15-s time interval. The lifetime of a single podosome was analyzed from these time-lapse videos by measuring the time until a podosome present at time point 0 disappeared. 10–30 podosomes were measured per cell. 2–10 cells were analyzed per condition in each of two to eight independent experiments. Podosome lifetime was analyzed using ImageJ software and the MTrackJ plugin (National Institutes of Health).

Actin core size was measured upon phalloidin staining. Two podosome containing regions were chosen per cell, and 10 podosome core diameters were measured per area. 4–10 cells were analyzed in each of five experiments by a person blinded to the genotype of the cells.

### Adhesion signaling

RAW cells were trypsinized and kept in serum-free DMEM in suspension for 3 h. Then cells were either kept in suspension or plated on a 6-cm cell culture dish coated with 5  $\mu$ g/ml fibronectin for 20 min. Cells were carefully washed with ice-cold PBS and lysed in RIPA buffer, containing protease inhibitors and phosphatase inhibitor cocktails (Sigma-Aldrich). 40  $\mu$ g of lysates was subjected to 10% SDS-PAGE and subsequent Western blot analyses.

### Sample preparation and in-solution digest

Proteins were extracted from pelleted and snap-frozen cells with 4% SDS, heated for 5 min to 95°C, and afterward precipitated with ice-cold acetone at  $-20^\circ\text{C}$  for 2.5 h. The proteins were dissolved in 300  $\mu$ l of 8 M urea buffer, and protein concentrations were determined using the Pierce 660 nm Protein Assay (Thermo Fisher Scientific). Per sample, 50  $\mu$ g of protein was reduced with 5 mM dithiothreitol for 60 min, followed by carbamidomethylation with 40 mM iodoacetamide for 45 min in the dark at RT. A predigest with the protease LysC (Wako Pure Chemicals Industries) was performed for 3 h, followed by a digest with trypsin (Promega) for 16 h. The digest was terminated by the acidification of the sample to 1% formic acid, and the resulting peptides were separated from salts and detergents using the C18 based Stop and Go extraction tips (Rappsilber et al., 2003).

### Liquid chromatography–tandem mass spectrometry analysis and data processing

An Easy nLC 1200 ultra-high-performance liquid chromatography coupled to a QExactive HF-X Hybrid Quadrupole-Orbitrap mass spectrometer (Thermo Fisher Scientific) was used for the proteomic analysis with the following settings. Peptides were fractionated using in-house-made 50-cm columns packed with 1.7- $\mu$ m C18 beads using a binary buffer system, consisting of Buffer A (0.1% formic acid) and Buffer B (80% acetonitrile in 0.1% formic acid). All samples were analyzed over a 90-min gradient, raising the content of Buffer B from 4% to 23% over 65 min, then from 23% to 55% over 13 min, followed by washing with 95% Buffer B. Spectra for full MS were acquired at a resolution of 60,000 at 200 m/z, and the automated gain control target was set to  $3 \times 10^6$  with a maximum injection time of 20



ms. The dynamic exclusion was set to 20 s. The MS2 measurements were acquired using a resolution of 15,000 at 200 m/z with a top 22 data-dependent mode. Here the automated gain control target was set to  $1 \times 10^5$  with an injection time of 22 ms. The normalized collision energy in the higher-energy collisional dissociation cell was 25.

The raw data were analyzed using the Andromeda search engine implemented in the MaxQuant software 1.5.3.8 (Cox et al., 2011). Parameters in MaxQuant were set to default with trypsin selected as protease for digestion. A mouse database from Uniprot (16.06.17) with contaminants was used for peptide and protein identification.

### Transwell assay

Cell migration was tested in Transwell cell culture inserts (24-well, 8- $\mu$ m pore, polyester membrane; Merck Millipore) coated with 1 mg/ml fibrinogen in TBS for 2 h at 37°C.  $10^5$  cells were stimulated with 2  $\mu$ g/ml TNF- $\alpha$  (R&D Systems) in DMEM/F-12 containing 0.1% FCS and added to the upper reservoir. 1 ml DMEM/F-12 with 0.1% FCS was filled in the lower reservoir. The experiment was started by adding 1  $\mu$ g/ml LPS to the lower reservoir. After 6 h, the cells were fixed for 15 min with 4% PFA and stained with DAPI. Not-transmigrated cells were removed with a cotton swab, and six pictures were taken per Transwell with an Evos FL cell imaging system (Thermo Fisher Scientific) with a 10 $\times$  objective to assess the number of transmigrated cells.

### Gelatin degradation assay

12-mm glass coverslips were coated with 10  $\mu$ g/ml Oregon Green 488-conjugated gelatin (Invitrogen) in PBS for 30 min. Slides were washed with PBS and fixed with 4% PFA for 15 min. Residual PFA was removed by extensive washing in PBS and incubation with full medium for 30 min.  $2 \times 10^5$  cells that were cultured in osteoclast differentiation medium for 24 h were seeded per coverslip. Cells were fixed with 4% PFA the following day and stained with DAPI. Five pictures were taken per slide with a Leica TCS SP5 X confocal microscope using a 40 $\times$  NA 1.25–0.75 oil objective. Gelatin degradation was quantified by measuring the degraded area using ImageJ software and correlated to the number of nuclei.

### Quantitative real-time PCR

mRNA expression level of Hic-5 was assessed by quantitative real-time PCR. An RNeasy Mini Kit (Qiagen) was used to isolate RNA, and reverse transcription was performed using a iScript cDNA Synthesis Kit (Bio-Rad Laboratories). Quantitative PCR was done with iQ SYBR Green Supermix (Bio-Rad Laboratories) in LightCycler 480 Multiwell Plate 96, white (Roche) on a LightCycler 480 II (Roche Molecular Systems) under standard conditions. The following primers were used: Hic-5 forward: 5'-GTAACCAACCCATCCGACAC-3', Hic-5 reverse: 5'-GCTGAGCATGGAAATGGTTT-3' (as published by Rashid et al., 2017); GAPDH forward: 5'-TCGTGGATCTGACGTGCCGCTG-3', and GAPDH reverse: 5'-CACCACCTGTTGCTGTAGCCGT-3'. All samples were measured in quadruplicate. Data were analyzed using the  $2^{-\Delta\Delta CT}$ -method (Livak and Schmittgen, 2001).

### Recombinant protein expression, purification, and pulldown

FL leupaxin, leupaxin NT, or leupaxin CT cDNAs were cloned into the bacterial expression vector pGEX-2T, kindlin-3 FO domain into pCoofy17 (Scholz et al., 2013). GST, N-terminally GST-tagged leupaxin FL, NT, or CT and HisSUMO-tagged kindlin-3 FO domain were expressed in Rosetta (DE3)-competent cells. Bacteria were cultured in 50–100 ml Luria-Bertani medium at 37°C to an OD<sub>600</sub> of 0.6 to 0.7. Proteins were expressed at 18°C overnight upon induction with 0.2 mM IPTG. For leupaxin expression, cultures were supplemented with 500  $\mu$ M ZnCl<sub>2</sub>. Protein purification, pulldowns, and wash steps were performed in 25 mM Tris buffer, pH 7.5, containing 150 mM NaCl, 5 mM MgCl<sub>2</sub>, 1 mM DTT, 0.01% NP-40 Substitute (Sigma-Aldrich), protease inhibitors, and 10  $\mu$ M ZnCl<sub>2</sub> (for leupaxin only). Bacteria pellets were lysed by incubation with lysozyme (10  $\mu$ g/ml) and sonication. Lysates were cleared by centrifugation. HisSUMO-kindlin-3 FO was batch-purified using PureCube 100 INDIGO Ni-Agarose beads (Cube Biotech). GST and GST-tagged leupaxin FL, NT, or CT were bound to 40  $\mu$ l Glutathione Magnetic Agarose Beads (Jena Bioscience) for 1 h at RT. After washing extensively, 10  $\mu$ l of loaded beads per condition were blocked with 5% BSA for 1.5 h at 4°C, and, subsequently, purified kindlin-3 FO domain was added for 1 h at 4°C in the presence of 0.5% BSA. After washing, bound proteins were eluted by incubation for 5 min at 95°C in Laemmli buffer. Samples were subjected to SDS-PAGE and Western blot.

### Statistical analysis

Data are presented as means  $\pm$  95% confidence interval. Statistical analyses were performed using the software GraphPad Prism. Fluorescence intensities were log-transformed before statistical analyses, as upon transformation, normal distribution can be assumed. For statistical evaluation of podosome lifetime measurements, we determined the time at which 50% of the observed podosomes had disappeared for each cell culture dish. These values were subjected to statistical analyses, assuming normal distribution.

Paired or unpaired Student's *t* tests were used to compare two different datasets if normal distribution could be assumed. A Mann-Whitney test was performed to compare two datasets if normal distribution could not be implied. To evaluate three or more datasets, one-way ANOVA was performed followed by a Tukey's or a Sidak's multiple comparison test, as recommended by GraphPad Prism.

Data were tested for significance as follows: paired Student's *t* test for fluorescence intensity measurements; unpaired Student's *t* test for podosome lifetime measurements, actin core diameter, and leupaxin expression; Mann-Whitney test for cells that form podosomes; one-way ANOVA with Tukey's multiple comparison test for fluorescence intensity measurements, actin core diameter, and gelatin degradation assay; and one-way ANOVA with Sidak's multiple comparison test for podosome lifetime measurements and Transwell assay.

A difference between datasets was considered to be significant if *P* < 0.05.

### Online supplemental material

Fig. S1 describes the generation of Flag-tagged kindlin-3 knockin mice, Flag-tagged kindlin-3 protein expression, and its



localization to podosomes. Fig. S2 shows by IF stainings and Western blotting that loss of leupaxin or a reduced kindlin-3 expression result in increased phosphorylation of paxillin at Y118. Overexpression of leupaxin in K3<sup>n/-</sup> cells is not sufficient to lower paxillin phosphorylation at Y31. Fig. S3 shows confocal images of IF stainings of various podosomal marker proteins in control and K3<sup>n/-</sup> cells. Fig. S4 shows that Hic-5 expression is not induced in paxillin/leupaxin dKO cells, and retroviral overexpression of Hic-5 cannot rescue the podosome defect of paxillin/leupaxin dKO RAW cells. Furthermore, immunoprecipitation and quantitative proteomics experiments reveal that leupaxin and paxillin do not compete for kindlin-3 binding. Table S1 shows a list of the main reagents and resources used in the study. Videos 1 and 2 show +/+ and K3<sup>n/-</sup> preosteoclasts expressing LifeAct-GFP, revealing shorter podosome lifetime at low kindlin-3 expression levels.

## Acknowledgments

The authors thank Soo Jin Min-Weissenhorn and the people from the transgenic facility of the Max Planck Institute of Biochemistry for help with generating the Flag-kindlin-3 mice. We thank Reinhard Fässler for his generous support and Arnoud Sonnenberg, Stefan Linder, and Nick Brown for critically reading the manuscript.

This work was supported by the Deutsche Forschungsgemeinschaft (SFB914 TP A01) and the Max Planck Society.

The authors declare no competing financial interests.

Author contributions: S. Klapproth, T. Bromberger, and M. Moser designed and performed the experiments and analyzed data. C. Türk and M. Krüger performed mass spectrometry and analyzed the data. M. Moser supervised the work, and S. Klapproth and M. Moser wrote the paper with input from all other authors.

Submitted: 18 March 2019

Revised: 8 July 2019

Accepted: 5 August 2019

## References

- Angers-Loustau, A., J.F. Côté, A. Charest, D. Dowbenko, S. Spencer, L.A. Lasky, and M.L. Tremblay. 1999. Protein tyrosine phosphatase-PEST regulates focal adhesion disassembly, migration, and cytokinesis in fibroblasts. *J. Cell Biol.* 144:1019–1031. <https://doi.org/10.1083/jcb.144.5.1019>
- Azimifar, S.B., R.T. Böttcher, S. Zanivan, C. Grashoff, M. Krüger, K.R. Legate, M. Mann, and R. Fässler. 2012. Induction of membrane circular dorsal ruffles requires co-signalling of integrin-ILK-complex and EGF receptor. *J. Cell Sci.* 125:435–448. <https://doi.org/10.1242/jcs.091652>
- Badowski, C., G. Pawlak, A. Grichine, A. Chabadel, C. Oddou, P. Jurdic, M. Pfaff, C. Albige-Rizo, and M.R. Block. 2008. Paxillin phosphorylation controls invadopodia/podosomes spatiotemporal organization. *Mol. Biol. Cell.* 19:633–645. <https://doi.org/10.1091/mbc.e06-01-0088>
- Ballestrem, C., N. Erez, J. Kirchner, Z. Kam, A. Bershadsky, and B. Geiger. 2006. Molecular mapping of tyrosine-phosphorylated proteins in focal adhesions using fluorescence resonance energy transfer. *J. Cell Sci.* 119:866–875. <https://doi.org/10.1242/jcs.02794>
- Betz, U.A., C.A. Vosschenrich, K. Rajewsky, and W. Müller. 1996. Bypass of lethality with mosaic mice generated by Cre-loxP-mediated recombination. *Curr. Biol.* 6:1307–1316. [https://doi.org/10.1016/S0960-9822\(02\)70717-3](https://doi.org/10.1016/S0960-9822(02)70717-3)
- Block, M.R., C. Badowski, A. Millon-Fremillon, D. Bouvard, A.P. Bouin, E. Faurobert, D. Gerber-Sckaert, E. Planus, and C. Albige-Rizo. 2008. Podosome-type adhesions and focal adhesions, so alike yet so different. *Eur. J. Cell Biol.* 87:491–506. <https://doi.org/10.1016/j.ejcb.2008.02.012>
- Böttcher, R.T., M. Veelders, P. Rombaut, J. Faix, M. Theodosiou, T.E. Stradal, K. Rottner, R. Zent, F. Herzog, and R. Fässler. 2017. Kindlin-2 recruits paxillin and Arp2/3 to promote membrane protrusions during initial cell spreading. *J. Cell Biol.* 216:3785–3798. <https://doi.org/10.1083/jcb.201701176>
- Brown, M.C., and C.E. Turner. 2004. Paxillin: adapting to change. *Physiol. Rev.* 84:1315–1339. <https://doi.org/10.1152/physrev.00002.2004>
- Brown, M.C., J.A. Perrotta, and C.E. Turner. 1996. Identification of LIM3 as the principal determinant of paxillin focal adhesion localization and characterization of a novel motif on paxillin directing vinculin and focal adhesion kinase binding. *J. Cell Biol.* 135:1109–1123. <https://doi.org/10.1083/jcb.135.4.1109>
- Calle, Y., S. Burns, A.J. Thrasher, and G.E. Jones. 2006. The leukocyte podosome. *Eur. J. Cell Biol.* 85:151–157. <https://doi.org/10.1016/j.ejcb.2005.09.003>
- Chen, P.W., and G.S. Kroog. 2010. Leupaxin is similar to paxillin in focal adhesion targeting and tyrosine phosphorylation but has distinct roles in cell adhesion and spreading. *Cell Adhes. Migr.* 4:527–540. <https://doi.org/10.4161/cam.4.4.12399>
- Cox, J., N. Neuhauser, A. Michalski, R.A. Scheltema, J.V. Olsen, and M. Mann. 2011. Andromeda: a peptide search engine integrated into the MaxQuant environment. *J. Proteome Res.* 10:1794–1805. <https://doi.org/10.1021/pr101065j>
- Deakin, N.O., and C.E. Turner. 2008. Paxillin comes of age. *J. Cell Sci.* 121:2435–2444. <https://doi.org/10.1242/jcs.018044>
- Destaing, O., F. Saltel, J.C. Géminard, P. Jurdic, and F. Bard. 2003. Podosomes display actin turnover and dynamic self-organization in osteoclasts expressing actin-green fluorescent protein. *Mol. Biol. Cell.* 14:407–416. <https://doi.org/10.1091/mbc.e02-07-0389>
- Digman, M.A., C.M. Brown, A.R. Horwitz, W.W. Mantulin, and E. Gratton. 2008. Paxillin dynamics measured during adhesion assembly and disassembly by correlation spectroscopy. *Biophys. J.* 94:2819–2831. <https://doi.org/10.1529/biophysj.107.104984>
- Fukuda, K., K. Bledzka, J. Yang, H.D. Perera, E.F. Plow, and J. Qin. 2014. Molecular basis of kindlin-2 binding to integrin-linked kinase pseudokinase for regulating cell adhesion. *J. Biol. Chem.* 289:28363–28375. <https://doi.org/10.1074/jbc.M114.596692>
- Gao, J., M. Huang, J. Lai, K. Mao, P. Sun, Z. Cao, Y. Hu, Y. Zhang, M.L. Schulte, C. Jin, et al. 2017. Kindlin supports platelet integrin αIIbβ3 activation by interacting with paxillin. *J. Cell Sci.* 130:3764–3775. <https://doi.org/10.1242/jcs.205641>
- Garton, A.J., A.J. Flint, and N.K. Tonks. 1996. Identification of p130(cas) as a substrate for the cytosolic protein tyrosine phosphatase PTP-PEST. *Mol. Cell Biol.* 16:6408–6418. <https://doi.org/10.1128/MCB.16.11.6408>
- Gupta, A., B.S. Lee, M.A. Khadeer, Z. Tang, M. Chellaiyah, Y. Abu-Amer, J. Goldknopf, and K.A. Hruska. 2003. Leupaxin is a critical adaptor protein in the adhesion zone of the osteoclast. *J. Bone Miner. Res.* 18:669–685. <https://doi.org/10.1359/jbmr.2003.18.4.669>
- Harburger, D.S., and D.A. Calderwood. 2009. Integrin signalling at a glance. *J. Cell Sci.* 122:159–163. <https://doi.org/10.1242/jcs.018093>
- Huet-Calderwood, C., N.N. Brahme, N. Kumar, A.L. Stiegler, S. Raghavan, T.J. Boggan, and D.A. Calderwood. 2014. Differences in binding to the ILK complex determines kindlin isoform adhesion localization and integrin activation. *J. Cell Sci.* 127:4308–4321. <https://doi.org/10.1242/jcs.155879>
- Humphries, J.D., M.R. Chastney, J.A. Askari, and M.J. Humphries. 2019. Signal transduction via integrin adhesion complexes. *Curr. Opin. Cell Biol.* 56:14–21. <https://doi.org/10.1016/j.ejcb.2018.08.004>
- Hynes, R.O. 2002. Integrins: bidirectional, allosteric signaling machines. *Cell.* 110:673–687. [https://doi.org/10.1016/S0092-8674\(02\)00971-6](https://doi.org/10.1016/S0092-8674(02)00971-6)
- Iwamoto, D.V., and D.A. Calderwood. 2015. Regulation of integrin-mediated adhesions. *Curr. Opin. Cell Biol.* 36:41–47. <https://doi.org/10.1016/j.ejcb.2015.06.009>
- Klapproth, S., F.A. Moretti, M. Zeiler, R. Ruppert, U. Breithaupt, S. Mueller, R. Haas, M. Mann, M. Sperandio, R. Fässler, and M. Moser. 2015. Minimal amounts of kindlin-3 suffice for basal platelet and leukocyte functions in mice. *Blood.* 126:2592–2600. <https://doi.org/10.1182/blood-2015-04-639310>
- Laukaitis, C.M., D.J. Webb, K. Donais, and A.F. Horwitz. 2001. Differential dynamics of alpha 5 integrin, paxillin, and alpha-actinin during formation and disassembly of adhesions in migrating cells. *J. Cell Biol.* 153:1427–1440. <https://doi.org/10.1083/jcb.153.7.1427>



- Legate, K.R., S.A. Wickström, and R. Fässler. 2009. Genetic and cell biological analysis of integrin outside-in signaling. *Genes Dev.* 23:397–418. <https://doi.org/10.1101/gad.1758709>
- Li, H., Y. Deng, K. Sun, H. Yang, J. Liu, M. Wang, Z. Zhang, J. Lin, C. Wu, Z. Wei, and C. Yu. 2017. Structural basis of kindlin-mediated integrin recognition and activation. *Proc. Natl. Acad. Sci. USA.* 114:9349–9354. <https://doi.org/10.1073/pnas.1703064114>
- Linder, S., and P. Kopp. 2005. Podosomes at a glance. *J. Cell Sci.* 118: 2079–2082. <https://doi.org/10.1242/jcs.02390>
- Lipsky, B.P., C.R. Beals, and D.E. Staunton. 1998. Leupaxin is a novel LIM domain protein that forms a complex with PYK2. *J. Biol. Chem.* 273: 11709–11713. <https://doi.org/10.1074/jbc.273.19.11709>
- Livak, K.J., and T.D. Schmittgen. 2001. Analysis of relative gene expression data using real-time quantitative PCR and the 2(-Delta Delta C(T)) Method. *Methods.* 25:402–408. <https://doi.org/10.1006/meth.2001.1262>
- Luxenburg, C., J.T. Parsons, L. Addadi, and B. Geiger. 2006. Involvement of the Src-cortactin pathway in podosome formation and turnover during polarization of cultured osteoclasts. *J. Cell Sci.* 119:4878–4888. <https://doi.org/10.1242/jcs.03271>
- Luxenburg, C., D. Geblinger, E. Klein, K. Anderson, D. Hanein, B. Geiger, and L. Addadi. 2007. The architecture of the adhesive apparatus of cultured osteoclasts: from podosome formation to sealing zone assembly. *PLoS One.* 2:e179. <https://doi.org/10.1371/journal.pone.0000179>
- Luxenburg, C., S. Winograd-Katz, L. Addadi, and B. Geiger. 2012. Involvement of actin polymerization in podosome dynamics. *J. Cell Sci.* 125:1666–1672. <https://doi.org/10.1242/jcs.075903>
- Marchisio, P.C., I. Bergui, G.C. Cortascio, O. Cremona, N. D'Urso, M. Schena, L. Tesio, and F. Caligaris-Cappio. 1988. Vinculin, talin, and integrins are localized at specific adhesion sites of malignant B lymphocytes. *Blood.* 72:830–833.
- Moser, M., B. Nieswandt, S. Ussar, M. Pozgajova, and R. Fässler. 2008. Kindlin-3 is essential for integrin activation and platelet aggregation. *Nat. Med.* 14:325–330. <https://doi.org/10.1038/nm1722>
- Moser, M., K.R. Legate, R. Zent, and R. Fässler. 2009. The tail of integrins, talin, and kindlins. *Science.* 324:895–899. <https://doi.org/10.1126/science.1163865>
- Motohashi, S., K. Koizumi, R. Honda, A. Maruyama, H.E. Palmer, and K. Mashima. 2014. Protein tyrosine phosphatase-PEST (PTP-PEST) regulates mast cell-activating signals in PTP activity-dependent and -independent manners. *Cell. Immunol.* 289:128–134. <https://doi.org/10.1016/j.cellimm.2014.04.003>
- Murphy, D.A., and S.A. Courtneidge. 2011. The 'ins' and 'outs' of podosomes and invadopodia: characteristics, formation and function. *Nat. Rev. Mol. Cell Biol.* 12:413–426. <https://doi.org/10.1038/nrm3141>
- Nakamura, K., H. Yano, H. Uchida, S. Hashimoto, E. Schaefer, and H. Sabe. 2000. Tyrosine phosphorylation of paxillin alpha is involved in temporospatial regulation of paxillin-containing focal adhesion formation and F-actin organization in motile cells. *J. Biol. Chem.* 275:27155–27164.
- Naviaux, R.K., E. Costanzi, M. Haas, and I.M. Verma. 1996. The pCL vector system: rapid production of helper-free, high-titer, recombinant retroviruses. *J. Virol.* 70:5701–5705.
- Petropoulos, C., C. Oddou, A. Emadali, E. Hiriart-Bryant, C. Boyault, E. Faurobert, S. Vande Pol, J.R. Kim-Kaneyama, A. Kraut, Y. Coute, et al. 2016. Roles of paxillin family members in adhesion and ECM degradation coupling at invadosomes. *J. Cell Biol.* 213:585–599. <https://doi.org/10.1083/jcb.201510036>
- Pfeifer, A., T. Kessler, S. Silletti, D.A. Cheresch, and I.M. Verma. 2000. Suppression of angiogenesis by lentiviral delivery of PEX, a noncatalytic fragment of matrix metalloproteinase 2. *Proc. Natl. Acad. Sci. USA.* 97: 12227–12232. <https://doi.org/10.1073/pnas.220399597>
- Pignatelli, J., S.E. LaLonde, D.P. LaLonde, D. Clarke, and C.E. Turner. 2012. Actopaxin ( $\alpha$ -parvin) phosphorylation is required for matrix degradation and cancer cell invasion. *J. Biol. Chem.* 287:37309–37320. <https://doi.org/10.1074/jbc.M112.385229>
- Rappsilber, J., Y. Ishihama, and M. Mann. 2003. Stop and go extraction tips for matrix-assisted laser desorption/ionization, nanoelectrospray, and LC/MS sample pretreatment in proteomics. *Anal. Chem.* 75:663–670. <https://doi.org/10.1021/ac026117i>
- Rashid, M., J. Belmont, D. Carpenter, C.E. Turner, and E.C. Olson. 2017. Neural-specific deletion of the focal adhesion adaptor protein paxillin slows migration speed and delays cortical layer formation. *Development.* 144:4002–4014. <https://doi.org/10.1242/dev.147934>
- Riedl, J., A.H. Crevenna, K. Kessenbrock, J.H. Yu, D. Neukirchen, M. Bista, F. Bradke, D. Jenne, T.A. Holak, Z. Werb, et al. 2008. Lifeact: a versatile marker to visualize F-actin. *Nat. Methods.* 5:605–607. <https://doi.org/10.1038/nmeth.1220>
- Robertson, L.K., and H.L. Ostergaard. 2011. Paxillin associates with the microtubule cytoskeleton and the immunological synapse of CTL through its leucine-aspartic acid domains and contributes to microtubule organizing center reorientation. *J. Immunol.* 187:5824–5833. <https://doi.org/10.4049/jimmunol.1003690>
- Sahu, S.N., M.A. Khadeer, B.W. Robertson, S.M. Núñez, G. Bai, and A. Gupta. 2007a. Association of leupaxin with Src in osteoclasts. *Am. J. Physiol. Cell Physiol.* 292:C581–C590. <https://doi.org/10.1152/ajpcell.00636.2005>
- Sahu, S.N., S. Nunez, G. Bai, and A. Gupta. 2007b. Interaction of Pyk2 and PTP-PEST with leupaxin in prostate cancer cells. *Am. J. Physiol. Cell Physiol.* 292:C2288–C2296. <https://doi.org/10.1152/ajpcell.00503.2006>
- Schmidt, S., I. Nakhbandi, R. Ruppert, N. Kawelke, M.W. Hess, K. Pfaller, P. Jurdic, R. Fässler, and M. Moser. 2011. Kindlin-3-mediated signaling from multiple integrin classes is required for osteoclast-mediated bone resorption. *J. Cell Biol.* 192:883–897. <https://doi.org/10.1083/jcb.201007141>
- Scholz, J., H. Besir, C. Strasser, and S. Suppmann. 2013. A new method to customize protein expression vectors for fast, efficient and background free parallel cloning. *BMC Biotechnol.* 13:12. <https://doi.org/10.1186/1472-6750-13-12>
- Shen, Y., G. Schneider, J.F. Cloutier, A. Veillette, and M.D. Schaller. 1998. Direct association of protein-tyrosine phosphatase PTP-PEST with paxillin. *J. Biol. Chem.* 273:6474–6481. <https://doi.org/10.1074/jbc.273.11.6474>
- Sun, Z., M. Costell, and R. Fässler. 2019. Integrin activation by talin, kindlin and mechanical forces. *Nat. Cell Biol.* 21:25–31. <https://doi.org/10.1038/s41556-018-0234-9>
- Tanaka, T., K. Moriwaki, S. Murata, and M. Miyasaka. 2010. LIM domain-containing adaptor, leupaxin, localizes in focal adhesion and suppresses the integrin-induced tyrosine phosphorylation of paxillin. *Cancer Sci.* 101:363–368. <https://doi.org/10.1111/j.1349-7006.2009.01398.x>
- Theodosiou, M., M. Widmaier, R.T. Böttcher, E. Rognoni, M. Veelders, M. Bharadwaj, A. Lambacher, K. Austen, D.J. Müller, R. Zent, and R. Fässler. 2016. Kindlin-2 cooperates with talin to activate integrins and induces cell spreading by directly binding paxillin. *eLife.* 5:e10130. <https://doi.org/10.7554/eLife.10130>
- Ussar, S., H.V. Wang, S. Linder, R. Fässler, and M. Moser. 2006. The Kindlins: subcellular localization and expression during murine development. *Exp. Cell Res.* 312:3142–3151. <https://doi.org/10.1016/j.yexcr.2006.06.030>
- Vanarotti, M.S., D.B. Finkelstein, C.D. Guibao, A. Nourse, D.J. Miller, and J.J. Zheng. 2016. Structural Basis for the Interaction between Pyk2-FAT Domain and Leupaxin LD Repeats. *Biochemistry.* 55:1332–1345. <https://doi.org/10.1021/acs.biochem.5b01274>
- Webb, D.J., K. Donais, L.A. Whitmore, S.M. Thomas, C.E. Turner, J.T. Parsons, and A.F. Horwitz. 2004. FAK-Src signalling through paxillin, ERK and MLCK regulates adhesion disassembly. *Nat. Cell Biol.* 6:154–161. <https://doi.org/10.1038/ncb1094>
- Zaidel-Bar, R., S. Itzkovitz, A. Ma'ayan, R. Iyengar, and B. Geiger. 2007. Functional atlas of the integrin adhesome. *Nat. Cell Biol.* 9:858–867. <https://doi.org/10.1038/ncb0807-858>
- Zou, W., T. Izawa, T. Zhu, J. Chappel, K. Otero, S.J. Monkley, D.R. Critchley, B.G. Petrich, A. Morozov, M.H. Ginsberg, and S.L. Teitelbaum. 2013. Talin1 and Rap1 are critical for osteoclast function. *Mol. Cell Biol.* 33: 830–844. <https://doi.org/10.1128/MCB.00790-12>



# Supplemental material

Klapproth et al., <https://doi.org/10.1083/jcb.201903109>

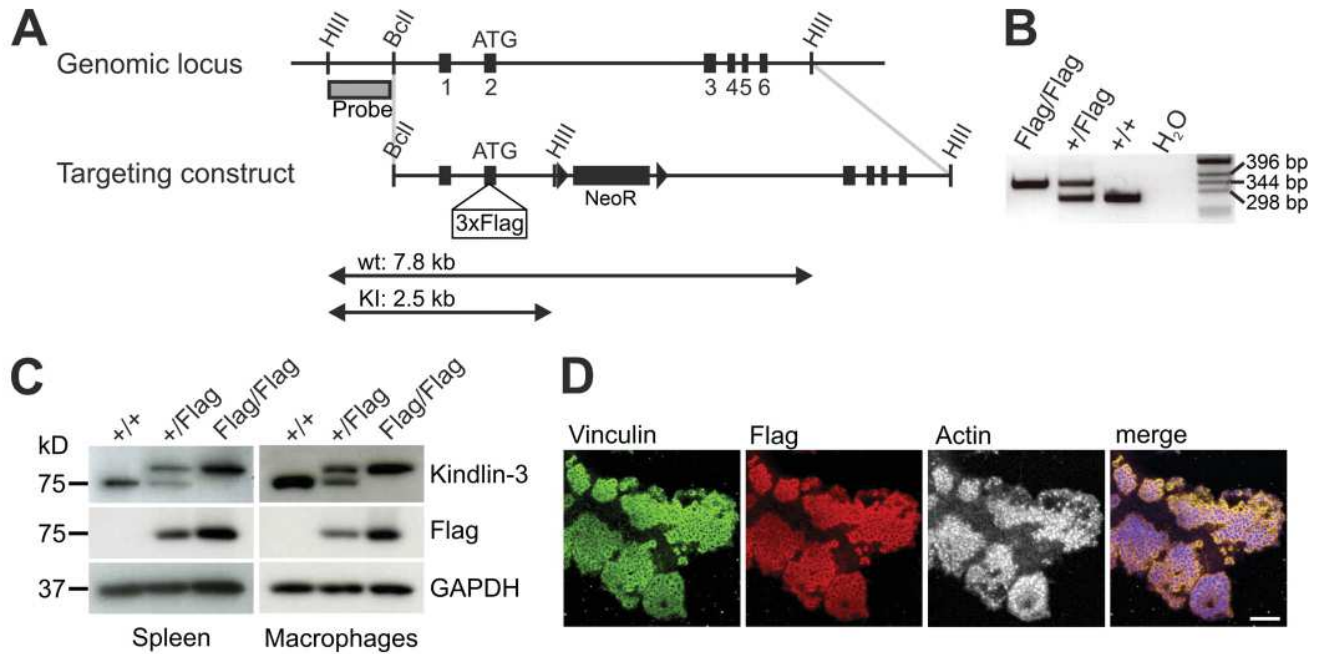
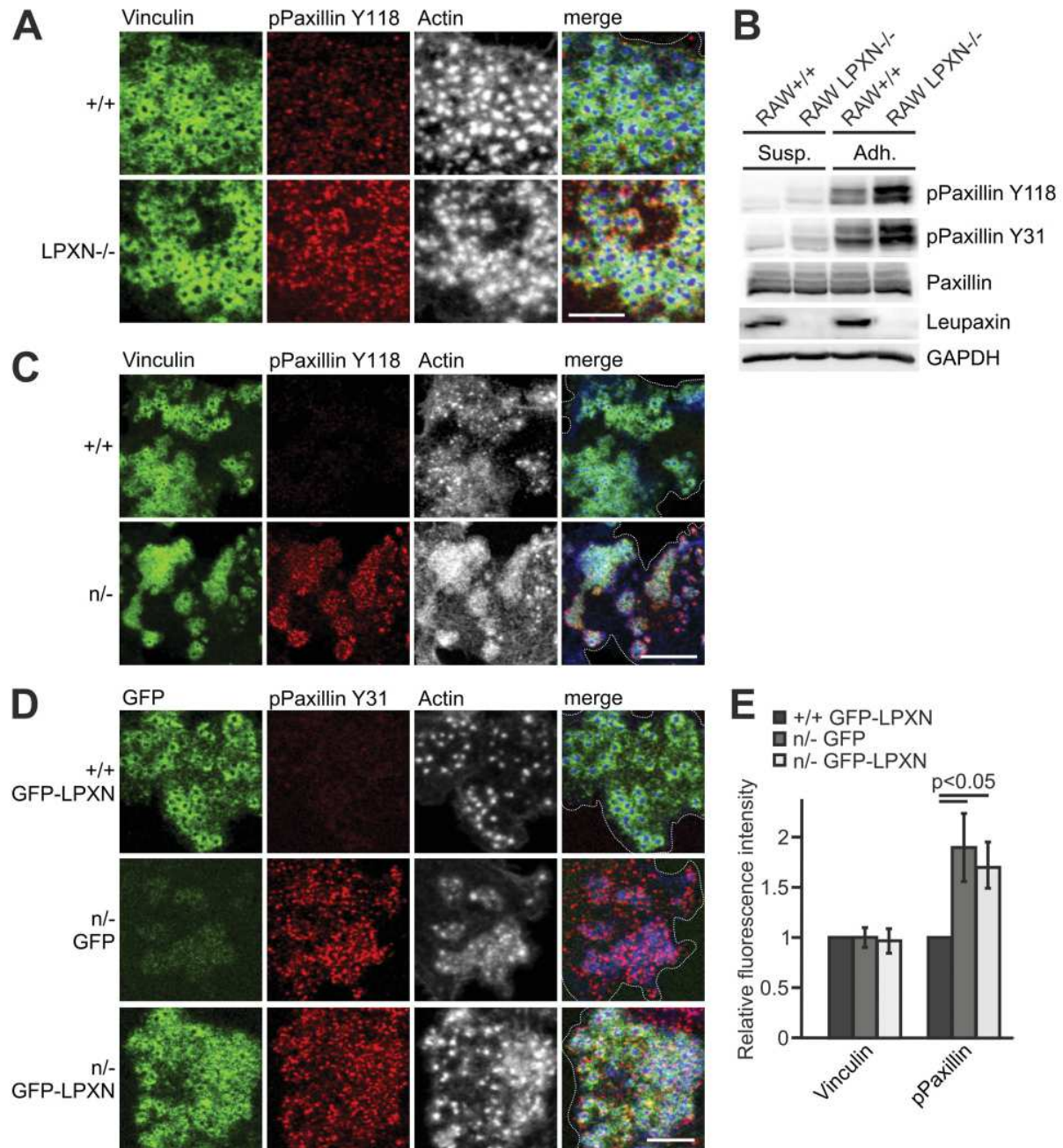


Figure S1. **Generation and characterization of Flag-tagged kindlin-3 knockin mice.** (A) Targeting strategy for the generation of mice expressing an N-terminally Flag-tagged version of kindlin-3, by targeting exon 2 of the endogenous kindlin-3 gene locus. (B) Genomic PCR for genotyping WT (+/+), heterozygous (+/Flag) and homozygous (Flag/Flag) mutant animals. (C) Western blot analyses of lysates of spleen and bone marrow-derived macrophages from +/+, +/Flag, and Flag/Flag mice. (D) IF staining for vinculin (green), flag peptide (red), and actin (white/blue in merge) of Flag/Flag preosteoclasts. Scale bar, 10 μm.



**Figure S2. Loss of leupaxin podosomal localization results in reduced paxillin phosphorylation.** (A) Confocal images of +/+ RAW cells and leupaxin<sup>-/-</sup> RAW cells stained for vinculin (green), paxillin phosphorylated at Y118 (red), and actin (white/blue in merge). Scale bar, 5  $\mu$ m. (B) Analysis of paxillin phosphorylation in +/+ and leupaxin<sup>-/-</sup> RAW cells kept either in suspension (Susp.) or adherent (Adh.) to fibronectin assessed by probing Western blots for paxillin phosphorylated at Y31 or Y118, total paxillin, and leupaxin. (C) Confocal images of vinculin (green), Y118-phosphorylated paxillin (red), and actin (white/blue in merge) IF stainings of preosteoclasts derived from WT and K3<sup>n/-</sup> mice. Scale bar, 10  $\mu$ m. (D) Confocal images of +/+ preosteoclasts overexpressing GFP-tagged leupaxin and K3<sup>n/-</sup> preosteoclasts transduced with either GFP alone or GFP-tagged leupaxin stained for phosphorylated paxillin at Y31 (red) and actin (white/blue in merge). Scale bar, 5  $\mu$ m. (E) Quantification of vinculin level and paxillin phosphorylation at Y31 in podosomal clusters of +/+ and n/- preosteoclasts transduced with GFP or GFP-tagged leupaxin by measuring MFI of confocal images. Values of WT cells expressing GFP-leupaxin were set to 1.  $n = 4$ . Dotted white lines mark cell borders.



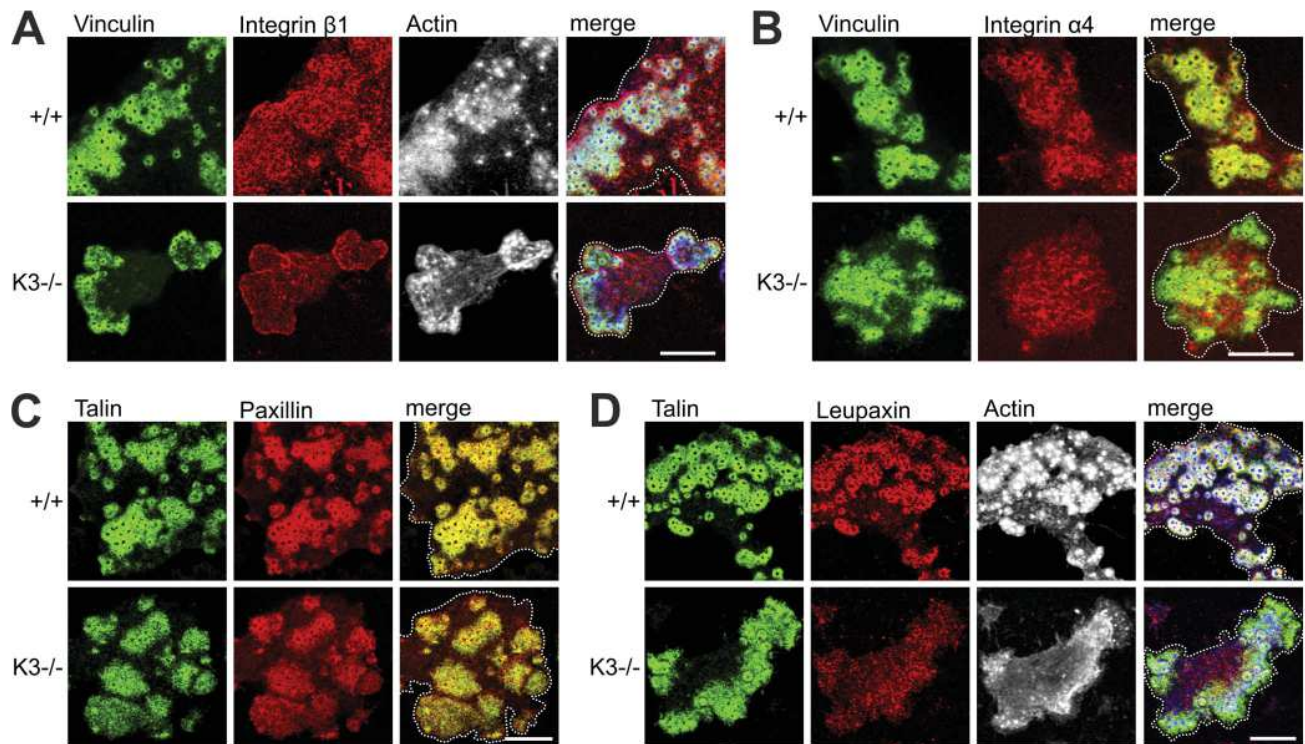
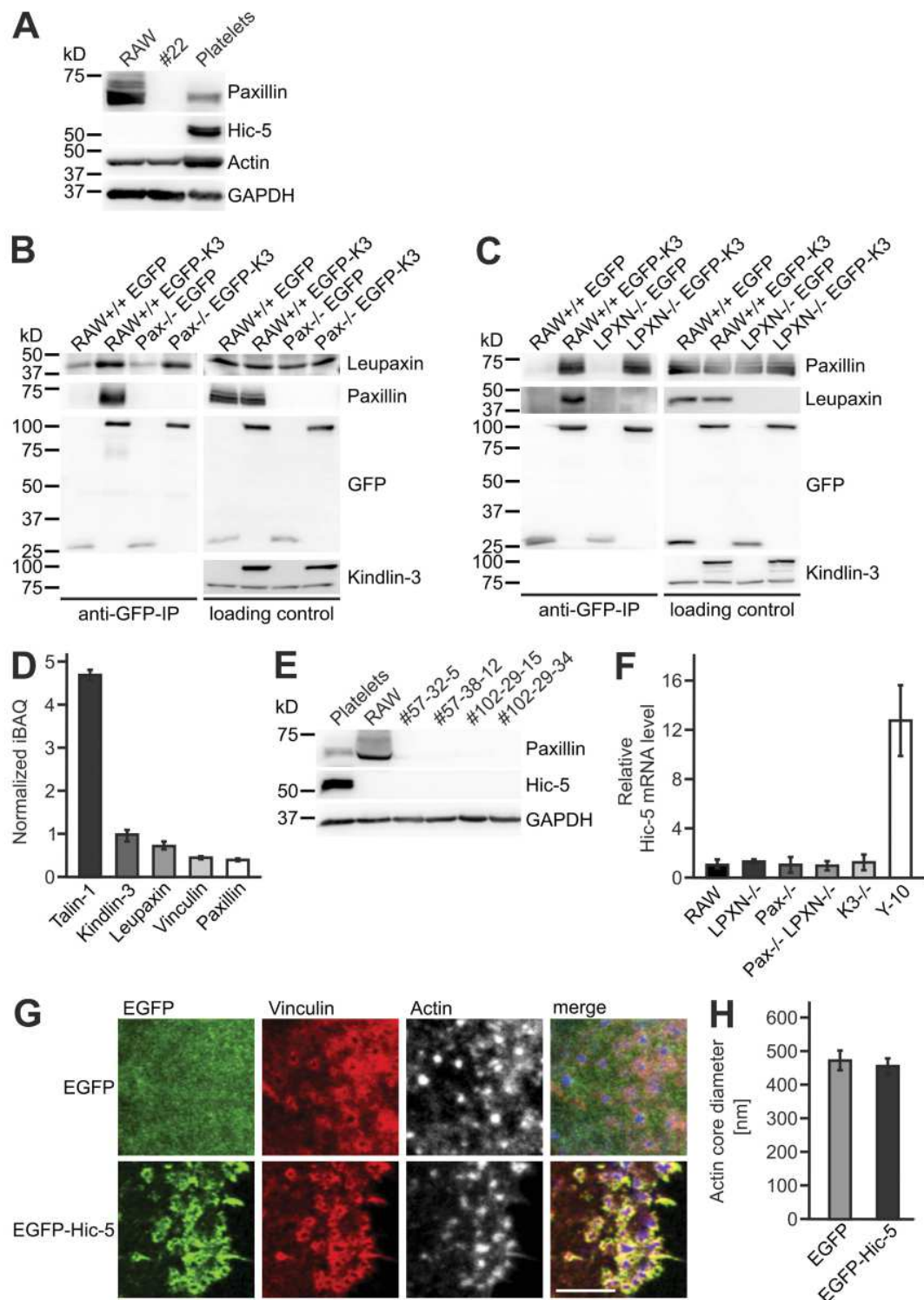


Figure S3. In contrast to the plaque proteins vinculin, talin, and paxillin,  $\beta 1$  and  $\alpha 4$  integrins are not recruited to adhesion patches of kindlin-3-deficient preosteoclasts. Confocal images of IF stainings for (A) vinculin (green), integrin  $\beta 1$  (red), and actin (white/blue in merge); (B) vinculin (green) and integrin  $\alpha 4$  (red); (C) talin (green) and paxillin (red); and (D) talin (green), leupaxin (red), and actin (white/blue in merge) in podosomes of K3<sup>+/+</sup> and K3<sup>-/-</sup> preosteoclasts. Scale bars, 10  $\mu$ m. Dotted white lines mark cell borders.



**Figure S4. Paxillin and leupaxin do not compete for kindlin-3 binding in RAW cells.** (A) Western blot analyses of  $+/+$ , paxillin $^{-/-}$  (#22) RAW cells, and platelets for paxillin and Hic-5 expression. Actin and GAPDH served as loading controls. (B) GFP-IP from lysates of  $+/+$  and paxillin $^{-/-}$  RAW cells expressing either EGFP or EGFP-K3 analyzed for leupaxin and paxillin binding. (C) GFP-IP from lysates of WT and leupaxin-deficient RAW cells expressing either EGFP or EGFP-K3 analyzed for paxillin and leupaxin binding. (D) Quantification of the protein abundance of talin-1, kindlin-3, leupaxin, paxillin, and vinculin in RAW cells by whole proteome mass spectrometry analyses. All values are given in relation to the amount of kindlin-3.  $n = 4$ . (E) Western blot analyses of platelets and  $+/+$  and different clones of paxillin/leupaxin dKO RAW cells for paxillin and Hic-5 expression. (F) Hic-5 mRNA level in  $+/+$ , leupaxin $^{-/-}$ , paxillin $^{-/-}$ , paxillin/leupaxin dKO, and K3 $^{-/-}$  RAW cells relative to GAPDH. WT controls were set to 1, and megakaryocyte precursor cell line Y-10 served as positive control.  $n = 4$ . (G) Confocal images of paxillin/leupaxin dKO RAW cells transfected with EGFP or EGFP-tagged Hic-5 stained for vinculin (red) and actin (white/blue in merge). Scale bar, 5  $\mu$ m. (H) Diameter of the podosomal actin cores in paxillin/leupaxin dKO RAW cells transfected with EGFP or EGFP-tagged Hic-5.  $n = 4$ .



Table S1. Key resources

Reagent type (species) or resource	Designation	Source or reference	Identifiers	Additional information
Genetic reagent ( <i>Mus musculus</i> )	K3 <sup>-/-</sup>	<a href="#">Moser et al., 2008</a>	RRID: MGI:2147790	R. Fässler (Max Planck Institute of Biochemistry)
Genetic reagent ( <i>M. musculus</i> )	K3 <sup>n/-</sup>	<a href="#">Klapproth et al., 2015</a>	RRID: MGI:3785479	R. Fässler
Antibody	Rabbit anti-actin	Sigma-Aldrich	Cat. no. A2066; RRID: AB_476693	WB (1:3,000)
Antibody	rabbit anti-cortactin	Cell Signaling Technology	Cat. no. 3502; RRID: AB_2115148	WB (1:1,000)
Antibody	Rabbit anti-phospho-Cortactin Y421	Cell Signaling Technology	Cat. no. 4569; RRID: AB_2276917	WB (1:1,000)
Antibody	Rabbit anti-FAK	Cell Signaling Technology	Cat. no. 3285; RRID: AB_2269034	WB (1:1,000)
Antibody	Rabbit anti-phospho-FAK Y397	Cell Signaling Technology	Cat. no. 3283S; RRID: AB_2173659	WB (1:1,000)
Antibody	Mouse anti-FLAG M2-Cy3	Sigma-Aldrich	Cat. no. A9594; RRID: AB_439700	IF (1:500)
Antibody	Mouse anti-GAPDH	Merck Millipore	Cat. no. CB1001; RRID: AB_2107426	WB (1:20,000)
Antibody	Mouse anti-GFP	Homemade cell culture supernatant		WB (1:3)
Antibody	Mouse anti-Hic-5	BD Biosciences	Cat. no. 611164; RRID: AB_398702	WB (1:500)
Antibody	Rabbit anti-His-tag	Cell Signaling Technology	Cat. no. 2365; RRID: AB_2115720	WB (1:1,000)
Antibody	Alexa Fluor 488-conjugated anti-mouse IgG	Thermo Fisher Scientific	Cat. no. A-11001; RRID: AB_2534069	IF (1:300)
Antibody	Alexa Fluor 546-conjugated anti-mouse IgG	Thermo Fisher Scientific	Cat. no. A-11003; RRID: AB_2534071	IF (1:300)
Antibody	Alexa Fluor 488-conjugated anti-rabbit IgG	Thermo Fisher Scientific	Cat. no. A-11034; RRID: AB_2576217	IF (1:300)
Antibody	Alexa Fluor 546-conjugated anti-rabbit IgG	Thermo Fisher Scientific	Cat. no. A-11010; RRID: AB_2534077	IF (1:300)
Antibody	Alexa Fluor 546-conjugated anti-rat IgG	Thermo Fisher Scientific	Cat. no. A-11081; RRID: AB_2534125	IF (1:300)
Antibody	IgG1 isotype control from murine myeloma	Sigma-Aldrich	Cat. no. M5284-1MG; RRID: AB_1163685	IP (5 µg)
Antibody	Anti-integrin α4-PE	BD Pharmingen	Cat. no. 553157; RRID: AB_394670	IF (1:100)
Antibody	Anti-integrin αV-PE	BD Pharmingen	Cat. no. 551187; RRID: AB_394088	IF (1:100)
Antibody	Anti-integrin β1	R. Fässler (Max Planck Institute of Biochemistry)		IF (1:5,000)
Antibody	Anti-integrin β3-PE	eBioscience	Cat. no. 12-0611-81; RRID: AB_465717	IF (1:100)
Antibody	Rabbit anti-kindlin-3	Markus Moser (Max Planck Institute of Biochemistry)		IF (1:100), WB (1:3,000)
Antibody	Mouse anti-leupaxin	Abcam	Cat. no. ab181621	IF (1:100), WB (1:1,000)
Antibody	Mouse anti-paxillin	Thermo Fisher Scientific	Cat. no. 610051; RRID: AB_397463	WB (1:5,000), IP (5 µg)
Antibody	Rabbit anti-paxillin	Abcam	Cat. no. ab32084; RRID: AB_779033	IF (1:300)

Table S1. Key resources (Continued)

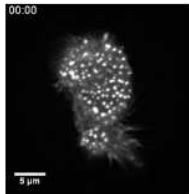
Reagent type (species) or resource	Designation	Source or reference	Identifiers	Additional information
Antibody	Rabbit anti-paxillin Y31	Thermo Fisher Scientific	Cat. no. 44-720G; RRID: AB_2533732	IF (1:100), WB (1:1,000)
Antibody	Rabbit anti-paxillin Y118	Thermo Fisher Scientific	Cat. no. 44-722G; RRID: AB_1501919	IF (1:100), WB (1:1,000)
Antibody	Mouse anti-PTP-PEST	Thermo Fisher Scientific	Cat. no. MA1-12377; RRID: AB_2175233	IF (1:100), WB (1:1,000)
Antibody	Rabbit anti-Pyk2	Cell Signaling Technology	Cat. no. 3292; RRID: AB_2174097	WB (1:1,000)
Antibody	Rabbit anti-phospho-Pyk2 Y402	Cell Signaling Technology	Cat. no. 3291; RRID: AB_2300530	WB (1:1,000)
Antibody	Anti-p-tyrosine (pY99)	Santa Cruz Biotechnology	Cat. no. sc-7020; RRID: AB_628123	IF (1:50)
Antibody	Mouse anti-talin	Sigma-Aldrich	Cat. no. T3287; RRID: AB_477572	WB (1:20,000)
Antibody	Rabbit anti-talin1	Abcam	Cat. no. ab71333; RRID: AB_2204002	IF (1:250)
Antibody	Mouse anti-vinculin	Sigma-Aldrich	Cat. no. V9131; RRID: AB_477629	IF (1:500)
Peptide, recombinant protein	GeneArt Platinum Cas9 Nuclease (3 µg/µL)	Thermo Fisher Scientific	Cat. no. B25641	
Peptide, recombinant protein	Fibronectin bovine plasma	Merck Millipore	Cat. no. 341631	5 µg/ml
Peptide, recombinant protein	Gelatin from pig skin, Oregon Green 488 Conjugate	Thermo Fisher Scientific	Cat. no. G13186	10 µg/ml
Peptide, recombinant protein	Recombinant mouse TNF-α	R&D Systems	Cat. no. 410-MT	2 µg/ml
Commercial assay or kit	µMACS GFP Isolation Kit	Miltenyi	Cat. no. 130-091-125	
Commercial assay or kit	µMACS DYKDDDDK Isolation Kit	Miltenyi	Cat. no. 130-101-591	
Commercial assay or kit	Mouse Macrophage Nucleofactor Kit	Lonza	Cat. no. VAPA-1009	
Commercial assay or kit	Glutathione Magnetic Agarose Beads	Jena Bioscience	Cat. no. AC-605-5	
Commercial assay or kit	Pierce Protein A/G Magnetic beads	Thermo Fisher Scientific	Cat. no. 88802	
Commercial assay or kit	PureCube 100 INDIGO Ni-Agarose beads	Cube Biotech	Cat. no. 75103	
Commercial assay or kit	GeneArt Precision gRNA Synthesis Kit	Thermo Fisher Scientific	Cat. no. A29377	
Commercial assay or kit	Neon Transfection System 10 µl Kit	Thermo Fisher Scientific	Cat. no. MPK1096	
Commercial assay or kit	Lipofectamine LTX Reagent with PLUS Reagent	Thermo Fisher Scientific	Cat. no. A12621	
Commercial assay or kit	Lipofectamine 3000 Transfection Reagent	Thermo Fisher Scientific	Cat. no. L3000015	
Commercial assay or kit	RNeasy Mini Kit	Qiagen	Cat. no. 74104	
Commercial assay or kit	iScript cDNA Synthesis Kit	Bio-Rad	Cat. no. 1708890	
Commercial assay or kit	iQ SYBR Green Supermix	Bio-Rad	Cat. no. 1708880	
Chemical compound, drug	M-CSF	Tebu-bio	Cat. no. 315-02-B	
Chemical compound, drug	Alexa Fluor 647 phalloidin	Thermo Fisher Scientific	Cat. no. A22287; RRID: AB_2620155	IF (1:40)
Chemical compound, drug	RANKL	Tebu-bio	Cat. no. 315-11-B	
Software, algorithm	GraphPad Prism	GraphPad	RRID:SCR_002798	



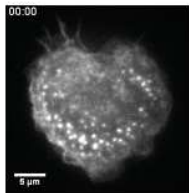
Table S1. Key resources (Continued)

Reagent type (species) or resource	Designation	Source or reference	Identifiers	Additional information
Software, algorithm	ImageJ	National Institutes of Health	RRID:SCR_003070	
Software, algorithm	Photoshop	Adobe	RRID:SCR_014199	
Other	Glass Bottom Microwell Dishes	MatTek Corporation	Cat. no. P35G-15-20-C	

WB, Western blot; PMID, PubMed ID; RRID, Research Resource identifiers.



Video 1. Time-lapse video of a WT preosteoclast expressing LifeAct-GFP acquired with a custom-made spinning disc confocal microscope. Pictures were taken every 15 s for 5 min.



Video 2. Time-lapse video of a K3<sup>N/-</sup> preosteoclast expressing LifeAct-GFP acquired with a custom-made spinning disc confocal microscope. Pictures were taken every 15 s for 5 min.

## References

- Klapproth, S., F.A. Moretti, M. Zeiler, R. Ruppert, U. Breithaupt, S. Mueller, R. Haas, M. Mann, M. Sperandio, R. Fässler, and M. Moser. 2015. Minimal amounts of kindlin-3 suffice for basal platelet and leukocyte functions in mice. *Blood*. 126:2592–2600. <https://doi.org/10.1182/blood-2015-04-639310>
- Moser, M., B. Nieswandt, S. Ussar, M. Pozgajova, and R. Fässler. 2008. Kindlin-3 is essential for integrin activation and platelet aggregation. *Nat. Med.* 14: 325–330. <https://doi.org/10.1038/nm1722>



## SHORT REPORT

# Rap1 and membrane lipids cooperatively recruit talin to trigger integrin activation

Thomas Bromberger<sup>1,\*</sup>, Liang Zhu<sup>2,\*</sup>, Sarah Klapproth<sup>1</sup>, Jun Qin<sup>2,‡</sup> and Markus Moser<sup>1,3,‡</sup>

## ABSTRACT

Recruitment and tethering of talin to the plasma membrane initiate the process of integrin activation. Multiple factors including the Rap1 proteins, RIAM (also known as APBB1IP) and PIP<sub>2</sub> bind talin proteins and have been proposed to regulate these processes, but not systematically analyzed. By expressing specific talin mutants into talin-null fibroblasts, we show that binding of the talin F0 domain to Rap1 synergizes with membrane lipid binding of the talin F2 domain during talin membrane targeting and integrin activation, whereas the interaction of the talin rod with RIAM was dispensable. We also characterized a second Rap1-binding site within the talin F1 domain by detailed NMR analysis. Interestingly, while talin F1 exhibited significantly weaker Rap1-binding affinity than talin F0, expression of a talin F1 Rap1-binding mutant inhibited cell adhesion, spreading, talin recruitment and integrin activation similarly to the talin F0 Rap1-binding mutant. Moreover, the defects became significantly stronger when both Rap1-binding sites were mutated. In conclusion, our data suggest a model in which cooperative binding of Rap1 to the talin F0 and F1 domains synergizes with membrane PIP<sub>2</sub> binding to spatiotemporally position and activate talins to regulate integrin activity.

**KEY WORDS:** Integrin, Small GTPase, Rap1, Talin, RIAM, NMR

## INTRODUCTION

Integrins are heterodimeric transmembrane receptors that mediate strong adhesion of cells to the extracellular matrix or other cells by connecting the extracellular ligand with the intracellular actin cytoskeleton. The formation of integrin adhesion complexes is either initiated by the extracellular ligand or by intracellular integrin activators such as talins that induce the conformational change of the integrin's extracellular domain towards a high affinity state for ligand binding.

Talin1 and talin2 are large (270 kDa) cytoplasmic adapter proteins consisting of an N-terminal 4.1 protein, ezrin, radixin, moesin (FERM)-like head domain, which binds the cytoplasmic domain of  $\beta$  integrin subunits, and a long C-terminal rod domain forming multiple connections with the actin cytoskeleton (Calderwood et al., 2013; Klapholz and Brown, 2017). In resting cells, a large portion of talin proteins (talin hereafter) reside in the

cytoplasm in a closed, auto-inhibited conformation (Banno et al., 2012; Goult et al., 2013), in which intramolecular interactions between the head and rod domains prevent integrin binding (Goksoy et al., 2008; Goult et al., 2009; Zhang et al., 2016). Upon stimulation, talin is efficiently recruited to the plasma membrane and released from its auto-inhibitory conformation to trigger integrin activation. However, the molecular mechanisms behind these crucial events are not fully understood.

Previous studies have suggested that talin-mediated integrin activation is highly dependent on the membrane-anchored small GTPase Rap1 protein family (Bos, 2005; Caron et al., 2000; Katagiri et al., 2000; Reedquist et al., 2000; Sebzda et al., 2002; Han et al., 2006). One model has suggested that talin membrane recruitment is triggered via the Rap1 effector RIAM (also known as APBB1IP), which binds the talin rod domain and thereby links it to the plasma membrane (Lagarrigue et al., 2016; Lee et al., 2009). However, this Rap1–RIAM–talin pathway is only crucial for leukocyte  $\beta 2$  integrin activation, but dispensable for integrin regulation in other cells such as platelets (Klapproth et al., 2015; Stritt et al., 2015; Su et al., 2015). We recently identified a direct 'Rap1–talin' membrane targeting pathway to regulate integrin activity in mammals, which was previously observed in *Dictyostelium discoideum* (Plak et al., 2016; Zhu et al., 2017). The physiological relevance of this pathway was subsequently demonstrated in mice and flies by us and others (Bromberger et al., 2018; Camp et al., 2018). However, while mutant flies that are deficient in Rab1 binding show embryonic lethality, a phenotype resembling that of talin-null mutants (Brown et al., 2002), Rap1-binding mutant mice comprising a talin knockin showed rather mild integrin defects in leukocytes and platelets (Bromberger et al., 2018). In particular, the weak platelet phenotype, when compared to that of mice in which both genes encoding Rap1 proteins (*Rap1a/b*) or *talin1* were genetically deleted in platelets (Nieswandt et al., 2007; Stefanini et al., 2018), suggests that the interaction mode between talin and Rap1 proteins (Rap1 hereafter) is more complex in mammals. Consistent with this assumption, a recent study suggested that talin F1 also binds to Rap1 and plays a major role in regulating integrin activation in CHO cells (Gingras et al., 2019). However, the physiological relevance of this interaction and how F0 and F1 are coordinated for Rap1 binding remained unsolved. Besides, interaction of talin with negatively charged membrane lipids (in particular PIP<sub>2</sub>) contributes to membrane tethering and activation of talin. Specifically, a helical loop in the F1 domain as well as positively charged patches in the F2 and F3 domains form electrostatic contacts with PIP<sub>2</sub> and stabilize talin at the plasma membrane (Goksoy et al., 2008; Goult et al., 2010; Martel et al., 2001; Saltel et al., 2009).

In this study, we investigated the relative contributions of different talin recruitment and/or activation factors to integrin activity in fibroblasts. Our results emphasize talin as a direct effector of Rap1, which binds to the talin F0 and F1 domains in a cooperative

<sup>1</sup>Max-Planck-Institute of Biochemistry, Department of Molecular Medicine, 82152 Martinsried, Germany. <sup>2</sup>Department of Cardiovascular & Metabolic Sciences, Lerner Research Institute, Cleveland Clinic, 9500 Euclid Ave., Cleveland, OH 44195, USA. <sup>3</sup>Center for Translational Cancer Research (TranslaTUM), TUM School of Medicine, Technische Universität München, 81675 Munich, Germany.

\*These authors contributed equally to this work

‡Authors for correspondence (qinj@ccf.org; m.moser@tum.de)

DOI: 10.1242/jcs.235531; L.Z., 0000-0002-6529-5706; S.K., 0000-0003-4723-056X; M.M., 0000-0001-8825-5566

Received 21 June 2019; Accepted 24 September 2019



manner and synergizes with membrane lipid PIP<sub>2</sub> to recruit and stabilize talin to/at the membrane to regulate integrin activity.

## RESULTS AND DISCUSSION

### Rap1 synergizes with PIP<sub>2</sub> to regulate talin-mediated integrin activation

To study the relative importance of different talin recruitment factors for integrin regulation, we used a previously established cell culture system of talin1 and talin2 double-deficient fibroblasts (talin<sup>1/2dKO</sup>), that allows reconstitution with wild-type (WT) and mutant talin to analyze integrin activity (Zhu et al., 2017). Cells were retrovirally transduced with constructs encoding C-terminally ypet-tagged talin fusion proteins, which carry mutations in the Rap1-binding site within the F0 domain (K15A/R35A, F0<sup>DM</sup>) (Bromberger et al., 2018; Zhu et al., 2017), the PIP<sub>2</sub>-binding domain in the F2 domain (K272A/K274A) (Song et al., 2012), or RIAM-binding sites in the talin rod domains R3 and R8 (V871Y/V1540Y) (Chang et al., 2014; Yang et al., 2014), as well as combined mutants carrying different combinations of these mutations (Fig. 1A). Cells expressing ypet-talin levels identical to endogenous talin protein levels of control cells (talin<sup>1<sup>fl</sup>/talin2<sup>-/-</sup>), were sorted and used for experiments (Fig. 1B,C). Note that all cell groups showed comparable surface integrin levels (Fig. 1C). We performed adhesion assays on the integrin ligands fibronectin (FN) and laminin-111. As expected, talin<sup>1/2dKO</sup> cells expressing ypet alone as a control hardly adhered to both ligands (Fig. 1D,E). Consistent with our previous study, Rap1-binding-deficient cells revealed an ~20% reduction in adhesion to both ligands compared to cells expressing WT talin (Zhu et al., 2017). The PIP<sub>2</sub>-binding mutant cells also showed a similar reduction in cell adhesion, confirming the role of PIP<sub>2</sub> in regulating integrin activation and cell adhesion. Interestingly, cells expressing a combined 'Rap1/PIP<sub>2</sub>' talin mutant showed further reduced adhesion on laminin-111, whereas loss of RIAM-binding to the talin rod had no impact on cell adhesion (Fig. 1D,E). Next, we plated the cells on FN and followed cell spreading for 2 h. While ypet-transduced talin<sup>1/2dKO</sup> cells remained roundish and did not spread, all talin variants rescued spreading but to a different extent. Cells expressing Rap1- or PIP<sub>2</sub>-binding mutants displayed a significant spreading defect, which was further exacerbated in combined mutants, whereas RIAM-binding mutants spread normally as cells expressing WT talin (Fig. 1F). Next, we wondered whether the reduced cell adhesion and spreading of Rap1- and PIP<sub>2</sub>-binding deficient cells are caused by impaired focal adhesion formation or integrin activation due to reduced talin recruitment. To this end, we seeded the cells on FN and investigated the formation of focal adhesions by quantification of paxillin-positive areas. Our measurements showed that the focal adhesion (FA) area per cell, the recruitment of talin to FAs (calculated by the ypet fluorescence intensity within FAs in correlation to the total cellular ypet fluorescence intensity), and the amount of active  $\beta$ 1 integrins within FAs (determined by staining with antibody clone 9EG7) were significantly reduced in Rap1- and PIP<sub>2</sub>-binding mutants compared to WT talin controls, whereas none of these parameters were affected in RIAM-binding mutants (Fig. 1G–I). Overall, these data indicate that Rap1 and PIP<sub>2</sub> act synergistically on talin membrane recruitment to regulate integrin activation, cell adhesion and spreading, while the interaction of the talin rod with RIAM is dispensable for these processes.</sup>

### The F1 domain of talin harbors a second Rap1-binding site

Both talin F0 and F1 domains form similar ubiquitin-like folds (Goult et al., 2010). Notably, the basic residues in the F0 domain,

which form critical contacts with Rap1 in *Dictyostelium*, *Drosophila* and mice (Bromberger et al., 2018; Camp et al., 2018; Plak et al., 2016; Zhu et al., 2017), are also conserved within the talin F1 domain (Fig. 2A). Although we did not detect an obvious interaction between Rap1 and a construct composed of the talin F1 and F2 domains (talin F1F2) in our previous study (Zhu et al., 2017), a recent study showed that Rap1 induced minor chemical shift changes of <sup>15</sup>N-labeled talin F1 (Gingras et al., 2019). To clarify this, we first compared the binding of talin F0 and F1 domains to Rap1 using heteronuclear single quantum coherence spectroscopy (HSQC). At relatively low Rap1 concentration (90  $\mu$ M, molar ratio between Rap1 and talin F0 or F1 is 2:1), the talin F0 domain showed effective binding to Rap1 but interaction between talin F1 and Rap1 was barely detectable (Fig. 2B,C), which was consistent with our previous observation (Zhu et al., 2017). However, an interaction became detectable when we used higher molar ratios between Rap1 and talin F1 domain (5:1). The addition of Rap1 induced chemical shift changes of multiple talin F1 residues but the overall spectral change of talin F1 was much smaller than that of talin F0 under the same conditions (Fig. 2D,E), suggesting a weaker affinity of Rap1 to talin F1 than to talin F0 domain. Indeed, HSQC-based competition experiments revealed a  $K_i$  of talin F1 of 1.06 mM, which is three times weaker than that of talin F0 ( $K_i$ =0.35 mM) (Fig. 2F). By contrast, the interaction is indeed specific, as double mutations in talin F1 (K98A, R118A; F1<sup>DM</sup>) that mimic those of talin F0 (K15A, R35A; F0<sup>DM</sup>) abolished Rap1 binding (Fig. 2G). Like the F0 domain, talin F1 also binds Rap1 in a GTP-dependent manner, as evidenced in Fig. 2H showing that Rap1 loaded with GDP induced smaller chemical shift changes of <sup>15</sup>N-labeled talin F1 than active Rap1 loaded with GMP-PNP.

Since the talin head domain adopts a linear conformation where the F1 is sandwiched between the F0 and F2 domains, which may affect the binding of talin F1 domain to Rap1 (Elliott et al., 2010), we performed additional HSQC experiments. Fig. S1A,B clearly shows that the talin F0–Rap1 interaction is dominant at low concentration as the interaction between Rap1 and a construct composed of talin F0<sup>DM</sup> and the F1 domains (talin F0<sup>DM</sup>F1) was predominantly blocked. Consistently, talin F0<sup>DM</sup>F1 only interacts with Rap1 at high concentration, in a manner similar to the isolated F1 domain (Fig. S1C). The similar observation applied also to talin F1F2 (Fig. S1D,E). Taken together, these data suggest that the flanking F0 and F2 domains have negligible effects on the talin F1–Rap1 interaction, which is significantly weaker than the talin F0–Rap1 interaction.

### Rap1-binding at talin F0 and F1 domains acts synergistically on integrin activation

Next, we wondered whether the weak talin F1–Rap1 interaction also regulates talin-mediated integrin activity. We first generated C-terminally GFP-tagged talin head domain expression constructs carrying mutations in the F0 (TH-F0<sup>DM</sup>), the F1 (TH-F1<sup>DM</sup>) or in both domains (TH-F0<sup>DM</sup>F1<sup>DM</sup>) (Fig. 3A) and transfected them into  $\alpha$ IIb $\beta$ 3 integrin-expressing CHO-A5 cells to measure integrin activity using a conformation-specific anti-active human  $\alpha$ IIb $\beta$ 3 integrin (clone PAC1) antibody. Both TH-F0<sup>DM</sup> and TH-F1<sup>DM</sup> showed reduced integrin activation levels compared to WT control, however, cells expressing the F1 mutant showed a stronger defect despite the lower affinity of the F1 domain for Rap1 (Fig. 3B). Of note, the combined mutants showed no further reduction in integrin activation. These data are partially in line with the recent study from Gingras et al. (2019). To solve the discrepancies between the CHO cell-based assays and our previous studies in fibroblasts and mice



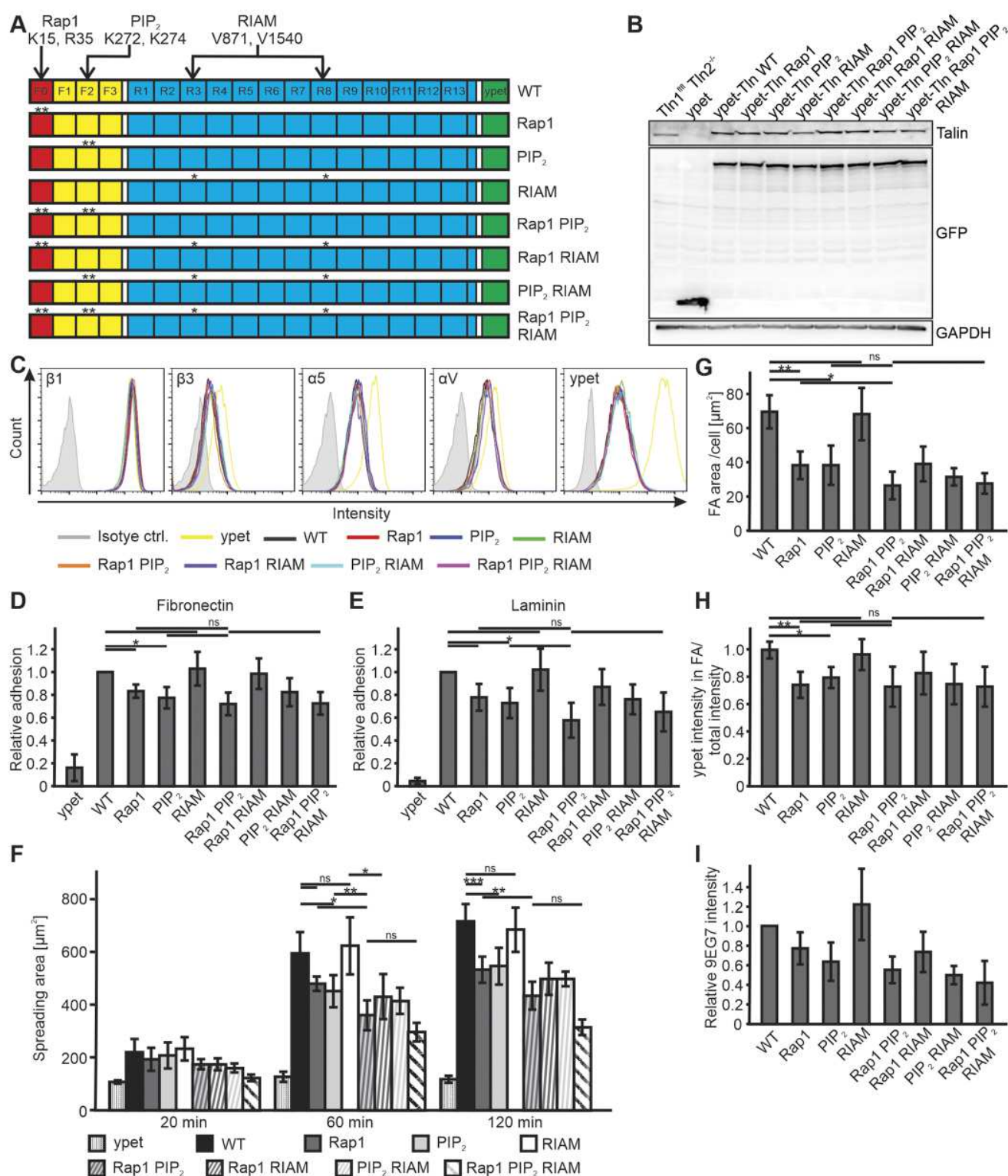


**Fig. 1. Rap1 and PIP<sub>2</sub> binding to talin regulate integrin activity in fibroblasts.** (A) Schematic overview of ypet-tagged talin variants for re-expression in talin<sup>1/2dKO</sup> fibroblasts. (B) Expression levels of talin variants assessed by western blotting. (C) FACS analysis of β1, β3, α5 and αV integrin surface levels and ypet intensity. (D,E) Relative adhesion of talin<sup>1/2dKO</sup> fibroblasts expressing ypet alone or ypet-tagged talin variants carrying the indicated mutations on fibronectin (D) and laminin (E) normalized to unspecific adhesion to poly-L-lysine. Values for cells expressing WT talin were set to 1 (n=8). (F) Spreading area of cells plated on fibronectin for 20, 60 and 120 min (n=6). (G–I) Quantitative analysis of immunofluorescence images of talin<sup>1/2dKO</sup> fibroblasts expressing various talin variants shown as focal adhesion area (G), ypet intensity in paxillin-positive areas relative to total cellular intensity (H) and intensity of anti-β1 integrin 9EG7 antibody signal within adhesion sites (I) (n=6). Data are presented as mean±95% CI. \*P<0.05; \*\*P<0.01; \*\*\*P<0.001; ns, not significant by one-way ANOVA followed by Sidak's multiple comparison test.



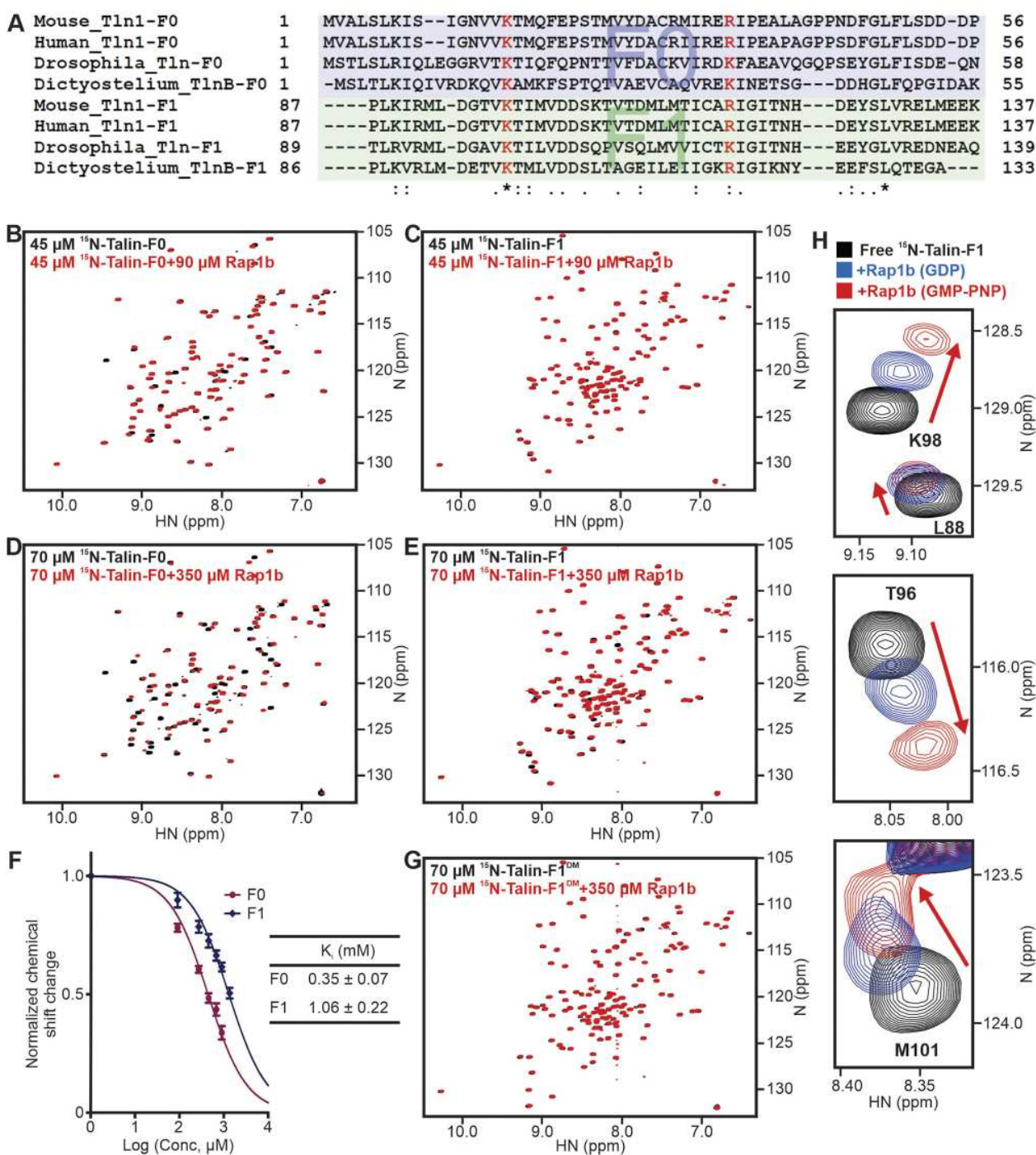


**Fig. 2. Rap1 interacts with both talin F0 and F1 domains in a GTP-dependent manner.** (A) Excerpt from the protein sequence alignment of mouse, human, *Drosophila* and *Dictyostelium* talin F0 and F1 domains. Conserved positively charged amino acids, corresponding to K15 and R35 in the murine talin F0 domain, are highlighted in red. '\*', ':' and '.' indicate conserved, highly and weakly similar residues, respectively. (B–E) HSQC spectra of 45  $\mu$ M  $^{15}$ N-labeled talin F0 (B) and 45  $\mu$ M  $^{15}$ N-labeled talin F1 (C) in the absence (black) and presence of 90  $\mu$ M GMP-PNP-loaded Rap1b (red), and 70  $\mu$ M  $^{15}$ N-labeled-talin F0 (D) and 70  $\mu$ M  $^{15}$ N-labeled-talin F1 (E) in the absence (black) and presence of 350  $\mu$ M GMP-PNP-loaded Rap1b (red). (F) HSQC-based competition experiment to compare the binding of Rap1 to talin F0 and F1. Data are presented as mean $\pm$ 95% CI. (G) HSQC spectra of 70  $\mu$ M  $^{15}$ N-labeled talin F1<sup>DM</sup> (K98A, R118A) in the absence (black) and presence of 350  $\mu$ M GMP-PNP-loaded Rap1b (red). (H) HSQC spectra (residues L88, K98, T96 and M101) of 70  $\mu$ M  $^{15}$ N-labeled talin F1 in the absence (black) and presence of 350  $\mu$ M GDP-loaded Rap1b (blue) or GMP-PNP loaded Rap1b (red).

(Zhu et al., 2017; Bromberger et al., 2018), we tested the relative importance of both Rap1-binding sites in our fibroblast system where full-length talin is expressed at physiological levels. Ypet-tagged full-length talin expression constructs carrying Rap1-

binding site mutations in the F0 (F0<sup>DM</sup>), the F1 (F1<sup>DM</sup>) or in both domains (F0<sup>DM</sup>F1<sup>DM</sup>), as well as talin constructs lacking the F0 domain in combination with WT or mutant F1 domains ( $\Delta$ F0 and  $\Delta$ F0F1<sup>DM</sup>) were retrovirally transduced into talin<sup>1/2dKO</sup> fibroblasts

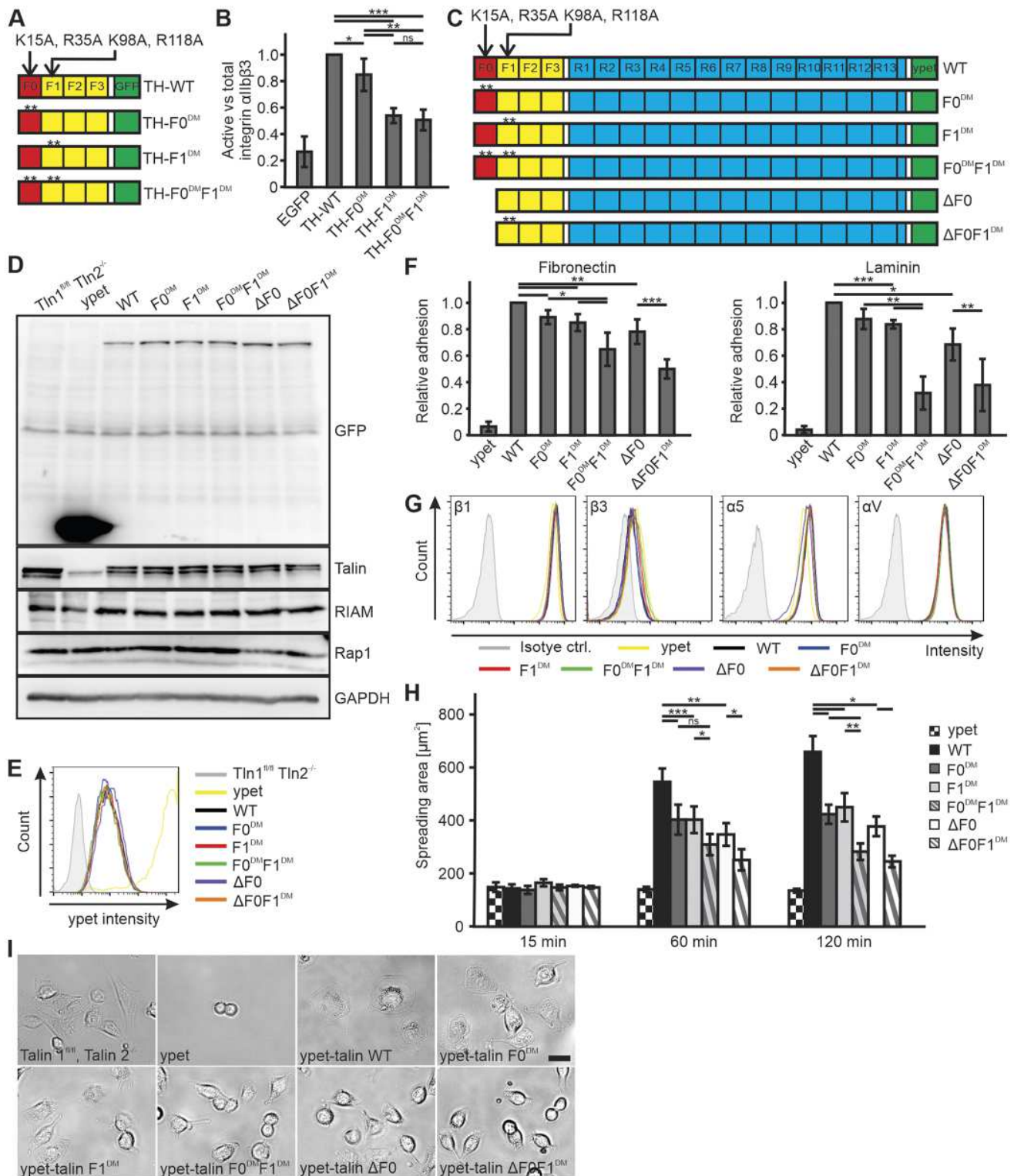


**Fig. 3. Binding of Rap1 to talin F0 and F1 domains synergize to promote cell adhesion and spreading.** (A) Overview of C-terminally EGFP-tagged talin head (TH) constructs. (B)  $\alpha$ IIb $\beta$ 3 integrin activation in CHO A5 cells expressing EGFP alone or EGFP-tagged TH variants assessed by FACS analysis of done PAC1 antibody binding. Values were normalized to  $\alpha$ IIb integrin surface levels. WT values were set to 1.  $n=5$ . (C) Schematic overview of ypet-tagged talin variants re-expressed in talin<sup>1/2dKO</sup> fibroblasts by retroviral transduction. (D) Western blot analyses of ypet-tagged talin variant-transduced cells for their expression of talin, RIAM and Rap1. (E) FACS analysis of ypet intensity in transduced cell lines. (F) Static adhesion of talin<sup>1/2dKO</sup> fibroblasts expressing ypet, ypet-tagged WT talin or variants on fibronectin and laminin. Values of WT talin-transduced cells were set to 1 ( $n=12/6$ ). (G) FACS analysis of  $\beta$ 1,  $\beta$ 3,  $\alpha$ 5 and  $\alpha$ V integrin surface levels in talin variant-transduced cells. (H) Spreading area of talin<sup>1/2dKO</sup> fibroblasts expressing ypet, ypet-talin WT and ypet-talin variants ( $n=6$ ). (I) Phase contrast images of talin<sup>1/2dKO</sup> cells and talin<sup>1/2dKO</sup> cells expressing talin variants. Scale bar: 25  $\mu$ m. Data are presented as mean $\pm$ 95% CI. \* $P<0.05$ ; \*\* $P<0.01$ ; \*\*\* $P<0.001$ ; ns, not significant by one-way ANOVA followed by Tukey's (PAC assay shown in B) or Sidak's (adhesion and spreading assays shown in F and H) multiple comparison tests.



and sorted for ypet levels that were identical to talin expression levels of control cells (Fig. 3C–E). Western blot analysis revealed normal Rap1 and RIAM expression in all groups (Fig. 3D). First, we performed cell adhesion assays on FN and laminin-111 and found that adhesion of F1<sup>DM</sup> cells to both integrin ligands was reduced by a similar level as in F0<sup>DM</sup> and  $\Delta$ F0 cells. Importantly, both double F0<sup>DM</sup>F1<sup>DM</sup> and  $\Delta$ F0F1<sup>DM</sup> mutants showed a further significant reduction in cell adhesion, indicating an additive effect (Fig. 3F). These alterations were not caused by changes in integrin surface expression levels (Fig. 3G). In line with impaired cell adhesion, F0<sup>DM</sup>, F1<sup>DM</sup> or  $\Delta$ F0 cells showed a comparable spreading defect, which was further exacerbated in F0<sup>DM</sup>F1<sup>DM</sup> and  $\Delta$ F0F1<sup>DM</sup> cells (Fig. 3H), where the spreading defects persisted and were visible in permanent cultures (Fig. 3I).

Furthermore, immunofluorescence staining (Fig. 4A) revealed that both FA area and number were strongly decreased in F0<sup>DM</sup> and F1<sup>DM</sup> cells and were even more dramatically reduced in combined mutant F0<sup>DM</sup>F1<sup>DM</sup> cells (Fig. 4B,C). Since most  $\Delta$ F0F1<sup>DM</sup> cells formed very low numbers of apparent FAs, we excluded cells that express talin mutants lacking the F0 domain from these analyses. Similarly, the recruitment of talin to paxillin-positive FAs was reduced to similar levels in F0<sup>DM</sup> and F1<sup>DM</sup> cells but was further diminished in F0<sup>DM</sup>F1<sup>DM</sup> cells (Fig. 4D). The same observation also applied to  $\beta$ 1 integrin activity (relative 9EG7:total  $\beta$ 1 integrin fluorescence intensity) within the adhesion sites (Fig. 4E). Taken together, these data strongly suggest that the two Rap1-binding sites act in a synergistic manner in regulating talin membrane recruitment, integrin activation and signaling, which significantly differs from the previous report (Gingras et al., 2019).

Although our study clearly shows that mutations in talin F0 and F1 domains block direct binding of Rap1, we cannot fully exclude that the mutations may affect binding of other Rap1-like small GTPases that additionally contribute to the integrin defects. To address this point, talin<sup>1/2dKO</sup> fibroblasts expressing WT and talin F0<sup>DM</sup>, F1<sup>DM</sup> or F0<sup>DM</sup>F1<sup>DM</sup> mutants were transfected with mCherry-tagged dominant-negative Rap1 (Rap1DN) or control plasmid. Cells were then plated on fibronectin for 1 h and the spreading areas were determined. Our data revealed that expression of Rap1DN strongly reduced spreading of WT, F0<sup>DM</sup> and F1<sup>DM</sup> cells to a similar level as observed in F0<sup>DM</sup>F1<sup>DM</sup> cells, but had little effect on spreading of Rap1-binding-deficient F0<sup>DM</sup>F1<sup>DM</sup> cells. These data suggest that talin-mediated integrin signaling is highly dependent on Rap1 (Fig. S2). Biochemically, we directly tested the small GTPases Rac1, Cdc42, RhoA and H-Ras, which are known for their roles in integrin signaling, for their interaction with the talin F0 and F1 domains by nuclear magnetic resonance (NMR) HSQC but found no obvious interaction for Rac1, Cdc42 or RhoA (Fig. S3A–F). Interestingly, while being highly homologous to Rap1, H-Ras barely interacted with talin F0 even at high concentration (Fig. S3G), but induced similar chemical shift changes of talin F1 as Rap1 did (Fig. S3H). Moreover, the chemical shift changes were also blocked by the double mutations in the talin F1 domain (Fig. S3I). Together with Fig. S3J,K, our data suggest that F0 is more selective than F1 in binding Rap1 GTPase, and H-Ras binding to F1 may play a compensatory or additive role to Rap1. This may explain the stronger defect of integrin activation caused by the F1 compared to the F0 talin head mutant in the overexpression-based CHO cell assay. More detailed investigations will be required to address this possibility in the future. Nonetheless, all evidence by us and others (Stefanini et al., 2018; Wynne et al., 2012) suggests that Rap1 is the major physiological GTPase involved in integrin activation.

In summary, our study provides a comprehensive analysis of how multiple factors cooperatively regulate talin-mediated integrin signaling.

First, while Rap1 and PIP<sub>2</sub> have been independently shown to be talin regulators (Han et al., 2006; Martel et al., 2001; Saltel et al., 2009), we showed here that Rap1 and PIP<sub>2</sub> synergize to promote potent integrin activation. We note that although only residues on talin F2 that interact with PIP<sub>2</sub> were studied, it is conceivable that additional contacts including a basic helical loop within the F1 domain and positively charged patches in the F3 domain, which both form electrostatic interactions with negatively charged membrane lipids, will further stabilize talin–membrane interactions (Elliott et al., 2010; Goult et al., 2010). These additional interactions are expected to contribute to the talin effect on integrin activation, which explains the modest synergistic effect of our Rap1/PIP<sub>2</sub> mutants. In contrast, the interaction of RIAM with the talin rod is dispensable for talin recruitment and integrin activity regulation in fibroblasts, which is consistent with the restricted function of RIAM in regulating leukocyte integrin activity (Klapproth et al., 2015; Stritt et al., 2015; Su et al., 2015). Although we cannot exclude the possibility that RIAM binding to the talin F3 domain is involved in talin activation (Yang et al., 2014), RIAM clearly plays a negligible role in talin membrane recruitment in the system we employed here.

Second, we have carefully characterized a second but weaker Rap1-binding site within the talin F1 domain, which shows a similar binding mode as the F0 domain. In a recent study, Gingras et al. (2019) used a CHO cell-based system and claimed that Rap1-binding to only F1 regulates integrin activation. They, thereby, supported their previous report, which suggested that the F0 domain does not contribute to Rap1-mediated integrin activation (Lagarigue et al., 2018). By using the same assay but a different mutation - i.e. one that causes a stronger defect in Rap1 binding - than the one inserted by Lagarigue et al. (2018), we did observe an integrin activation defect in F0 mutant cells, which was less strong compared to that in F1 mutant cells. However, data from this *in vitro* assay require careful interpretation as it relies on overexpression of an integrin, which is normally not expressed in this cell line, and a truncated talin lacking the regulatory rod domain. As mentioned above, the stronger defect caused by the F1 mutant in this CHO cell system could be simply due to the disruption of both Rap1 and H-Ras binding to talin F1. In sharp contrast, we employed a more physiological model system to show that interactions of both talin F0 and F1 domains with Rap1 are equally important and they cooperate to regulate talin membrane recruitment and integrin activity. Given that mice with deficient talin F0–Rap1 interaction showed mild phenotypes (Bromberger et al., 2018), it will be interesting to see whether the lower affinity interaction between Rap1 and talin F1 is also of physiological relevance *in vivo* and to what extent both Rap1 binding sites can compensate each other in a mutant mouse model.

How do the interactions of talin F0 and F1 domains with two Rap1 molecules cooperate during integrin activation? We previously observed that the direct interaction between Rap1 and full-length talin or the talin head domain at relatively low concentration resembles the talin F0–Rap1 interaction (Zhu et al., 2017). Together with our findings shown here that talin F1 binds more weakly than talin F0 to Rap1, we propose that talin F0 domain is likely to form initial contact with Rap1 to regulate talin membrane recruitment. This increases the chance of talin F1 binding to another Rap1. The two membrane-bridged Rap1s in Rap1-enriched microdomains would bind talin F0 and F1 with much higher affinity than talin F0 or talin



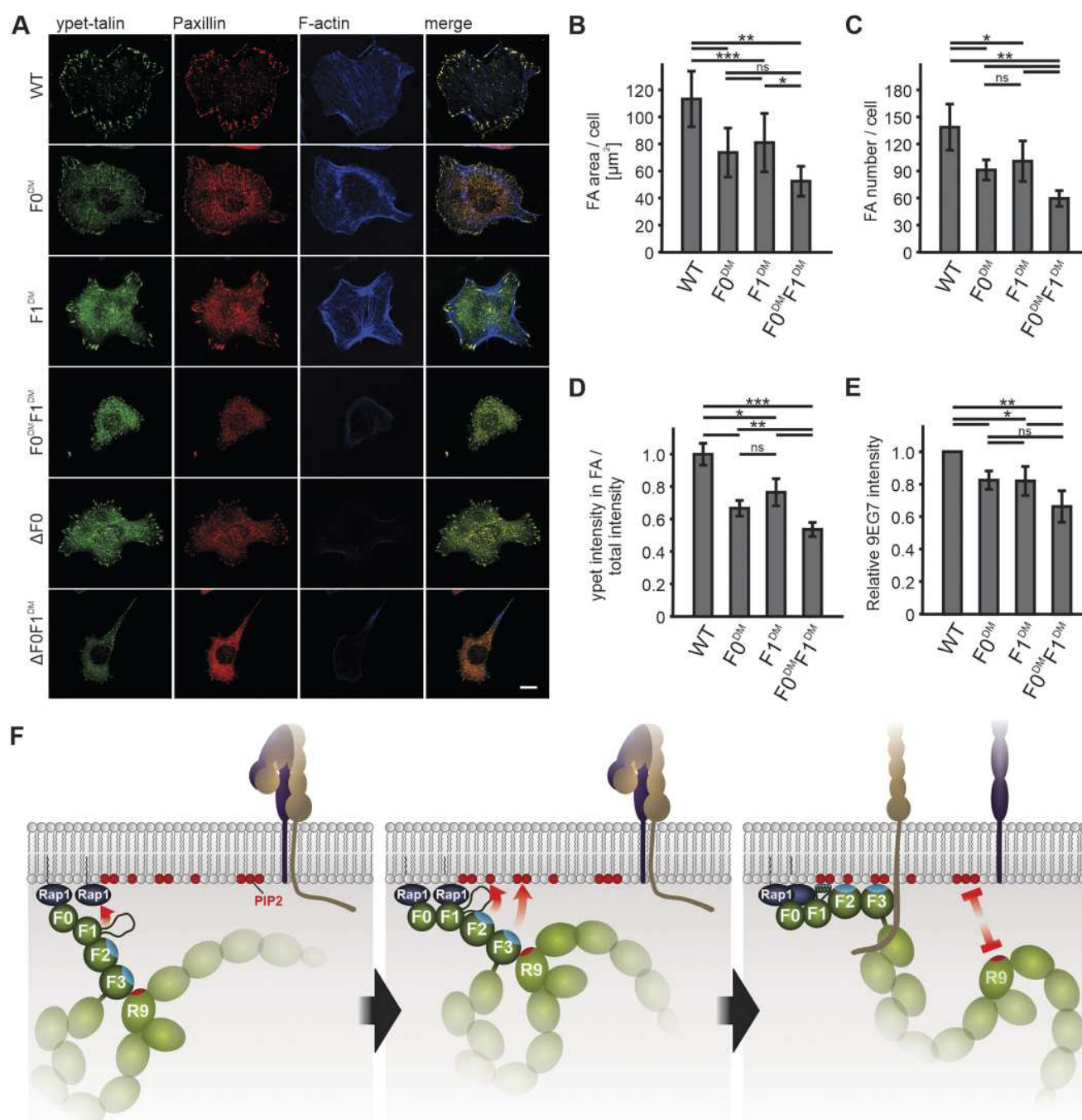


**Fig. 4.** Rap1 interactions with talin F0 and F1 domains facilitate talin recruitment and regulate integrin activity. (A) Confocal images of talin<sup>1/2dKO</sup> cells transduced with ypet-talin WT or indicated mutants (green) plated on fibronectin and stained for paxillin (red) and F-actin (blue). Scale bar: 10 μm. (B–E) In fibroblasts expressing ypet-tagged WT talin or ypet-talin variants, focal adhesion area (B) and number per cell (C) were measured (*n*=6). (D) ypet intensities measured within paxillin-positive areas were normalized to total cellular ypet fluorescence (*n*=6). (E) Ratio of active (done 9EG7 staining) to total β1 staining intensities within focal adhesions (*n*=6). Eight cells were analyzed per experiment and genotype. Data are presented as mean±95% CI. \**P*<0.05; \*\**P*<0.01; \*\*\**P*<0.001; ns, not significant by one-way ANOVA followed by Tukey's multiple comparison test. (F) Schematic illustration of the proposed model suggesting that talin1 (depicted in green) is recruited to adhesion sites by interaction with the small GTPase Rap1 via both binding sites in its F0 and F1 domain. Rap1 recruits talin to the membrane favorably via the talin F0 domain and further stabilizes the talin head domain at the membrane site by binding to the F1 domain and synergizing with PIP<sub>2</sub>–talin F1(loop)F2F3 interaction to trigger integrin activation and cell adhesion.

F1 alone, leading to a synergistic effect in talin membrane recruitment. Membrane tethering of talin is further strengthened by the presence of PIP<sub>2</sub>, which leads to strong talin activation, talin–integrin interaction and subsequent integrin activation (Fig. 4F).

Consistent with such a targeted recruitment mechanism of talin to Rap1-enriched microdomains, talin was found to be directly recruited to, but not laterally diffuse at, the membrane before it reaches the adhesion sites (Rossier et al., 2012).



## MATERIALS AND METHODS

### Cell culture and cell line generation

Talin1 and talin2 double knock-out (talin<sup>1/2dKO</sup>) cells (Theodosiou et al., 2016) were cultured and infected using the Phoenix cell system (Austen et al., 2013, 2015) as described earlier (Zhu et al., 2017). Briefly, talin<sup>1/2dKO</sup> fibroblasts were retrovirally transduced with pLPCX expression constructs containing either ypet alone or C-terminally ypet-tagged murine talin1 cDNA variants: WT talin1, Rap1- (K15A, R35A), PIP<sub>2</sub>- (K272A, K274A), or RIAM- (V871Y, V1540Y) binding-deficient single mutants, and double or triple mutant combinations accordingly for one set of experiments. For the second set of experiments, variants unable to bind Rap1 by the F0 domain (F0<sup>DM</sup>; K15A, R35A), F1 domain (F1<sup>DM</sup>; K98A, R118A) or both (F0<sup>DM</sup>F1<sup>DM</sup>; K15A, R35A, K98A, R118A), as well as mutants lacking the whole F0 domain with intact ( $\Delta$ F0) or mutant ( $\Delta$ F0F1<sup>DM</sup>) F1 Rap1-binding site were used. Cells were FACS-sorted to equal ypet intensity using a FACSaria IIIu cell sorter (BD Biosciences).

Talin<sup>1/2dKO</sup> cells expressing the various talin mutants were transfected with pmCherry-C1 or pmCherry-C1 Rap1aDN (dominant-negative S17N Rap1a mutant) using Lipofectamine 2000 (Thermo Fisher Scientific) following the manufacturer's protocol.

Generated cell lines were characterized by means of western blot following standard protocols. The following antibodies were used: mouse anti-GFP (in-house), mouse anti-talin (Sigma-Aldrich, T3287; 1:20,000), rabbit anti-RIAM (Abcam, 76090; 1:1000), rabbit anti-Rap1 (Santa Cruz Biotechnology, sc-65; 1:500), mouse anti-GAPDH (Merck Millipore, CB1001; 1:20,000), goat anti-mouse-HRP and goat anti-rabbit-HRP (Jackson ImmunoResearch Laboratories, 115-035-003 and 111-035-003; 1:15,000). Surface levels of relevant integrins were determined by FACS analysis using an LSRFortessa X-20 flow cytometer (BD Biosciences) as described earlier (Zhu et al., 2017). The following antibodies were used at a dilution of 1:200: Alexa Fluor 647 hamster IgM isotype control, Alexa Fluor 647 hamster anti-rat CD29, Alexa Fluor 647 hamster anti-mouse CD61, Alexa Fluor 647 rat anti-mouse CD49e and biotin rat anti-mouse CD51 (all BD Biosciences; 562110, 562153, 563523, 564312 and 551380), followed by Cy5-labeled streptavidin (Jackson ImmunoResearch Laboratories, 016-170-084; 1:500). FACS data were analyzed using FlowJo software.

All cells were cultured in DMEM GlutaMAX supplemented with 10% fetal bovine serum, 100 U ml<sup>-1</sup> penicillin, 100  $\mu$ g ml<sup>-1</sup> streptomycin, 2 mM L-glutamine and non-essential amino acids (all from Thermo Fisher Scientific) under standard conditions.

### PAC1 integrin activation assay

Wild-type talin head (amino acids 1–405) domain, talin head F0<sup>DM</sup>, F1<sup>DM</sup> and F0<sup>DM</sup>F1<sup>DM</sup> constructs were cloned into a pEGFP-N1 vector. CHO A5 cells, which express  $\alpha$ IIb $\beta$ 3 integrin (kind gift from Dr David Calderwood, Yale School of Medicine, New Haven, CT), were transiently transfected with empty pEGFP-N1 vector or indicated talin head constructs using Lipofectamine 2000. Integrin activation assays were performed one day after transfection. Briefly, cells were trypsinized and resuspended in Tyrode's buffer (136 mM NaCl, 0.43 mM NaH<sub>2</sub>PO<sub>4</sub>, 2.7 mM KCl, 12 mM NaHCO<sub>3</sub>, 5 mM HEPES, 0.1% glucose, 0.35% BSA; pH 7.35) supplemented with 2 mM CaCl<sub>2</sub> and 1 mM MgCl<sub>2</sub>. Cells were incubated with 0.4 mg ml<sup>-1</sup> RGDS peptide (Sigma-Aldrich) as negative control or left untreated for 10 min and subsequently incubated with Alexa Fluor 647 pre-labeled mouse anti-active human  $\alpha$ IIb $\beta$ 3 antibody (clone PAC1, Thermo Fisher Scientific, MA5-28523; 1:50) for 30 min at room temperature. The PAC1 antibody was labeled using an Alexa Fluor 647 Antibody Labeling Kit (Thermo Fisher Scientific) following the manufacturer's protocol prior to the experiments and stored at 4°C until use. After washing, cells were analyzed using an LSRFortessa X-20 flow cytometer. To assess total levels of  $\alpha$ IIb integrin, cells were stained with mouse anti-human CD41a (BD Biosciences, 555465; 1:200) or mouse IgG isotype control (eBioscience, 13-4714-85; 1:200) antibodies, and subsequently with donkey anti-mouse Alexa Fluor 647 antibody (Thermo Fisher Scientific, A31571; 1:200). To calculate integrin activation, the mean fluorescence intensity (MFI) of PAC1 that binds to RGDS-treated cells was subtracted from the MFI of PAC1 that binds to untreated cells and divided by the isotype control-corrected MFI of total  $\alpha$ IIb integrin [(MFI<sub>untreated</sub> – MFI<sub>RGDS</sub>)/(MFI <sub>$\alpha$ IIb</sub> – MFI<sub>isotype ctrl</sub>)]. Values obtained for cells transfected with WT talin head were set to 1.

### Adhesion and spreading assays

Adhesion and spreading assays were performed as described earlier (Zhu et al., 2017). Polystyrol flat-bottom 96-well microplates (Greiner Bio-One) were coated with 10  $\mu$ g ml<sup>-1</sup> laminin, 5  $\mu$ g ml<sup>-1</sup> fibronectin or 0.01% poly-L-lysine (both Sigma-Aldrich) in coating buffer (20 mM Tris-HCl pH 9.0, 150 mM NaCl, 2 mM MgCl<sub>2</sub>) overnight at 4°C for adhesion assays. After blocking with 3% BSA/PBS, 2.5  $\times$  10<sup>4</sup> cells were seeded per well in adhesion medium (DMEM containing 0.1% fetal bovine serum). Plates were washed with PBS after 1 h incubation and adherent cells subsequently fixed with 4% paraformaldehyde and stained with 5 mg/ml Crystal Violet in 2% ethanol. After washing, remaining cell-bound dye was solved in 2% SDS and absorbance was measured at 595 nm using a microplate reader (Tecan). Quadruplets were measured for all groups in each experiment. Results for fibronectin and laminin were normalized to values for poly-L-lysine.

Cell spreading areas were assessed 15, 60 and 120 min after plating the cells on fibronectin-coated dishes (5  $\mu$ g ml<sup>-1</sup> in coating buffer, overnight at 4°C). An EVOS FL Auto life cell microscope (Thermo Fisher Scientific) was used to take phase contrast pictures. Spreading area of 20 cells per group was measured in each experiment using ImageJ software (US National Institutes of Health).

### Immunostaining and confocal microscopy

Number and area of focal adhesions, talin recruitment and level of active  $\beta$ 1 integrin were assessed by immunofluorescence microscopy as previously described (Bromberger et al., 2018; Zhu et al., 2017). Cells were cultured on fibronectin-coated glass coverslips (Thermo Fisher Scientific) for 4 h and either fixed immediately or incubated with rat anti-active  $\beta$ 1 integrin antibody (clone 9EG7, BD Biosciences, 553715; 1:100 in PBS) for 30 min on ice and subsequently fixed with 4% paraformaldehyde. Cells were further stained with mouse anti-paxillin (BD Transduction, 610051; 1:300) and phalloidin-conjugated Alexa Fluor 647 (Thermo Fisher Scientific, A22287; 1:100) or, if pre-incubated with 9EG7 antibody, rabbit anti-total  $\beta$ 1 integrin (in-house, described in Azimifar et al., 2012; 1:5000). The following secondary antibodies were used: goat anti-mouse Alexa Fluor 546, goat anti-rat Alexa Fluor 546 and goat anti-rabbit Alexa Fluor 647 (all Thermo Fisher Scientific, A11003, A11081 and A21244; 1:300). Images were acquired using a Leica TCS SP5 X confocal microscope (Leica Microsystems) equipped with a 63 $\times$  NA 1.4 oil objective and processed with Photoshop (Adobe Systems). Quantitative image analyses were carried out with ImageJ software.

### Protein purification

The following constructs for bacterial expression were used in this study: mouse talin1-F0 domain (amino acids 1–86), talin1-F1 (83–202), talin1-F0F1 (1–206) and talin1-F1F2 (83–309) subcloned into pHis-1 vectors, and human Rap1b, human Rap1b (G12V) and human H-Ras (G12V) subcloned into pET28a vectors (Zhu et al., 2017). Human RhoA (1–193, Q63L) and Cdc42 (2–178, Q61L) subcloned into pET28a vectors, and human Rac-1 (2–192, Q61L) subcloned into a pET19b vector were kind gifts from Dr Matthias Buck at Case Western Reserve University, Cleveland, OH, USA. Construct mutagenesis was conducted by using QuikChange Lightning site-directed mutagenesis kit (Agilent Technologies). Mutated constructs generated in this study include talin1-F1\_DM (K98A, R118A) and talin1-F0F1\_DM (K15A, R35A). Each talin fragment was expressed in *E. coli* BL21 (DE3) strain, and <sup>15</sup>N isotope-labeled talin fragment expression was achieved by growing bacteria in minimal medium with <sup>15</sup>NH<sub>4</sub>Cl as the sole nitrogen source. Protein was purified using a nickel affinity column and then incubated with TEV protease to remove the recombinant N-terminal 6 $\times$ His-tag. Untagged protein was collected by means of flow through the nickel affinity column, and then subjected to gel filtration by using Superdex-75 (10/300 or 16/60, GE Healthcare), which was pre-equilibrated with buffer containing 20 mM NaH<sub>2</sub>PO<sub>4</sub>/Na<sub>2</sub>HPO<sub>4</sub> (pH 6.6), 50 mM NaCl and 2 mM dithiothreitol (DTT). Protein concentration was determined by measuring absorbance at 280 nm. All GTPases including Rap1b, Rap1b (G12V), H-Ras (G12V), Rac-1, RhoA and Cdc42 with N-terminal 6 $\times$ His tag were purified by nickel affinity column, followed by gel filtration using Superdex-75 (16/60, GE Healthcare). Purified wild-type Rap1b was loaded with guanosine 5'-[ $\beta$ -thio] diphosphate trilithium salt (GDP- $\beta$ -S, Sigma-Aldrich) and all other mutant GTPases were loaded with guanosine



5'-[ $\beta$ ,  $\gamma$ -imido] triphosphate trisodium salt (GMP-PNP, Sigma-Aldrich) for experimental use. Protein concentrations of all GTPases were measured using Pierce 660 nm protein assay reagent (Thermo Fisher Scientific).

# Nuclear magnetic resonance spectroscopy

2D-HSQC experiments were performed on a Bruker 600 MHz NMR spectrometer. Samples containing  $^{15}\text{N}$ -labeled talin fragment (WT or mutant) in the absence or presence of GDP- $\beta$ -S or GMP-PNP loaded GTPases were studied. Experiments were performed at 25°C in buffer containing 20 mM  $\text{NaH}_2\text{PO}_4/\text{Na}_2\text{HPO}_4$  (pH 6.6), 50 mM NaCl, 5 mM  $\text{MgCl}_2$ , 2 mM dithiothreitol (DTT) and 5%  $\text{D}_2\text{O}$ . For HSQC-based competition experiment, increasing amounts of unlabeled talin F0 or talin F1 were mixed with 45  $\mu\text{M}$   $^{15}\text{N}$ -labeled talin F0 in the presence of 90  $\mu\text{M}$  GMP-PNP-loaded Rap1b (G12V). Chemical shift changes of five selected residues (S9, I10, N12, K15, M17) of  $^{15}\text{N}$ -labeled talin F0 were calculated. Chemical shift change ( $\Delta\delta_{\text{obs}} [\text{HN}, \text{N}]$ ) of each residue was calculated with the equation  $\Delta\delta_{\text{obs}} [\text{HN}, \text{N}] = [(\Delta\delta_{\text{HN}} W_{\text{HN}})^2 + (\Delta\delta_{\text{N}} W_{\text{N}})^2]^{1/2}$  where  $\Delta\delta$  (ppm) =  $\delta_{\text{bound}} - \delta_{\text{free}}$  and  $W_{\text{HN}}$  and  $W_{\text{N}}$  are weighting factors,  $W_{\text{HN}} = 1$ ,  $W_{\text{N}} = 0.154$ . Chemical shift change of each residue was normalized to that observed in the initial sample containing only 45  $\mu\text{M}$   $^{15}\text{N}$ -labeled talin F0 and 90  $\mu\text{M}$  GMP-PNP-loaded Rap1b (G12V). The  $K_i$  was fitted by using 'One site - Fit  $K_i$ ' mode in GraphPad Prism.

# Protein sequence analyses

Sequences were aligned using the Clustal Omega multiple sequence alignment tool (Madeira et al., 2019).

# Statistical analysis

All data are presented as mean  $\pm$  95% confidence interval (CI). Prism 6 (GraphPad Software) was used for statistical analysis. The given sample size  $n$  represents the number of independent experiments. Differences between groups were considered statistically significant if  $P < 0.05$ . The degree of significance is indicated as follows in figures: \* $P < 0.05$ , \*\* $P < 0.01$ , \*\*\* $P < 0.001$ . One-way ANOVA followed by a Tukey's multiple comparison test was carried out to test for overall statistical significance, when each experimental condition was compared to every other condition. In cases in which only selected conditions were compared, one-way ANOVA followed by a Sidak's multiple comparison test was performed.

# Acknowledgements

We thank Reinhard Fässler (Max-Planck-Institute of Biochemistry, Martinsried, Germany) for providing us with talin1/2 double knockout fibroblasts.

# Competing interests

The authors declare no competing or financial interests.

# Author contributions

Conceptualization: J.Q., M.M.; Formal analysis: T.B., L.Z., S.K.; Investigation: T.B., L.Z., S.K.; Writing - original draft: J.Q., M.M.; Writing - review & editing: T.B., L.Z., S.K.; Visualization: T.B., L.Z.; Supervision: J.Q., M.M.; Funding acquisition: J.Q., M.M.

# Funding

This work was supported by the National Institutes of Health (NIH P01HL073311 to J.Q.), the Max-Planck-Gesellschaft and the Deutsche Forschungsgemeinschaft (SFB914 TP A01 to M.M.). Deposited in PMC for release after 12 months.

# Supplementary information

Supplementary information available online at <http://jcs.biologists.org/lookup/doi/10.1242/jcs.235531.supplemental>

# References

Austen, K., Kluger, C., Freikamp, A., Chrostek-Grashoff, A. and Grashoff, C. (2013). Generation and analysis of biosensors to measure mechanical forces within cells. *Methods Mol. Biol.* **1066**, 169-184. doi:10.1007/978-1-62703-604-7\_15  
Austen, K., Ringer, P., Mehlich, A., Chrostek-Grashoff, A., Kluger, C., Klingner, C., Sabass, B., Zent, R., Rief, M. and Grashoff, C. (2015). Extracellular rigidity sensing by talin isoform-specific mechanical linkages. *Nat. Cell Biol.* **17**, 1597-1606. doi:10.1038/ncb3268  
Azimifar, S. B., Bottcher, R. T., Zanivan, S., Grashoff, C., Kruger, M., Legate, K. R., Mann, M. and Fassler, R. (2012). Induction of membrane circular dorsal

ruffles requires co-signalling of integrin-ILK-complex and EGF receptor. *J. Cell Sci.* **125**, 435-448. doi:10.1242/jcs.091652  
Banno, A., Goult, B. T., Lee, H., Bate, N., Critchley, D. R. and Ginsberg, M. H. (2012). Subcellular localization of talin is regulated by inter-domain interactions. *J. Biol. Chem.* **287**, 13799-13812. doi:10.1074/jbc.M112.341214  
Bos, J. L. (2005). Linking Rap to cell adhesion. *Curr. Opin. Cell Biol.* **17**, 123-128. doi:10.1016/j.cob.2005.02.009  
Bromberger, T., Klapproth, S., Rohwedder, I., Zhu, L., Mittmann, L., Reichel, C. A., Sperandio, M., Qin, J. and Moser, M. (2018). Direct Rap1/Talin1 interaction regulates platelet and neutrophil integrin activity in mice. *Blood* **132**, 2754-2762. doi:10.1182/blood-2018-04-846766  
Brown, N. H., Gregory, S. L., Rickoll, W. L., Fessler, L. I., Prout, M., White, R. A. and Fristrom, J. W. (2002). Talin is essential for integrin function in Drosophila. *Dev. Cell* **3**, 569-579. doi:10.1016/S1534-5807(02)00290-3  
Calderwood, D. A., Campbell, I. D. and Critchley, D. R. (2013). Talins and kindlins: partners in integrin-mediated adhesion. *Nat. Rev. Mol. Cell Biol.* **14**, 503-517. doi:10.1038/nrm3624  
Camp, D., Haage, A., Solianova, V., Castle, W. M., Xu, Q. A., Lostchuck, E., Goult, B. T. and Tanentzapf, G. (2018). Direct binding of Talin to Rap1 is required for cell-ECM adhesion in Drosophila. *J. Cell Sci.* **131**, Jcs225144. doi:10.1242/jcs.225144  
Caron, E., Self, A. J. and Hall, A. (2000). The GTPase Rap1 controls functional activation of macrophage integrin  $\alpha\text{M}\beta 2$  by LPS and other inflammatory mediators. *Curr. Biol.* **10**, 974-978. doi:10.1016/S0960-9822(00)00641-2  
Chang, Y. C., Zhang, H., Franco-Barraza, J., Brennan, M. L., Patel, T., Cukierman, E. and Wu, J. (2014). Structural and mechanistic insights into the recruitment of talin by RIAM in integrin signaling. *Structure* **22**, 1810-1820. doi:10.1016/j.str.2014.09.020  
Elliott, P. R., Goult, B. T., Kopp, P. M., Bate, N., Grossmann, J. G., Roberts, G. C., Critchley, D. R. and Barsukov, I. L. (2010). The structure of the talin head reveals a novel extended conformation of the FERM domain. *Structure* **18**, 1289-1299. doi:10.1016/j.str.2010.07.011  
Gingras, A. R., Lagarrigue, F., Cuevas, M. N., Valadez, A. J., Zorovich, M., McLaughlin, W., Lopez-Ramirez, M. A., Seban, N., Ley, K., Kiosses, W. B. et al. (2019). Rap1 binding and a lipid-dependent helix in talin F1 domain promote integrin activation in tandem. *J. Cell Biol.* **218**, 1799-1809. doi:10.1083/jcb.201810061  
Goksoy, E., Ma, Y. Q., Wang, X., Kong, X., Perera, D., Plow, E. F. and Qin, J. (2008). Structural basis for the autoinhibition of talin in regulating integrin activation. *Mol. Cell* **31**, 124-133. doi:10.1016/j.molcel.2008.06.011  
Goult, B. T., Bate, N., Anthis, N. J., Wegener, K. L., Gingras, A. R., Patel, B., Barsukov, I. L., Campbell, I. D., Roberts, G. C. and Critchley, D. R. (2009). The structure of an interdomain complex that regulates talin activity. *J. Biol. Chem.* **284**, 15097-15106. doi:10.1074/jbc.M900078200  
Goult, B. T., Bouaouina, M., Elliott, P. R., Bate, N., Patel, B., Gingras, A. R., Grossmann, J. G., Roberts, G. C., Calderwood, D. A., Critchley, D. R. and et al. (2010). Structure of a double ubiquitin-like domain in the talin head: a role in integrin activation. *EMBO J.* **29**, 1069-1080. doi:10.1038/emboj.2010.4  
Goult, B. T., Xu, X. P., Gingras, A. R., Swift, M., Patel, B., Bate, N., Kopp, P. M., Barsukov, I. L., Critchley, D. R., Volkman, N. et al. (2013). Structural studies on full-length talin1 reveal a compact auto-inhibited dimer: implications for talin activation. *J. Struct. Biol.* **184**, 21-32. doi:10.1016/j.jsb.2013.05.014  
Han, J., Lim, C. J., Watanabe, N., Soriani, A., Ratnikov, B., Calderwood, D. A., Puzon-McLaughlin, W., Lafuente, E. M., Boussiotis, V. A., Shattil, S. J. and et al. (2006). Reconstructing and deconstructing agonist-induced activation of integrin  $\alpha\text{IIb}\beta 3$ . *Curr. Biol.* **16**, 1796-1806. doi:10.1016/j.cub.2006.08.035  
Katagiri, K., Hattori, M., Minato, N., Irie, S., Takatsu, K. and Kinashi, T. (2000). Rap1 is a potent activation signal for leukocyte function-associated antigen 1 distinct from protein kinase C and phosphatidylinositol-3-OH kinase. *Mol. Cell. Biol.* **20**, 1956-1969. doi:10.1128/MCB.20.6.1956-1969.2000  
Klappholz, B. and Brown, N. H. (2017). Talin - the master of integrin adhesions. *J. Cell Sci.* **130**, 2435-2446. doi:10.1242/jcs.190991  
Klapproth, S., Sperandio, M., Pinheiro, E. M., Prunster, M., Soehnlein, O., Gertler, F. B., Fassler, R. and Moser, M. (2015). Loss of the Rap1 effector RIAM results in leukocyte adhesion deficiency due to impaired beta2 integrin function in mice. *Blood* **126**, 2704-2712. doi:10.1182/blood-2015-05-647453  
Lagarrigue, F., Kim, C. and Ginsberg, M. H. (2016). The Rap1-RIAM-talin axis of integrin activation and blood cell function. *Blood* **128**, 479-487. doi:10.1182/blood-2015-12-638700  
Lagarrigue, F., Gingras, A. R., Paul, D. S., Valadez, A. J., Cuevas, M. N., Sun, H., Lopez-Ramirez, M. A., Goult, B. T., Shattil, S. J., Bergmeier, W. and Ginsberg, M. H. (2018). Rap1 binding to the talin F1 domain makes a minimal contribution to murine platelet GPIIb-IIIa activation. *Blood Adv* **2**, 2358-2368. doi:10.1182/bloodadvances.2018020487  
Lee, H. S., Lim, C. J., Puzon-McLaughlin, W., Shattil, S. J. and Ginsberg, M. H. (2009). RIAM activates integrins by linking talin to ras GTPase membrane-targeting sequences. *J. Biol. Chem.* **284**, 5119-5127. doi:10.1074/jbc.M807117200  
Madeira, F., Park, Y. M., Lee, J., Buso, N., Gur, T., Madhusoodanan, N., Basutkar, P., Tivey, A. R. N., Potter, S. C., Finn, R. D. et al. (2019). The EMBL-



- EBI search and sequence analysis tools APIs in 2019. *Nucleic Acids Res.* 47, 636–641. doi:10.1093/nar/gkz268
- Martel, V., Racaud-Sultan, C., Dupe, S., Marie, C., Paulhe, F., Galmiche, A., Block, M. R. and Albiges-Rizo, C. (2001). Conformation, localization, and integrin binding of talin depend on its interaction with phosphoinositides. *J. Biol. Chem.* 276, 21217–21227. doi:10.1074/jbc.M102373200
- Nieswandt, B., Moser, M., Pleines, I., Varga-Szabo, D., Monkley, S., Critchley, D. and Fassler, R. (2007). Loss of talin1 in platelets abrogates integrin activation, platelet aggregation, and thrombus formation in vitro and in vivo. *J. Exp. Med.* 204, 3113–3118. doi:10.1084/jem.20071827
- Plak, K., Pots, H., Van Haastert, P. J. and Kortholt, A. (2016). Direct interaction between TalinB and Rap1 is necessary for adhesion of Dictyostelium cells. *BMC Cell Biol.* 17, 1. doi:10.1186/s12860-015-0078-0
- Reedquist, K. A., Ross, E., Koop, E. A., Wolthuis, R. M., Zwartkruis, F. J., Van Kooyk, Y., Salmon, M., Buckley, C. D. and Bos, J. L. (2000). The small GTPase, Rap1, mediates CD31-induced integrin adhesion. *J. Cell Biol.* 148, 1151–1158. doi:10.1083/jcb.148.6.1151
- Rossier, O., Oceau, V., Sibarita, J. B., Leduc, C., Tessier, B., Nair, D., Gatterdam, V., Destaing, O., Albiges-Rizo, C., Tampé, R. et al. (2012). Integrins beta1 and beta3 exhibit distinct dynamic nanoscale organizations inside focal adhesions. *Nat. Cell Biol.* 14, 1057–1067. doi:10.1038/ncb2588
- Saltel, F., Mortier, E., Hytönen, V. P., Jacquier, M.-C., Zimmermann, P., Vogel, V., Liu, W. and Wehrle-Haller, B. (2009). New PI(4,5)P<sub>2</sub>- and membrane proximal integrin-binding motifs in the talin head control beta3-integrin clustering. *J. Cell Biol.* 187, 715–731. doi:10.1083/jcb.200908134
- Sebzda, E., Bracke, M., Tugal, T., Hogg, N. and Cantrell, D. A. (2002). Rap1A positively regulates T cells via integrin activation rather than inhibiting lymphocyte signaling. *Nat. Immunol.* 3, 251–258. doi:10.1038/ni765
- Song, X., Yang, J., Hirbawi, J., Ye, S., Perera, H. D., Goksoy, E., Dwivedi, P., Plow, E. F., Zhang, R. and Qin, J. (2012). A novel membrane-dependent on/off switch mechanism of talin FERM domain at sites of cell adhesion. *Cell Res.* 22, 1533–1545. doi:10.1038/cr.2012.97
- Stefanini, L., Lee, R. H., Paul, D. S., O'shaughnessy, E. C., Ghaloussi, D., Jones, C. I., Boulaftali, Y., Poe, K. O., Piatt, R., Kechele, D. O. et al. (2018). Functional redundancy between RAP1 isoforms in murine platelet production and function. *Blood* 132, 1951–1962. doi:10.1182/blood-2018-03-838714
- Stritt, S., Wolf, K., Lorenz, V., Vogtle, T., Gupta, S., Bosl, M. R. and Nieswandt, B. (2015). Rap1-GTP-interacting adaptor molecule (RIAM) is dispensable for platelet integrin activation and function in mice. *Blood* 125, 219–222. doi:10.1182/blood-2014-08-597542
- Su, W., Wynne, J., Pinheiro, E. M., Strazza, M., Mor, A., Montenont, E., Berger, J., Paul, D. S., Bergmeier, W., Gertler, F. B. and et al. (2015). Rap1 and its effector RIAM are required for lymphocyte trafficking. *Blood* 126, 2695–2703. doi:10.1182/blood-2015-05-644104
- Theodosiou, M., Widmaier, M., Bottcher, R. T., Rognoni, E., Veelders, M., Bhargava, M., Lambacher, A., Austen, K., Muller, D. J., Zent, R. et al. (2016). Kindlin-2 cooperates with talin to activate integrins and induces cell spreading by directly binding paxillin. *eLife* 5, e10130. doi:10.7554/eLife.10130
- Wynne, J. P., Wu, J., Su, W., Mor, A., Patsoukis, N., Boussiotis, V. A., Hubbard, S. R. and Phillips, M. R. (2012). Rap1-interacting adapter molecule (RIAM) associates with the plasma membrane via a proximity detector. *J. Cell Biol.* 199, 317–330. doi:10.1083/jcb.201201157
- Yang, J., Zhu, L., Zhang, H., Hirbawi, J., Fukuda, K., Dwivedi, P., Liu, J., Byzova, T., Plow, E. F., Wu, J. et al. (2014). Conformational activation of talin by RIAM triggers integrin-mediated cell adhesion. *Nat. Commun.* 5, 5880. doi:10.1038/ncomms6880
- Zhang, H., Chang, Y. C., Huang, Q., Brennan, M. L. and Wu, J. (2016). Structural and functional analysis of a talin triple-domain module suggests an alternative talin autoinhibitory configuration. *Structure* 24, 721–729. doi:10.1016/j.str.2016.02.020
- Zhu, L., Yang, J., Bromberger, T., Holly, A., Lu, F., Liu, H., Sun, K., Klapproth, S., Hirbawi, J., Byzova, T. V. et al. (2017). Structure of Rap1b bound to talin reveals a pathway for triggering integrin activation. *Nat. Commun.* 8, 1744. doi:10.1038/s41467-017-01822-8

# Figure S1

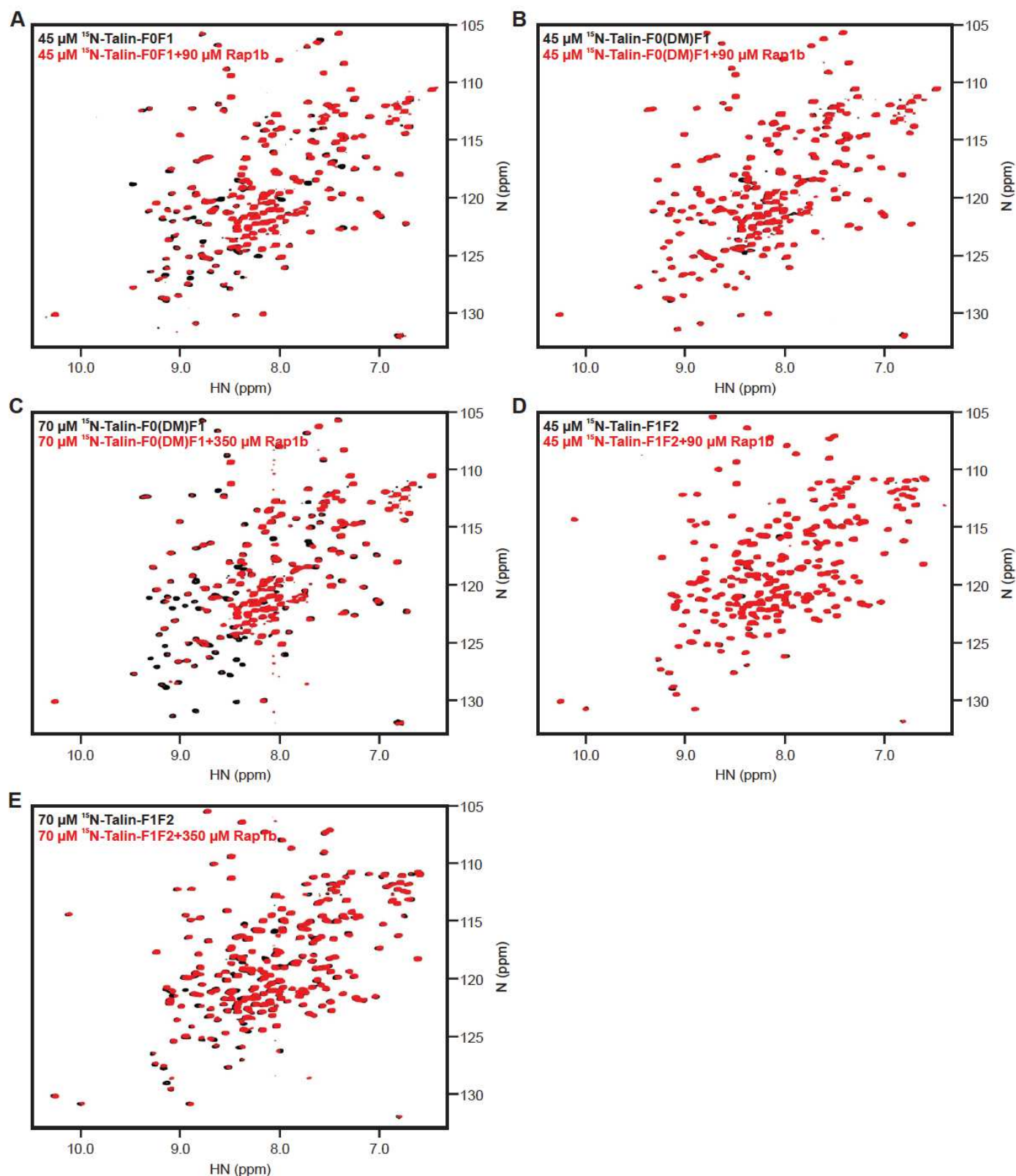


**Figure S1:** (A) The HSQC spectra of 45  $\mu\text{M}$   $^{15}\text{N}$ -labeled talin-F0F1 in the absence (black) and presence of 90  $\mu\text{M}$  GMP-PNP loaded Rap1b (red). (B) The HSQC spectra of 45  $\mu\text{M}$   $^{15}\text{N}$ -labeled talin-F0(DM)F1 (K15A, R35A) in the absence (black) and presence of 90  $\mu\text{M}$  GMP-PNP loaded Rap1b (red). (C) The HSQC spectra of 70  $\mu\text{M}$   $^{15}\text{N}$ -labeled talin-F0(DM)F1 (K15A, R35A) in the absence (black) and presence of 350  $\mu\text{M}$  GMP-PNP loaded Rap1b (red). (D) The HSQC spectra of 45  $\mu\text{M}$   $^{15}\text{N}$ -labeled talin-F1F2 in the absence (black) and presence of 90  $\mu\text{M}$  GMP-PNP loaded Rap1b (red). (E) The HSQC spectra of 70  $\mu\text{M}$   $^{15}\text{N}$ -labeled talin-F1F2 in the absence (black) and presence of 350  $\mu\text{M}$  GMP-PNP loaded Rap1b (red).



## Figure S2

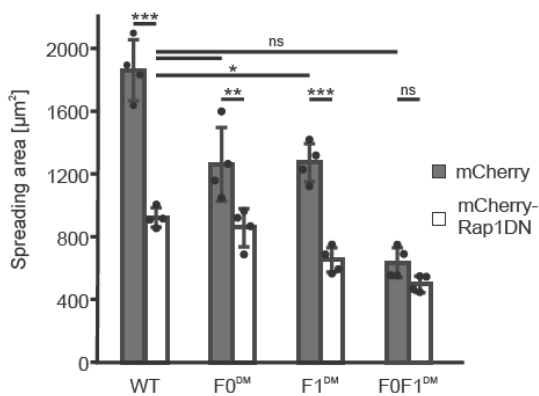


**Figure S2: Talin-mediated cell spreading is highly dependent on Rap1.** Spreading area of talin<sup>1/2dKO</sup> fibroblasts expressing ypet-talin WT, ypet-talin F0<sup>DM</sup>, F1<sup>DM</sup> or F0F1<sup>DM</sup> combined with either mCherry alone or a mCherry-tagged dominant negative S17N Rap1a mutant (n=4). Spreading area was assessed 1 h after seeding the cells on fibronectin. Data are represented as mean±c.i.; statistical significance was tested by two-way ANOVA followed by Tukey's multiple comparison test.

# Figure S3

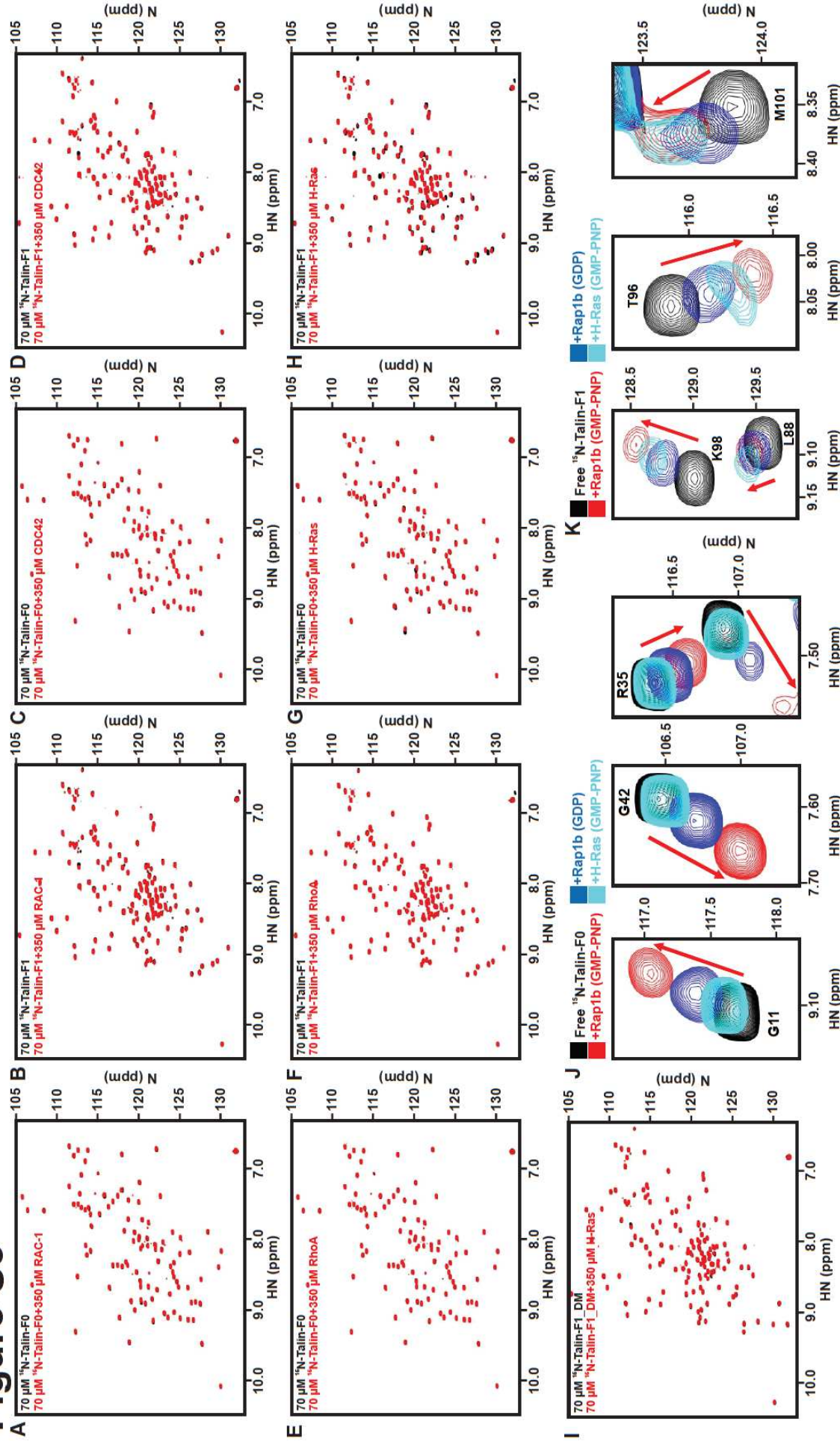


**Figure S3: Interactions between Talin F0 or F1 domains with Rac-1, Cdc42, RhoA or H-Ras tested by NMR HSQC.** The HSQC spectra of 70  $\mu\text{M}$   $^{15}\text{N}$ -labeled talin-F0 (A/C/E/G) and 70  $\mu\text{M}$   $^{15}\text{N}$ -labeled talin-F1 (B/D/F/H) in the absence (black) and presence (red) of 350  $\mu\text{M}$  GMP-PNP loaded Rac-1 (A/B), Cdc42 (C/D), RhoA (E/F) or H-Ras (G/H). (I) The HSQC spectra of 70  $\mu\text{M}$   $^{15}\text{N}$ -labeled talin-F1 DM (K98A, R118A) in the absence (black) and presence of 350  $\mu\text{M}$  GMP-PNP loaded H-Ras. (J/K) Zoomed HSQC spectra (representative residues are shown) of 70  $\mu\text{M}$   $^{15}\text{N}$ -labeled talin-F1 (I) and 70  $\mu\text{M}$   $^{15}\text{N}$ -labeled talin-F0 (J) in the absence (black) and presence of 350  $\mu\text{M}$  GDP loaded Rap1b (dark blue), GMP-PNP loaded Rap1b (red) or GMP-PNP loaded H-Ras (cyan). For binding talin-F0, Rap1b GMPPNP > Rap1b GDP >> H-Ras GMPPNP. For binding talin-F1, Rap1b GMPPNP > (slightly) H-Ras GMPPNP > Rap1b GDP. These suggest that talin F0 is more selective than F1 in binding GTPase.